

Stimulating In Situ Denitrification in an Aerobic, Highly Conductive Municipal Drinking Water Aquifer

by

Catharine Elizabeth Critchley

A thesis
presented to the University of Waterloo
in fulfillment of the
thesis requirement for the degree of
Master of Science
in
Earth Sciences

Waterloo, Ontario, Canada, 2010

© Catharine Elizabeth Critchley 2010

Author's Declaration

I hereby declare that I am the sole author of this thesis. This is a true copy of the thesis, including any required final revisions, as accepted by my examiners.

I understand that my thesis may be made electronically available to the public.

Abstract

Best or beneficial management practices (BMPs) are often relied upon as a mitigation strategy for nitrate contamination throughout Canada. At a regional scale, reducing the quantity of nutrients applied to agricultural land is one BMP approach that has been implemented internationally. While these BMP strategies have been proven to successfully reduce the environmental impact of agriculture on water systems, the time interval between BMP implementation and a noticeable improvement in groundwater quality can be quite extensive. This lag time has been observed at the agriculturally impacted Thornton Well Field in Oxford County. Despite seven years of significant reductions in fertilizer application within the capture zone of this municipal well field, declining nitrate concentrations have yet to be observed in the production water wells. In order to accelerate nitrate reductions at the Thornton Well Field, an integrated approach, combining BMPs with a stimulated in situ denitrification strategy, was implemented.

This research focused on the use of a cross-injection scheme to stimulate in situ denitrification within the production aquifer units, up-gradient of the Thornton Well Field. Briefly, this strategy involves injecting a carbon source and electron donor into a high flux aquifer zone using an injection and extraction system positioned perpendicular to the regional flow field. Through altering the geochemical conditions, the injections stimulate indigenous bacteria to reduce harmful nitrate to innocuous dinitrogen gas. The main objectives of this research included: characterizing the hydrogeologic and geochemical properties of the target aquifer; pilot scale testing of the proposed in situ denitrification system; and suggesting an approach for up-scaling to a full-scale treatment scheme capable of remediating the elevated nitrate concentrations at the Thornton Well Field.

Core logging, electrical resistivity studies, several methods of hydraulic characterization, tracer testing, and three-dimensional groundwater modelling were used to quantify the physical properties of the target aquifer and to develop a hydrogeologic conceptual model of the site. The aquifer unit was found to be unconfined in the experiment vicinity,

consisting of a complex system of six main hydrostratigraphic layers of sand and gravel featuring variable hydraulic conductivity (K) values. Despite the hydrogeologic complexity, the geochemical properties of the aquifer were relatively uniform with depth. Anion, cation, alkalinity, pH, dissolved oxygen, and nitrous oxide data all contributed to this conjecture. Of particular interest, however, were the elevated dissolved oxygen concentrations, which rivalled atmospheric saturation throughout the entire aquifer sequence. The background physical and chemical characterization identified two main challenges that would potentially influence the performance of the in situ denitrification process: stimulating uniform denitrification in the fast flowing, complex aquifer system and overcoming the elevated oxygen concentrations to achieve the necessary anaerobic conditions.

Following the initial site characterization phase, several preliminary cross-injection experiments were designed and performed. These experiments featured an injection-extraction circulation cycle which spanned five metres and was operated normal to groundwater flow. Acetate was selected as the electron donor and carbon substrate. The first test involved a single acetate injection followed by an extensive period of groundwater sampling. Unfortunately, this initial test provided no indication of stimulated in situ denitrification. All anion, cation, and nitrous oxide concentration and isotope data collected during and following this injection remained within the range of background estimates.

Following the first injection experiment, a subsequent test involving multiple, repetitive acetate injections was implemented to overcome the highly aerobic nature of the aquifer and support the growth and reproduction of denitrifying bacterial populations. The second injection phase included 19 individual injections that were operated at intervals of every day to every other day over a total period of 26 days. These injections successfully lowered the dissolved oxygen concentrations within the target aquifer to an average range of 0 to 4 mg/L. The least conductive layers featured the lowest oxygen concentrations, while the higher K layers maintained elevated oxygen concentrations. The nitrite, nitrate, and enriched $\text{NO}_3\text{-}^{15}\text{N}$ and $\text{NO}_3\text{-}^{18}\text{O}$ isotope data suggested a high degree of stimulated

denitrification in the least conductive layers and a limited degree in the high-K layers. The lower-K units corresponding to multi-level well ports ML7-2, ML7-5, and ML7-6 achieved a 46 percent reduction in nitrate, while the layer represented by ML7-1 attained a 100 percent reduction in nitrate. Alternatively, due to the constant influx of dissolved oxygen and limited residence times, very little denitrification was observed in the fast flowing layers corresponding to ports ML7-3, ML7-4, and ML7-7. Overall, a percent reduction, in terms of nitrate mass crossing the 5-m wide treatment lens, of only eleven percent was calculated. These results clearly demonstrate that the K-profile had a significant impact on stimulating in situ bioremediation.

Two major system challenges were observed, including an inability to successfully stimulate denitrification within the highly permeable layers and the generation of harmful nitrite at nearly all aquifer depths. Based on these significant challenges, it was concluded that additional experimentation is required before this remediation technique can be expanded to a full-scale in situ treatment scheme. The most significant recommendation requested the development and execution of a third injection phase, consisting of multiple, consecutive substrate injections designed to systematically test various pulsing intervals, injection concentrations, and electron donors. Despite the current limitations, this approach has great potential. It is believed that with additional research, the in situ stimulation of denitrification could be used to successfully reduce the elevated nitrate concentrations at the Thornton Well Field.

Acknowledgements

I extend many thanks to my mentor and supervisor Dr. David Rudolph for providing me with this opportunity. He has given me a great deal of guidance, knowledge, and encouragement over the past several years, in addition to an ideal research project that I have loved being involved in. Thanks also to my committee members Dr. Rick Devlin, for providing additional technical and personal support, and Dr. Ramon Aravena, for introducing me to the wonderful world of isotopes. I am also appreciative of the guidance provided by Dr. Brewster Conant, who was always a quick e-mail or phone call away when help was needed.

Thank you to Paul Johnson and Bob Ingleton for their technical expertise and assistance. I could not have done this research without them. In addition to installing wells, collecting core, building packers systems and sampling manifolds, they were great teachers, providing me with many new skills that will be useful throughout life.

Special thanks to Peter Schillig who made the thirty-hour sampling expeditions both manageable and entertaining. It was great to have a partner, someone to learn from, share the ups and downs with, and challenge me to perform at my best. I would also like to thank all of the researchers and students who have helped me with field, lab, and modelling work: Richard Elgood, Jeff Melchin, Joanna Passmore, Cynthia Davis, Marcelo Sousa, Greg Boonstra, Jamie Koch, Mike Christie, Cameron McNaughton, Melissa Bunn, Justin Harbin, Stan Smith, Dave Snider, Tyler Gale, Scott Piggott, Kayla Siefried, Graham Pope, Kelly Molnar, Christina Miceli, Ashley Rudy, and Candice Williams. They have all gone above and beyond, contributing knowledge, encouragement, patience, and friendship.

I am grateful to the Natural Sciences and Engineering Council of Canada, the Ontario Graduate Scholarship Program, the County of Oxford, the Canadian Water Network, and the Ontario Ministry of the Environment for providing generous financial support. In addition, thank you to the people at Oxford County for providing access to the study site.

Finally, thank you to my old and new friends for the laughs and diversion; to my family who have always told me I could do anything I put my mind to; and to Joel for the hours spent proof reading, listening, and encouraging.

Table of Contents

Author’s Declaration	ii
Abstract.....	iii
Acknowledgements.....	vi
Table of Contents.....	vii
List of Figures	xi
List of Tables	xv
1. Introduction	1
1.1 Nitrate, Agriculture, and Groundwater.....	1
1.2 Conventional Use of Land Management BMPs for Nitrate Mitigation.....	1
1.3 Coupling BMPs and Remediation Strategies for Enhanced Treatment	2
1.4 Field Application of the Integrated Approach: Woodstock, Ontario	3
1.5 Hypothesis and Objectives	3
1.6 Study Approach	4
2. Background	5
2.1 Literature Review	5
2.1.1 Nitrate and Human Health	5
2.1.2 Regulatory Framework for Nutrient Management in Ontario.....	6
2.1.3 Nutrient Management Strategies in the Literature	7
2.1.4 The Integrated Use of Groundwater Remediation Strategies	10
2.1.5 In Situ Denitrification as a Treatment Option	10
2.1.5.1 Permeable Reactive Barriers for Denitrification.....	11
2.1.5.2 Injection-Withdrawal Systems for Denitrification	12
2.1.5.3 Site Characterization Challenges Relating to In Situ Treatment.....	13
2.2 Study Site.....	14
2.2.1 Site Description and Topography	14
2.2.2 Previous Research.....	15
2.2.3 Geology	16
2.2.4 Hydrogeology.....	17
2.2.5 The Average Regional Groundwater Flow Field	17
2.2.6 History of Nutrient Management at the Study Site	18
3. Methods.....	27
3.1 Site Instrumentation	27
3.1.1 Injection-Extraction Wells	27
3.1.2 Multi-Level Monitoring Wells.....	27
3.1.3 Existing Monitoring Wells.....	28
3.2 Core Logging.....	29

3.3 Electrical Resistivity Surveys.....	30
3.4 Hydraulic Testing.....	31
3.4.1 Grain Size Analysis	31
3.4.2 Conventional Slug Tests.....	32
3.4.3 Multi-level Slug Tests.....	33
3.4.4 Borehole Flowmeter Testing	34
3.5 Determining the Regional Hydraulic Gradient.....	36
3.6 Tracer Tests	36
3.6.1 Predictive Analytical Modelling.....	36
3.6.2 Forced Gradient Testing	37
3.6.3 Natural Gradient Testing	38
3.6.4 Analysis of the Breakthrough Data.....	39
3.7 Three-Dimensional Groundwater Modelling.....	40
3.7.1 Finite-Difference Groundwater Modelling Approach	41
3.7.2 Model Input Parameters	42
3.7.3 The Preliminary Homogeneous Model.....	42
3.7.4 Stratified Model Development and Calibration	43
3.8 Groundwater Sampling and Analysis	43
3.8.1 Anion Samples	44
3.8.2 Cation Samples	44
3.8.3 Alkalinity	44
3.8.4 Dissolved Oxygen.....	45
3.8.5 Nitrous Oxide Sampling	45
3.9 Isotope Sampling and Analysis.....	46
3.9.1 ¹⁵ N and ¹⁸ O in Nitrate	47
3.9.2 ¹⁵ N and ¹⁸ O in Nitrous Oxide.....	47
3.9.3 Tritium-Helium Age Dating.....	48
3.10 Lateral Nitrate Flux through the Treatment Zone	48
3.11 Substrate Additions.....	49
3.11.1 Selection of the Cross-Injection Scheme	49
3.11.2 Electron Donor Selection.....	50
3.11.3 The C:N Ratio	51
3.11.4 Injection Procedure	52
3.11.5 Groundwater Sampling Routine.....	54
3.11.6 Evaluating the Effectiveness of the In Situ Treatment System	56
3.11.7 Developing an Approach for Up-scaling Treatment.....	56
4. Results and Discussion	65
4.1 Hydrogeologic Conceptual Model.....	65
4.1.1 Core Logging	65
4.1.2 Electrical Resistivity Surveys.....	66
4.1.3 Hydraulic Characterization	67
4.1.3.1 Grain Size Analysis	67

4.1.3.2 Conventional Slug Tests	68
4.1.3.3 Multi-level Slug Tests	69
4.1.3.4 Borehole Flowmeter Testing.....	69
4.1.4 The Regional Hydraulic Gradient.....	70
4.1.5 Tracer Testing Results.....	72
4.1.5.1 Forced Gradient Tracer Test 1	72
4.1.5.2 Forced Gradient Tracer Test 2	73
4.1.5.3 Natural Gradient Tracer Test	75
4.1.5.4 Comparison of Tracer Test Results	76
4.1.6 Three-Dimensional Groundwater Modelling Results.....	78
4.1.6.1 Results from the Preliminary Homogeneous Model	78
4.1.6.2 Stratified Model Development	78
4.1.6.3 Calibration of the Five-Layer Model	79
4.1.6.4 Application of the Calibrated Model: The Six Cases of Interest	80
4.1.6.5 Case 1 Results (5 m separation distance, single extraction well).....	82
4.1.6.6 Case 2 Results (5 m separation distance, two extraction wells)	82
4.1.6.7 Case 3 Results (10 m separation distance, single extraction well).....	83
4.1.6.8 Case 4 Results (10 m separation distance, two extraction wells)	83
4.1.6.9 Case 5 Results (15 m separation distance, single extraction well).....	84
4.1.6.10 Case 6 Results (15 m separation distance, two extraction wells)	84
4.1.6.11 Substrate Dilution	84
4.1.6.12 Comments on the Injection Duration and Concentration.....	85
4.1.6.13 The Ideal Well Configuration	86
4.1.6.14 Sources of Uncertainty	86
4.1.6.15 Model-Based Recommendations for the Treatment System.....	87
4.1.7 Estimating the Hydraulic Conductivity Profile.....	88
4.1.7.1 The Hydrogeologic Conceptual Model	90
4.1.7.2 Implications of the K Profile on Stimulating In Situ Denitrification.....	92
4.2 Geochemical Characterization	93
4.2.1 Quality Assurance and Quality Control (QA/QC).....	93
4.2.2 Anion Samples	93
4.2.3 Cation Samples	94
4.2.4 Alkalinity, Dissolved Oxygen, and Other Field Parameters	95
4.2.5 Nitrous Oxide	96
4.2.6 ¹⁵ N and ¹⁸ O in Nitrate	96
4.2.7 Tritium-Helium Age Dating.....	97
4.3 Implications of the Lateral Nitrate Flux through the Treatment Zone	97
4.4 Cross-Injection Experiments.....	98
4.4.1 Results from Injection Phase 1	98
4.4.2 Results from Injection Phase 2	100
4.4.2.1 Oxygen Monitoring Throughout Injection Phase 2	101
4.4.2.2 Injection 13: Subsurface Distribution of Acetate and Bromide.....	103
4.4.2.3 Injection 13: The Fate of Nitrous Oxide	105

4.4.2.4 Injection 13: The Fate of Manganese, Iron, and Sulphate.....	106
4.4.2.5 Injection 13: The Fate of Nitrate and Nitrite	107
4.4.2.6 Injection 13: Trends in Groundwater Isotope Composition	110
4.4.2.7 Additional Anion Monitoring Throughout Injection Phase 2	112
4.5 Site-Specific Challenges.....	113
4.6 Critical Next Steps and an Approach for Up-Scaling Treatment	115
4.7 Application of the System beyond the Study Site.....	116
4.8 Overall Implications.....	116
5. Conclusions and Recommendations	164
5.1 Conclusions.....	164
5.2 Recommendations	165
Bibliography.....	167
Appendices	178
Appendix A: Well Location and Construction Information	178
Appendix B: Geologic Core Logs.....	185
Appendix C: Grain Size Analysis Data	215
Appendix D: Manual Water Level Measurements	219
Appendix E: Complete CLOUDPE and PULSEPE Tracer Test Results	220
Appendix F: Background Geochemical Data	223
Appendix G: Geochemical Results from Acetate Injection Phase 1.....	236
Appendix H: Geochemical Results from Acetate Injection Phase 2.....	241

List of Figures

Figure 2.1: Map displaying the study site location within Southern Ontario. Map contains data from DMTI CanMap Streetfiles (2005) and DMTI Census Geography (2003).	20
Figure 2.2: Municipal supply well locations in the Thornton and Tabor Well Fields. Map contains data from CanMap Streetfiles (2005) and Southwestern Ontario Orthoimagery Project (2006).....	21
Figure 2.3: Trends in nitrate concentrations in Municipal Wells 1, 3, and 5 (Bekeris, 2007).	22
Figure 2.4: Topography of the study site and surrounding area. Map contains data from CanMap Streetfiles (2005) and Natural Resources and Values Information System (2008).....	23
Figure 2.5: Quaternary geology of the study site and surrounding area. Map contains data from The Corporation of the County of Oxford (2001, 2003b, 2003c) (Modified from Bekeris, 2007).	24
Figure 2.6: Stratigraphic cross-section along Curry Road (Haslauer, 2005; Bekeris, 2007). ..	25
Figure 2.7: Hydraulic head contour maps representing conditions in May of 2008 in (a) Aquifer 2 and (b) Aquifer 3 (modified from Koch, 2009).....	26
Figure 3.1: Layout of the monitoring wells at the study site. Map contains data from CanMap Streetfiles (2005) and Southwestern Ontario Orthoimagery Project (2006)...	58
Figure 3.2: Core locations relative to the monitoring wells. Map contains data from CanMap Streetfiles (2005) and Southwestern Ontario Orthoimagery Project (2006).	59
Figure 3.3: Location map of resistivity survey lines 1 and 2.	60
Figure 3.4: Multi-level slug testing apparatus (modified from Zlotnik and McGuire, 1998)..	61
Figure 3.5: (a) The impeller flowmeter used for borehole logging. (b) The Mount Sopris 4MXA-1000 winch used to control the measurement depths. (c) The surface instrumentation, including the tri-pod and pulley system used to suspend the instrument and the Honda WH15XK1C1 high-pressure pump.....	62
Figure 3.6: Preliminary homogeneous conceptual model (not to scale) (Gale, 2009).....	63

Figure 3.7: (a) Map indicating tritium-helium sampling locations and (b) photograph of one of the in situ diffusion samplers.	64
Figure 4.1: The August 19, 2009 and September 10, 2009 resistivity results for Line 1.	130
Figure 4.2: The August 19, 2009 and September 10, 2009 resistivity results for Line 2.	131
Figure 4.3: Grain size analysis results plotted as hydraulic conductivity with depth.	132
Figure 4.4: Borehole flowmeter test results for wells WO77, WO78, WO79, and WO80. ..	133
Figure 4.5: Hydraulic head contour plot displaying direction of ambient groundwater flow.	134
Figure 4.6: Bromide breakthrough curves from the first forced gradient tracer test.	135
Figure 4.7: Breakthrough curves from the second forced gradient tracer test for (a) ML5, (b) ML6, (c) ML7, and (d) ML8.	136
Figure 4.8: Natural gradient tracer test breakthrough curves for (a) bromide and (b) acetate.	137
Figure 4.9: Comparison of hydraulic conductivity values determined from tracer testing; note the different horizontal scales.	138
Figure 4.10: Observed and simulated breakthrough curves for (a) the homogeneous case, (b) the three-layer case, (c) the initial five-layer case, and (d) the calibrated five-layer case (Gale, 2009).	139
Figure 4.11: Five-layer conceptual model (not to scale) (Gale, 2009).	140
Figure 4.12: Prospective pumping and injection well (PW, IW) arrangements (Gale, 2009).	141
Figure 4.13: Case 1 (5 m separation distance, single extraction well) model-generated acetate plume along the injection-extraction well plane at (a) t = 50 minutes, (b) t = 240 minutes, (c) t = 720 minutes, and (d) t = 1440 minutes (Gale, 2009).	142
Figure 4.14: Plan view diagrams illustrating the injectate plume in the third layer ($K = 1.2 \times 10^{-1}$ cm/s) for (a) Case 1 at 240 minutes, (b) Case 2 at 240 minutes, (c) Case 3 at 720 minutes, (d) Case 3 at 1440 minutes, (e) Case 4 at 720 minutes, (f) Case 4 at 1440 minutes, (g) Case 5 at 1440 minutes, and (h) Case 6 at 1440 minutes (modified from Gale, 2009).	143

Figure 4.15: Case 2 (5 m separation distance, two extraction wells) model-generated acetate plume along the injection-extraction well plane at (a) t = 50 minutes, (b) t = 240 minutes, (c) t = 720 minutes, and (d) t = 1440 minutes (Gale, 2009)..... 144

Figure 4.16: Case 3 (10 m separation distance, single extraction well) model-generated acetate plume along the injection-extraction well plane at (a) t = 50 minutes, (b) t = 240 minutes, (c) t = 720 minutes, and (d) t = 1440 minutes (Gale, 2009)..... 145

Figure 4.17: Case 4 (10 m separation distance, two extraction wells) model-generated acetate plume along the injection-extraction well plane at (a) t = 50 minutes, (b) t = 240 minutes, (c) t = 720 minutes, and (d) t = 1440 minutes (Gale, 2009)..... 146

Figure 4.18: Case 5 (15 m separation distance, single extraction well) model-generated acetate plume along the injection-extraction well plane at (a) t = 50 minutes, (b) t = 240 minutes, (c) t = 720 minutes, and (d) t = 1440 minutes (Gale, 2009)..... 147

Figure 4.19: Case 6 (15 m separation distance, two extraction wells) model-generated acetate plume along the injection-extraction well plane at (a) t = 50 minutes, (b) t = 240 minutes, (c) t = 720 minutes, and (d) t = 1440 minutes (Gale, 2009)..... 148

Figure 4.20: Graphical summary of all hydraulic conductivity profile estimates. 149

Figure 4.21: The hydrogeologic conceptual model for the study site. 150

Figure 4.22: Background nitrate, sulphate, and chloride concentration profiles for (a) WO74-ML, (b) ML5, and (c) ML10. 151

Figure 4.23: Vertical profiles of (a) alkalinity, (b) dissolved oxygen, (c) electrical conductivity, and (d) pH. 152

Figure 4.24: 2007 and 2009 nitrate isotope data plotted amongst various categories of nitrate sources (modified from Bleifuss et al., 2001). 153

Figure 4.25: ML7 (a) Bromide, (b) acetate, (c) nitrate, and (d) nitrite results from the first injection phase. 154

Figure 4.26: Dissolved oxygen results from the second injection phase. 155

Figure 4.27: Cross-sectional contour plots along the line of multi-level wells representing concentrations of (a) acetate at T-to = 7.5 hours and (b) bromide at T-to = 7.5 hours. 156

Figure 4.28: ML7 (a) bromide and (b) acetate breakthrough curves from the 25-hour sampling effort that took place during and following injection 13. 157

Figure 4.29: Nitrous oxide concentrations determined from samples collected during injection 13. 158

Figure 4.30: ML7 (a) nitrate and (b) nitrite results from the 25-hour sampling effort. 159

Figure 4.31: Cross-sectional contour plots along the line of multi-level wells representing concentrations of (a) nitrate at T-to = 0.5 hours, (b) nitrate at T-to = 7.5 hours, (c) nitrite at T-to = 0.5 hours, and (d) nitrite at T-to = 7.5 hours..... 160

Figure 4.32: Nitrate concentration plotted against nitrite concentration for experiment times of (a) T – to = 0.5 hours and (b) T – to = 7.5 hours. 161

Figure 4.33: ML5, ML6, and ML7 nitrate isotope results from the second injection phase. 162

Figure 4.34: Additional (a) nitrate and (b) nitrite monitoring throughout Injection Phase 2. 163

List of Tables

Table 3.1: Summary of acetate injections.	57
Table 4.1: Hydraulic conductivity results from conventional slug tests.	120
Table 4.2: Hydraulic conductivity results from multi-level slug testing.	120
Table 4.3: 2008 monthly gradients across the study site.	121
Table 4.4: Summary of CLOUDPE and PULSEPE tracer test results.	122
Table 4.5: Hydrogeologic parameters for the three-layer model (Gale, 2009).	123
Table 4.6: Hydrogeologic parameters for the initial five-layer model (Gale, 2009).	123
Table 4.7: Layer-specific parameters for the calibrated five-layer model (Gale, 2009).	123
Table 4.8: Universal parameters for the calibrated five-layer model (Gale, 2009).	123
Table 4.9: Summary of normalized sensitivity coefficients; the grey cells represent NSC values greater than 0.1 and less than -0.1, indicating significant sensitivity (modified from Gale, 2009).	124
Table 4.10: Summary of hydraulic conductivity estimates generated by various methods.	125
Table 4.11: Nitrate mass flux calculations for municipal supply wells 01, 03, 05, 08, and 11.	126
Table 4.12: Nitrate mass flux calculations for the aquifer layers, including supply well impact estimates.	127
Table 4.13: Calculations comparing the nitrate mass flux prior to the addition of acetate and following the 13 th injection.	128
Table 4.14: Estimates of nitrogen isotope enrichment factors for denitrification.	129

1. Introduction

1.1 Nitrate, Agriculture, and Groundwater

It is suggested that nitrate is the single most common groundwater contaminant worldwide (Freeze and Cherry, 1979; Spalding and Exner, 1993; Appelo and Postma, 2005), emanating from both point sources, such as septic tanks and agricultural waste lagoons, and non-point sources, such as nutrients applied to farm fields and geological sources (Canter, 1997).

Appelo and Postma (2005) suggest that the main cause of increasing nitrate levels in shallow aquifers is the excessive agricultural application of fertilizers and manure since the 1960s. In rural settings where municipal and private wells tend to be surrounded by agricultural land, this direct connection between nutrient application and groundwater quality must be recognized.

1.2 Conventional Use of Land Management BMPs for Nitrate Mitigation

The accumulation of nitrate in the hydrologic cycle resulting from agricultural operations has drawn the international attention of government regulators, researchers, and water resources managers, who have established a collection of mandatory and voluntary standards for agricultural practice (Bekeris, 2007). The primary focus of these standards is limiting the loss of nutrients to the environment. In addition to meeting strict nutrient management regulations, such as restrictions on winter applications and set-back distances from groundwater wells and surface water bodies, farmers typically further soil and water protection efforts by implementing other best or beneficial management practices (BMPs) (Bekeris, 2007). These practices include any action that considers the balance of nutrients in agriculture, with an overall goal of protecting environmental resources without sacrificing successful crop production (Crop Nutrients Council, 2009). Examples of BMPs include the use of a crop rotation, reducing nitrogen application rates, synchronizing nitrogen supply and plant demand, the use of buffer strips and riparian zones, and the use of cover crops (Di and Cameron, 2002; Mckague et al., 2005).

1.3 Coupling BMPs and Remediation Strategies for Enhanced Treatment

Land management BMPs are commonly relied upon as a mitigation strategy for nitrate contamination throughout Canada. While this technique has been shown to successfully reduce the environmental impact of agriculture on groundwater systems, the time interval between BMP implementation and a noticeable improvement in groundwater quality can be quite extensive. For example, Meissner et al. (2002) observed a strong correlation between a 50 percent reduction in fertilizer input and the amount of nutrient leaching through the unsaturated zone; however, the positive outcome was not observed until 13 years following implementation. In addition, a second study suggests that nitrate concentrations in the saturated zone of the Abbotsford-Sumas aquifer, which spans the Western Canada-United States border, have not notably changed following ten years of established agricultural BMPs (Wassenaar et al., 2006). Non-compliance issues revolving around the fertilizer application requirements and the employment of inorganic chemical fertilizers, however, may have affected these results (Wassenaar et al., 2006). Cole (2008) examined the long-term effects of a 46 percent reduction in nutrient application on shallow groundwater nitrate concentrations. An average reduction of 35 percent was observed, with more significant improvements occurring near the water table. While the decrease in nutrient loading was found to significantly reduce the nitrate mass exiting the farm property, these positive results were not observed until 10 years following implementation. Research studies by Tomer and Burkart (2003) and Honisch et al. (2002) also support the notion that it may take several years to decades for changes in agricultural management practices to have an impact on groundwater quality due to extensive travel times through the vadose zone.

It is clear that a lengthy lag time exists between regional scale BMP implementation and a decrease in groundwater nitrate concentrations at certain sites. Therefore, the adoption of an integrated approach, combining BMPs with various groundwater remediation strategies, seems intuitive. While the BMPs provide a relatively low maintenance, longer term solution, groundwater remediation strategies, such as permeable reactive barriers and other in situ

treatment methods, provide a more intense, shorter term solution. Integrating these two approaches combines the benefits of both methods and may provide a reliable, enduring treatment system with a significantly reduced lag time. The focused remedial approach would be designed to function until the effects of the regional scale BMPs are realized in the production aquifer.

1.4 Field Application of the Integrated Approach: Woodstock, Ontario

The City of Woodstock, Ontario, located within the County of Oxford, relies on groundwater from glacial sediments to meet all domestic and industrial water demands. The Thornton Well Field, located in a rural setting southwest of the city, provides the majority of the water supply. Over the last three decades, nitrate concentrations at this well field have been progressively increasing, likely due to the influence of excess fertilizer application on the surrounding agricultural land. As a result, in 2003 the County purchased 111 hectares of agricultural land within the capture zone of the Thornton Well Field. The land is now rented back to farmers who must abide by strict nutrient application guidelines and various BMPs. Following this effort, it was assumed that nitrate concentrations would gradually decline in the supply wells. Seven years later, no decline has been observed and the County of Oxford has shifted its focus to an integrated approach involving a combination of regional reductions in nutrient application and focused in situ denitrification. This research project addresses the supplementary in situ remediation strategy.

1.5 Hypothesis and Objectives

In an effort to mitigate the nitrate problems at the Thornton Well Field, an in situ bioremediation strategy was proposed. Briefly, this strategy involves injecting a carbon source and electron donor into a high flux aquifer zone, up-gradient of the supply wells. With these key ingredients and under proper reduction-oxidation conditions, naturally-occurring aquifer bacteria will reduce the nitrate to innocuous dinitrogen gas. At full scale, it is thought that this type of system has the potential to lower nitrate concentrations in the supply wells to below the MAC. This project will provide the initial research required to

determine whether or not the described system will perform well at the Woodstock site. The overall hypothesis of this research is: large-scale in situ denitrification can be initiated in a heterogeneous, aerobic aquifer through the introduction of a carbon source and electron donor using a controlled injection system. Based on this hypothesis, the main objectives of this work are to:

- Thoroughly characterize the chemical and physical properties of the subsurface in the experiment vicinity.
- Establish and evaluate the performance of a method for stimulating in situ denitrification in a highly aerobic, fast-flowing aquifer.
- Suggest an approach for up-scaling to a full in situ treatment scheme with the capacity to remediate the elevated nitrate concentrations at the Thornton Well Field.

1.6 Study Approach

The overall approach of this research can be broken up into two main phases. In Phase 1 emphasis was placed on physical and chemical site characterization. This was done with a series of field and lab techniques, including core logging, grain size analysis, geophysics, tracer testing, groundwater sampling, and three-dimensional modelling. Phase 2 involved the actual acetate injections. Several injections were executed over a period of about six months. During the injections, intense groundwater sampling was used to track the extent of denitrification and geochemical variability.

Chapter 2 of this thesis provides background information related to the field site and in situ remediation technologies. Chapter 3 describes the methodology used for various experiments. Chapter 4 presents the results of all field and modelling work, in addition to discussion and interpretation. Finally, Chapter 5 contains the conclusions of this research as well as future recommendations.

2. Background

2.1 Literature Review

2.1.1 Nitrate and Human Health

Elevated nitrate concentrations in drinking water have most commonly been associated with methemoglobinemia, also known as “blue baby syndrome” (Johnson et al., 1987; Gelberg et al., 1999; Knobeloch et al., 2000), and various types of gastrointestinal cancers (Ward et al., 1996; Yang et al., 1998). Medical research also suggests a potential linkage between maternal nitrate exposure and adverse reproductive and developmental outcomes (Fan and Steinberg, 1996; Manassaram et al., 2005).

The potentially fatal methemoglobinemia, affecting bottle-fed infants, is perhaps the most well known condition associated with nitrate-contaminated drinking water. This illness begins when large amounts of nitrate are consumed by the infant and reduced to nitrite in the digestive system. The nitrite then oxidizes hemoglobin in the blood to form methemoglobin, a compound which lacks the ability to transport oxygen. The buildup of methemoglobin deprives the infant’s body tissues of oxygen, resulting in hypoxia and the development of an abnormal blue-grey skin colour. Methemoglobin levels greater than 50 percent can result in coma or death of the infant (Knobeloch et al., 2000).

While the connection between elevated nitrate levels in drinking water and methaemoglobinaemia appears to be a secure one, the relationship between nitrate and cancer is a debated issue. Addiscott and Benjamin (2004) suggest that there are theoretical reasons for proposing a connection between nitrate consumption and stomach cancer. Nitrite produced from nitrate reduction has the potential to react with protein digestion products in the stomach to form carcinogenic N-nitroso compounds (Addiscott and Benjamin, 2004).

It appears that further epidemiological studies are required to understand the full impact of elevated nitrate levels on human health. In the mean time, due to the potential of adverse

effects, a MAC of 10 mgNO₃-N/L for nitrate in drinking water has been established by Health Canada (Health Canada, 2008).

2.1.2 Regulatory Framework for Nutrient Management in Ontario

The potential health and environmental risks associated with agricultural practice have resulted in the development of legislation, regulations, and protocols designed to reduce nutrient pollution. In Ontario, the management of agricultural nutrients is governed by the Nutrient Management Act, developed by the Ontario Ministry of the Environment and the Ontario Ministry of Agriculture, Food, and Rural Affairs and passed on June 27, 2002 (Ontario Ministry of the Environment, 2008). This Act provides a complete nutrient management framework for the agricultural industry at the municipal scale, including comprehensive environmental protection guidelines (Ontario Ministry of the Environment, 2008). It gives current BMPs the force of law and defines enforceable, province-wide standards which regulate the management of all nutrient-rich materials applied to the land (Ontario Ministry of the Environment, 2008). Under this act, the Nutrient Management Regulation (O. Reg. 267/03) was passed in September of 2003 and amended in September 2005 (O. Reg. 511/05) (Ontario Ministry of Agriculture, Food, and Rural Affairs, 2009). This regulation defines a set of specific protocols aimed at protecting the environment and human health. Examples of these protocols include (Ontario Ministry of Agriculture, Food, and Rural Affairs, 2009):

- Design and construction standards for manure holdings
- Nutrient application setbacks from wells and surface water bodies
- Restrictions on winter spreading of nutrient-rich materials
- Requirements for vegetated buffer zones along surface water bodies

The implementation of these protocols is the responsibility of the farm operator, who may choose to supplement them with additional BMPs. Compliance and enforcement programs are defined in the Nutrient Management Act and farm-based inspections can be planned or

performed in response to complaints (Ontario Ministry of Agriculture, Food, and Rural Affairs, 2009).

2.1.3 Nutrient Management Strategies in the Literature

Dinnes et al. (2002) examined the effectiveness of many strategies for improved nutrient management. These practices are commonly used together and include the timing of nutrient applications, diversified crop rotations, cover crops, riparian buffers, and significant reductions in the nutrient application rate.

The timing and rate of nutrient application has been proven to play a dominant role in the loss of nitrate to groundwater and surface water (Dinnes et al., 2002). As the time between nutrient application and crop uptake increases, so does the risk of nitrogen losses due to leaching, runoff, and volatilization (Dinnes et al., 2002; Meisinger and Delgado, 2002). In certain areas North American farmers apply nutrients in the fall as opposed to the spring due to labour availability, favourable weather and soil conditions, and lower fertilizer prices (Dinnes et al., 2002). This practice concentrates nutrients in the soil well before it is required by crops, greatly increasing the leaching potential. In a study by Sanchez and Blackmer (1988) it was shown that 49 to 64 percent of fall-applied nitrogen was lost from the upper soil zone prior to plant uptake in the spring. Furthermore, a 36 percent reduction in nitrate losses from tile drainage was observed by Randall and Mulla (2001) when the application time was changed from fall to spring.

Diversified crop rotations, especially changing from continuous corn to a corn-soybean rotation, have also proven to be an effective method for minimizing nutrient losses (Weed and Kanwar, 1996; Albus and Knighton, 1998; Dinnes et al., 2002). Weed and Kanwar (1996) reported that the total $\text{NO}_3\text{-N}$ losses over a three year period were 164 kg/ha for continuous corn, 77 kg/ha for rotation corn plots, 84 kg/ha for rotation soybean. In addition to this, adding perennial species to the crop rotation has also been shown to reduce $\text{NO}_3\text{-N}$ losses in subsurface drainage (Randall et al., 1997). Randall et al. (1997) compared nitrate losses

from tile drainage between fields planted with continuous corn, a corn-soybean rotation, alfalfa, and an alfalfa-perennial grass mixture. The results indicated that $\text{NO}_3\text{-N}$ losses from perennial crops ranged from 30 to 50 times less than from row crops (Randall et al., 1997).

A third common nutrient management strategy is the use of a cover crop. This strategy targets the non-crop period, following the fall harvest and prior to crop development in the spring. This critical time of year, which generally runs from November to May, typically features the highest $\text{NO}_3\text{-N}$ losses from subsurface drainage (Cambardella et al., 1999). In a three year study, Drury et al. (1996) demonstrated that 88 to 95 percent of total annual $\text{NO}_3\text{-N}$ losses occurred during this time period. The cultivation of cover crops during the non-crop interval had been proven to effectively reduce the potential for nitrate leaching from agricultural fields (Martinez and Guiraud, 1990; Meisinger et al., 1991; Dinnes et al., 2002). Cover crops operate by accumulating inorganic soil nutrients and holding them in an organic form, thus preventing leaching to groundwater systems (Dinnes et al., 2002). The bound nutrients are then released to the next crop upon decomposition (Dinnes et al., 2002). Martinez and Guiraud (1990) measured $\text{NO}_3\text{-N}$ concentrations in drainage water from a field with a corn-wheat rotation both with and without a ryegrass cover crop. They determined that, during the intercrop period, the average $\text{NO}_3\text{-N}$ concentration in drainage water was 40 mg/L when the field was bare and 0.25 mg/L when there was a cover crop (Martinez and Guiraud, 1990). In addition, over the course of the study 110 kg/ha was leached under bare fallow, while only 40 kg/ha was leached under the catch crop (Martinez and Guiraud, 1990).

The preservation of uncultivated strips of land separating agricultural fields from streams, also termed riparian buffers, is yet another method of nutrient management. These riparian zones, which feature natural trees, shrubs, and grasses, have frequently been proven to decrease the nitrate concentration of shallow groundwater that encounters them (Addy et al., 1999; Cey et al., 1999; Spruill et al., 2000; Young and Briggs, 2005). While the effectiveness of these buffers is widely accepted, the mechanism of nutrient control is often

debated or unclear (Dinnes et al., 2002). There are several possible mechanisms, including dilution resulting from increased recharge in the buffer zone, nutrient uptake by buffer zone vegetation, and naturally enhanced denitrification resulting from an increase in organic carbon (Dinnes et al., 2002). These mechanisms may work individually or in combination to reduce nitrate concentrations. For example, Spruhill et al. (2000) observed a 95 percent reduction in nitrate concentrations in buffer zones, with approximately 30 to 35 percent being attributed to dilution and 65 to 70 percent being credited to plant assimilation and/or denitrification.

Another common nutrient management strategy involves significantly reducing the nutrient application rate over agricultural land. This strategy is of particular interest as it has been employed at the Woodstock site since 2003. As previously mentioned, Meissner et al. (2002) observed a strong correlation between a 50 percent reduction in fertilizer input and the amount of nutrient leaching through the unsaturated zone and Cole (2008) concluded that a 46 percent reduction in nutrient application resulted in declining shallow groundwater nitrate concentrations. In addition to the previously discussed lengthy lag times, a second potential limitation of this technique is maintaining crop yields while minimizing the amount of applied fertilizer. This drawback was not observed by Cole (2008), who concluded that the considerable nutrient application reduction did not significantly alter crop yields.

In summary, multiple nutrient management strategies have been thoroughly explored in the literature, with proof of success at a number of field sites. Due to the diversity of subsurface conditions, however, exceptions do exist. For these exceptions, alternative mitigation options must be explored, with particular emphasis on integrating a variety of strategies. This is explored in the following section.

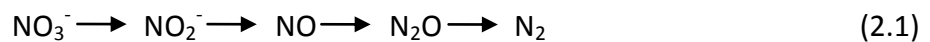
2.1.4 The Integrated Use of Groundwater Remediation Strategies

Following regulatory guidelines and adopting a variety of agricultural nutrient management strategies alone may not be enough to satisfactorily reduce groundwater nitrate concentrations at certain sites (Dinnes et al., 2002). Also, as previously mentioned, the time lag between the implementation of nutrient management strategies and a noticeable improvement in groundwater quality can be quite extensive (Meissner et al., 2002; Wassenaar et al., 2006). At sites where this is the case, integrating nutrient management techniques with groundwater remediation strategies may provide a feasible solution to contamination.

Groundwater remediation strategies for the treatment of inorganic groundwater contaminants generally fall into two categories: in situ and ex situ. Ex situ treatments typically include excavating the contaminant source and pump and treat methods. These approaches, however, are usually expensive and better suited for point source problems. The non-point source nature of nitrate contamination affecting many agricultural sites, including the Woodstock site, requires a more progressive, in situ, and passive approach to treatment. In situ methods, such as permeable reactive barriers and injection-withdrawal systems, rely on stimulating chemical or biological reactions directly within the contaminated aquifer. The following sections describe the available in situ treatment options for agricultural nitrate contamination.

2.1.5 In Situ Denitrification as a Treatment Option

Under proper conditions nitrate is readily transformed to innocuous nitrogen gas by a wide range of facultative anaerobic organisms (Foth, 1984). Following the consumption of all oxygen, these organisms rely on nitrate to generate energy via cellular respiration (Foth, 1984). The denitrification process involves the formation of several intermediate products and can be summarized as (Soares, 2000):



As the final product, nitrogen gas simply escapes to the atmosphere. For this process to continue to completion the denitrifying bacteria require an electron donor, a source of organic carbon, and proper environmental conditions.

Although nitrate is readily converted to nitrogen gas in the natural environment, it remains a top groundwater contaminant because many aquifers lack the optimum reduction-oxidation conditions and steady source of carbon and electrons. This recognition has led to the development of many in situ denitrification technologies revolving around the addition of various carbon sources and electron donors. There are two main categories of in situ, semi-passive treatment schemes: (1) permeable reactive barriers, and (2) injection-withdrawal systems.

2.1.5.1 Permeable Reactive Barriers for Denitrification

The installation of permeable reactive barriers (PRBs) has proven to be an effective method for treating inorganic groundwater contaminants, including nitrate (Robertson and Cherry, 1995; Blowes et al., 2000; Robertson et al., 2000). This technology involves positioning chemically or biologically reactive materials across the flow path of a contaminant plume. As the plume migrates through the PRB, the constituents are transformed to nontoxic or immobile derivatives (Scherer et al., 2000). A great deal of time and money are required for the initial PRB design phase; following this, however, the system can operate passively on the order of years to decades.

A main limitation of the reactive barrier method is achieving the minimum required residence time to ensure the reactions reach completion (Gierczak et al., 2007). This problem is not typically encountered when natural gradients are controlling groundwater flow. However, when municipal supply wells are operating in close proximity, which is the case at the Woodstock site, this can be a major constraint. A second limitation involves maintaining a sufficient hydraulic conductivity (Gierczak et al., 2007). If the hydraulic conductivity of the PRB is less than that of the aquifer material, the contaminated

groundwater may completely bypass the barrier. This may also occur on a smaller scale within the actual barrier due to improper installation. In addition, constructing and installing a PRB deep below the water table is typically very difficult and expensive. The effectiveness of a PRB at the Woodstock site is questionable, therefore, due to the high hydraulic conductivity of the target aquifer, the close proximity to the Thornton Well Field, and the difficult and expensive nature of the approach.

2.1.5.2 Injection-Withdrawal Systems for Denitrification

There are three main categories of injection-withdrawal systems for denitrification: single-well injection-withdrawal systems, dual-well injection-withdrawal systems, and daisy-well systems (Gierczak et al., 2007). The simple single-well systems operate by injecting an electron donor solution directly into the plume, allowing denitrification to occur, and then extracting the treated water from the same well at a later time (Gierczak et al., 2007). This type of test may be utilized to evaluate the denitrifying potential of the aquifer before a larger scale system is designed and built.

Dual-well injection-withdrawal systems involve injecting an electron donor and nutrient substrate into one well while simultaneously pumping another nearby well. This arrangement is typically used to establish an underground “cloud” of dissolved nutrients which migrates downgradient while promoting the necessary reactions. Again, this relatively simple system can be used to assess the feasibility of denitrification at a specific site before up-scaling to a multi-well system. Gierczak et al. (2007) notes that a single well doublet is rarely sufficient for a full-scale denitrification project.

Daisy-well injection-withdrawal systems are characterized by a single, central extraction well surrounded by several injection wells (Gierczak et al., 2007). The water table that results from the daisy-well pumping scheme is thought to depict the petals of a daisy flower (Khan and Spalding, 2003). Typically, this type of well arrangement is used for large-scale remediation projects due to the relatively large zone of influence. The literature relays

several successful field-scale applications of the daisy-well system for stimulating in situ denitrification (Hamon and Fustec, 1991; Kahn and Spalding, 2003; Kahn and Spalding, 2004).

It has continually been demonstrated that these injection-withdrawal systems perform optimally when the electron donor substrate is introduced in a series of discrete pulses, as opposed to a continuous injection (Devlin and Barker, 1996; Peyton, 1996; Khan and Spalding, 2003;). The pulses help to reduce the formation of biofilms, which can lead to aquifer and screen clogging, a typical problem associated with injection-withdrawal systems (Devlin and Barker, 1994). Other possible disadvantages of these treatment systems include gas formation, the accumulation of harmful intermediate products, and difficulty distributing the substrate and promoting the reaction homogeneously throughout the aquifer (Soares, 2000). In addition to this, the groundwater system at the site of interest should be well characterized both physically and chemically, which can be time consuming and expensive (Soares, 2000). This aspect is discussed further in the following section.

2.1.5.3 Site Characterization Challenges Relating to In Situ Treatment

Site characterization is a crucial aspect of all bioremediation projects. It is required to determine the extent of contamination, set feasible remediation goals, design an affordable and effective remediation program, and predict the outcome of the remediation effort (Mackay, 1990). Several research studies have focused on the complex nature of the subsurface and how it controls biostimulated reactions and the fate of groundwater contaminants (Freeze and Cherry, 1979; Mackay et al., 1985; Mackay and Cherry, 1989; Lee et al., 2000; Yang et al., 2003; Englert et al., 2009). These publications suggest that a limited initial understanding of the chemical and physical hydrogeology at a particular site will lead to an inefficient, costly, and prolonged remediation program (Mackay, 1990).

Despite the obvious need for a thorough understanding of subsurface conditions, the various methods of site characterization are imperfect and sometimes unavailable (Mackay,

1990). Typical characterization problems revolve around issues of scale. Mackay and Cherry (1989) relate that slight, small-scale variations in permeability can be of great detriment to remediation strategies, especially when designed under impressions of homogeneity. Classic techniques such as aquifer tests and geologic coring tend to miss such small-scale variations and fine stratification (Mackay, 1990). In addition, monitoring wells with long screened intervals tend to blur the chemical details (Mackay, 1990).

The greater Woodstock site has been well characterized on a broad scale; however, it is clear that much more detail was required in the direct vicinity of the study site to design a successful in situ bioremediation program. To overcome the limitations discussed above, a series of evidential lines at various scales were relied upon for thorough characterization. Data from core logging, grain size analysis, geophysical methods, tracer tests, three-dimensional modelling, and several rounds of geochemical sampling were amalgamated to produce a comprehensive conceptual model of subsurface conditions prior to the remediation effort. In addition, several multi-level wells with short screens were installed for detailed chemical monitoring before, during, and after the remediation injections.

2.2 Study Site

2.2.1 Site Description and Topography

The site of interest is located approximately three kilometers south of Woodstock, Ontario in Oxford County (Figure 2.1). The eastern edge of the site is bordered by the Thornton Well Field, which provides the City of Woodstock with approximately half of its water supply via five major production wells (Wells 1, 3, 5, 8, and 11). A second principal well field, the Tabor Well Field (Wells 2 and 4), is located approximately three kilometers southeast of the Thornton property (Figure 2.2). Agriculture, the dominant land use in the area, has resulted in elevated nitrate levels in the municipal wells. While concentrations at the Tabor Well Field have generally remained below the MAC of 10mg-N/L, water produced at the Thornton Well Field has been surpassing this limit since the mid-1990s (Figure 2.3) (Haslauer, 2005). In order to maintain concentrations in the production groundwater supply

below the MAC, the current solution involves controlling pumping rates, alternating between production wells, and blending the nitrate laden water with low nitrate water from the Tabor Well Field (Bekeris, 2007).

The ground surface in the area surrounding the study site can be described as gently rolling, with two distinct hill features identified as drumlins (Figure 2.4). The longitudinal axes of these landforms are oriented from south-west to north-east (Haslauer, 2005). The study site is located in a low-lying area directly between these two features.

2.2.2 Previous Research

Since the late-1990s a series of research projects have focused on characterizing the physical and geochemical setting of the Thornton Well Field and the surrounding area. Heagle (2000) was the first to provide a detailed assessment of the site geochemistry, with an emphasis on nitrate contamination. To accompany this chemical piece, Padusenko (2001) characterized the regional physical hydrogeology of the area. This research also focused on evaluating and mitigating the impacts of agriculture on groundwater quality at the regional scale.

Haslauer (2005), Bekeris (2007), and Koch (2009) continued research at the site following the County of Oxford's 2003 decision to purchase the 111 hectares of agricultural land. Haslauer (2005) focused on refining the site conceptual model through a series of field investigations including geophysical testing, drilling, core logging, and water sampling. The result of this research was a three-dimensional digital model of the hydrostratigraphic units at both the regional and local scales. Bekeris (2007) combined hydrologic, geologic, and meteorological information to derive estimates of nitrate mass loading across the purchased land parcel in an effort to evaluate the effectiveness of the reduction in applied fertilizer. Koch (2009) continued to evaluate mass loading while also assessing aquifer vulnerability and refining the geologic conceptual model.

These previous projects have all focused on a very large area, which surrounds the compact study site of this research endeavor. As a result, the greater Woodstock site is well characterized on a broad scale. Alternatively, this project requires a much deeper understanding of the small scale variations in the chemical and physical properties of the subsurface.

2.2.3 Geology

The Paleozoic geology of the Woodstock area is characterized by Silurian dolostone and shale overlain by Devonian limestone (Cowan, 1975). The bedrock surface is flat to gently rolling and slopes to the south (Cowan, 1975). Haslauer (2005) encountered limestone bedrock approximately 69 m below ground surface with the installation of a deep monitoring well about one kilometer south-west of the study site. The fossiliferous nature of the limestone helped identify it as the Detroit River Formation of Devonian age (Haslauer, 2005).

The Quaternary geology of the area, illustrated in Figure 2.5, was shaped by glacial outflows from the Ontario-Erie, Huron, and Georgian Bay ice lobes during the Wisconsinan (Cowan, 1975). The alternating advances of these lobes mixed the sediments in the area, forming a complex interlobate zone composed of lithologically similar tills (Cowan, 1975). The late Wisconsinan Tavistock Till, characterized by its stiff, stony, and silty composition, dominates the surficial Quaternary geology of the study site (Cowan, 1975; Bekeris, 2007). Cowan (1975) notes that this till unit typically occurs as ground moraine or in drumlins in the Woodstock area. Bekeris (2007) suggests that the Catfish Creek Till and perhaps the Port Stanley Till occur deeper at the site. The Catfish Creek Till is dominated by stiff silt and is frequently associated with glaciofluvial sand and gravel units (Cowan, 1975). The Port Stanley Till is a clayey silt till, which occurs as ground moraine in the area (Cowan, 1975). Over the broad area surrounding the site, these tills comprise what is best described as a drumlinized ground moraine (Bekeris, 2007). Of particular interest are the glaciofluvial sand and gravel deposits occurring directly in the site vicinity. These highly permeable materials

were deposited in a significant glacial meltwater channel (Cowan, 1975). Haslauer (2005) identified this channel as a principal pathway for nitrate transport to the production wells of the Thornton Well Field. Further information regarding the site geology is provided by Padusenko (2001), Haslauer (2005), Bekeris (2007), and Koch (2009).

2.2.4 Hydrogeology

The intense glacial history of the Woodstock area has produced a complex distribution of aquifers and aquitards at the site. In the area surrounding the Thornton Well Field, these units, as well as the groundwater flow system, have been thoroughly explored by Padusenko (2001) and Haslauer (2005). The existing conceptual model, produced by Haslauer (2005), features an overburden system of four aquifers interlayered amongst four aquitards, all overlying a conductive bedrock aquifer. These aquifers and aquitards range from zero to tens of metres in thickness across the site (Bekeris, 2007). Figure 2.6 is a cross-section along Curry Road displaying the generalized stratigraphy. Of particular interest are Aquifers 2 and 3. Koch (2009) suggests that these two aquifers converge to form one large unconfined aquifer in the area of interest. Drill logs, geophysical surveys, and a rapidly responding water table support this conjecture (Bekeris, 2007). The absence of Aquitards 1, 2, and 3 in this vicinity greatly increases the vulnerability of the aquifer to nitrate contamination. This is of particular importance as the Thornton Well Field supply wells are located down-gradient of this location in Aquifers 3 and 4. Padusenko (2001), Haslauer (2005), Bekeris (2007), and Koch (2009) provide further information regarding the site hydrogeology.

2.2.5 The Average Regional Groundwater Flow Field

Koch (2009) contoured hydraulic head measurements collected at wells screened in both Aquifer 2 and Aquifer 3 in May of 2008 (Figure 2.7). The groundwater flow direction across the greater Woodstock site in both Aquifer 2 and Aquifer 3 is predominantly east to southeastward (Koch, 2009). In Aquifer 2, eastward flow dominates near the northern edge of the greater site area, while southeastward flow is observed along the glaciofluvial

outwash channel identified in Figure 2.5 (Koch, 2009). Alternatively, in Aquifer 3, southeastward groundwater flow dominates in the northwestern portion of the greater Woodstock site, while eastward flow is observed in the southern portion of the figure (Koch, 2009). Koch (2009) also noted the hydraulic head measurements recorded for Aquifer 2 were slightly lower than those measured for Aquifer 3, suggesting the presence of an upward gradient. This gradient, however, declined as the well field was approached. In the direct vicinity of the study site, a downward vertical gradient was noted. A final observation by Koch (2009) indicated that the direction of groundwater was not largely influenced by the seasons.

2.2.6 History of Nutrient Management at the Study Site

As previously mentioned, nitrate concentrations at the Thornton Well Field, directly adjacent to the study site, have been progressively increasing over the past three decades as a result of excess fertilizer application. To deal with this issue, the County of Oxford purchased two parcels of agricultural land just north of the Thornton Well Field. Parcel A is 38 hectares in area and is bounded to the northwest by Curry Road, to the southwest by Dodge Line, and to the southeast by another farming property (Koch, 2009). Parcel B is 73 hectares in area and is bounded to the northwest by Curry Road and to the east by the Thornton Well Field (Koch, 2009). Both parcels are located directly within the capture zone of the production wells.

There are seven individual agricultural fields comprising Parcel B, which are currently rented to farmers who must abide by strict nutrient application guidelines. This effort is part of a nutrient management strategy aimed at significantly reducing the amount of nitrate loading to the subsurface. The amount of fertilizer currently applied to each field is dictated by the type of crop grown (Bekeris, 2007). Bekeris (2007) indicates that corn is given a starter fertilizer which coincides with planting and a side-dress in late spring. No nitrogen fertilizer is applied to soybean crops as they are capable of nitrogen fixation (Bekeris, 2007).

Crop rotations were also altered as part of the nutrient management strategy. Prior to 2003, most of the Parcel B fields featured a grass and wheat-corn-soybean rotation (Bekeris, 2007). This rotation has been maintained, however, the wheat has been changed from hard red winter wheat to soft red winter wheat, which requires 50 percent less nitrogen (Bekeris, 2007).

To supplement this nutrient management strategy, continuous monitoring of groundwater nitrate concentrations has been performed since 2003. This effort has started to show some reductions in nitrate across the greater Woodstock site. These reductions, however, have been slow to appear and there has been no obvious decline in nitrate concentrations at the Thornton Well Field.

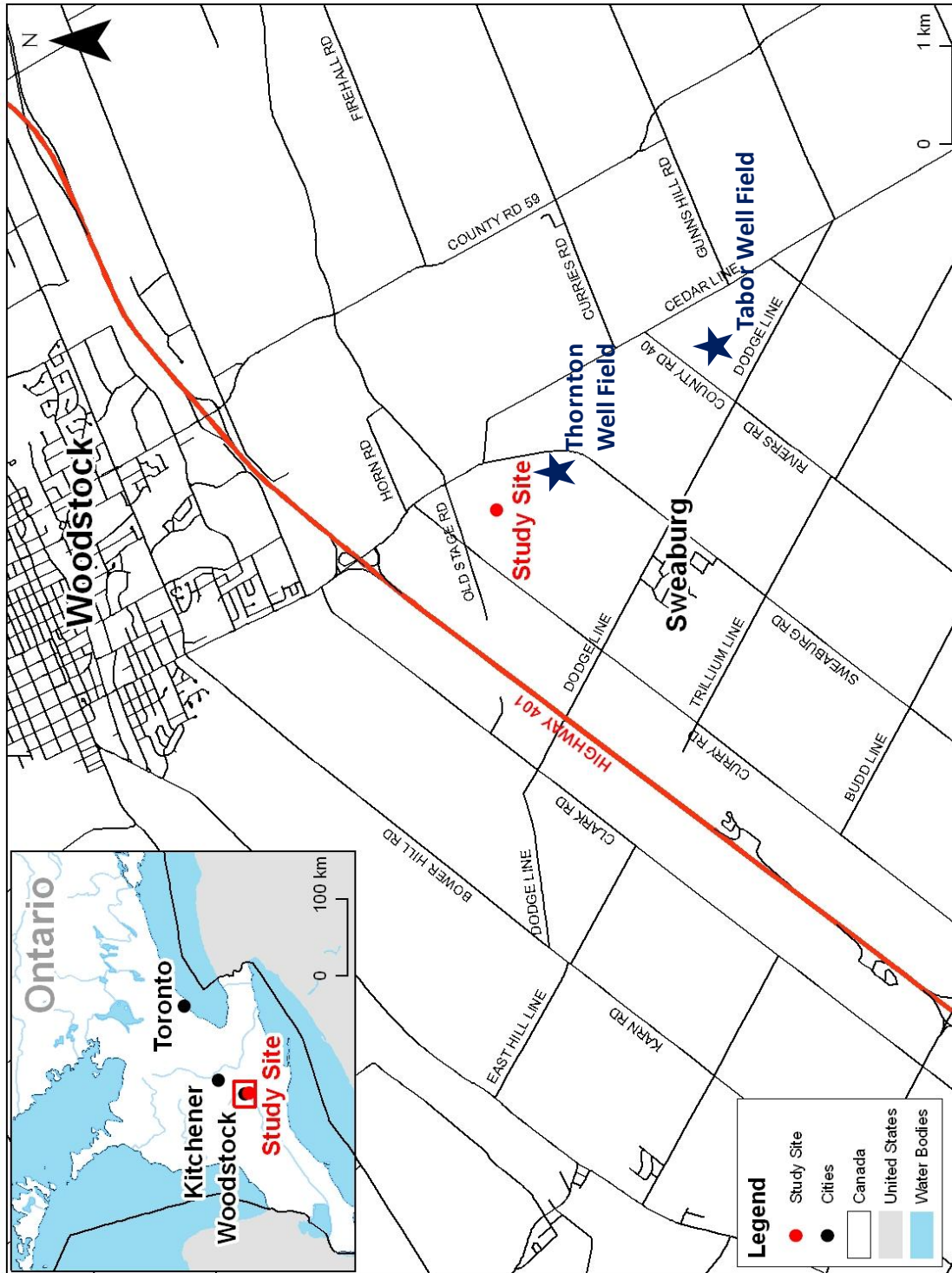


Figure 2.1: Map displaying the study site location within Southern Ontario. Map contains data from DMTI CanMap Streetfiles (2005) and DMTI Census Geographv (2003).

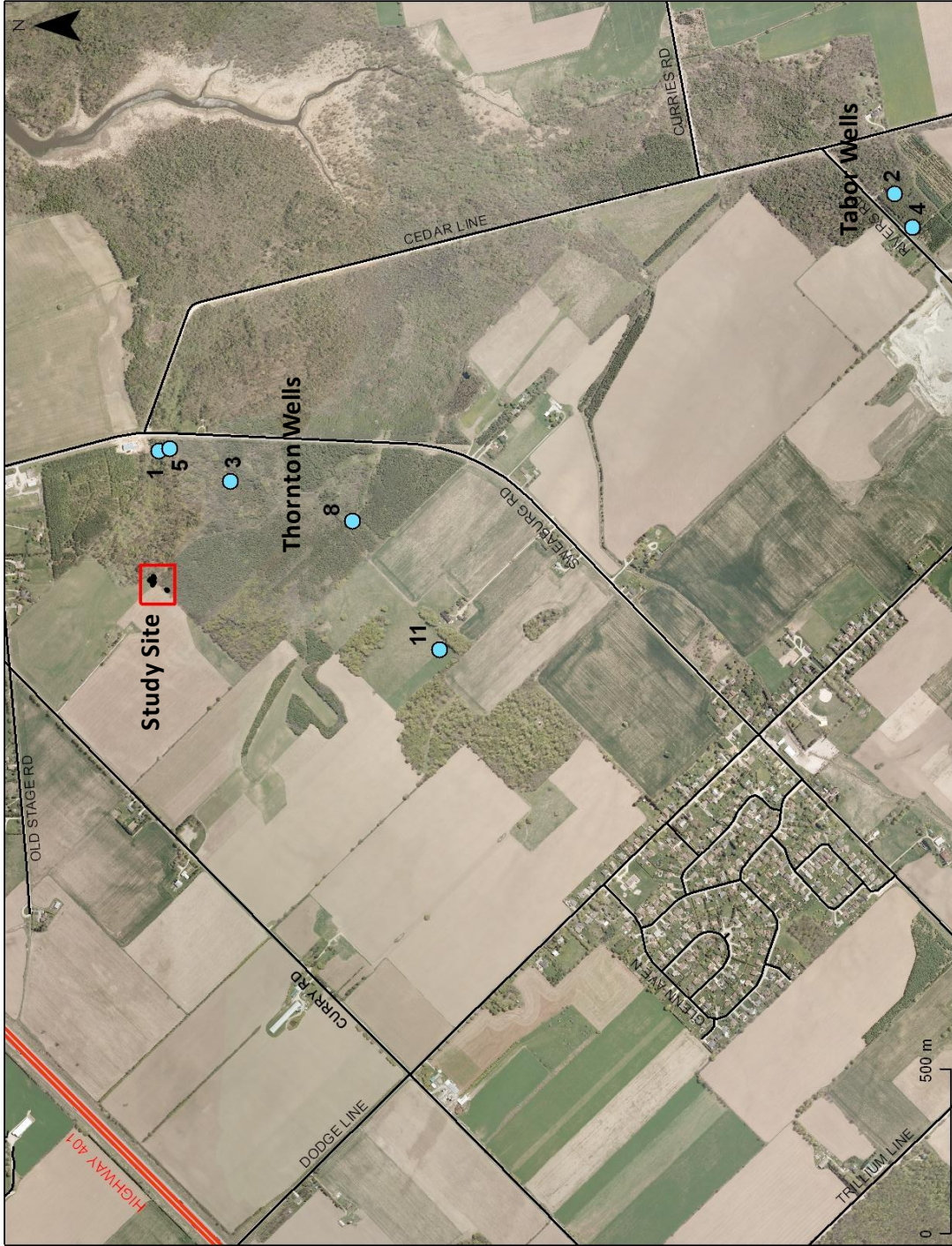


Figure 2.2: Municipal supply well locations in the Thornton and Tabor Well Fields. Map contains data from CanMap Streetfiles (2005) and Southwestern Ontario Orthoimagery Project (2006).

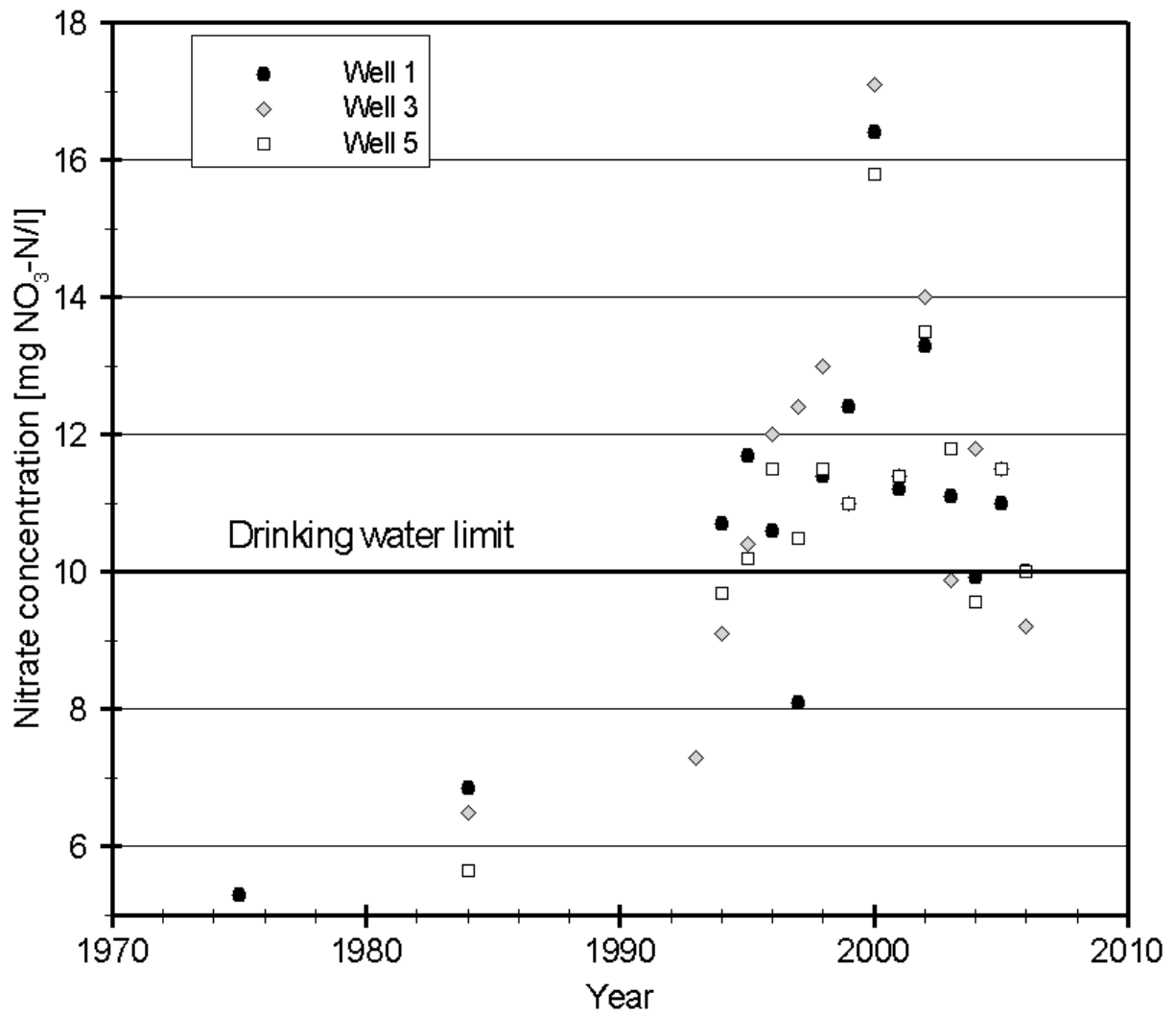


Figure 2.3: Trends in nitrate concentrations in Municipal Wells 1, 3, and 5 (Bekeris, 2007).

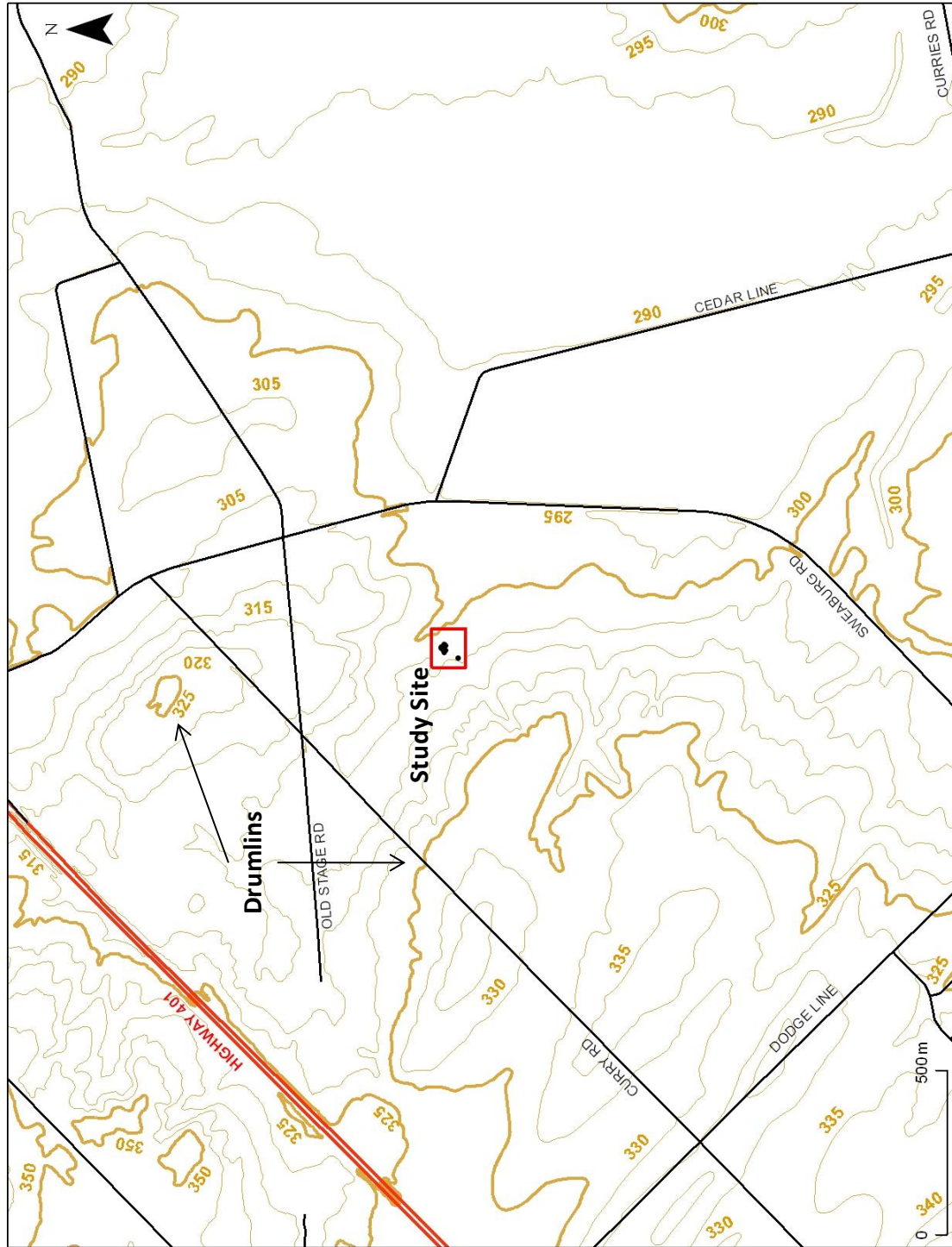


Figure 2.4: Topography of the study site and surrounding area. Map contains data from CanMap Streetfiles (2005) and Natural Resources and Values Information System (2008).

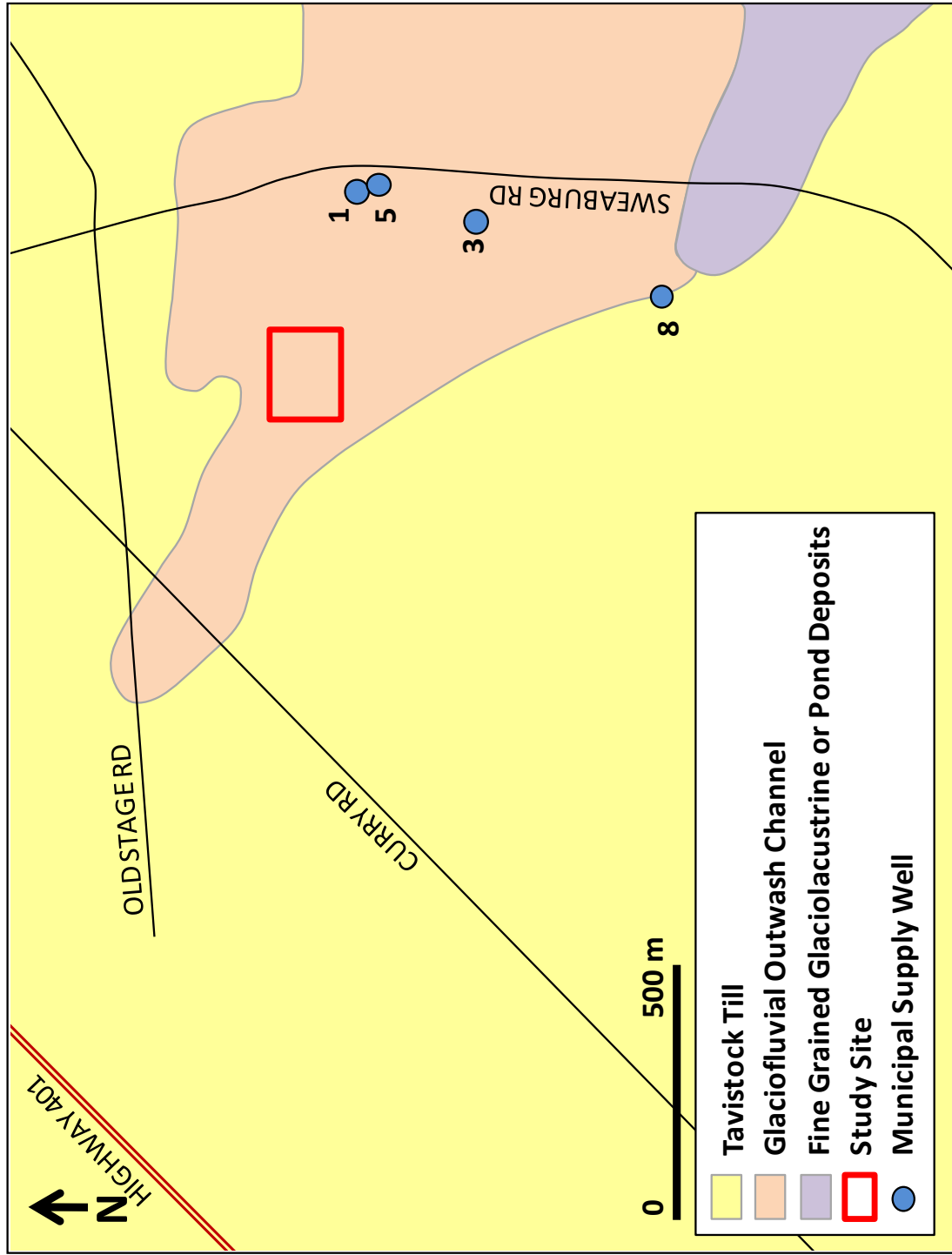


Figure 2.5: Quaternary geology of the study site and surrounding area. Map contains data from The Corporation of the County of Oxford (2001, 2003b, 2003c) (Modified from Bekeris, 2007).

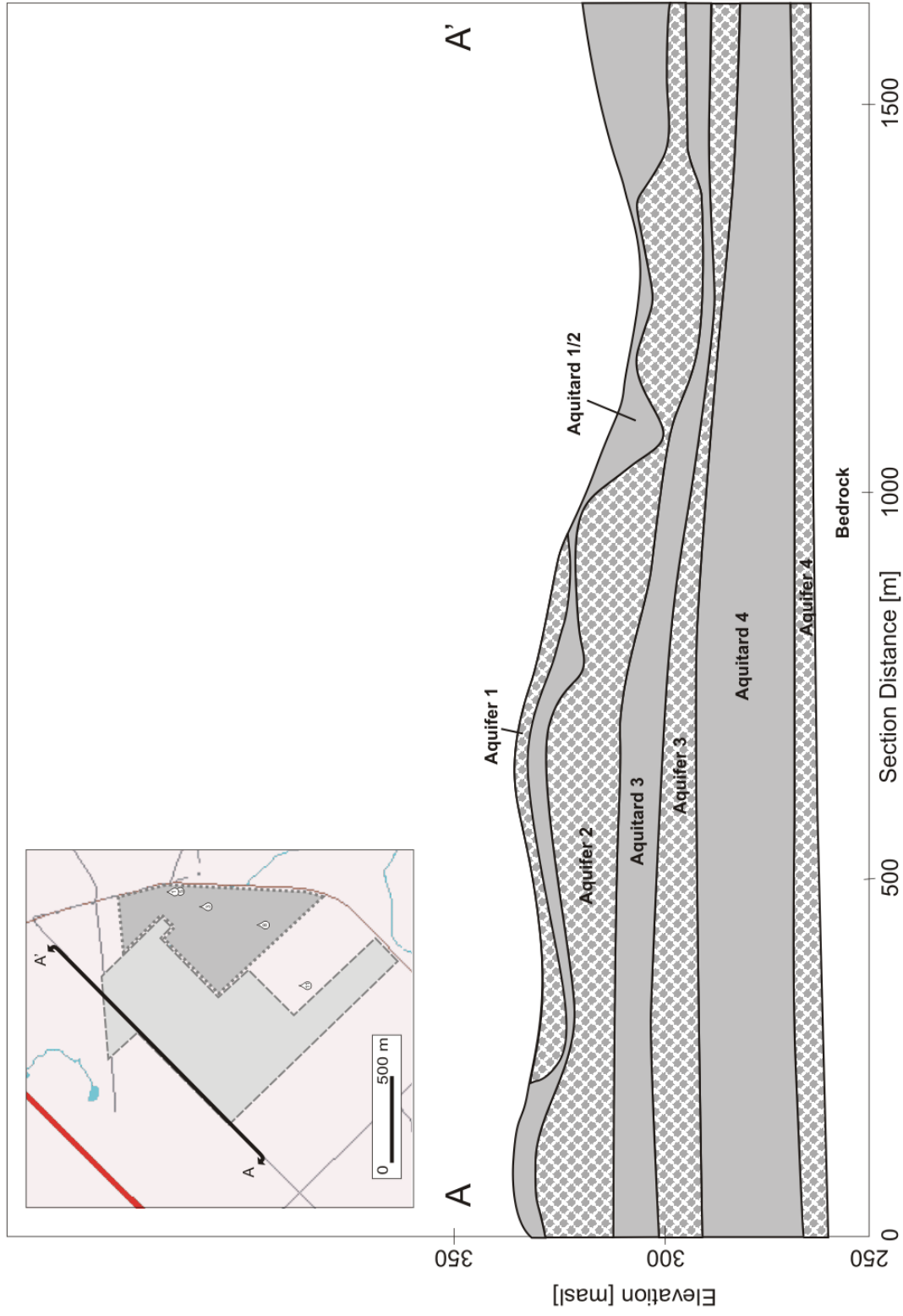


Figure 2.6: Stratigraphic cross-section along Curry Road (Haslauer, 2005; Bekeris, 2007).

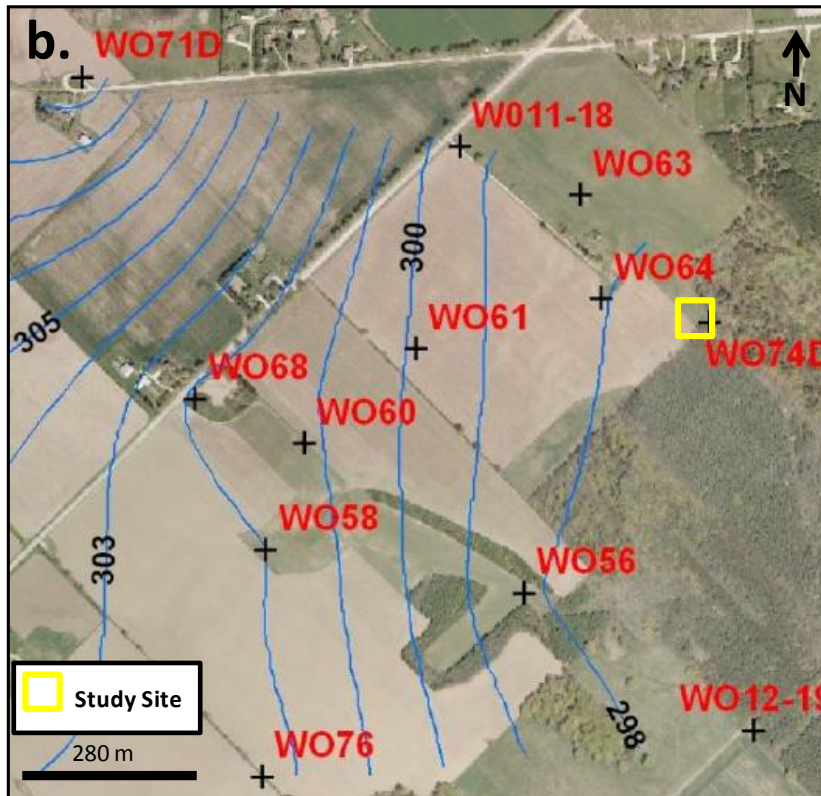
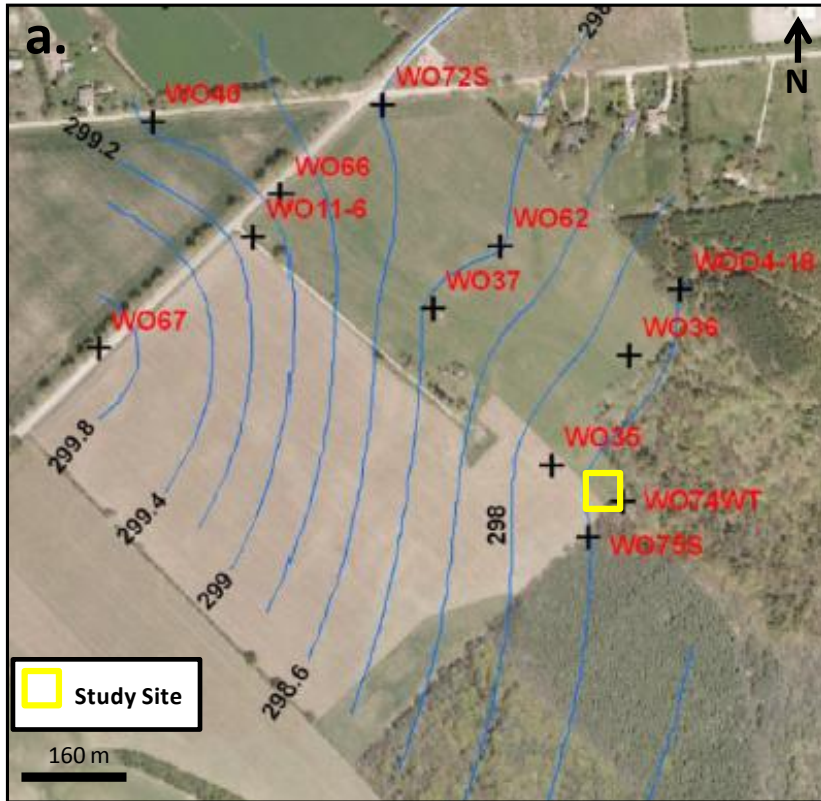


Figure 2.7: Hydraulic head contour maps representing conditions in May of 2008 in (a) Aquifer 2 and (b) Aquifer 3 (modified from Koch, 2009).

3. Methods

3.1 Site Instrumentation

3.1.1 Injection-Extraction Wells

A total of four injection-extraction wells, WO77, WO78, WO79, and WO80, were installed in the summer and fall of 2008 (Figure 3.1). They each feature a 50.8-mm (2-inch) diameter 10-slot PVC screen and Schedule 40 PVC riser pipe. The total depths of the wells and the screen lengths vary due to local elevation changes of an underlying clay layer. WO77, WO78, and WO80 all have 7.62-m (25-foot) long screens and reach a depth of about 17 metres below the ground surface. Alternatively, WO79 has a 6.10-m (20-foot) long screen and reached a depth of about 15 metres below the ground surface. The four wells were installed to form a straight line perpendicular to the regional flow field, with a separation distance of 5 metres. This orientation was selected to facilitate the creation of a uniform dissolved nutrient cloud between the injection-extraction wells. Following the injections, this substrate cloud is permitted to migrate downgradient, promoting denitrification along its path. The similar design of the four wells permitted the comparison and assessment of various well separation distances, including 5 metres, 10 metres, and 15 metres. Table A.1 in Appendix A provides further construction and location information pertaining to these four wells.

3.1.2 Multi-Level Monitoring Wells

Twelve bundle-type multi-level monitoring wells, ML1 to ML12, were also installed in the summer and fall of 2008. These wells were principally used to monitor tracer distribution during initial hydrogeologic testing, gather detailed background chemical data, and track geochemical changes during the acetate injections. Each multi-level well features eight individual screens, 10 centimeters in length and placed at vertical increments of 1.7 metres. The bundles were constructed by securing seven 9.5-mm inner diameter polyethylene tubes around a central 12.7-mm inner diameter PVC pipe. The screen tips were created from slotted 9.5-mm inner diameter polyethylene tubing wrapped in fine Nitex™ screen. These bundles were transported to the field in pieces and assembled on-site. For all multi-level

bundles, the sampling ports are labeled one to eight, one corresponding to the shallowest port and eight corresponding to the deepest port. The multi-level bundles were positioned to form a tight grid situated downgradient of the injection-extraction wells. The orientation of the grid allows for detailed geochemical monitoring in both space and time during the substrate injection experiments. Table A.2 in Appendix A provides detailed construction and location information for these monitoring wells.

All of the wells constructed in 2008, including the injection-pumping wells and multi-level bundles, were installed with a Geoprobe® Model 7720DT direct push drill rig. Due to the gravelly composition of the unsaturated zone, augers were used to drill to a depth of approximately 4.6 metres (15 feet). The augers were then removed and 82.6-mm (3.25-inch) outer diameter probe rods were installed to the desired depth. The wells were then lowered into the hole and secured as the rig pulled the casing sections to the surface. The formation was assumed to collapse uniformly around the wells below the water table. Above the saturated zone, the annulus was filled with the auger cuttings, followed by bentonite chips near the ground surface.

3.1.3 Existing Monitoring Wells

Geochemical and water level datasets from the WO74 and WO75 series wells, installed during the course of previous research work, were frequently relied upon. The close proximity of these wells to the multi-level network in addition to the abundance of existing chemical and physical data made these monitoring wells an asset. Also, the various depths of the WO74 and WO75 series wells spanned the entire experiment zone, permitting a direct comparison of datasets collected at these wells and the network of injection-extraction and multi-level wells.

The WO74 well grouping is comprised of five individual wells, including a Solinst® CMT Multi-level System (WO74-ML) and four 50.8-mm (2-inch) diameter wells screened over various aquifer depths (WO74-WT, WO74-S, WO74-M, and WO74-D). The WO75 series

consists of only three wells, including a second Solinst® CMT Multi-level System (WO75-ML) and two 50.8-mm (2-inch) diameter wells (WO75-S and WO75-D). The two CMT systems feature six 10-mm diameter and one 9.5-mm diameter channels, all reaching various depths within the aquifer. The larger wells feature a 50.8-mm (2-inch) diameter 10-slot PVC screen and Schedule 40 PVC riser pipe. All WO74 and WO75 series wells were installed with a Boart Longyear Rotosonic Mini Drill Rig over a period spanning December of 2006 to January of 2007. The wells were constructed with an artificial filter pack consisting of uniform sand. Above the sand pack, bentonite chips were used to seal the annulus. The relative locations of these wells, in addition to the new injection-pumping and multi-level wells, are displayed in Figure 3.1.

In addition to these well groupings, other existing monitoring wells including WO35 and WO02-D-14 were relied upon for water level and quality data. WO35 is located approximately 70 metres up-gradient from the multi-level grid and features a 38.1-mm (1.5-inch) diameter 10-slot PVC screen and Schedule 40 PVC riser pipe. WO02-D-14 is located within the limits of the Thornton Well Field, approximately 130 metres down-gradient from the multi-level well network. This well has a 34.9-mm (1.375-inch) diameter slotted PVC screen and Schedule 40 PVC riser pipe. Both WO35 and WO02-D-14 are screened in Aquifer 2, with depths corresponding to the experiment zone at the study site.

Table A.3 and Table A.4 in Appendix A provide construction and location information for the previously existing multi-level wells and larger diameter, single-screen wells, respectively. These tables provide location co-ordinates and screen depths in metres above sea level (masl).

3.2 Core Logging

A total of four geologic cores were collected, their locations relative to the monitoring wells are displayed in Figure 3.2. Cores 1, 2, and 4 were collected in the summer and fall of 2008 with the Geoprobe® Model 7720DT direct push drill rig and sampling system. Core 3 was

collected in the spring of 2008 using a Vibra-Push® direct push rig equipped with an Enviro-Core® sampling system. The core collection was used to explore the stratigraphy in the area directly surrounding the intended injection-extraction site. Grain size analyses were also performed from core sub-samples in an initial effort to define the hydraulic conductivity profile.

The four cores were logged in the laboratory according to the Unified Soil Classification System (American Society for Testing Materials, 2006). The stony composition of the subsurface resulted in relatively poor core recovery overall. While logging, it was assumed that the top of each core section was truly representative of the shallowest material and all missing material corresponded to the deepest material at the bottom of the core section. This assumption is based on the idea that the core tube will collect material until it encounters a rock which blocks its opening. Following this, the tube pushes the rock deeper through the sediment, preventing the material from entering the core barrel.

Additional core logging was performed in the winter of 2007 following the method described above, producing thorough geologic logs for wells WO74-S, WO74-WT, WO74-M, WO74-D, WO75-S, and WO75-D. These core logs are displayed in Appendix B.

3.3 Electrical Resistivity Surveys

As the inverse of electrical conductivity, the resistivity of a medium is a measure of how well the material impedes the flow of electrical current (Herman, 2001). Monitoring resistivity as the distribution of an induced electrical current below ground surface with a series of electrode pairs can provide information regarding the distribution of various soil types, including the general extents of aquifers and aquitards. In general, the resistivity of a medium is dependent on its moisture content, clay content, and the ion concentration of the pore water (Haslauer, 2005). Combining previously collected information regarding these key factors with resistivity surveys provides a reliable means of delineating underground layers (Herman, 2001).

Two electrical resistivity surveys were completed in August and September of 2009 in an effort to initially characterize the aquifer of interest with a non-destructive, non-invasive approach. A Syscal Junior Switch 48 resistivity imaging system from IRIS Instruments was employed for the surveys. The two resistivity survey lines, including individual electrode locations, are displayed in Figure 3.3. Both the Wenner and Dipole-Dipole electrode arrays were used to gain a thorough understanding of the subsurface resistivity distribution. An electrode separation distance of 2.5 m was used and a maximum penetration depth of approximately 20 m was achieved. The dataset was corrected for topography using ground surface elevations collected with a Sokkia SET 600 Total Station.

3.4 Hydraulic Testing

Several lines of evidence were relied upon to determine the subsurface distribution of hydraulic conductivity. These methods include grain size analyses performed on core sub-samples, conventional slug tests, multi-level slug tests, and borehole flowmeter tests. The following sections describe these techniques in detail.

3.4.1 Grain Size Analysis

102 individual grain size analyses were performed on core sub-samples taken at an interval of twenty to thirty centimeters in the winter of 2008. The procedure was based on a standard method described in American Society for Testing Materials (2007). All samples were air dried prior to sieving. Due to the coarse nature of the material, a method developed by Terzaghi (1925) was used for the analysis of sieve data. The hydraulic conductivity (K) of each sample was calculated as:

$$K = \left(\frac{S}{V} \right) \cdot (d_{10})^2 \cdot \left(\frac{(n - 0.13)}{(1 - n^{0.333})^2} \right) \quad (3.1)$$

where S is an empirical constant, assumed to be 0.1048 for smooth grains and 0.0602 for angular grains; V is the viscosity, assumed to be $0.0131 \text{ g cm}^{-1} \text{ s}^{-1}$, corresponding to an

average groundwater temperature of 10 degrees Celsius; d_{10} is the grain size diameter at which ten percent of the particles are finer; and n is the porosity, assumed to be 0.33. Due to the uniform mixture of angular and smooth specimens in each sample, all final K-estimates were calculated by averaging the results produced by the Terzaghi (1925) method for angular grains ($S = 0.0602$) and the Terzaghi (1925) method for smooth grains (0.1048).

3.4.2 Conventional Slug Tests

Conventional slug testing is a relatively quick and inexpensive method for determining the hydraulic conductivity of an aquifer in the direct vicinity of a well screen. This type of test involves inducing a near-instantaneous head change in a well, followed by detailed monitoring of the resultant recovery.

Several slug tests were performed on the WO74 and WO75 series wells in the winter of 2007. The initial head changes were generated by the introduction or removal of a mechanical PVC slug, resulting in either a falling or rising head test, respectively. Before, during, and following the induced head change, water level information was collected with a Solinst Model 3001 Levelogger LT pressure transducer. A minimum of four rising and four falling head tests were completed for each of the seven wells, with the initial displacement being altered for each test. In addition, the wells were all thoroughly developed via extended pumping prior to the slug testing. The various initial displacements and ample well development were required to deal with potential skin effects resulting from well installation. Following this, the field data and specific well parameters were entered into AQTESOLVE Pro 4.0 for analysis. The water level displacement datasets were analyzed using a mathematical solution developed by Springer and Gelhar (1991) designed exclusively for unconfined aquifers. This solution was able to accommodate the oscillatory water level response curves obtained during testing. Visual curve matching was performed to obtain the best fit to the raw data. A hydraulic conductivity estimate was generated for each of the rising and falling tests at the seven well locations.

3.4.3 Multi-level Slug Tests

The use of multi-level slug testing to characterize the vertical profile of hydraulic conductivity has been successfully demonstrated by many researchers (Zlotnik and McGuire, 1998; Svenson et al., 2005; Zemansky and McElwee, 2005; Ross and McElwee, 2007). While conventional slug tests only generate one bulk estimate of hydraulic conductivity per well, multi-level slug tests have the ability to produce several estimates with depth, generating a comprehensive profile. These tests can be performed in individual wells installed at different depths or by sealing off discrete intervals along a borehole or continuous well screen (Svenson et al., 2005). Similar to conventional slug testing, these experiments involve inducing a near-instantaneous pressure change and monitoring the resultant response with a pressure transducer.

Two rounds of multi-level slug tests were performed on WO77 in May of 2009. This well features a 10.7-metre long continuous screen which was sealed off at various intervals to achieve a detailed K-profile. The apparatus used for the testing is displayed in Figure 3.4. In simplified terms, the system consisted of a double packer unit, compressed air source, well-head manifold, pressure transducer, and PVC riser pipe (Svenson et al., 2005). The double packer assembly featured two 4.3-cm diameter N-Packers manufactured by RST Instruments. These packers were connected by a perforated pipe acting as a permeable spacer, creating a test interval of one metre in length. A 1.25-cm inner diameter access pipe running through the upper packer connected the double packer system to the 2.54-cm diameter PVC riser pipe, which housed the pressure transducer and extended to ground surface. To ensure a good seal, Teflon tape and silicon were used to seal the joints of the PVC riser pipe. The well-head manifold was constructed of PVC pipe, an air-tight fitting for the transducer cable, and two ball valves, one for pressurizing the system and one for instantaneously releasing the pressure. A tank of compressed nitrogen was used to inflate the packers while a portable air compressor was used for system pressurization. Suspended in the water column in the riser pipe, a non-vented Level TROLL 300 pressure transducer manufactured by In-Situ Inc. was employed to log pressure changes. Via a direct-read cable,

the transducer was connected to a field laptop where real-time water level data could be observed. The entire system was suspended from a large aluminum tripod, with a boat winch controlling the depth of the apparatus.

A total of ten depths were tested along the well screen of WO77 at an interval of one metre. Three to four repetitive tests were performed at each of the ten depths, with the initial displacement being induced by a pressurization of between 10 and 20 PSI. Similar to the conventional slug tests, a minimum of two different initial displacements were used for each depth. The tests began by assembling the field equipment and lowering the packer system to the required depth. The packers were then inflated and the system was permitted to return to equilibrium. Once the transducer had been initiated, the air compressor was used to pressurize the test interval and the water level in the riser pipe was depressed. The system was then allowed to equilibrate. Following this, the pressure was instantaneously released by opening the ball valve on the manifold. The pressure was logged by the transducer at an interval of 0.25 seconds before, during, and following each test. The tests were rendered complete when the water level returned to its static position. Upon completion of testing at a specific depth, the packers were deflated, riser pipe was added, and the system was lowered to the next depth of interest.

Following the field work, the collected data and specific well parameters were entered into AQTESOLVE Pro 4.0. Once again, the Springer and Gelhar (1991) analytical solution was selected for analysis based on characteristics of the well, the aquifer, and the water level response. Using visual curve matching, a hydraulic conductivity estimate was generated for each of the three to four tests conducted at the ten depths. These values were then averaged and plotted, producing a profile of hydraulic conductivity.

3.4.4 Borehole Flowmeter Testing

Borehole flowmeter testing has proven to be a convenient method for gaining insight into vertical variations in horizontal hydraulic conductivity (Moltz et al., 1989). A series of these

tests were performed on wells WO77, WO78, WO79, and WO80 in November of 2008 and February of 2009. For each test, a Honda WH15XK1C1 high-pressure pump extracted water at a near-constant rate of about 230 L/minute from just above the well screen. Prior to the testing, the wells required approximately one hour of pumping for proper development and to achieve pseudo-steady-state conditions (Moltz et al. 1989). For each test, the Mount Sopris FLP2492 Impeller Flowmeter was lowered into the wells using a Mount Sopris 4MXA-1000 winch. The first measurement was always taken just above the bottom of the screened interval. The device was then lifted by the winch system and flow measurements were taken every ten centimeters over the entire screen length. Figure 3.5 displays several pictures illustrating the general setup of the experiment.

The conversion of the raw flowmeter output in rotations per second to hydraulic conductivity followed a method developed by Moltz et al. (1989). This method is based on a fluid flow study by Javandel and Witherspoon (1969), which states that in simple, layered aquifers, flow towards a pumping well becomes horizontal and flow into the well from layer i is proportional to the transmissivity of layer i . With this information, Moltz et al. (1989) developed an equation relating hydraulic conductivity to flowmeter output:

$$\frac{K_i}{K} = \frac{\Delta Q_i / \Delta z_i}{Q_p / B} \quad (3.2)$$

where K_i is the horizontal hydraulic conductivity of layer i , K is the average hydraulic conductivity of the aquifer, ΔQ_i is the flow into the pumping well from layer i , Δz_i is the thickness of layer i , Q_p is the pumping rate, and B is the screen length (Moltz et al. 1989).

A limitation of this profiling technique is the threshold velocity, which the flowmeter must overcome before spinning will occur. This issue may result in inaccurate data when examining the hydraulic conductivity at the bottom of a deep well or in low permeability units (Moltz et al., 1989). This information was kept in mind while performing these tests and processing the data.

3.5 Determining the Regional Hydraulic Gradient

The spatial distribution of hydraulic head is the driving force behind groundwater flow (Haslauer, 2005). Due to seasonal fluctuations in temperature and precipitation, this distribution is constantly changing. Water level measurements taken at individual wells can be used to track hydraulic head at discrete points. Amalgamating this information across a site provides information regarding the magnitude and direction of horizontal groundwater flow (Haslauer, 2005). In addition to this, multi-level wells can be relied upon for information concerning vertical groundwater flow (Haslauer, 2005).

The regional horizontal hydraulic gradient at the study site was measured using water levels taken at multiple wells, including the WO74 and WO75 series wells, WO35, and WO02-D-14. The dataset consisted of manual water levels collected over the entire year of 2008 at an interval of approximately one month, excluding March and November. The 2008 water level dataset was selected as it was the most recent, complete dataset available at the time of analysis. These water levels were contoured using Surfer 8 (version 8.01), a contouring program created by Golden Software Incorporated. From the contoured surface, a gradient was calculated as the change in hydraulic head over the distance between measurements. This procedure was performed ten times, corresponding to the ten months that had available water level data. In a similar procedure, the vertical hydraulic gradient was estimated using manual water levels collected at the twelve multi-level wells.

3.6 Tracer Tests

3.6.1 Predictive Analytical Modelling

Before each tracer test was performed, the scenario was simulated with an analytical solution for one-dimensional solute transport, ONED_1. The solution, derived by the application of integral transform methods, relates to a system with a constant influent concentration and an initial concentration of zero (Neville, 2001). Estimates of the darcy flux, porosity, travel distance, dispersion and diffusion values, retardation and decay properties, and concentration information are specified in the model input. The output

consists of a series of concentration breakthrough curves representing tracer arrival at the extraction well and a series of downgradient wells. This modelling was used to predict the required durations of the tracer tests and the breakthrough times for the down-gradient multi-level wells.

3.6.2 Forced Gradient Testing

A total of two forced gradient tracer tests were performed prior to the substrate additions. Both tests involved injecting a tracer into one well while pumping another nearby well. This system was operated perpendicular to groundwater flow in an effort to create a “wall” of tracer in the aquifer between the two wells. Bromide, in the form of potassium bromide, was used as a groundwater tracer in both cases. It was selected due to its relatively harmless nature and high solubility in water. These tracer tests were required to gain a thorough understanding of solute movement in the subsurface prior to the addition of acetate.

The first tracer test was performed in November of 2008. Groundwater was extracted from WO77 (screen depth: 283.90 to 294.56 masl) at an average rate of approximately 200 litres per minute, amended with a concentrated bromide solution at the surface, and re-injected into WO78 (screen depth: 283.70 to 294.37 masl). The 250,000 mg/L bromide solution was mixed with the groundwater in-line at a rate of 0.19-0.20 litres per minute for a period of four hours. This translates into an injection concentration of approximately 242 mg/L. Following the four hour injection, the circulation cycle operated for an additional 11 hours. The 3.8-cm diameter pump intake tubing was positioned in the centre of the screen in WO77. The circulation cycle was driven by a high pressure centrifugal water pump, the Honda WH15XK1C1. The flow rate was measured in-line with an F-1000 Digi-Meter Paddlewheel Flowmeter manufactured by Blue-White Industries Limited. Bromide injection was facilitated via a T-connector and a much smaller Geopump Series II peristaltic pump. The bromide-amended groundwater was re-injected into a 2.5-cm diameter PVC riser and screen centered within the larger 5.1-cm diameter riser and screen of WO78. Similar to the

screen of WO78, the smaller diameter injection screen was a 10-slot well screen; however, the insert screen was taped at regular intervals to mimic an 8-slot screen. This was done to create a slight back pressure within the well during injection, ensuring an even distribution of tracer with depth. Throughout this test, ML12 was sampled for anions, including bromide, nitrate, nitrite, sulfate, and chloride, at approximately 0.5 hour intervals. Real time bromide concentrations were obtained in the field using an electrical conductivity probe.

The second tracer test was performed in April of 2009. This time groundwater was extracted from WO78 (screen depth: 283.70 to 294.37 masl) at an average rate of approximately 190 litres per minute, amended with a concentrated bromide solution at the surface, and re-injected into WO79 (screen depth: 285.32 to 294.47 masl). Again, the 250,000 mg/L bromide solution was mixed with the groundwater in-line at a rate of 0.20 litres per minute for a period of just under four hours. This yields an injection concentration of approximately 263 mg/L. Following the injection period, the circulation cycle operated for an additional 2.5 hours. This time, the pump intake tubing in WO78 was positioned within the casing, just above the screened interval. All other design aspects of Tracer Test 1, including the pumps and screen insert, were maintained for this test. Four multi-level bundles, ML5, ML6, ML7, and ML8, were monitored and sampled for Tracer Test 2. Samples were collected both during and following the injection for a total period of 17 hours. Again, anion samples were taken for bromide, nitrate, nitrite, sulfate, and chloride. Due to the poor performance of the electrical conductivity probe, real time bromide concentrations were obtained in the field using a bromide ion-selective electrode manufactured by Cole-Parmer.

3.6.3 Natural Gradient Testing

WO80 was used to inject the tracer solution for the natural gradient, reactive tracer test, performed in April of 2009. Groundwater was pumped from WO77 (screen depth: 283.90 to 294.56 masl) at an average rate of 186 L/min, amended with both a potassium bromide and sodium acetate solution, and re-injected into WO80 (screen depth: 284.00 to 294.66 masl),

fifteen metres away. It was assumed that the pumping at WO77 would not directly impact the test in the vicinity of WO80 due to the large separation distance and brief pumping schedule. The 104,000 mg/L bromide and 35,000 mg/L acetate solutions were mixed with the groundwater in-line at a rate of about 0.20 L/min for a period of one hour. This yields an injection concentration of about 112 mg/L of bromide and 37 mg/L of acetate. All pumping and injection equipment were turned off following one hour. Once again, the pump intake in WO77 was positioned within the casing, just above the screened interval. All other design aspects of Tracer Test 1 and Tracer Test 2 were maintained for this test. Multi-level bundle ML10 was sampled at 0.5 hour increments for approximately 7.5 hours, during and following the injection. Samples were collected for analysis of bromide, acetate, nitrate, nitrite, sulfate, nitrous oxide, and carbon dioxide.

It was recognized that this relatively small addition of acetate was likely to be inadequate for stimulating in situ denitrification. The carbon would most definitely be consumed by aerobes and denitrifiers for growth and reproduction (Gierczak et al., 2007). Acetate was included for the sole purpose of examining its subsurface behaviour. In particular, a comparison of bromide and acetate transport was performed, with emphasis being placed on the peak arrival times. This test was therefore considered to be a tracer test instead of an acetate injection.

3.6.4 Analysis of the Breakthrough Data

For each tracer test estimates of the average linear groundwater velocity and subsurface dispersivity at the multi-level points were determined by fitting the bromide breakthrough data with one-dimensional solutions of the advection-dispersion equation (Gierczak et al., 2006). Assuming a pulsed injection and a finite source width, the first solution, PULSEPE, uses the following equations (Devlin and Barker, 1996; Gierczak et al., 2006):

$$C(x,t) = \frac{C_o}{2} \left[\operatorname{erfc} \left(\frac{x - w/(2) - vt}{2(Dt)^{1/2}} \right) - \operatorname{erfc} \left(\frac{x + w/(2) - vt}{2[D(t - w/v)]^{1/2}} \right) \right] \quad (3.3)$$

$$D = v\alpha + D^* \quad (3.4)$$

where C_o is the injection concentration (mg/L); x is the distance from the source (m); w is the source width (m); D is the dispersion coefficient (m²/s); t is time (s); α is the dispersivity (m); D^* is the effective diffusion coefficient (m²/s); and v is the average linear groundwater velocity (m/s). For a given breakthrough curve, using this solution it was possible to optimize estimates of w , α , and v simultaneously (Gierczak et al., 2006).

The bromide breakthrough curves from the down-gradient multi-level wells were also fit with CLOUDPE, a second solution. This code assumes a point injection and finite mass, and relies on the following equation (Devlin and Barker, 1996; Gierczak et al., 2006):

$$C(x, t) = \frac{M / n}{(4\pi Dt)^{1/2}} \exp\left[-\frac{(x - vt)^2}{4Dt}\right] \quad (3.5)$$

where M is the tracer mass injected (mg); n is the porosity (dimensionless); and all other parameters correspond to those found in Equations 3.3 and 3.4. Note that a porosity value of 0.33 was assumed for all calculations. This value is based on previous research by Bekeris (2007), who reported a porosity range of 0.30 to 0.36 for aquifer-type soils. Using CLOUDPE a given breakthrough curve is matched by optimizing M , n , and v concurrently (Gierczak et al., 2006).

3.7 Three-Dimensional Groundwater Modelling

If calibrated properly, groundwater modelling provides a powerful tool for predicting subsurface behaviour and planning an in situ remediation scheme. Therefore, a finite difference analysis approach, relying on ModFlow and MT3D, was adopted to demonstrate the effects of substrate injection and circulation and to test the various design parameters of the Woodstock injection experiment. More specifically, the original goal of the modelling

was to determine the pumping rate and duration required to draw the solute perpendicular to the ambient flow direction between the injection-extraction well pair. It was then used to comment on the most efficient injection configuration, with particular attention being paid to the separation distance between the injection-extraction wells. ModFlow was used to compute the physical system, solving for a steady-state, constant density, saturated flow field, while MT3D was used to compute the chemical system by modelling solute transport by advection and dispersion. The two codes were operated by the Visual ModFlow software suite. Note that the author of this research set up all simulation scenarios, provided raw field data, and supervised the modelling work, which was performed and summarized by Gale (2009).

3.7.1 Finite-Difference Groundwater Modelling Approach

As previously mentioned, the modelling of subsurface solute transport requires two individual codes, the first used to model the physical flow field. Variations in the flow field with respect to space and time are computed by a particular version of the three-dimensional groundwater flow equation using specific physical properties of the aquifer. In this case, simplifying assumptions of uniform water density, uniform saturation, and steady state flow were established.

Once the physical flow field has been successfully modeled, a version of the three-dimensional solute transport equation is used to simulate the movement of the solute in the subsurface. The physical flow field output provides the advection term used for solute transport. A fourth simplifying assumption of reaction having a negligible effect on the transport of acetate was made. Therefore, only advection, dispersion, and diffusion were considered for solute transport modelling of the Woodstock injection system.

Both ModFlow, used to generate the flow field, and MT3D, used to simulate solute transport, rely on a block-centred, finite difference solution method. The finite difference solution method uses truncated Taylor series to numerically estimate the spatial derivatives

of the governing flow and solute transport equations (Rausch et al., 2005). These derivatives are computed between discrete nodes, arranged to form a grid within the model domain (Logan, 2001). Block-centred indicates that each node is centred within the cells of the domain. Average groundwater velocity and concentration values can only be determined at these discrete nodes. It is important to note that other strategies exist for modelling advective solute transport. Of particular interest is the method of characteristics (MOC). For this project, advection was simulated using both the finite difference method and the MOC. The MOC solves the advection term with a conventional particle tracking method (Zheng and Wang, 1999). This method relies on tracking particles of known concentration as they move through the domain due to advection alone over several time steps (Zheng and Wang, 1999).

3.7.2 Model Input Parameters

The determination of proper hydrogeologic parameters is extremely important to the successful development of an accurate groundwater flow and solute transport model. Therefore, a variety of laboratory and field techniques were relied upon for estimates of the average gradient and hydraulic conductivity. Information was amalgamated from the previously discussed 2008 water level data, core logs, grain size analyses, conventional slug tests, and the initial forced gradient tracer test to devise the preliminary homogeneous model. This information was later refined based on trends in the hydraulic conductivity datasets to develop a five-layer representation.

3.7.3 The Preliminary Homogeneous Model

The preliminary homogeneous model was created assuming a homogeneous and isotropic distribution of hydraulic conductivity throughout the domain. Dispersivity and porosity were also assumed to be uniform. A cross-section of the conceptual model for the homogeneous case is illustrated in Figure 3.6. In accordance with core logs from Cores 1 to 4 and the WO74 and WO75 series wells, the model depicts an unconfined sand and gravel aquifer underlain by a clay aquitard at a depth of 19 metres below ground surface (mbgs). An

average hydraulic conductivity for this unit was generated based on conventional slug test data and grain size analysis results. The calculated gradient reflects the average annual gradient based on manual water level measurements taken at WO35, WO02-D-14, and the WO74 and WO75 series wells. Consistent with the tracer test breakthrough curve analyses, a porosity value of 0.33 was chosen based on work by Bekeris (2007). Finally, values of longitudinal and transverse dispersivity were generated from the tracer test breakthrough curves. This conceptual model was discretized and superimposed on a finite difference grid in Visual Modflow to begin the simulations. Injection and extraction wells were added to the domain to simulate the cross-injection scheme.

3.7.4 Stratified Model Development and Calibration

The development of a more accurate stratified model involved a progressive process of adding layers, altering hydraulic conductivity estimates, and continually comparing the modelling results to the ML12 breakthrough curves from the first tracer test. Each model run was set up to reproduce the tracer test, including matching of pumping rates, bromide concentration, and test duration. In addition, an observation well was incorporated into each model run at the same relative location as ML12, allowing for direct comparison of the modelling results to the observed curves. Several layered scenarios were investigated to generate the most appropriate representation of the hydrostratigraphic model.

Calibration methods were used to refine the fit of the observed data to curves generated by the multi-layer model. The process involved altering the conductivity and dispersivity values of the five layers iteratively. A total of 42 individual iterations were performed for the calibration. In addition, two solute transport modelling approaches were examined, including an upstream finite difference method and the method of characteristics (MOC).

3.8 Groundwater Sampling and Analysis

A multitude of sample types were required to thoroughly characterize the background geochemistry at the site and track changes resulting from the acetate additions. Prior to

sampling, at least three well volumes were purged to ensure the collection of formation water. Depending on the sample type, this purging was performed with either a Geopump Series II peristaltic pump, a 7-channel constructed manifold, or a Waterra inertial pump. The following sections describe the various procedures for collecting each sample type.

3.8.1 Anion Samples

Anion sampling played a vital role in tracking geochemical changes resulting from the acetate injections. The majority of these samples were analyzed for nitrate, nitrite, acetate, bromide, sulfate, and chloride. All anion samples were collected in 25 mL scintillation vials. To prevent biological activity, these samples were frozen shortly after being collected. Sample analysis was performed on a Dionex ICS 3000 ion chromatograph featuring a Dionex IonPac AS18 analytical column. Prior to the analysis, the samples were thawed completely in the refrigerator and agitated to prevent the effects of stratification due to freezing. Duplicate samples were collected and analyzed approximately every ten samples.

3.8.2 Cation Samples

Numerous rounds of cation samples were collected during each acetate injection. These samples were analyzed for calcium, aluminum, silicon, iron, and manganese. Each sample was field-filtered with a 0.45 μm filter and directed into a 60 mL high density polyethylene bottle. The bottles were pre-acidified with 1.2 mL of concentrated nitric acid. The reduced pH is required to prevent the precipitation of the ions in solution. Duplicate samples were collected approximately every eight samples. All samples were sent to the Plasma Analytical Laboratory (KU-PAL) at the University of Kansas where they were analyzed using inductively coupled plasma atomic emission spectrometry (ICPAES), a method developed for the detection of trace ions in solution.

3.8.3 Alkalinity

Alkalinity was measured a few times throughout this project, both prior to and during the acetate injections. The procedure for measuring alkalinity involves a field titration using a

HACH Model AL-DT Alkalinity Kit. Briefly, 100 mL of sample is measured and thoroughly mixed with an indicator, Bromcresol Green-Methyl Red in this case. The solution is then titrated with concentrated sulfuric acid until there is a colour change, which indicates the endpoint has been reached. The results are expressed as mg/L as CaCO₃, the range of the test kit is 10 to 4,000 mg/L, and the accuracy is ±1 percent.

3.8.4 Dissolved Oxygen

Dissolved oxygen is a very important aspect of this research as denitrification is an anaerobic reaction that will only proceed following the consumption of all available oxygen. For this reason, the concentration of dissolved oxygen was carefully monitored before, during, and after all injections. It was often used as a surrogate parameter to determine the effectiveness of the injections before nitrate values became available. Measuring dissolved oxygen in groundwater is a procedure that takes place in the field, immediately following sample collection. The process involves a 25 mL groundwater sample, CHEMetrics dissolved oxygen vacu-vials, and a CHEMetrics Model V-2000 Photometer. The vacu-vial tip is snapped off in the sample and fills with water. This vial is then placed in the photometer, where it is processed for two minutes. The system relies on the indigo carmine method. Each vacu-vial contains the reduced form of indigo carmine, which reacts with the dissolved oxygen in the sample to form a bright blue product (Gilbert et al., 1982). The photometer measures the intensity of the blue product and relates it to the amount of dissolved oxygen, generating a measurement in milligrams per litre as O₂. The indigo carmine method is quite reliable as it is not affected by temperature, salinity, or the presence of other dissolved gases (Gilbert et al., 1982).

3.8.5 Nitrous Oxide Sampling

Nitrous oxide sampling was also used to track geochemical changes resulting from the acetate additions. Nitrous oxide is an intermediate product that forms along the denitrification pathway. Although there are many mechanisms for its creation, during enhanced in situ bioremediation it is typically created by the incomplete reduction of

nitrate (Anderson and Levine, 1986). Therefore, it was anticipated that fluctuations in nitrous oxide concentrations from the background level could provide insight into the reduction-oxidation conditions of the aquifer and the progress along the denitrification chain. For example, nitrous oxide concentrations which increase or remain unchanged might indicate that dissolved oxygen is still present in the aquifer and either no denitrification or partial denitrification is occurring. Alternatively, a decrease in nitrous oxide may indicate that reducing conditions have been achieved and all nitrogen compounds are being converted to nitrogen gas.

Nitrous oxide concentration samples were collected in 60 mL glass serum bottles. When collecting these samples, it was very important to ensure that no head space or bubbles were created. The samples were preserved with 0.2 mL of saturated HgCl₂ and refrigerated until analysis. Duplicates were collected approximately every ten samples. For analysis, the samples were submitted to the Environmental Geochemistry Laboratory at the University of Waterloo shortly after collection. The analysis method involves equilibrating the N₂O in a 5 mL headspace and manually injecting it onto a Varian CP-3800 gas chromatograph with an ECD detector (Rempel, 2008).

3.9 Isotope Sampling and Analysis

Stable nitrogen and oxygen isotope compositions ($\delta^{15}\text{N}$ and $\delta^{18}\text{O}$) can provide unique information regarding denitrification and N₂O production in the subsurface (Barford et al., 1999). While a great deal is known about the isotopic effect denitrification has on ¹⁵N and ¹⁸O in nitrate, less is understood about the influence of denitrification on the isotopic composition of N₂O (Barford et al., 1999). Despite this, both $\delta^{15}\text{N}$ and $\delta^{18}\text{O}$ in N₂O and $\delta^{15}\text{N}$ and $\delta^{18}\text{O}$ in nitrate were analyzed for this research. In addition, tritium (³H) and helium-3 (³He) isotope concentrations were measured to gain insight into groundwater age.

3.9.1 ^{15}N and ^{18}O in Nitrate

It has been well established that microbial denitrification results in the enrichment of both $\delta^{15}\text{N}$ and $\delta^{18}\text{O}$ in residual nitrate (Bottcher et al., 1990; Aravena and Robertson, 1998; Lund et al., 2000; Cole, 2008). As nitrate concentrations decrease from in situ denitrification, isotopic fractionation of nitrogen and oxygen molecules occurs due to the preferential reduction of the lighter ^{14}N and ^{16}O isotopes in nitrate by the denitrifying bacteria (Aravena and Robertson, 1998). The result is linear isotopic enrichment of the heavier isotopes in the residual nitrate, typically by a factor of 2.1:1 on a plot of $\delta^{15}\text{N}$ and $\delta^{18}\text{O}$ in nitrate (Bottcher et al., 1990; Aravena and Robertson, 1998).

Samples were collected in either 500 mL or 1.5 L plastic bottles for the analysis of ^{15}N and ^{18}O in nitrate. The amount of sample collected was dependant on the anticipated nitrate concentration of the groundwater. More water was required for samples with lower nitrate concentrations and less water was needed for samples with higher nitrate concentrations. Therefore, prior to the addition of acetate, most background samples were collected in 500 mL bottles. Following the acetate injections, larger 1.5 L bottles were required due to the anticipated drop in nitrate. All samples were frozen as soon as possible following collection. Once the nitrate concentrations of the samples were determined, they were submitted to the Environmental Geochemistry Lab for processing and then to the Environmental Isotope Laboratory for analysis, both at the University of Waterloo.

3.9.2 ^{15}N and ^{18}O in Nitrous Oxide

Samples for ^{15}N and ^{18}O in nitrous oxide were collected in 160 mL glass serum bottle. Similar to the N_2O concentration samples, it was very important to ensure that no head space or bubbles were created. The samples were preserved with 0.4 mL of saturated HgCl_2 and refrigerated as soon as possible following collection. Again, duplicates were collected approximately every ten samples. Once the N_2O concentrations of the samples were determined, they were submitted to the Environmental Geochemistry Lab for processing

and then to the Environmental Isotope Laboratory for analysis, both at the University of Waterloo.

3.9.3 Tritium-Helium Age Dating

Measuring the ratio of tritium (^3H) to helium-3 (^3He) in water samples can produce estimates of groundwater age (Sebol, 2004). The decay is governed by a 12.34 year half-life and can be used to generate relatively precise (± 1 year) age values (Sebol, 2004). The $^3\text{H}/^3\text{He}$ groundwater age can be calculated with the following equation (Solomon and Sudicky, 1991):

$$t = \lambda^{-1} \ln \left(\frac{^3\text{He}^*}{^3\text{H}} + 1 \right) \quad (3.6)$$

where t is the $^3\text{H}/^3\text{He}$ age of the groundwater; λ is the ^3H decay constant; $^3\text{He}^*$ is the concentration of tritogenic ^3He ; and ^3H is the measured concentration of ^3H .

To gain insight into the age of groundwater at the Woodstock site, several tritium-helium samples were collected from wells WO12, WO35, and WO40 in August of 2009. Figure 3.7 (a) presents a map of the greater Woodstock site, illustrating the locations of these wells. The in situ diffusion sampler technique was used for gas collection (Figure 3.7 (b)). Briefly, the samplers are filled with air using a simple hand pump, deployed in the well at a depth of interest, and allowed to equilibrate with dissolved gases at that depth (Hendry et al., 2005). Following a 24-hour equilibration period, the device is retrieved and the sample tip is isolated using pinch-off clamps. Prior to sample collection, the three wells were purged with a Waterra inertial pump. All samples were analyzed using mass spectrometry at the Dissolved and Noble Gas Laboratory at the University of Utah in Salt Lake City, Utah.

3.10 Lateral Nitrate Flux through the Treatment Zone

Prior to the substrate additions, the lateral mass flux of nitrate through the large-scale treatment zone was calculated. This zone is comprised of a section of aquifer approximately

53.6 metres wide and 14.6 metres deep, spanning the distance between the WO74 and WO75 series wells. Based on core logs and previous research at the site, this portion of the aquifer has been identified as extremely conductive. It can be pictured as a fast-flowing conduit, continuously transporting a great deal of nitrate mass to the supply wells of the Thornton Well Field. The mass flux calculation was performed to generate a percentage of the nitrate mass produced at the supply wells coming directly from this zone.

To begin the calculation, the treatment zone was divided into six distinct layers based on the hydrogeologic conceptual model. The average annual regional hydraulic gradient computed using manual water level data, hydraulic conductivity values outlined in the conceptual model, and an assumed porosity of 0.33 were used to generate estimates of the average linear groundwater velocity for each of these six zones. These values were then combined with area estimates and an average nitrate concentration of 13 mg-N/L to produce six lateral mass flux values, which were summed to produce a total flux in metric tons of nitrogen per year.

Comparing the nitrate mass passing through the proposed treatment zone to the nitrate mass produced at the supply wells provided insight into the relative impact this zone has on the wells. For this comparison, estimates of mass flux at Thornton Wells 01, 03, 05, 08, and 11 were computed using average aqueous nitrate concentration records from 1999 to 2006 and average 2008 flow rates for each supply well. These individual fluxes were summed to produce a total flux value representing the entire well field, which could be compared to the total mass flux of the treatment zone.

3.11 Substrate Additions

3.11.1 Selection of the Cross-Injection Scheme

Gierczak et al. (2007) pioneered the cross-injection scheme (CIS) for a pilot-scale study in Baden, Ontario, approximately 45 kilometers northeast of the Woodstock site. The method is an adaptation of the nutrient injection wall (NIW) described by Devlin and Barker (1994).

The NIW method is characterized by a highly permeable wall installed across the path of a contaminant plume (Devlin and Barker, 1994). Injection and pumping wells operate within the NIW, circulating the required nutrients perpendicular to groundwater flow. Following the injection phase, the wells are turned off and the nutrient pulse migrates into the aquifer under natural gradient conditions (Devlin and Barker, 1994). This active-passive pattern is repeated throughout the treatment, with dispersion being relied upon to mix the contaminated groundwater with the injected pulse down-gradient.

The high cost associated with the excavation and installation of a physical wall, as well as the naturally high hydraulic conductivity of the target aquifer, has led to the selection of the CIS for bioremediation at the Woodstock site. The CIS follows the same procedure as the NIW method; however, there is no wall to facilitate nutrient delivery (Gierczak et al., 2007). Alternatively, the injection-extraction system operates directly within the aquifer. The CIS combines the design flexibility of a daisy-well system with the predominantly passive operation of a PRB (Gierczak et al., 2007). In addition, previous studies have clearly demonstrated the success of this technology for stimulating in situ denitrification (Dybas et al., 2002; Gierczak et al., 2007). These advantages have led to the selection of the CIS for stimulating denitrification at the Woodstock site.

3.11.2 Electron Donor Selection

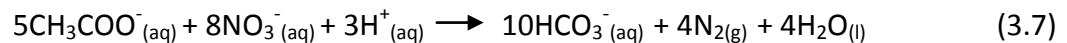
For stimulated in situ denitrification to proceed to completion, a source of electrons must be supplied. There are several electron donor choices to consider, including both organic compounds, such as simple organic acid anions, and inorganic compounds, such as ferrous iron, hydrogen, and reduced sulfur (Gierczak et al., 2007). Selecting a soluble organic substrate as an electron donor is beneficial as it supplies both the electrons and carbon required to drive the denitrification reaction. Common examples of these substrates include glucose, sucrose, formate, methanol, ethanol, and acetate. Several studies have identified acetate as the preferred carbon source and electron donor based on reports that it produces less biomass than other carbon substrates leading to fewer instances of clogging

(Mateju et al., 1992; Constantin and Fick, 1997; Devlin et al., 2000) and due to its proven success at stimulating complete denitrification (Kahn and Spalding, 2003; Kahn and Spalding, 2004; Gierczak et al., 2007). For these reasons, in addition to the relatively innocuous and accessible nature of acetate, it was selected as the carbon source and electron donor for this research.

3.11.3 The C:N Ratio

The ratio of available carbon consumed to the amount of nitrogen reduced, also known as the C:N ratio, has been identified as one of the key factors governing the efficiency of in situ denitrification (Sobieszuk and Szewczyk, 2006). An insufficient amount of carbon can result in partial denitrification, potentially leading to an accumulation of nitrite in the subsurface (Hamon and Fustec, 1991).

The biologically-mediated denitrification reaction with acetate as the electron donor is summarized as follows (Devlin et al., 2000):



This equation, which assumes complete denitrification, states that 5 moles of acetate are required to reduce 8 moles of nitrate. Background nitrate concentrations at the Woodstock site are typically very close to 13.0 mg-N/L or 57.6 mg-NO₃/L, which is equivalent to approximately 0.93 mmoles/L. Applying the stoichiometric balance of the above equation generates a required acetate concentration of approximately 0.58 mmoles/L or 34.3 mg/L. This required concentration is the absolute minimum as it assumes ideal, anaerobic conditions. It was hypothesized that a much greater acetate concentration would be required to achieve complete denitrification at Woodstock due to the highly aerobic nature of the aquifer. Before any nitrate consumption could occur, excess carbon would be required to achieve reducing conditions via stimulated bacterial consumption of oxygen. Further, it was also thought that additional carbon would be required to foster and develop

a subsurface community of denitrifiers. Due to these considerations, C:N ratios ranging from 1.9 to 2.8, approximately 3 to 4 times the theoretical requirement, were employed for the injections. These high ratios also reflect the close proximity of this experiment to the Thornton Well Field, where high nitrite concentrations could be problematic.

3.11.4 Injection Procedure

Over the course of this research project, two main substrate injection efforts were carried out. The two injection phases followed a similar procedure and relied upon WO78 (screen depth: 283.70 to 294.37 masl) as the pumping well and WO79 (screen depth: 285.32 to 294.47 masl) as the injection well. Similar to the forced gradient tracer tests, the system was operated perpendicular to groundwater flow, creating a “wall” of substrate in the aquifer between WO78 and WO79. A concentrated solution of sodium acetate and potassium bromide was injected during the two phases. Acetate was used to stimulate the denitrification reaction while bromide was used as a conservative tracer to track the distribution of the injected solution.

The pilot acetate experiment involved a single day injection on July 14, 2009. Groundwater was extracted from WO78 at an average rate of approximately 174 litres per minute, amended with the concentrated acetate-bromide solution at the surface, and re-injected into WO79. The 83,657 mg/L acetate and 236,796 mg/L bromide solution was mixed with groundwater in-line at an average rate of 0.214 litres per minute for a period of approximately six hours. This translates into injection concentrations of approximately 103 mg/L and 291 mg/L for acetate and bromide, respectively. The acetate injection concentration reflects a C:N ratio of approximately 1.9, on a mole-per-mole basis. Following the nearly six hour injection, the circulation cycle operated for an additional hour to ensure the solution was well distributed between the injection and extraction points. The 3.8-cm diameter pump intake tubing was positioned in the casing of WO78, just above the screened interval. The circulation cycle was driven by a high pressure centrifugal water pump, the Honda WH15XK1C1, and the flow rate being was in-line via with an F-1000 Digi-

Meter Paddlewheel Flowmeter manufactured by Blue-White Industries Limited. The injection of the concentrated acetate-bromide solution was facilitated via a T-connector and Geopump Series II peristaltic pump. The substrate-amended groundwater was re-injected into a 2.5-cm diameter PVC riser and screen centered within the larger 5.1-cm diameter riser and screen of WO79. Similar to the screen of WO79, the smaller diameter injection screen was a 10-slot well screen; however, the insert screen was taped at regular intervals to mimic an 8-slot screen. This was done to create a slight back pressure within the well during injection, ensuring an even distribution of acetate with depth.

A second injection phase was planned and executed following the realization that a single injection day could not possibly provide enough carbon to facilitate the consumption of all dissolved oxygen within the aquifer while supporting the growth and reproduction of denitrifying populations. This phase featured twelve consecutive injections which took place every day from September 14, 2009 to September 25, 2009, directly followed by seven injections performed on an every other day basis spanning September 27, 2009 to October 9, 2009. Nearly all design aspects of the first injection phase, including the pumps and the screen insert, were maintained for this round of injections. Each individual injection was intended to run for approximately six hours, followed by an additional hour of circulation. The target injection and pumping rates were 0.2 L/min and 200 L/min, respectively. With these pumping rates, the intended average acetate injection concentration was planned to be approximately 135 mg/L for each injection, leading to an average C:N ratio of 2.5, on a mole-per-mole basis. Table 3.5 features a summary of all acetate injections, including the single Phase 1 injection and the 19 Phase 2 injections. It is clear from this table that the target values for pumping and injections rates, the acetate injection concentration, and the C:N ratio were not always achieved. This can be attributed to the unpredictable nature of the large centrifugal pump, which gradually generated lower and lower pumping rates over the 19 Phase 2 injections. The injection rate, controlled by a Geopump Series II peristaltic pump, was also relatively difficult to set and maintain for the duration of an injection.

Table 3.5 also indicates that potassium bromide was injected as a conservative tracer for two of the second phase injections. On September 15, 2009 the bromide was used to determine the ideal afternoon sampling time for the injections to follow and on September 25, 2009 the bromide was used to track complete breakthrough, assisting with the organization of a detailed sampling regimen. Real time bromide concentrations were obtained in the field using a bromide ion-selective electrode manufactured by Cole-Parmer and an electrical conductivity probe.

3.11.5 Groundwater Sampling Routine

Before beginning this section it is important to note that all samples collected during the acetate injections followed the procedures outlined in the previous sections dedicated to sampling protocol.

During the first acetate injection phase, four multi-level bundles, ML5, ML6, ML7, and ML8, were closely monitored and sampled. Samples were collected before, during, and following the injection for a total period of almost 28 hours. Anion samples were collected and analyzed for acetate, bromide, nitrate, nitrite, sulfate, and chloride. These samples were collected at an interval of approximately 30 minutes for the first 9 hours of the experiment. Following this, the sampling rate gradually decreased overnight and into the following morning to one, two, and then three hours. Groundwater samples were also collected for analysis of ^{15}N and ^{18}O in nitrate and ^{15}N and ^{18}O in nitrous oxide. A total of 48 samples were obtained for each of these parameters, corresponding to four of the ports, at each of the multi-level bundles, at three time periods. The idea behind this sampling routine was to track the progress and extent of the denitrification reaction in space at the three distinct times. Nitrous oxide concentration samples, corresponding to the isotope samples, were also collected according to this regimen. In addition, dissolved oxygen, pH, and alkalinity measurements were taken and samples were collected for cation analysis (Ca, Al, Si, Mn, Fe).

The sampling program for the second acetate injection phase involved simple daily sampling, with more intense collections on September 25, 2009 and October 9, 2009. The daily sampling entailed collecting anion samples from the ports of ML7 in the morning, just as the injection was beginning, and in the afternoon, following the cessation of all pumping. These samples were analyzed for acetate, bromide, nitrate, nitrite, sulfate, and chloride. In addition, daily dissolved oxygen measurements were taken at the ports of ML7. These numbers were typically collected once a day, following the injection termination and before the collection of anion samples. On a few occasions dissolved oxygen was also measured in the morning as the injection was beginning.

September 25, 2009 marked the twelfth and final daily injection. The four multi-level bundles, ML5, ML6, ML7, and ML8, were closely monitored and sampled for a total period of over 27 hours. Anion samples were collected from the four multi-level bundles at an interval of approximately one hour for the first 10 hours of the experiment. Following this, the sampling rate gradually decreased to two and then three hours overnight and into the following morning and afternoon. Once again, the anion samples were analyzed for acetate, bromide, nitrate, nitrite, sulfate, and chloride. Similar to the experiment in the first injection phase, groundwater samples were also collected for analysis of ^{15}N and ^{18}O in nitrate and in nitrous oxide. A total of 32 samples were obtained for each of these parameters, corresponding to four of the ports, at each of the multi-level bundles, at two time periods. Nitrous oxide concentration samples, corresponding to the isotope samples, were also required. Finally, 28 samples were collected for cation analysis (Ca, Al, Si, Mn, Fe) and a series of dissolved oxygen, pH, and alkalinity measurements were taken.

The second injection phase was completed with the nineteenth injection, taking place on October 9, 2009. The ports of ML5, ML6, ML7, and ML8 were sampled for anions three times. The first round was collected in the morning before the start of the final injection, the second round was collected mid-day, and the third sampling round was performed

following the cessation of all pumping. Dissolved oxygen measurements were taken at ML7 in the afternoon.

Post-experiment sampling was performed on October 13, 2009 and October 19, 2009. Once again, the ports of ML5, ML6, ML7, and ML8 were sampled for anions and analyzed for acetate, bromide, nitrate, nitrite, sulfate, and chloride. In addition, dissolved oxygen measurements were taken at ML7 on both days.

3.11.6 Evaluating the Effectiveness of the In Situ Treatment System

The effectiveness of each acetate injection phase was evaluated based on several geochemical parameters, including manganese, iron, sulphate, nitrous oxide, dissolved oxygen, nitrate, nitrite, and $\text{NO}_3\text{-}^{15}\text{N}$ and $\text{NO}_3\text{-}^{18}\text{O}$ isotopes. Concentration data collected during and following the acetate injections were compared to background information to track significant geochemical changes. While changes in manganese, iron, sulphate, nitrous oxide and dissolved oxygen were used to track the establishment of new reduction-oxidation conditions, nitrate and nitrite concentrations were required to confirm the formation of a denitrifying environment. For this reason, emphasis was placed on nitrate and nitrite monitoring and concentration analysis. A significant decrease in nitrate with little to no nitrite production was determined to be the optimal outcome of initial testing, indicating a very effective treatment system.

3.11.7 Developing an Approach for Up-scaling Treatment

One of the main objectives of this research revolves around developing an approach for up-scaling treatment to a large-scale system capable of remediating the elevated nitrate concentrations at the Thornton Well Field. Several key factors were considered during this development, including the injection and extraction durations, the pulsing interval, the injection concentration, and the injection-extraction well spacing. In addition, the lateral extent of the treatment area was examined. These parameters were considered throughout this research in an effort to characterize the optimum treatment system for the study site.

Table 3.1: Summary of acetate injections.

Injection Phase	Injection Number	Date	Total Injection Time (hours)	Total Pumping Time (hours)	Average Honda Pump Rate (L/min)	Average Injection Pump Rate (L/min)	Average Bromide Injection Concentration (mg/L)	Average Acetate Injection Concentration (mg/L)	C:N Ratio ^a (moles/mole)	
1	1	14-Jul-09	5.6	6.9	174	0.214	291	103	1.9	
	2	14-Sep-09	5.5	6.5	206	0.219	-	133	2.4	
	3	15-Sep-09	6	7	202	0.202	237	141	2.6	
	4	16-Sep-09	6.1	7.1	202	0.198	-	130	2.4	
	5	17-Sep-09	6	7	199	0.202	-	134	2.4	
	6	18-Sep-09	6.4	7.4	199	0.189	-	125	2.3	
	7	19-Sep-09	6.2	7.2	199	0.195	-	130	2.4	
	8	20-Sep-09	6	7	198	0.202	-	134	2.5	
	9	21-Sep-09	6.2	7.2	198	0.195	-	130	2.4	
	10	22-Sep-09	6	7.1	198	0.202	-	134	2.4	
	2	11	23-Sep-09	6.4	7.4	196	0.189	-	127	2.3
		12	24-Sep-09	6.4	7.3	197	0.189	-	127	2.3
		13	25-Sep-09	6.1	7.1	198	0.198	237	148	2.7
		14	27-Sep-09	5.8	6.8	192	0.209	-	143	2.6
		15	29-Sep-09	5.8	6.8	193	0.209	-	143	2.6
		16	01-Oct-09	5.6	6.7	195	0.216	-	146	2.7
		17	03-Oct-09	5.9	7.1	193	0.205	-	140	2.6
		18	05-Oct-09	5.4	6.5	195	0.224	-	152	2.8
		19	07-Oct-09	5.7	6.7	191	0.212	-	147	2.7
		20	09-Oct-09	5.7	6.7	192	0.212	-	146	2.7

^a Calculated assuming average nitrate concentration of 13 mg-N/L.



Figure 3.1: Layout of the monitoring wells at the study site. Map contains data from CanMap Streetfiles (2005) and Southwestern Ontario Orthoimagery Project (2006).

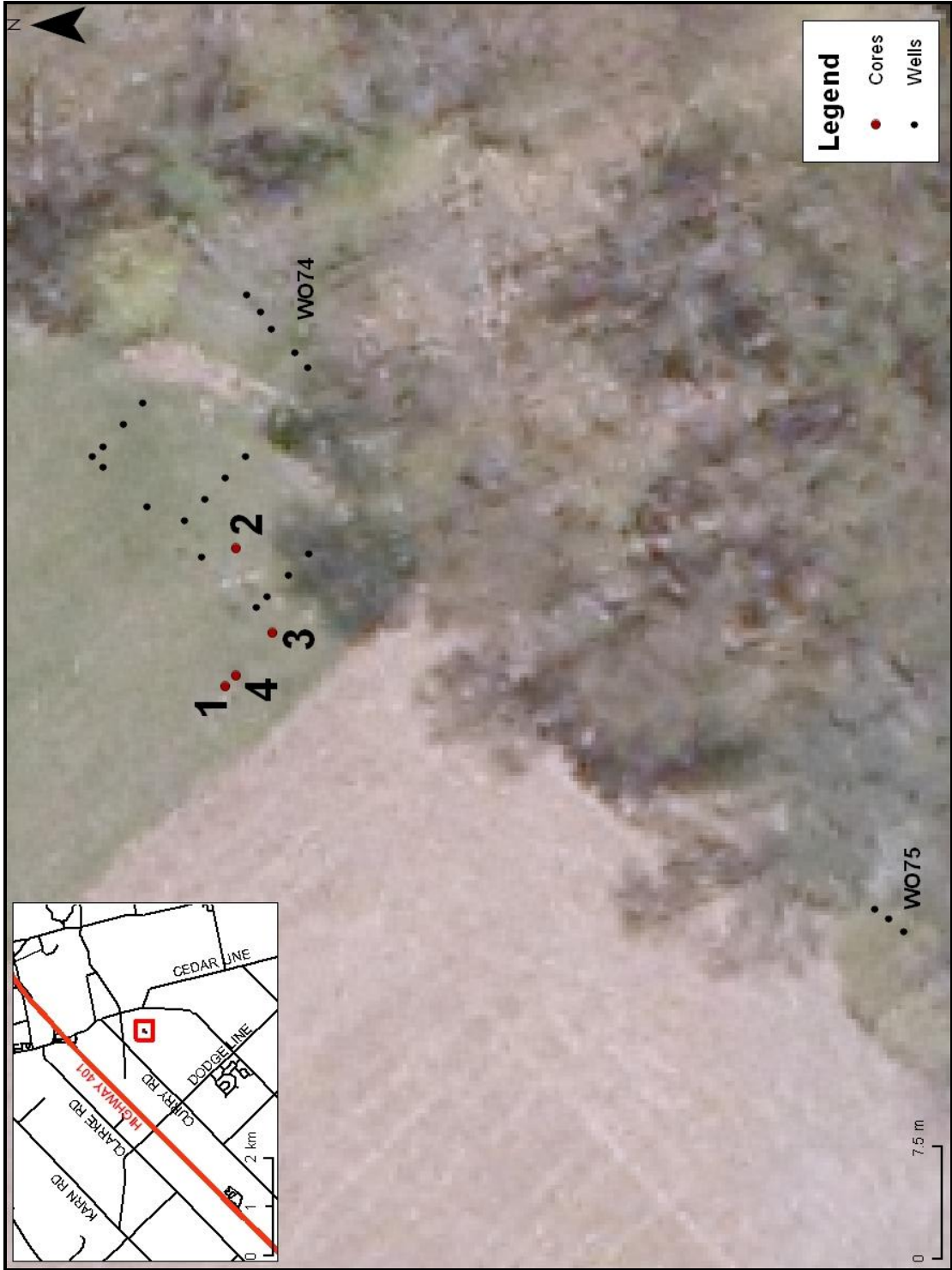


Figure 3.2: Core locations relative to the monitoring wells. Map contains data from CanMap Streetfiles (2005) and Southwestern Ontario Orthoimagery Project (2006).

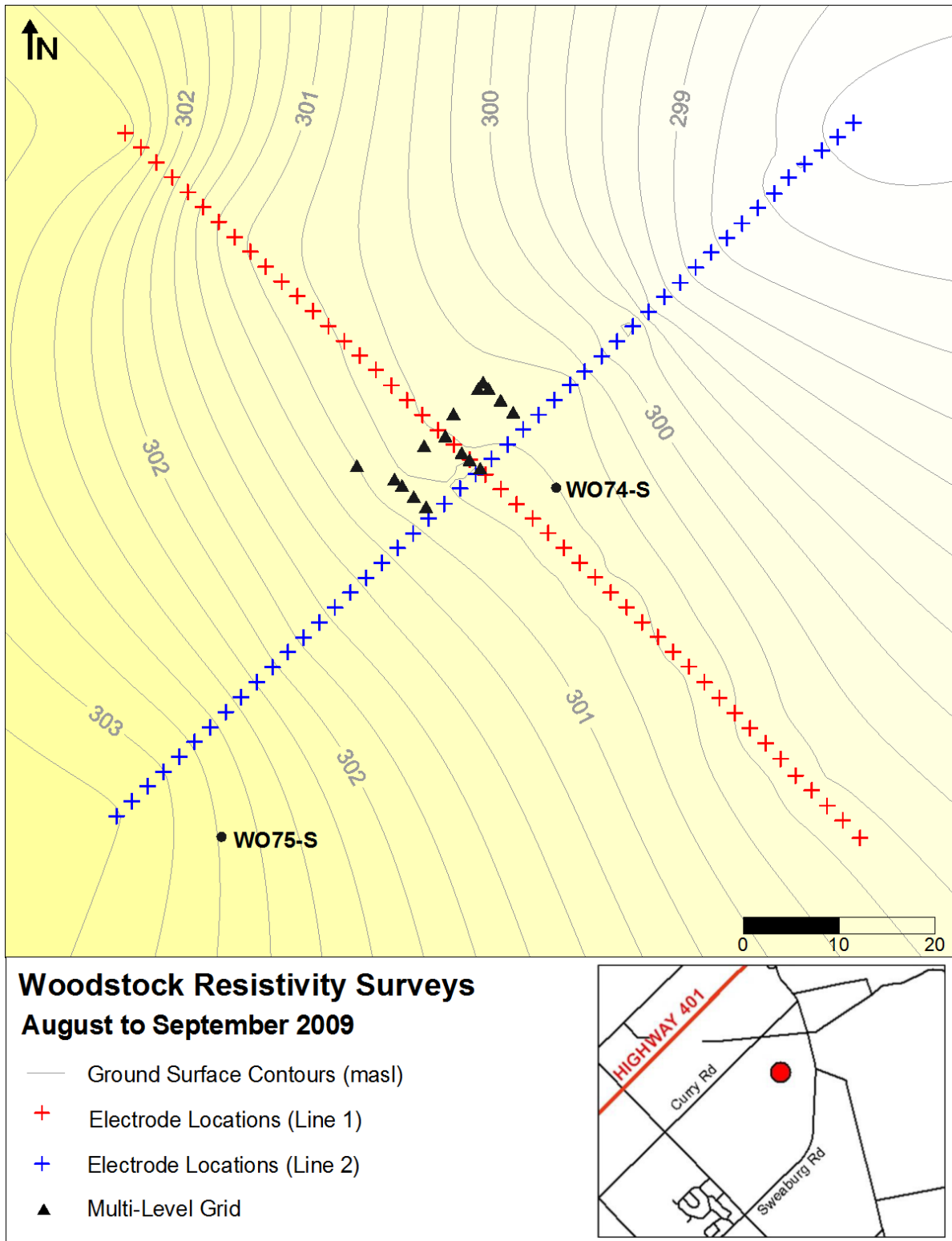


Figure 3.3: Location map of resistivity survey lines 1 and 2.

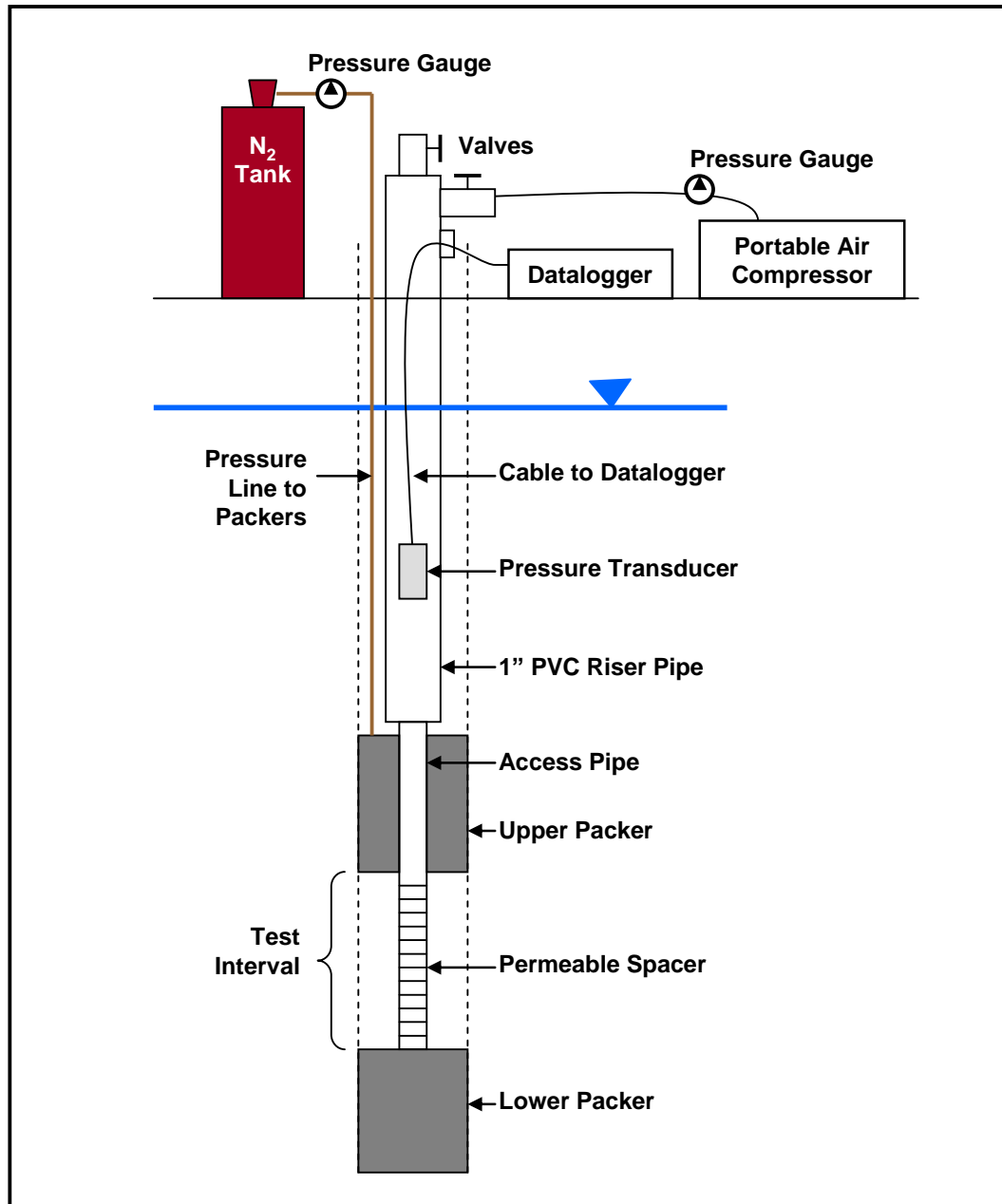


Figure 3.4: Multi-level slug testing apparatus (modified from Zlotnik and McGuire, 1998).

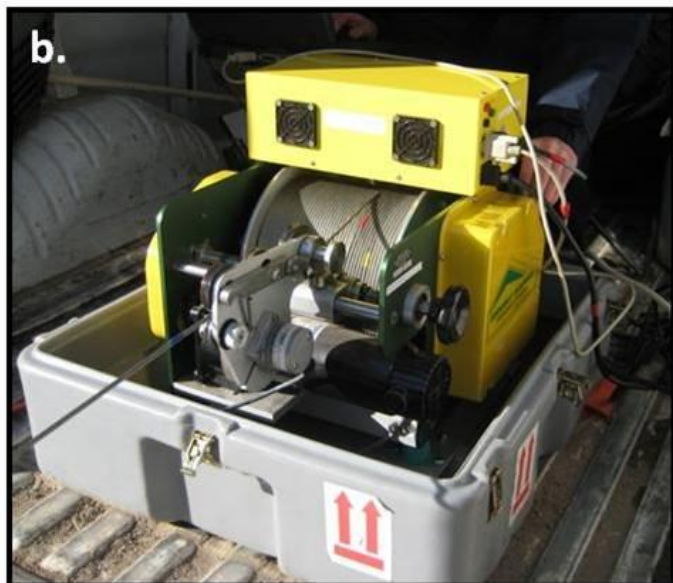


Figure 3.5: (a) The impeller flowmeter used for borehole logging. (b) The Mount Sopris 4MXA-1000 winch used to control the measurement depths. (c) The surface instrumentation, including the tri-pod and pulley system used to suspend the instrument and the Honda WH15XK1C1 high-pressure pump.

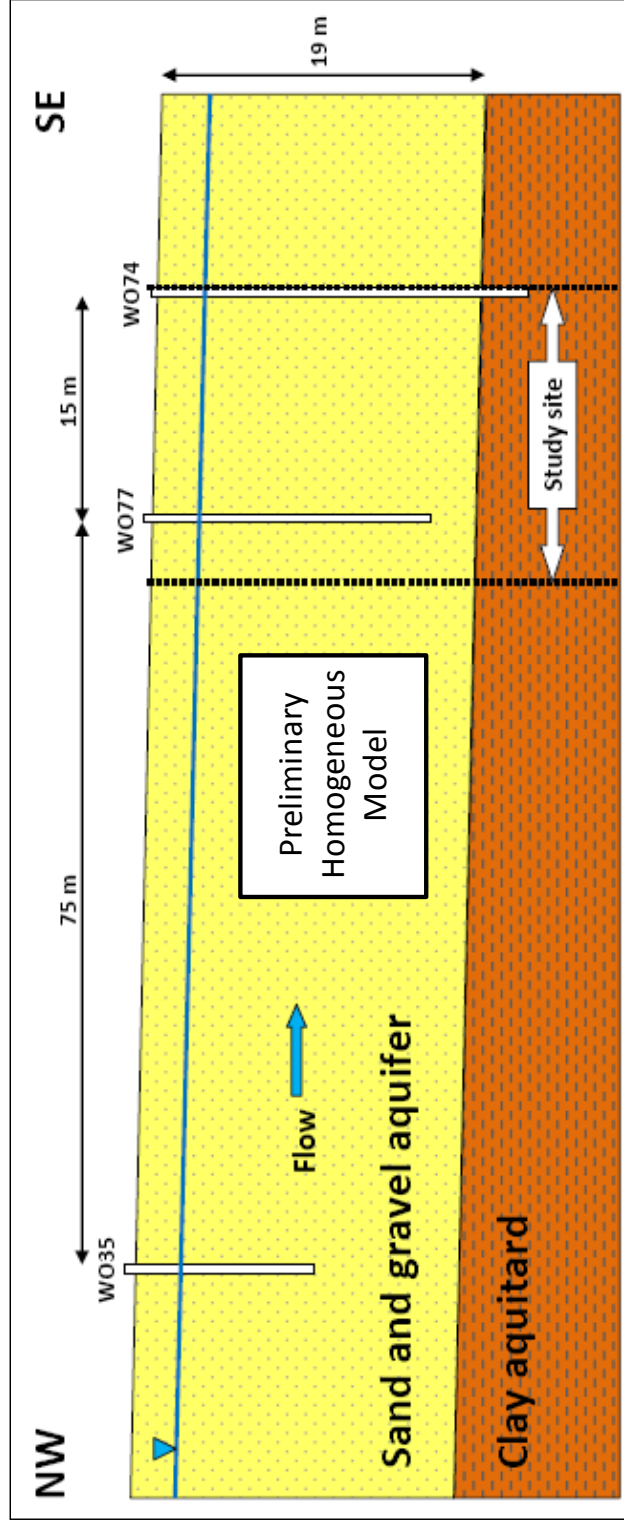


Figure 3.6: Preliminary homogeneous conceptual model (not to scale) (Gale, 2009).

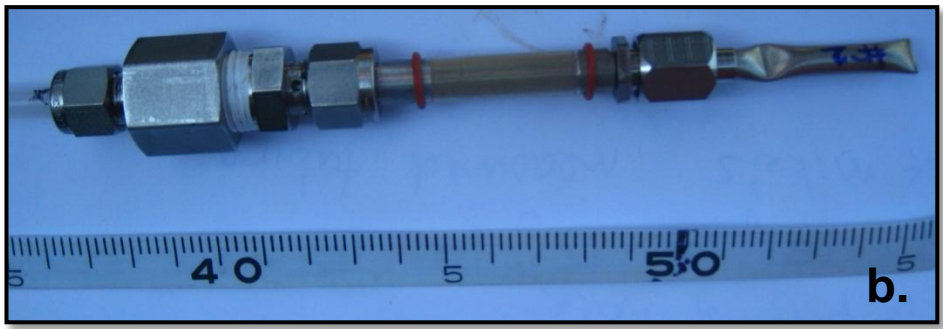
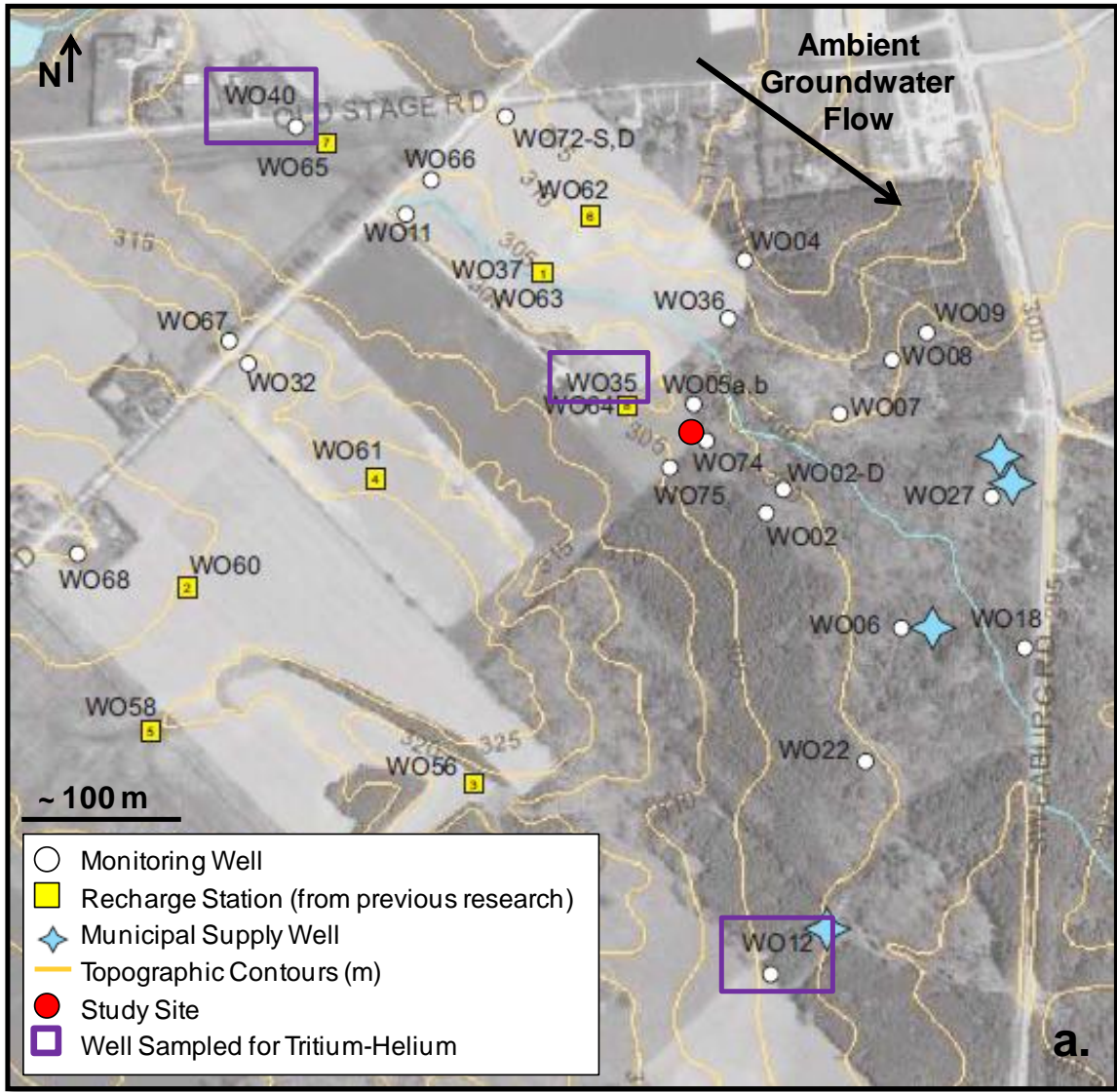


Figure 3.7: (a) Map indicating tritium-helium sampling locations and (b) photograph of one of the in situ diffusion samplers.

4. Results and Discussion

4.1 Hydrogeologic Conceptual Model

The development of the hydrogeologic conceptual model for the study site required input from several lab and field experiments performed at various scales. Results from core logging, resistivity surveys, grain size analyses, conventional slug tests, multi-level slug tests, borehole flowmeter tests, tracer tests, and three-dimensional numerical simulations were amalgamated for this effort. The results of these experiments are presented, discussed, compared, combined, and subsequently used to establish the physical conceptual model in this section.

4.1.1 Core Logging

A complete set of all geologic logs used for this research is presented in Appendix B. These logs include WO74-S, WO74-WT, WO74-M, WO74-D, WO75-S, WO75-D, and Cores 1 to 4. All geologic logs appear to be dominated by variably sorted sands and gravels. A few small, discontinuous silt and clay layers can also be found in most of the logs at various depths. Overall, the logs suggest the presence of a heterogeneous unconfined aquifer unit. The cores representing WO74-D and WO75-D provide insight into the depth of this conductive unit at the study site. From these logs, it is clear that a prominent clay aquitard exists below a depth of approximately 18.9 mbgs (281.9 masl) at WO74-D and 21.6 mbgs (281.2 masl) at WO75-D. Koch (2009) refers to this aquitard unit as Aquitard 4, which has a variable depth throughout the greater Woodstock site (Figure 2.6). Within the experiment vicinity, the depth of Aquitard 4 remains unknown due to the relatively shallow logs that exist for the area. In summary, based on core logging alone, the initial hydrogeologic conceptual model for the immediate study site features a fairly complex unconfined aquifer system with an average thickness of 20 metres, underlain by a clay aquitard at an average elevation of 281.5 masl. An average water table elevation of 297.6 masl (approximately 3.2 mbgs) was calculated for the unconfined aquifer system using monthly manual water level measurements taken at well WO74-WT over the year of 2008.

4.1.2 Electrical Resistivity Surveys

The electrical resistivity monitoring was used to provide a relatively simple, initial picture of the subsurface via a non-invasive approach. The August and September resistivity results for Lines 1 and 2 are displayed as contour plots in Figures 4.1 and 4.2, respectively. Note that the locations of these lines were presented in Figure 3.3. The results correspond to the Wenner electrode array, which relies on groups of four electrodes equidistant from each other (Herman, 2001). This array is known for its sensitivity to vertical changes in resistivity, allowing it to resolve horizontal structures such as the aquifer-aquitard units at the study site (Loke, 1999). Unfortunately, the Dipole-Dipole electrode array, which does not feature equidistant spacing, produced a low signal to noise ratio, generating obscure results which have not been presented for discussion. For both Lines 1 and 2, the resistivity contour plots generated in August clearly match those produced in September, suggesting consistency over time. Before examining Figures 4.1 and 4.2, it is important to mention that, in this case, the higher resistivity values correspond to units of suspected lower hydraulic conductivity, while the lower resistivity values represent suspected high-K layers. This is despite the surface conduction of the clay within the lower-K aquitard zones. In fully-saturated aquifers featuring typical total dissolved solids (TDS) values, electrolytic conduction of the groundwater tends to dominate over the clay effects, producing the relationship observed in the figures (Bunn, 2010; Endres, 2010). Also note the peculiar shape of the cross-sectional plots, which results from an inability to maintain horizontal coverage with depth.

The contour plots for Line 1, which runs directly along the line of multi-level bundles ML5, ML6, ML7, and ML8, illustrate a two-layer system. This is consistent with the plots generated for Line 2, which intersects Line 1 directly between ML7 and ML8. The elevated resistivity values at depth represent a potential aquitard unit, while the lower resistivity zone in the middle of the profile corresponds to the aquifer of interest. The high resistivity values near ground surface were generated by the dry surface conditions, a phenomenon referred to as contact resistance, and do not represent a second aquitard unit (Bunn, 2010). Based on observations corresponding to a depth range of 285 to 255 masl on all four plots,

the low resistivity target aquifer appears to be underlain by a significant aquitard unit at an elevation of approximately 280 masl. This is consistent with the core logging results, which place this aquifer-aquitard boundary at approximately 281.50 masl. Also similar to the core logs, which depict a fairly complex aquifer, the resistivity results suggest a relatively heterogeneous aquifer system with depth. Overall, the resistivity surveys were useful as an initial step towards physical characterization, yielding a general profile with depth. A much greater degree of detail, however, is required within the aquifer unit in preparation of the in situ remediation effort. Several methods of hydraulic characterization, described in the following sections, will be employed to achieve this.

4.1.3 Hydraulic Characterization

As previously mentioned, several lines of evidence were relied upon to determine the subsurface distribution of hydraulic conductivity of the aquifer. Results from this effort, including grain size analysis, conventional slug tests, multi-level slug tests, and borehole flowmeter tests, are presented in detail.

4.1.3.1 Grain Size Analysis

The grain size analysis results are presented in Figure 4.3 and Appendix C. Figure 4.3 graphically displays the results, while Tables C.1, C.2, C.3, and C.4 in Appendix C provide raw hydraulic conductivity estimates relative to depth for Cores 1, 2, 3, and 4, respectively. Refer to Figure 3.2 for a map illustrating the locations of Cores 1 to 4 relative to the grid of multi-level wells.

The hydraulic conductivity values derived from Cores 1, 2, and 4 have nearly identical arithmetic means, ranging from 1.3×10^{-3} m/s to 1.5×10^{-3} m/s. Due to the relatively short length and position of Core 3, it produced an arithmetic mean value of 2.5×10^{-4} m/s. Figure 4.3 displays a jagged conductivity profile with hydraulic conductivity values ranging from 6.5×10^{-6} m/s (Core 3) to 1.4×10^{-2} m/s (Core 4). The overlap of profiles from Cores 1, 2, and 4 suggests the potential presence of two main high conductivity zones, spanning 292 to 295

masl and 288 to 290 masl, although further testing is required to confirm this general observation. Several additional peaks exist for the individual core locations; however, these are thought to be the result of smaller, localized units. Overall, the grain size analysis results appear to suggest a fairly complex and conductive unconfined aquifer system, supporting the previously mentioned hydrogeologic conceptual model for the immediate study site (Section 4.1.1).

4.1.3.2 Conventional Slug Tests

The conventional slug tests performed on WO74-S, WO74-M, WO74-D, WO75-S, and WO75-D produced both underdamped and critically damped response curves. The oscillatory nature of the recovery data can be attributed to the high permeability of the aquifer of interest. All tests were rendered complete in a matter of seconds.

As previously mentioned, the water level displacement datasets were analyzed using a mathematical solution developed by Springer and Gelhar (1991). The hydraulic conductivity results generated by this solution are displayed in Table 4.1. These values range from 3.6×10^{-4} m/s (WO75-D) to 2.0×10^{-3} m/s (WO74-M). The hydraulic conductivities produced by the conventional slug tests (average of 8.5×10^{-4} m/s) are relatively similar to those determined from the grain size analyses (average of 1.3×10^{-3} m/s), with the average values differing by less than a factor of two. Discrepancies between these two datasets can be attributed to issues of scale. Also, despite being located within the study site boundaries, the cores used for grain size analysis and the wells used for slug testing were all in different locations. Unfortunately, conventional slug testing provides only a single hydraulic conductivity estimate per well and, therefore, a profile with depth could not be created for direct comparison. Also note that the slug test results corresponding to WO74-S and WO74-D appear to depend on whether a rising or falling head test was performed. This may indicate the presence of an evolving well skin resulting from insufficient development (Butler et al., 1996).

4.1.3.3 Multi-level Slug Tests

Similar to the results of the conventional slug testing, the multi-level slug tests performed on WO77 produced oscillatory response curves. Once again, the high permeability of the aquifer was credited with producing this response and the Springer and Gelhar (1991) solution was selected to fit the water level displacement data. The slug testing was performed with a packer system that isolated discrete intervals within the continuous well screen of WO77. The hydraulic conductivity values generated for each test depth are displayed in Table 4.2. While three to four slug tests were performed at every test depth using various pressures, only the mean conductivity value for each depth is presented. The conductivity values have a very narrow range of 2.3×10^{-4} m/s to 3.2×10^{-4} m/s. In addition, they are relatively low compared to the conductivities generated by the conventional slug tests and grain size analysis. The narrow range and relatively low values suggest artificial constraints on the estimated hydraulic conductivities. It was hypothesized that the water level response within the multi-level packer system was controlled by flow through the 1.25-cm inner diameter access pipe running through the upper packer rather than flow through the aquifer. Due to the questionable accuracy of the multi-level slug testing results, these hydraulic conductivity values were not taken into consideration during development of the final K profile.

4.1.3.4 Borehole Flowmeter Testing

The November 2008 and February 2009 borehole flowmeter test results corresponding to wells WO77, WO78, WO79, and WO80 are displayed in Figure 4.4. Unfortunately, only relative hydraulic conductivity estimates, presented as K_i/K , are generated by the borehole flowmeter tests. This limits the comparison of the flowmeter results to those produced by the grain size analyses and slug tests to a relative one.

Figure 4.4 displays another jagged profile of relative hydraulic conductivity, featuring K_i/K values ranging from undetectable to 12.8. In general, the profile seems to suggest the presence of a relatively high permeability zone above 292 masl and a relatively low

permeability zone below this depth. This is inconsistent with the grain size analysis profile presented in Figure 4.3, which identifies a second high conductivity zone spanning 288 to 290 masl. The flowmeter plots display very little activity at this depth. Also, an extensive no flow zone is seen below a depth of approximately 290 masl on all plots in Figure 4.4. The apparent presence of this zone may be the result of flowmeter sensitivity. It appears the threshold velocity of the flowmeter was too high to reliably measure relative conductivity with depth. In addition, a small amount of fine material in the water column continually clogged the flowmeter during testing. When this occurred, the flowmeter was extracted from the well, disassembled, and thoroughly cleaned. As a second hypothesis, perhaps the high conductivity zone at depth is a discontinuous lens, which cannot support groundwater flow.

In addition to the discrepancy between the flowmeter and grain size analysis results, the November 2008 and February 2009 flowmeter results for each of the wells do not match up particularly well. This disagreement may be the result of well development. Prior to the November 2008 testing, the wells were extensively pumped to remove fines. In January, however, further development was performed by injecting compressed air. The more thorough January well development, performed between the two tests, may have mobilized the fine formation material in the direct vicinity of the well screen, ultimately resulting in inconsistent flowmeter results. Due to the rapid groundwater flow and month-long interval between air injection and flowmeter testing, it is thought that the injected air did not directly influence the February results. In support of this statement, the February flowmeter tests suggested K-estimates similar to or higher than the November tests.

4.1.4 The Regional Hydraulic Gradient

Monthly estimates of the regional hydraulic gradient across the study site are displayed in Table 4.3. The manual water level data from wells WO35, WO74, WO75, and WO02-D-14 used to compute these gradient estimates are displayed in Table D.1 in Appendix D. Note that no manual water level measurements were taken during March and November of 2008

and, therefore, gradient estimates do not exist for these months. The gradients range from 2.4×10^{-3} in October to 4.3×10^{-3} in September and feature a mean value of 3.3×10^{-3} . It was intuitively assumed that the highest gradient would be observed in the spring and the lowest gradient would occur in late summer or over the frozen winter months. This was not the case, however, and the maximum and minimum values were found to correspond to adjacent months in the fall. The narrow range of gradient values may suggest that continuous pumping at the Thornton Well Field is the dominant force behind groundwater flow at the study site, as opposed to seasonal effects.

The water level data suggest the direction of groundwater flow resulting from the hydraulic gradient is from north-west to south-east across the study site for all months of 2008. Figure 4.5, displaying contours of hydraulic head and the resultant direction of ambient groundwater flow for the April 2008 dataset, is presented to demonstrate this. Note that it appears the flow direction is not quite perpendicular to the multi-level well grid as was intended. It was assumed that the injection and extraction efforts would not be negatively impacted by this.

It is important to acknowledge the uncertainty surrounding the monthly hydraulic gradient estimates and direction of groundwater flow at the study site. There were very few wells in close proximity to the site with consistent, comprehensive datasets available to generate monthly full flow field plots and regional gradient estimates. The water level data collected at the multi-level bundles did not correlate with the WO35, WO74, WO75, and WO02-D-14 data in terms of measurement timing throughout the year and, therefore, were not included in the flow field plots and gradient calculations. In addition, the high density of data points in the multi-level grid resulted in contouring issues. Leading to additional uncertainty, the head differences across the study site were very small, making it difficult to conclusively determine the exact orientation of groundwater flow.

In addition to the horizontal gradient, the vertical hydraulic gradient was also examined using water level data. Levels were taken throughout the study site at the multi-level bundles on multiple occasions in an effort to quantify the vertical gradient. The water level measurements, however, do not support the existence of vertical flow. This may be due to the relatively shallow nature of the multi-level bundles. A multi-level well that penetrates the underlying aquitard may be required to detect the presence of a vertical gradient between the layers. In addition, it has been demonstrated that detecting vertical gradients based on water level data alone is difficult due to measurement error and local variations in vertical flow related to heterogeneity or transient phenomena such as pumping or recharge events (Silliman and Mantz, 2000). This is especially true when measurement occurs over short distances and where gradients are small.

4.1.5 Tracer Testing Results

4.1.5.1 Forced Gradient Tracer Test 1

The bromide concentration breakthrough curves representing the results of the first forced gradient tracer test are displayed in Figure 4.6. These curves were produced using data collected at multi-level bundle ML12, situated between the injection-extraction well pair (Figure 3.1). Clearly, the vast majority of the bromide mass was transported through a highly permeable zone spanning ports ML12-2, ML12-3, and ML12-4 (289.68 to 293.08 masl). All other ML12 sampling ports reported only trace bromide concentrations. The bromide concentrations measured at ML12-4 peaked after only four hours of monitoring and nearly reached the injection concentration of approximately 242 mg/L. ML12-2 and ML12-3 featured lower bromide concentrations and a slower peak arrival time of approximately 6 hours. This peak concentration and arrival time discrepancy within the zone of high permeability, in addition to the unresponsive nature of the other ML12 ports, suggests an aquifer with a great deal of heterogeneity. While this observation of general aquifer heterogeneity correlates well with results of the core logging, grain size analysis, flowmeter tests, and slug tests, the rapid peak arrival times and extremely fast flowing groundwater observed at ports ML12-2, ML12-3, and ML12-4 were not anticipated based

on previous research. This discrepancy may result from several factors, including the influence of the injection-extraction procedure on groundwater flow in the experiment vicinity and the various scales used for investigation.

The breakthrough curves for ML12-2, ML12-3, and ML12-4 were fit with both CLOUDPE and PULSEPE. The results of these solutions are displayed in Table E.1 in Appendix E. The table includes best fit estimates of groundwater velocity, dispersivity, source width, and total mass, in addition to the approximate 95 percent confidence intervals for these parameters. A comparison of the generated curves suggested that PULSEPE provided the best fit to all three curves. This solution yielded an average groundwater velocity of 2.3×10^{-4} m/s, equivalent to approximately 20 m/day, and an average dispersivity of 0.5 m for the zone of high permeability. An average hydraulic conductivity was not calculated based on this velocity estimate due to the ambiguous nature of the gradient between the injection and extraction wells during circulation.

4.1.5.2 Forced Gradient Tracer Test 2

The results of the second forced gradient tracer test are displayed as several bromide concentration breakthrough curves in Figure 4.7. These curves were produced using data collected at multi-level bundles ML5, ML6, ML7, and ML8, located along a line bisecting the injection-extraction plane at downgradient distances of 1 metre, 3 metres, 5 metres, and 7 metres, respectively. Note that the ML5 and ML6 breakthrough curves are much more complete than the ML7 and ML8 curves. In particular, there is insufficient early time data from ML8 to properly define the curves. This is also the case with ports 6 and 7 of ML7. At the interpretation stage this was kept in mind and emphasis was placed on the complete breakthrough curves corresponding to ML5 and ML6. Also, while the ports of ML6 and ML7 all line up below ground surface, the ports of ML5 and ML8 are approximately 2 metres shallower and 0.7 metres deeper, respectively, due to installation issues. This means that all comparisons should be performed using exact depths as opposed to port numbers. To assist with data comparison, all relevant port depth information is summarized in the tables

corresponding to the tracer test results. For additional port depth information please refer to Appendix A.

Once again, the tracer test results indicate the presence of preferential pathways through the aquifer. Examining only the complete breakthrough curves recorded at ML5 and ML6 reveals a high permeability zone spanning ports 3 to 5 on ML5 (290.44 to 293.84 masl) and ports 2 to 4 on ML6 (290.05 to 293.45 masl), which correspond to nearly identical elevations. This is consistent with the results of the first forced gradient tracer test, which also identified a high-K zone spanning these depths. Unlike the first tracer test results, however, most of the other ports of ML5 and ML6 measured elevated bromide concentrations. Overall, the ML5 and ML6 peak concentrations and arrival times seem to suggest a profile featuring four layers. These units include a lower-K zone near the surface, underlain by a zone of very high permeability, underlain again by another lower-K zone, and bounded on the bottom by a second relatively high-K zone. In general, these observations agree with the hydraulic characterization results and initial conceptual model, however, a greater degree of detail has been established with the tracer testing.

The breakthrough curves for ML5, ML6, ML7, and ML8 were fit with both CLOUDPE and PULSEPE. Note that only complete breakthrough curves were analyzed with these solutions. If there was any inclination that the peak was missed, no curve fit was thought to be reliable. The results of these solutions are displayed in Table E.2 in Appendix E. The table includes best fit estimates of groundwater velocity, dispersivity, source width, and total mass, in addition to the approximate 95 percent confidence intervals for these parameters. The PULSEPE- and CLOUDPE-generated curves were compared for each port to determine the best fit. In some instances, the solution curves were identical and the two sets of parameters were averaged to determine the best fit values. For this tracer test, the best fit velocity estimates were converted to relative numbers and calibrated with the results of the natural gradient tracer test tracked at ML10. This calibration was performed to generate approximate velocity values representative of natural groundwater flow conditions. An

overall average groundwater velocity of 5.3×10^{-5} m/s and an average dispersivity of 0.8 m were calculated. While the first forced gradient tracer test measured breakthrough at a multi-level bundle aligned with the injection-extraction plane, the second tracer test featured breakthrough monitoring at downgradient multi-level ports, allowing hydraulic conductivity values to be calculated using the average ambient gradient at the site (Section 4.1.4). Based on the calibrated velocities, hydraulic conductivities were tabulated for each complete breakthrough curve using gradient and porosity values of 3.3×10^{-3} and 0.33, respectively (results presented in Table E.2). The K-estimates ranged from 6.8×10^{-4} m/s (ML5-2) to 5.1×10^{-2} m/s (ML7-4) and generated an average value of 5.3×10^{-3} m/s. This average conductivity falls well within the range of acceptable values for coarse aquifer materials. Further discussion regarding this value and the other tracer test results is presented in Section 4.1.5.4.

4.1.5.3 Natural Gradient Tracer Test

The bromide and acetate concentration breakthrough curves representing the results of the natural gradient tracer test are displayed in Figure 4.8. These curves were produced using data collected at multi-level bundle ML10, situated three metres directly downgradient of the injection well. Once again, a high permeability zone can be identified at a depth corresponding to ML10-4 (289.49 masl). This port of interest featured the shortest peak arrival times and highest peak concentrations for both acetate and bromide. Ports ML10-3 (291.19 masl) and ML10-7 (284.39 masl) also produced bromide and acetate breakthrough curves with relatively rapid peak arrival times. The other ports display delayed arrival times and relatively small peaks. Similar to the results of the forced gradient tracer testing, the peak concentrations and arrival times corresponding ML10 suggest a heterogeneous profile. It is thought that this profile features a lower-K zone near the surface, underlain by a zone of very high permeability, underlain again by another lower-K zone, and bordered on the bottom by a second relatively high-K zone.

The complete bromide breakthrough curves for ML10-3, ML10-4, and ML10-7, corresponding to the higher permeability layers, were fit with both CLOUDPE and PULSEPE. The results of these solutions are displayed in Table E.3 in Appendix E. The table includes best fit estimates of groundwater velocity, dispersivity, source width, and total mass, in addition to the approximate 95 percent confidence intervals for these parameters. Based on a comparison of the generated curves, it was determined that CLOUDPE provided the best fit to all three curves. This solution yielded an average groundwater velocity of 3.3×10^{-4} m/s and an average dispersivity of 0.68 m for the three higher permeability layers. Hydraulic conductivity values were also tabulated for these three zones using gradient and porosity values of 3.3×10^{-3} and 0.33, respectively (results presented in Table E.3). An average K-value of 3.3×10^{-2} m/s was generated. Further discussion regarding the tracer test results is presented in Section 4.1.5.4.

A secondary objective of the natural gradient tracer test was to compare the subsurface transport of acetate and bromide, with emphasis being placed on the peak arrival times. Figure 4.8 clearly demonstrates that bromide is a good surrogate for gauging the transport of acetate within the aquifer of interest. The peak arrival times for the two compounds were very similar. Alternatively, the peak arrival concentrations were quite different. This can be attributed to the consumption of acetate by indigenous microorganisms. Overall, the two solutes migrate in a similar fashion and, therefore, bromide can be used during the acetate injections to track the migration of the injected plume. This tracking will provide insight regarding where and when to collect groundwater samples.

4.1.5.4 Comparison of Tracer Test Results

Table 4.4 provides a summary of the tracer test results, including best fit dispersivity, velocity, and hydraulic conductivity estimates for all ports that produced complete breakthrough curves. The dispersivity values range from 0.23 to 23.2 metres, however, the accuracy of this maximum value is questionable on the basis of magnitude. The velocity and hydraulic conductivity estimates range from 6.8×10^{-6} to 5.1×10^{-4} m/s and 6.8×10^{-4} to 5.1×10^{-2}

² m/s, respectively. On average, these hydraulic conductivity values are very similar to the estimates produced by the grain size analyses and slug tests, differing by less than an order of magnitude in many cases. Any discrepancy that is apparent can likely be attributed to the variety of scales used for analysis. It is well established that the hydraulic conductivity of a given hydrogeologic unit appears to increase as the scale of measurement increases (Bradbury and Muldoon, 1990; Schulze-Makuch et al., 1999). Bradbury and Muldoon (1990) suggest hydraulic conductivity values estimated from laboratory methods can be one to two orders of magnitude lower than those generated from field tests on the same materials.

The tracer test results are graphically summarized in Figure 4.9. This plot features four vertical conductivity profiles corresponding to wells ML5, ML6, ML7, and ML10. Note that two different horizontal scales were required to properly display the data. All plots display a lower-K unit near the top of the aquifer. Below this, the graphical peaks suggest the presence of an extremely conductive layer at a depth of approximately 290 masl. The curves suggest the hydraulic conductivity decreases once again below a depth of 290 masl, eventually reaching a conductivity value similar to that of the first layer. Beyond this, the ML5 and ML6 plots suggest the hydraulic conductivity increases once again. In summary, the tracer test results depict a four-layer aquifer with alternating low- and high-K layers. Additional layers may exist, however, if these larger units are not completely uniform with respect to hydraulic conductivity or if the scale of examination is decreased. Section 4.1.7 provides further discussion regarding all hydraulic conductivity estimates generated during the physical characterization phase.

The tracer test results also provided information regarding the direction of ambient groundwater flow at the site. The discussion presented in Section 4.1.4 suggested that the groundwater flow direction in the experiment vicinity is not quite perpendicular to the well network. It was then assumed that the injection and extraction efforts would not be negatively impacted by this. The results of the tracer testing validate this assumption by portraying successful tracer breakthrough at the downgradient multi-level bundles. This is

especially apparent in the results of the second forced gradient tracer test, which depict bromide breakthrough at four multi-level wells representing downgradient distances of 1 m, 3 m, 5 m, and 7 m.

4.1.6 Three-Dimensional Groundwater Modelling Results

Before discussing the modelling results it is important to note once again that the author of this research set up all simulation scenarios, provided raw field data, and supervised the modelling work, which was performed and summarized by Gale (2009).

4.1.6.1 Results from the Preliminary Homogeneous Model

To test the validity of the preliminary homogeneous model, a scenario reproducing the first tracer test was simulated and the output was compared to the actual test results. This comparison is illustrated in Figure 4.10 (a). The observed and simulated results were extremely different, making it clear that a homogeneous medium was not representative of the field conditions and further work would be required.

4.1.6.2 Stratified Model Development

Further analysis of the core logging and grain size analysis results was the first step in delineating hydrostratigraphic layers. The presence of three potential layers became apparent on a logarithmic plot of point hydraulic conductivity measurements with depth. The uppermost unit, ranging from ground surface to 294.50 metres above sea level (masl), displayed a wide range of hydraulic conductivity values; the middle unit, which spanned 289.50 to 294.50 masl, displayed a much narrower, elevated range of hydraulic conductivity values; and finally, the lower unit, ranging from 289.50 masl to the top of the clay aquitard, was quite similar to the uppermost unit in terms of heterogeneity. The geometric averages of hydraulic conductivity for these three units were determined and applied to their corresponding layers. Table 4.5 provides a summary of the hydrogeologic parameters used for the three-layer model. The breakthrough curves generated by this initial stratified

model, displayed in Figure 4.10 (b), were a better match to the observed curves than the homogeneous model; however, further development was clearly required.

Comparing the simulated versus observed peak arrival times provided insight into the required next phase of model development. It was clear that the middle unit needed to be subdivided into three unique layers, producing a model with five distinct layers. Once again, the geometric averages of hydraulic conductivity values derived from the grain size analysis were used to estimate the conductivity of the five layers. Table 4.6 provides a summary of the hydrogeologic parameters used for the initial five-layer model. The longitudinal dispersivity values for layers 2, 3, and 4 were obtained directly from the tracer test result. The average longitudinal dispersivity value of 0.5 m was retained for layers 1 and 5 which had no available dispersivity data. As anticipated, the generated breakthrough curves more closely resembled the observed curves than the three-layer model (Figure 4.10 (c)). The peak arrival times greatly improved for ports 2 and 4, while port 3 requires some additional attention. In addition, the five-layer model is relatively consistent with the core logs. In general, the higher conductivity layers correspond to core sections with greater amounts of gravel and sand, while the lower conductivity layers correspond to poorly sorted core sections, with a mixture of grain sizes from clay to gravel. For these reasons, the five-layer representation was selected for further development.

4.1.6.3 Calibration of the Five-Layer Model

Calibration methods, involving altering the conductivity and dispersivity values of the five layers iteratively, were used to refine the fit of the curves generated by the five-layer model to the observed tracer test data. Following this process, the observed and simulated peak breakthrough times matched quite well and the relative calculated concentrations between the multi-level ports were reasonable. The total solute mass passing ML12 in the simulation, however, was much lower than in reality. It was hypothesized that this mass deficit may have resulted from unrealistically high dispersion introduced by the solute transport modelling approach. Logan et al. (2001) confirms that the finite difference method has a

tendency to exaggerate dispersion processes. To resolve this problem, the modelling approach was changed from an upstream finite difference method to the method of characteristics (MOC). The MOC substantially reduced the mass deficit, producing simulated breakthrough curves that were very similar to the observed breakthrough curves. Following this discovery, further calibration of conductivity and dispersion parameters was performed and a final five-layer conceptual model was established. Figure 4.10 (d) displays the calculated and observed breakthrough curves for the calibrated five-layer case. This scenario appears to have generated the best possible fit using a simplified, horizontally stratified five-layer model. A superior fit may have been possible with a more complex conceptual model; however, additional information was not available at this stage to support increased complexity. Tables 4.7 and 4.8 summarize the layer-specific and universal hydrogeologic parameters of the calibrated five-layer model, respectively. In addition, a cross-section of the conceptual model for the calibrated five-layer case is illustrated in Figure 4.11. It is also important to note that the ambient flow field is oriented perpendicular to the injection-extraction plane in the calibrated model. This assumption is based on the tracer test results discussed in Section 4.1.5.4.

4.1.6.4 Application of the Calibrated Model: The Six Cases of Interest

Flow and solute transport modelling using the calibrated multi-layer representation was principally used to compare various acetate injection scenarios. These scenarios were based on the arrangement of the injection and extraction wells, including the separation distance and number of operating wells. Theoretically, the ideal injection-extraction case produces a uniform horizontal and vertical distribution of substrate within the target aquifer. Due to heterogeneity, however, this ideal scenario may not be possible in reality. Also, concentrations in the direct vicinity of the injection and extraction well screens should remain as low as possible to prevent biological clogging. It was also determined that the ideal case features the widest possible span between injection and extraction wells, which minimizes the costs and resource consumption associated with well installation and monitoring. These criteria were kept in mind when assessing the modelling results.

A total of six cases, featuring a variety of well arrangements, were investigated with the calibrated 5-layer model (Figure 4.12). The simulations were performed with a circulating pumping rate of 200 L/min and a total substrate injection time of 4 hours (240 minutes). An injection concentration of 100 mg/L was selected as it provides a convenient means of assessing relative concentrations. The simulations were run for a total period of 24 hours (1440 minutes), with the injection-extraction circulation cycle operating for the entire duration. This extended duration was chosen to examine and quantify a shorter, sufficient pumping interval. Also, it was assumed that operating the circulation cycle for more than 24 hours would be impractical. The injection-extraction cycle consists of clean water for the 20-hour circulation interval following the 4-hour substrate injection in the simulations. Alternatively, in reality, the system would be circulating the acetate-rich water captured by the extraction well following the initial substrate injection interval. This discrepancy is especially noteworthy for the cases with small well separation distances since greater acetate concentrations reach the extraction well. Note that the modelling was never intended to completely replicate the field tests. Rather, the main goals were to demonstrate the effects of injection and flushing and to develop a set of reasonable simulation scenarios for comparison purposes.

The results of the six cases are presented as a series of cross-sectional maps along the injection-extraction well plane, each representing a specific time during the simulation (50 minutes, 240 minutes, 720 minutes, and 1440 minutes). To examine solute movement in the third dimension, several plan view maps have also been provided. These maps correspond to the third aquifer layer, which was selected based on its mid-range-K value of 1.2×10^{-1} cm/s (Figure 4.11). Note that only plan view diagrams illustrating the most uniform distribution of acetate between the injection and extraction wells have been displayed. For all cross-sectional and plan view maps, acetate concentrations have been contoured using an identical colour pallet that emphasizes the lower concentration range. The maps also feature dark blue contour lines, representing hydraulic head, and white and burgundy

arrows, indicating the direction of groundwater flow. The well spacing is indicated in the following section titles and the injection and pumping wells are labeled as IW and PW in the first cross-section of every figure. Also note there are three vertical white lines on each cross-sectional diagram corresponding to concentration observation ports. These ports, which do not affect the simulations, simply provide a secondary means of examining the acetate concentration distribution in space and time.

4.1.6.5 Case 1 Results (5 m separation distance, single extraction well)

The results for the first scenario are presented in Figure 4.13 and Figure 4.14 (a). This case features a single injection well paired with a single extraction well, separated by a distance of 5 metres. The acetate plume is most uniformly distributed between the injection and pumping wells following 240 minutes of circulation (Figures 4.13 (b) and 4.14 (a)). The cross-sections indicate that heterogeneity has strongly influenced the substrate distribution with depth. Following 240 minutes, the substrate injection was suspended while the injection-extraction circulation cycle continued for a total duration of 1440 minutes. Figures 4.13 (c) and (d) indicate the extra circulation resulted in the injection of a large quantity of acetate-free groundwater between the wells. At these later times, the acetate plume in the top four model layers was centred around the pumping well instead of forming a nutrient-rich wall between the wells. For this relatively small separation distance, it is clear that the pumping duration following injection should be kept short, providing just enough time to flush the substrate away from the injection screen to prevent clogging.

4.1.6.6 Case 2 Results (5 m separation distance, two extraction wells)

The results for the second case are displayed in Figure 4.14 (b) and Figure 4.15. This case features a single injection well centred between two extraction wells, with a well spacing of 5 metres. The substrate distributions illustrated in the cross-sectional maps are quite similar to those presented in Figure 4.13, especially early in time. The main difference is the symmetry of the acetate plume in Figure 4.15, resulting from the incorporation of a second pumping well. This difference is especially apparent in the plan view maps corresponding to

Cases 1 and 2 (Figures 4.14 (a) and (b)). It appears as though greater overall substrate spread was achieved with the second pumping well. Once again, the acetate plume is most uniformly distributed between the injection and pumping wells following 240 minutes of circulation (Figures 4.14 (b) and 4.15 (b)). In addition, the powerful effects of heterogeneity and the emplacement of acetate-free groundwater between the injection and extraction wells can be observed for this case (Figures 4.15 (c) and (d)).

4.1.6.7 Case 3 Results (10 m separation distance, single extraction well)

The plan view and cross-sectional maps for the third case are presented in Figures 4.14 (c), 4.14 (d), and 4.16. This case features a single injection well and single extraction well, separated by a distance of 10 metres. It appears as though the acetate plume is most uniformly distributed between the injection and pumping wells sometime between 720 minutes and 1440 minutes of circulation (Figures 4.14 (c), 4.14 (d), 4.16 (c), and 4.16 (d)). These two spans of time include 240 minutes of substrate injection followed by 480 minutes and 1200 minutes of additional pumping, respectively. Unlike the first two cases, the injection period alone was not sufficient to distribute the acetate evenly between the injection-extraction well pair for Case 3 (Figures 4.16 (a) and (b)). For this extended separation distance, it is clear that extended pumping is required to establish a nutrient-rich wall. Once again, the effects of heterogeneity dominate the substrate distribution.

4.1.6.8 Case 4 Results (10 m separation distance, two extraction wells)

The results for the fourth case are displayed in Figures 4.14 (e), 4.14 (f), and 4.17. This case features a single injection well centred between two pumping wells, with a well spacing of 10 metres. The acetate contours presented in the cross-sectional maps of Figure 4.17 are quite similar to those illustrated in Figure 4.16. Once again, the symmetrical distribution of acetate and greater overall spread in the Case 4 results are the main differences. Similar to Case 3, the acetate plume is most uniformly distributed between the injection and pumping wells sometime between 720 minutes and 1440 minutes of circulation (Figures 4.14 (e), 4.14 (f), 4.17 (c), and 4.17 (d)).

4.1.6.9 Case 5 Results (15 m separation distance, single extraction well)

The cross-sectional maps for the fifth case are presented in Figure 4.14 (g) and Figure 4.18. This case features a single injection-extraction well pair, separated by a distance of 15 metres. Within the 1440-minute time domain, the acetate does not become uniformly distributed between the two wells. It appears as though the extraction well will likely never capture the injected acetate, even in the most conductive layers. It is hypothesized that the ambient gradient is too great to overcome with a circulation distance of 15 meters.

4.1.6.10 Case 6 Results (15 m separation distance, two extraction wells)

The results for the sixth case are displayed in Figure 4.14 (h) and Figure 4.19. Case 6 features an injection well centred between two extraction wells, with a spacing of 15 metres. The substrate distributions illustrated in the plan view and cross-sectional maps for this case are identical to those presented in Figures 4.14 (g) and 4.18. There is no difference in symmetry or the degree of spread. Once again, the acetate does not become uniformly distributed between the two wells within the 1440-minute time domain due to the powerful ambient gradient. It is clear that a circulating distance of 15 metres is too large for the site.

4.1.6.11 Substrate Dilution

The simulations also provide an indication of how the concentration of the injected acetate changes over the course of the injection-extraction cycle. Figures 4.13 to 4.19 all display a correlation between extended circulation time and increased substrate dilution. This observation is of critical importance to the cross-injection scheme, which requires acetate concentrations to be maximized in order to stimulate the required reactions. Cases 1 and 2, which feature a well separation distance of 5 metres, require less circulating time to evenly distribute the acetate plume between the injection-extraction well pair, thereby minimizing the effects of dilution. Alternatively, the cases corresponding to larger separation distances require extended circulation to uniformly distribute the acetate between the injection and extraction wells. This leads to increased dilution, possibly lowering acetate concentrations

to below an effective range for stimulated in situ denitrification. If a larger well separation distance is selected for future work, increasing the acetate injection concentration and duration should be considered.

4.1.6.12 Comments on the Injection Duration and Concentration

The modelling results suggest that the required injection duration and concentration are dependent on the well spacing. To negate the effects of dilution, larger well separation distances require extended substrate injection periods at elevated concentrations.

Alternatively, shorter injection periods and lower substrate concentrations appear to be sufficient for smaller well separation distances, such as the 5 metre spacing simulated in Cases 1 and 2. In addition to this, the injection concentration and duration are also

dependent on the biology and geochemistry of the subsurface. In particular, the dissolved oxygen concentration and capabilities of the existing biological communities will affect the amount of substrate required. Based on this dependence, commenting on the ideal injection duration and concentration, based on the modelling results alone, is challenging.

However, combining these results with information from the literature provides insight into suitable estimates. Of particular interest is the research of Gierczak et al. (2007), which involved using the cross-injection scheme to stimulate in situ denitrification in a heterogeneous aquifer with nitrate concentrations rivaling those observed at the Woodstock site. Gierczak et al. (2007) performed several acetate injections, with concentrations ranging from 34 mg/L (C:N of 0.7) to 82 mg/L (C:N of 1.6). Results indicated that complete denitrification did not occur until elevated acetate concentrations, equivalent to 2.3 times the stoichiometric requirement, were employed. Based on this, it is hypothesized that an acetate injection concentration of 100 mg/L, consistent with the concentration used in the modelling, will be sufficient to stimulate denitrification at the Woodstock site. This concentration corresponds to approximately three times the stoichiometric requirement. It is concluded, therefore, that the acetate concentration and duration used in the modelling are most likely sufficient to create the desired input pulse,

especially when the injection-extraction well separation distance is small (5 m). However, preliminary field testing is required to test this conjecture.

4.1.6.13 The Ideal Well Configuration

Despite the effects of dilution, it is hypothesized that the scenario described by Case 4 represents the ideal injection-extraction well configuration. This case was selected as it produced a high degree of substrate spreading on either side of the injection well, as opposed to the unsymmetrical distribution created by Case 3. Also, the 10 metre well spacing is less expensive to implement than the 5 metre well spacing. When considering a full-scale treatment system, a well spacing of 10 metres will require half the number of wells required by a 5 metre interval, conserving a great deal of resources. The modelling results also suggest that a 15 metre well separation distance would not be advantageous due to the extreme substrate dilution and inability to overcome the ambient gradient.

4.1.6.14 Sources of Uncertainty

An analysis of model sensitivity was performed to identify which flow and solute transport parameters had a high degree of control over the model output. The concentration data collected during the first tracer test at ports ML12-2, ML12-3, and ML12-4 were used for this analysis. These ports were selected as they had sufficient concentration data to generate complete breakthrough curves. The sensitivity analysis was performed by varying the value of a specific parameter in the model input and determining the outcome of this change in the model output, with particular attention being paid to peak concentrations and arrival times. As part of the analysis, normalized sensitivity coefficients (NSC) were quantified:

$$NSC = \frac{\Delta x}{x_o} * \frac{Y_o}{\Delta Y} \quad (4.1)$$

The NSC computes the sensitivity of x with respect to changes in Y . It is the product of the proportional change in x and the proportional change in Y . For this case, x is the output parameter (peak concentration and arrival time) and Y is the input parameter that was

changed. The results of this analysis are displayed in Table 4.9. Many parameters were examined, including hydraulic conductivity, dispersivity, pumping rate, and effective porosity. For each parameter, the simulation was run using the value listed in Table 4.9, while all other parameters were set according to the calibrated five-layer model.

The grey cells in Table 4.9 highlight NSC values greater than 0.1 and less than -0.1, indicating significant sensitivity. Negative NSC values represent an inverse relationship between the input parameter change and resulting output. The results of the sensitivity analysis suggest that solute transport was particularly sensitive to changes in hydraulic conductivity and porosity, and fairly robust to changes in dispersivity. When the hydraulic conductivity of a particular layer was varied, the breakthrough curves produced for all layers were affected. Alternatively, changing the dispersivity of a particular layer only affected the results produced for that individual layer. The simulation was also quite sensitive to the pumping rate, a very important aspect of the cross-injection scheme.

A qualitative approach was adopted for examining the sensitivity of the model to changes in the ambient hydraulic gradient. The model was run with gradients of 0.001, 0.003, and 0.006. The migration of acetate between the injection-extraction well pair did not substantially change when the gradient was changed from 0.003 to 0.001. Alternatively, the elevated gradient resulted in the transport of mass away from the well pair. Despite this, however, the model output still met the criteria of a successful injection-extraction scheme (Section 4.1.6.4). This is because an arc of elevated acetate concentration still spanned the injection-extraction well pair to form a nutrient-rich wall, located just downgradient of the well alignment.

4.1.6.15 Model-Based Recommendations for the Treatment System

The modelling concluded that the well configuration represented by Case 4 provided the most positive results. This configuration, which includes a single injection well, two extraction wells, and a separation distance of 10 metres, achieves an ideal balance between

cost effectiveness and an ability to generate successful solute transport between the injection-extraction well pair. Based on the modelling, it is recommended that the full-scale treatment system mimic this configuration. For preliminary testing, however, a smaller well spacing may prove useful. The smaller separation distance means that shorter injection and extraction durations are required to evenly distribute the substrate between the wells, which ultimately means that less mass is needed for the injection. Therefore, a smaller scale system with a well spacing of 5 metres is recommended for preliminary testing of the bioremediation potential of the aquifer.

In addition, a further recommendation involves the use of a packer system to promote even vertical mixing of the injected acetate. It is clear from Figures 4.13 to 4.19 that the acetate has a much wider spread in the top half of the aquifer than in the bottom half. Using a packer system to isolate these two sections from each other may hold the solution to this problem. Once the packer system is deployed, lower injection and extraction rates could be employed in the upper portion of the aquifer, slowing the horizontal spread of acetate. At the same time, higher injection and extraction rates used in the lower portion of the aquifer could stimulate faster horizontal spreading. The overall effect would likely be a more uniform distribution of acetate with depth.

4.1.7 Estimating the Hydraulic Conductivity Profile

The average hydraulic conductivity estimates generated from the grain size analysis, borehole flowmeter tests, conventional slug tests, tracer tests, and the calibrated 5-layer model are summarized in Table 4.10. Note that a comparison of the individual values is inappropriate due to inconsistent averaging. While the averages generated from the grain size analysis, borehole flowmeter tests, conventional slug tests, and calibrated 5-layer model take the entire aquifer profile into account, the tracer test averages only reflect the highest-K layers that dominated tracer movement. Therefore, Table 4.10 provides only a summary of the data and should not be used for comparison purposes. The presented K values feature a range spanning two orders of magnitude, which can be accounted for by

the various scales of investigation, the different testing locations throughout the study site, and the variety of individual subsurface units that were examined within the aquifer. All estimates presented in Table 4.10 fall within the expected conductivity range for aquifer materials (sands and gravels) and correlate well with the core logs.

Figure 4.20 provides a visual representation of the hydraulic conductivity profiles generated with data from the grain size analysis, borehole flowmeter testing, tracer testing, and the calibrated 5-layer model. Note that instead of plotting absolute conductivity values, normalized values (K_i/K) were employed, where K_i is an individual hydraulic conductivity estimate in a particular dataset and K is the average hydraulic conductivity of that dataset. This plotting method revolves around ideas presented by Moltz et al. (1989), which suggest that many of the errors related to various methods of data analysis are multiplicative in nature and, therefore, cancel out upon normalization. The profiles generated by the various methods do not appear to match up particularly well. One source of discrepancy may be the degree of detail used for each method. The grain size analyses were performed on core subsamples taken at an interval of twenty to thirty centimeters, flowmeter testing was performed at an interval of only 10 centimeters, and the tracer test results were collected at multi-level sampling ports with a vertical spacing of 1.7 metres. Furthermore, the vertical profiles represent many different locations throughout the study site, and therefore, cannot be expected to correlate perfectly.

Based on the core logs, electrical resistivity surveys, and all available hydraulic conductivity data, it appears as though the aquifer consists of a variably conductive multi-layered system, with K -values ranging over nearly four orders of magnitude. Considering the applications of this study, the relative profile is likely best described using the tracer test results, which describe actual solute transport through the subsurface, and are therefore most relevant to the acetate injections. Depending on the degree of detail examined, these results reveal a 4- to 6-layer system, featuring a lower- K zone near the surface, underlain by a zone of very high permeability, underlain again by another lower- K zone, and bounded on

the bottom by a second relatively high-K zone. Also important to consider is the calibrated model, which depicts a 5-layer aquifer system. The model layers feature a realistic range of hydraulic conductivity and dispersivity values. In addition, the model output displays a strong resemblance to field data collected during the first trace test.

In summary, the relative hydraulic conductivity profile appears to be composed of a complex 4- to 6-layer aquifer system with alternating low- and high-K layers. Of particular interest is the highest hydraulic conductivity layer, which straddles a depth of approximately 290 masl. This layer was the main conduit for tracer transport and is therefore anticipated to play a major role in the distribution of the injected acetate. Note that the tracer tests may have missed an important K-layer at an elevation of approximately 294 masl. The borehole flowmeter tests and grain size analyses corresponding to Cores 1 and 2 support this.

4.1.7.1 The Hydrogeologic Conceptual Model

Data collected from the core logs, electrical resistivity surveys, grain size analysis, borehole flowmeter tests, conventional slug tests, tracer tests, and the calibrated 5-layer model were used to develop the hydrogeologic conceptual model for the study site (Figure 4.21). While these sources of information were all examined, emphasis was placed on the core logs, grain size analysis, tracer testing, and calibrated 5-layer model during conceptual model development.

Initially, the vertical limits of the model were defined. The water table delineates the upper limit and was calculated to be 297.57 masl based on monthly manual water level measurements taken at well WO74-WT over the year of 2008. A lower limit of 281.50, marking the top of the underlying clay aquitard, was originally suggested based on the WO74-D and WO75-D core logs. This estimate, however, was later refined to 283.00 masl due to the unresponsive nature of the deeper multi-level sampling ports, thought to be screened in the aquitard. Following this, the domain was broken into six distinct layers

based on the tracer test and three-dimensional modelling results. Particular emphasis was placed on the ML5 and ML6 breakthrough curves observed during the second forced gradient tracer test. The complete nature of these curves made it possible to track changes in solute transport behaviour with depth. The final step involved assigning hydraulic conductivity values to these six aquifer layers. For this step, all available grain size analysis, modelling, and tracer test data were amalgamated for each layer.

The resulting hydrogeologic conceptual model is illustrated in Figure 4.21. The first layer, spanning 297.60 masl to 294.50 masl, is dominated by sand and features a hydraulic conductivity of 4.8×10^{-4} m/s. The second layer, located between 294.50 masl and 292.50 masl, is also composed mostly of sand and exhibits a K-estimate of 1.6×10^{-3} m/s. Spanning 292.50 masl to 290.50 masl, the third layer features an elevated hydraulic conductivity of 5.9×10^{-3} m/s and is composed of sand and gravel. The fourth layer, located between 290.50 masl and 289.40 masl, boasts the highest hydraulic conductivity value of 1.9×10^{-2} m/s and appears to be composed of clean gravel. As previously mentioned, this layer is anticipated to play a major role in the distribution of injected acetate in the next phase of this research. From 289.40 masl to 285.00 masl, the fifth layer mimics the second layer, featuring a K-estimate of 1.2×10^{-3} m/s and an abundance of sand. Finally, the sand and gravel dominated sixth layer, spanning 285.00 masl to 283.00 masl, features increased flow and a K-estimate of 4.9×10^{-3} m/s.

Note that this representation of the model only spans wells ML5, ML6, ML7, and ML8, covering a section of aquifer that was thoroughly examined during the second forced gradient tracer test. The layers of the conceptual model are assumed to be present throughout the study site, however, although natural spatial variability clearly exists across the coring and testing points. This variability is best illustrated by the core logs. It is important to emphasize that up-scaling the injection-extraction scheme to support well separation distances of 10 to 15 meters may be critically influenced by this spatial variability. To accommodate this, the conceptual model may require future refinement.

4.1.7.2 Implications of the K Profile on Stimulating In Situ Denitrification

The aquifer properties, especially the vertical distribution of horizontal hydraulic conductivity, control the subsurface migration and dispersal of injected solutes. It is well established that a heterogeneous conductivity profile will yield a heterogeneous solute distribution. At the Woodstock site, this phenomenon was clearly demonstrated by the uneven nature of the tracer test breakthrough curves and the three-dimensional modelling results. In terms of the acetate injections, this means that not all aquifer areas will receive an equal dose of acetate. The higher-K layers will have a greater capacity to transport acetate mass than the lower-K layers, leading to an anticipated uneven distribution of stimulated denitrification with depth. Based on this, it is hypothesized that the high-K layers will exhibit greater denitrification rates than the low-K layers. If this is the case, the use of packer system may be required to even out the acetate distribution. This technique was previously discussed in Section 4.1.6.15.

A secondary consideration that may challenge the previous hypothesis is the transport of dissolved oxygen through the aquifer of interest. In the same way the high-K layers dominate the movement of acetate, dissolved oxygen is also preferentially transported through these layers. As previously mentioned, denitrification is an anaerobic reaction that will only occur in the absence of oxygen. Therefore, the excess flow of dissolved oxygen through the high-K zones may counteract the effects of increased acetate concentrations.

In summary, the hydraulic conductivity profile is one of the most important factors controlling the spread of acetate in the aquifer. For this reason, multiple lines of evidence, including grain size analyses, borehole flowmeter tests, conventional slug tests, tracer tests, and modelling, were relied upon for its estimation. Following a thorough geochemical characterization, the clear next step is a pilot-scale acetate injection. This is the only concrete way to qualitatively and quantitatively determine how the hydraulic conductivity profile will affect the stimulation of in situ denitrification.

4.2 Geochemical Characterization

4.2.1 Quality Assurance and Quality Control (QA/QC)

Several QA/QC procedures were employed to ensure accurate geochemical data. At the field level, a minimum of three well volumes were purged prior to sampling, ensuring the collection of formation water. Also, as mentioned throughout Section 3.8, many duplicate field samples were collected for each parameter to ensure measurement precision. This involved collecting two groundwater samples simultaneously from the same sampling location and under identical conditions. Using de-ionized water, field and laboratory blanks were also collected and analyzed. In addition, several standards were incorporated into each analysis to monitor accuracy. These standards spanned the sample concentrations and were run multiple times throughout analysis. Unfortunately, a charge balance could not be performed as a complete ion analysis was not performed at a single specific time. Overall, all duplicate samples were found to be within 10 percent of each other, all standards were determined to be within a maximum of 15 percent of target concentrations, and all field and lab blanks had concentrations below the detection limit for each analysis method.

4.2.2 Anion Samples

Background nitrate, nitrite, sulphate, chloride, bromide, and acetate concentration results from ion samples collected between the winters of 2007 and 2009 are summarized in chronological order in Table F.1 (Appendix F). The arithmetic mean for all nitrate samples is 13.0 mg-N/L, with a standard deviation of 2.6 mg-N/L. In addition, the arithmetic means for all sulphate and chloride samples are 32.9 mg-SO₄/L and 38.1 mg-Cl/L, with standard deviations of 5.2 mg-SO₄/L and 10.5 mg-Cl/L, respectively. All nitrite, bromide, and acetate samples yielded concentrations below the detection limit of 0.5 mg/L.

Overall, the concentration profiles produced from the multi-level well data are fairly uniform with depth for all ion species. The typical profile features a nearly straight vertical line hovering around the ion concentration average, suggesting a fairly homogeneous geochemical system. Contradicting this conjecture, however, are two clear exceptions. The

ion concentration profiles produced by the WO74-ML and ML5 data feature much lower ion concentrations closer to ground surface than at depth. The shallow installation of both WO74-ML and ML5 allowed for the detection of this phenomenon. All other multi-level wells were installed approximately one to two metres deeper and, as a result, missed this occurrence. A comparison of ion concentration profiles corresponding to WO74-ML, ML5, and ML10 is displayed in Figure 4.22. The plot relating to ML10 was included to represent the typical profile. It is clear that nitrate, sulphate, and chloride concentrations above an elevation of approximately 295 masl are much lower than those below this elevation. Perhaps this unique geochemical signature is the first indication of BMP success within the saturated zone. Natural in situ denitrification has been ruled out due to elevated dissolved oxygen concentrations, which are discussed further in Section 4.2.4. In summary, the aquifer of interest appears to be fairly uniform with respect to geochemistry below an elevation of 295 masl. Above this point, however, ion concentrations are much lower, indicating the presence of cleaner water.

4.2.3 Cation Samples

Background calcium, aluminum, silicon, manganese, and iron concentration results from samples collected in the winter of 2009 are summarized in Table F.2 in Appendix F. The arithmetic means for the calcium and silicon samples are 104.0 mg/L and 5.9 mg/L, with standard deviations of 3.5 mg/L and 0.3 mg/L, respectively. The manganese results produced only one measurable concentration of 0.1 mg/L corresponding to ML5-8. All other manganese samples yielded concentrations below the lowest quantifiable concentration of 0.01 mg/L. In addition, all aluminum and iron samples yielded concentrations below their corresponding lowest quantifiable concentrations of 0.02 mg/L and 0.1 mg/L, respectively.

Similar to the anion profiles, the ML5 and ML8 calcium and silicon concentrations are fairly uniform with depth. The main deviation corresponds to shallow calcium concentrations recorded at ML5. ML5-1 and ML5-2 features calcium values of 112.0 mg/L and 96.3 mg/L, respectively. These concentrations differ from the mean value by approximately 8 mg/L. All

other calcium concentrations differ from the mean by less than 5 mg/L. This trend is faintly present in the silicon data, where the ML5-1 concentration features the largest deviation from the mean of 0.9 mg/L. Overall, however, all calcium and silicon concentrations are quite similar, suggesting a uniform geochemical profile with respect to the cation species.

4.2.4 Alkalinity, Dissolved Oxygen, and Other Field Parameters

A series of alkalinity, dissolved oxygen, electrical conductivity, and pH measurements were taken at multi-level bundles ML5, ML6, ML7, and ML8 over the winter, spring, and summer of 2009. This information is graphically displayed in Figure 4.23 and summarized in chronological order in Table F.3 (Appendix F). Note that the electrical conductivity values have been corrected for temperature. The alkalinity measurements feature a mean value of 267.2 mg/L, with a standard deviation of 10.6 mg/L; the dissolved oxygen values revolve around a mean value of 8.7 mg/L, with a standard deviation of 1.4 mg/L; and the electrical conductivity and pH measurements have mean values of 550.7 uS and 7.3, with standard deviations of 36.3 uS and 0.1, respectively.

The alkalinity and pH values are quite uniform with depth. The pH values form almost a perfect vertical line, while the alkalinity measurements are more scattered around the mean value. Both profiles indicate near geochemical homogeneity. Alternatively, the electrical conductivity measurements increase with depth and the dissolved oxygen profile is quite irregular. Dissolved oxygen is extremely hard to accurately measure due to atmospheric exposure and, as a result, consistent oxygen values cannot always be expected. The oxygen range of 6.4 to 12.5 presented here is thought to be reasonable, especially considering the number of different depths and locations represented. Despite the increase in conductivity with depth and the irregularity of the oxygen profile, a generally uniform profile is once again suggested by these data.

The elevated dissolved oxygen values are of particular importance to the in situ bioremediation experiment as denitrification is an anaerobic process. The background

estimates are close to atmospheric saturation and portray a highly aerobic aquifer. For denitrification to be successfully stimulated, nearly all of this oxygen must be consumed by indigenous bacteria. Eliminating the oxygen will be one of the most challenging aspects of this experiment.

4.2.5 Nitrous Oxide

Background nitrous oxide concentration samples were collected from ML8 in July of 2009. The results from this sampling are summarized in Table F.4 in Appendix F. Seven samples were collected and analyzed for nitrous oxide. A mean value of 37.8 $\mu\text{g-N/L}$ and standard deviation of 2.1 $\mu\text{g-N/L}$ were calculated for this dataset. The nitrous oxide values seem to be fairly uniform with depth. Data from additional multi-level wells, however, are required to confirm this general observation.

Nitrous oxide isotope samples were collected from the ports of ML8 for background analysis on July 13, 2009 as well. For the purposed of this work, only one of these samples was analyzed for $\delta^{15}\text{N}$ and $\delta^{18}\text{O}$ in nitrous oxide. This sample corresponded to ML8-3 and produced $\delta^{15}\text{N}$ and $\delta^{18}\text{O}$ estimates of -14.9 ‰ and 34.0 ‰, respectively.

4.2.6 ^{15}N and ^{18}O in Nitrate

Water samples collected in August and September of 2007 and in March of 2009 were analyzed for background values of $\delta^{15}\text{N}$ and $\delta^{18}\text{O}$ in nitrate. This information is displayed in Table F.5 in Appendix F. The 2007 values were collected and reported by Koch (2009) and feature data from multiple wells, all within an approximate 500 m radius of the study site. Alternatively, the 2009 values were generated from samples collected at ML5, directly within the study site limits. The mean $\delta^{15}\text{N}$ and $\delta^{18}\text{O}$ values are 6.3 ‰ and 1.3 ‰, with standard deviations of 0.7 ‰ and 1.1 ‰, respectively. Overall, the 2007 and 2009 datasets are very similar for both $\delta^{15}\text{N}$ and $\delta^{18}\text{O}$ in nitrate, suggesting a uniform isotopic signature in both space and time.

The background 2007 and 2009 $\delta^{15}\text{N}$ and $\delta^{18}\text{O}$ values are plotted in Figure 4.24, which also displays the limits of various nitrate source categories. The ^{15}N and ^{18}O isotope fractionation associated with the 2007 and 2009 samples is consistent with the NH_4^+ fertilizer source range. This is with the exception of one data point corresponding to ML5-1. The NH_4^+ fertilizer range suggests that the nitrate contamination at the Woodstock site stems mainly from a commercial fertilizer. Note, however, that the data points form a cluster towards the enriched section of this range, perhaps suggesting a small degree of mixing between commercial fertilizer and manure nitrate sources (Koch, 2009).

4.2.7 Tritium-Helium Age Dating

The tritium-helium analysis yielded groundwater ages of 5.88 ± 0.56 years for WO40, 5.95 ± 0.59 years for WO35, and 11.47 ± 0.73 years for WO12, revealing relatively young groundwater. It appears that the youngest groundwater corresponds to the wells located further upgradient, potentially closer to a main recharge area. Alternatively, the older water corresponds to WO12 which is located much further downgradient, away from the recharge area. These ages are consistent with the findings of Sebol (2004), who also studied tritium-helium ages across the Woodstock site. She indicated the presence of young groundwater, with all samples producing ages of less than ten years.

4.3 Implications of the Lateral Nitrate Flux through the Treatment Zone

The calculation behind the nitrate mass flux estimates for Thornton Wells 01, 03, 05, 08, and 11 is presented in Table 4.11. In accordance with the table headings, these values were computed using average aqueous nitrate concentration records from 1999 to 2006 and average 2008 flow rates for each supply well. Combining the five individual supply well estimates produced a total mass flux of 16.2 metric tons of nitrate (as nitrogen) per year. This value was then compared to the lateral nitrate mass flux values associated with the six aquifer layers of the hydrogeologic conceptual model. The mass flux calculations and comparisons for the individual layers are summarized in Table 4.12. The total mass flux through the window of interest and across all six layers is 3.76 metric tons of nitrate (as

nitrogen) per year. This translates to approximately 23 percent of the total flux produced by the supply wells. In the context of a remediation strategy, this percentage is substantial. The nitrate mass flux calculations suggest that if a 54-m wide section of the aquifer is targeted with a successful in situ bioremediation strategy, the total nitrate mass produced by the supply wells should theoretically decline by up to 23 percent. At the Woodstock site, this 23 percent would likely be the difference between pumping groundwater with nitrate concentrations above the MAC and pumping water with acceptable concentrations. Note that this percentage seems quite high when you consider the small size of the 54-m wide window in comparison to the entire capture zone of the well field. The elevated percentage may be the result of the hydraulic conductivity values included in this calculation. These values were determined from the tracer tests, grain size analysis, and three-dimensional modelling, which focused directly on the grid of multi-level wells. Perhaps this section of the aquifer is a great deal more conductive than other sections included in the 54-m wide window. Further research and the installation of additional wells spanning the entire window would be required to confirm this hypothesis. Despite this seemingly elevated percentage, the calculation confirms that a full-scale in situ bioremediation strategy has the potential to effectively address the persistent nitrate problems of the Thornton Well Field.

4.4 Cross-Injection Experiments

4.4.1 Results from Injection Phase 1

The first injection phase featured a single 6-hour injection effort driven by wells WO78 and WO79. A number of groundwater samples were collected from ML5, ML6, ML7, and ML8 for analysis of anions, cations, N₂O concentration, N₂O isotopes, and NO₃ isotopes. Upon examining the first round of anion data from ML7, it became clear that the injection effort failed to stimulate in situ denitrification. As a result, sample analysis was largely halted to conserve both time and money. For this reason, only partial datasets corresponding to anion analysis, cation analysis, N₂O concentration analysis, and N₂O isotope analysis are available to present and discuss.

The ML7 bromide, acetate, nitrate, and nitrite concentrations are plotted relative to experiment time in Figure 4.25 and listed in Table G.1 (Appendix G). The bromide and acetate breakthrough curves display very similar shapes and peak arrival times for the seven ports. Alternatively, the peak arrival concentrations are quite different. This is consistent with the results of the natural gradient tracer test and can be attributed to the consumption of acetate by subsurface microorganisms. Also consistent with the tracer test results is the irregular assortment of peak concentrations and arrival times for the seven ports. The curves corresponding to ML7-3, ML7-4, ML7-5, and ML7-7 all reach peak breakthrough following approximately 7 hours of testing. Despite this similarity, however, the peak concentrations for these ports vary substantially for both acetate and bromide. The curves representing ML7-3 and ML7-4 reach the highest bromide C/C_o values of 0.9 to 1.0, while the curves corresponding to ML7-5 and ML7-7 only reach bromide C/C_o values of approximately 0.6 and 0.3, respectively. The peak arrival times at ML7-2 and ML7-6 are delayed relative to these four ports, while no visible peak is present at all for ML7-1. Similar to the results of the three tracer tests, the peak concentrations and arrival times corresponding to the ML7 bromide and acetate data suggest a heterogeneous aquifer profile, composed of four to six distinct layers. The bromide and acetate breakthrough curves also reveal that the greatest acetate consumption is associated with the most permeable layers. This is most apparent from the curves representing ML7-3 and ML7-4, which display a large difference between peak bromide and acetate concentrations.

The nitrate and nitrite plots displayed in Figure 4.25 mimic those produced by background data. The nitrate values feature a mean of 14.7 mg-N/L and standard deviation of 1.1 mg-N/L. This mean value is higher than the background estimate of 13.0 mg-N/L; however, it still falls well within the background range of values. In addition, all ML7 nitrite samples yielded concentrations below the detection limit of 0.5 mg/L, as was observed for the background samples. The nitrate and nitrite data collected during the pilot acetate injection provide absolutely no evidence of in situ denitrification.

Calcium, aluminum, silicon, manganese, and iron concentration results from samples collected during the pilot acetate injection are summarized in Table G.2 in Appendix G. The post-injection arithmetic means for the calcium and silicon samples are 115.4 mg/L and 5.7 mg/L, respectively. These estimates are nearly identical to background values. This consistency is also observed in the aluminum, manganese, and iron datasets, which feature estimates below the detection limit for both the background and injection experiment concentrations. The similarity between the pre- and post-injection cation data supports the notion that no in situ denitrification was stimulated by the pilot acetate injection.

Table G.3 in Appendix G lists the nitrous oxide concentration data collected during the initial acetate injection. The mean value of this dataset is 35.4 $\mu\text{g-N/L}$, with a standard deviation of 2.9 $\mu\text{g-N/L}$. These estimates are very close to the background mean and standard deviation values of 37.8 $\mu\text{g-N/L}$ and 2.1 $\mu\text{g-N/L}$, respectively. In addition, no significant change was noted in the nitrous oxide isotope data, listed in Table G.4 in Appendix G. This table compares the single background sample collected at ML8-3 with three samples collected from ML5-4 at experiment times of 4.3, 8.5, and 15.4 hours. Consistent with all data collected during this initial injection phase, all nitrous oxide $\delta^{15}\text{N}$ and $\delta^{18}\text{O}$ values are nearly identical.

In summary, the anion, cation, and nitrous oxide concentration and isotope data collected during and following the first acetate injection phase provide no indication of stimulated in situ denitrification. Nearly all values remained within the range of background estimates. Following this effort, it was clear a second injection phase, featuring multiple, repetitive acetate injections at higher concentrations, would be required to more completely consume the dissolved oxygen within the aquifer and support the growth of denitrifying populations.

4.4.2 Results from Injection Phase 2

The second injection phase included 19 injections over 26 days and consisted of three main stages, including: (I) daily injections 2 to 12, (II) comprehensive injection 13, and (III)

injections 14 to 20, taking place every other day (refer to Table 3.5 for summary of all injections). The first stage was required to promote microbial consumption of dissolved oxygen directly within the experiment vicinity and to support the growth and development of denitrifying populations. The second stage, consisting of the thirteenth injection, included detailed groundwater sampling for a period of approximately 25 hours, providing snapshots of aquifer geochemistry relative to space and time. Finally, the third stage was utilized to determine whether a 2-day injection interval could sustain stimulated in situ denitrification following the establishment of denitrifying populations. The results of these three stages are discussed below in sections dedicated to specific parameters. Throughout the discussion, particular emphasis is placed on injection 13, which produced the greatest amount of chemical data and insight into subsurface processes.

4.4.2.1 Oxygen Monitoring Throughout Injection Phase 2

Dissolved oxygen is one of the most important parameters controlling subsurface chemical reactions, especially anaerobic denitrification. As previously discussed, nearly all dissolved oxygen within the highly aerobic target aquifer must be consumed before stimulated denitrification can occur. The dissolved oxygen concentrations collected before, during, and following the second injection phase are tabulated in Table H.1 (Appendix H) and plotted in Figure 4.26. These numbers represent point concentration measurements corresponding to the ports of ML7. Multi-level bundle ML7 was selected for detailed monitoring based on its location, 5 metres downgradient of the injection-extraction plane. It was hypothesized that, if oxygen monitoring was performed too close to the injection-extraction wells, there would not be sufficient space or time available for the required mixing and reactions to occur. It was also thought that background chemistry would overwhelm the monitoring if it was performed too far from the injection-extraction plane. With this in mind, a downgradient distance of 5 meters was selected for oxygen monitoring. Prior to evaluating the data, it is important to note the oxygen concentrations were measured directly following each injection. Therefore, the results may be elevated due to the relatively high oxygen concentration of the injectate.

Figure 4.26 indicates the oxygen concentrations began to decline in the first injection stage, between September 16 (injection 4) and September 18 (injection 6). This confirms the hypothesis that several consecutive injections are required to facilitate oxygen consumption and bacterial acclimation. In general, the dissolved oxygen concentrations remained quite low, ranging between 0 and 4 mg/L, until the injection on September 25 (injection 13). During this injection, the concentrations partially rebounded, reaching values between 4 and 6 mg/L. This phenomenon is also observed on September 15 (injection 3), when concentrations reached peak values ranging from 9 to 12 mg/L. Coincidentally, these two dates represent the only injections of both acetate and bromide. It was originally hypothesized that the increased mixing required to dissolve both acetate and bromide in the injectate may have resulted in elevated dissolved oxygen values. This explanation is questionable, however, due to the relative injection rates of the mixed solution (0.2 L/min) and the circulating water (200 L/min). As a secondary hypothesis, perhaps the elevated ion concentrations resulting from the injection of both potassium bromide and sodium acetate negatively affected the bacterial populations responsible for dissolved oxygen consumption. The high ion concentrations may have created a more saline environment which the bacteria were not accustomed to, slowing or arresting cellular respiration. Whatever the mechanism, mechanical or biochemical, it is clear the injections corresponding to both bromide and acetate resulted in elevated oxygen concentrations.

The third stage of acetate injections (injections 14 to 20) feature diminished oxygen levels, once again ranging from approximately 0 to 4 mg/L. These values mimic those produced in the first injection stage, providing evidence that an injection interval of every other day is sufficient following the establishment of proper bacterial populations. It is also possible that denitrifying conditions could have been initially established with a pulsing interval of every other day, although another injection phase would be required to test this hypothesis. Following the final injection on October 9, the dissolved oxygen concentrations increased towards background levels. The rebound was slower than anticipated, however, with

oxygen concentrations reaching a maximum of only 6.6 mg/L following ten days of recovery. This suggests the reducing capacity of the aquifer sediment may have increased during the 26-day injection period.

Figure 4.26 also indicates that the oxygen concentrations corresponding to ports ML7-3, ML7-4, and ML7-7 were higher than those representing the other ports throughout the entire duration of Injection Phase 2. The average dissolved oxygen concentrations for these three ports, over a period spanning September 10 to October 19, were between 4.2 and 4.8 mg/L. Alternatively, the averages corresponding to ports ML7-1, ML7-2, ML7-5, and ML7-6 over the same time period ranged from 2.2 to 3.4 mg/L. Based on tracer test data and other hydraulic testing results, it is thought that ports ML7-3, ML7-4, and ML7-7 represent the high-K zones, while ports ML7-1, ML7-2, ML7-5, and ML7-6 represent lower-K units within the aquifer. The dissolved oxygen concentrations appear to have been affected by the K-profile.

4.4.2.2 Injection 13: Subsurface Distribution of Acetate and Bromide

Injection 13 involved the addition of both acetate and bromide and featured a 25-hour sampling period to track their migration within the aquifer. The results from this effort are displayed in Figures 4.27 and 4.28. Figure 4.27 features cross-sectional bromide and acetate concentration contour plots along the line of multi-level wells at an experiment time of approximately 7.5 hours. In addition, Figures 4.28 (a) and (b) feature bromide and acetate breakthrough curves for the ports of ML7, respectively. All raw concentration information is summarized in Table H.2 (Appendix H).

Figure 4.27 clearly displays a plunging acetate and bromide plume within principle high-K layer. At a lateral distance of one metre, the highest concentrations are located at an elevation of approximately 294 masl. Alternatively, at a lateral distance of seven metres, these concentrations correspond to an elevation of approximately 290 masl, a vertical difference of four metres. It is hypothesized that density effects may explain this migration

pattern within the fast flowing unit. The elevated solute concentrations in this layer likely produced a high-density plume, which descended under the force of gravity as it travelled with the natural gradient. If this is the case, lower bromide concentrations should be considered for future testing. As alternate hypotheses, perhaps the hydrostratigraphic units within the aquifer are dipping or the deep municipal wells are introducing an element of vertical flow. Additional work is needed to evaluate these possibilities more thoroughly, however, before firm conclusions can be made. In addition to the plunging plume, Figure 4.27 also illustrates aquifer heterogeneity. The concentration contours depict a layered system with alternating higher- and lower-K units. Further discussion regarding this heterogeneity is presented in reference to the breakthrough curves displayed in Figure 4.28.

The ML7 bromide and acetate breakthrough curves illustrated in Figure 4.28 display very similar shapes and peak arrival times, while peak concentrations are quite different. Once again, this can be attributed to the consumption of acetate by subsurface microorganisms. Also consistent with the tracer test results is the irregular assortment of peak concentrations and arrival times for the seven ports. Of particular interest are the peaks corresponding to ML7-3, ML7-4, and ML7-7, which feature very rapid peak arrival times and high concentrations. While ports ML7-3 and ML7-4 were also highly active during the first injection phase, ML7-7 did not display this behaviour. Perhaps the initial 11 injections of Phase 2 altered the subsurface system by further developing the immediate area surrounding injection well WO79. Regardless of the reason, ML7-3, ML7-4, and ML7-7 clearly correspond to extremely fast flowing layers. This observation correlates well with the hydrogeologic conceptual model presented in Figure 4.21. Interestingly, despite transporting the largest amount of acetate mass, these units maintained elevated oxygen concentrations throughout the second injection phase, suggesting continual oxygen replenishment via the rapid groundwater flow.

The breakthrough curves corresponding to ports ML7-5 and ML7-6 are nearly identical with respect to both peak concentration and arrival time. This observation confirms that

consecutive ports ML7-5 and ML7-6 represent the same hydrogeologic unit, as indicated in the site conceptual model. The ML7-2 breakthrough curves are similar to those produced by ML7-5 and ML7-6 in terms of peak concentration; however the peak arrival time is approximately five hours delayed. The final port, ML7-1, features consistent bromide and acetate concentrations throughout the sampling period, hovering around C/C_o values of 0.1 to 0.2. This amount of acetate mass is very small, especially in comparison to the levels observed at the other ports. Despite this, ML7-1 featured the lowest dissolved oxygen concentrations throughout the second injection phase, with many measurements being less than 1.0 mg/L, suggesting the successful establishment of reducing conditions.

In summary, the cross-sectional contour plots and ML7 bromide and acetate breakthrough curves produced by injection 13 support the hydrogeologic conceptual model of a heterogeneous, multi-layered aquifer system. In addition, a comparison of the breakthrough curves and dissolved oxygen data suggests that a high acetate mass flux does not necessarily translate to the successful establishment of reducing conditions in a highly aerobic aquifer.

4.4.2.3 Injection 13: The Fate of Nitrous Oxide

Nitrous oxide concentrations were monitored during the comprehensive sampling effort which took place during and directly following injection 13. Samples were collected from ML5, ML6, ML7, and ML8 at four depths of interest. These depths were selected to represent a wide range of aquifer K-values. Depth 1 corresponds to ports ML5-2, ML6-1, ML7-1, and ML8-1 and represents a known low-K unit; Depth 2 corresponds to ML5-3, ML6-2, ML7-2, and ML8-2 and represents a mid-range-K layer; Depth 3 corresponds to ML5-5, ML6-4, ML7-4, and ML8-4 and represents a known high-K unit; and finally, Depth 4 corresponds to ML5-7, ML6-6, ML7-6, and ML8-6 and represents a second mid-range-K layer. Two samples were collected at each of these ports, representing experiment times of approximately 5.5 and 9.5 hours. The nitrous oxide concentration results are graphically displayed in Figure 4.29 and listed in Table H.3 (Appendix H). Note that the mean value of

this dataset is 18.8 $\mu\text{g-N/L}$, with a standard deviation of 14.3 $\mu\text{g-N/L}$. This mean value is much lower than both the background mean (37.8 $\mu\text{g-N/L}$) and the mean generated by the results of the first injection phase (35.4 $\mu\text{g-N/L}$). The decreased dissolved oxygen and nitrous oxide values imply that Injection Phase 2 was able to alter the redox conditions of the target aquifer. However, due to the presence of dissolved oxygen at concentrations greater than 1 mg/L, the achievement of full reducing conditions remains uncertain.

Overall, Figure 4.29 suggests the N_2O concentrations decreased significantly in the low-K and mid-range-K layers. This is consistent with the oxygen dataset, which portrays lower oxygen levels in the slower moving layers. With this in mind, it is thought that these lower-K units achieved reducing conditions during Injection Phase 2, resulting in the conversion of all available N_2O to nitrogen gas. Alternatively, it appears as though the high-K layer depicted in Figure 4.28 has maintained N_2O concentrations similar to background values. The oxygen values measured at this depth also reflect background concentrations. It is hypothesized that the injection scheme was unable to generate reducing conditions in this layer and therefore, N_2O reduction was not possible. Note there are a few clear exceptions to the N_2O concentration observations, perhaps suggesting a higher degree of heterogeneity than originally anticipated.

4.4.2.4 Injection 13: The Fate of Manganese, Iron, and Sulphate

During the stimulation of in situ denitrification, it is possible to provide subsurface microorganisms with excess substrate, resulting in the development of various redox zones. Once oxygen and nitrate become depleted, the microbes rely on manganese (IV), iron (III), sulphate, and finally carbon dioxide as terminal electron acceptors (Appelo and Postma, 2005). These processes can release manganese (II), iron (II), HS^- , and CH_4 into solution, potentially degrading water quality. Due to the close proximity of this research to municipal production wells, manganese, iron, and sulphate concentrations were closely monitored during and following the acetate injections. The manganese, iron, and other cation concentration data accompanying the second injection phase are displayed in Table H.4

(Appendix H). In addition, sulphate numbers are presented in Table H.2 (Appendix H). All manganese, iron, and sulphate numbers remained very similar to background values throughout the duration of Injection Phase 2, indicating the redox environment was never pushed past denitrifying conditions by the addition of acetate.

4.4.2.5 Injection 13: The Fate of Nitrate and Nitrite

Figure 4.30 graphically displays the nitrate and nitrite concentration data collected from ML7 over the 25-hour sampling period accompanying injection 13. In addition, all results are summarized in Table H.2 (Appendix H). This information confirms varying degrees of denitrification were stimulated within the aquifer. In general, the concentrations collected from the high-K units indicate limited denitrification, while the information gathered from the lower-K units suggests nearly complete denitrification. This observation is consistent with the dissolved oxygen and nitrous oxide results. Note that all nitrate concentration reductions are assumed to be the result of stimulated in situ denitrification as opposed to the effects of dilution since the injection-extraction circulation cycle was driven by high nitrate aquifer water.

Consistent with expectations based on the dissolved oxygen data, the least denitrification occurred at depths corresponding to ports ML7-3, ML7-4, and ML7-7. The nitrate concentrations at these ports over the 25-hour sampling period ranged from approximately 11.2 to 14.0 mg-N/L, falling within the span of background values. Despite this, the elevated nitrite concentrations establish that some denitrification did occur. These values, collected over the same 25-period, ranged from 0.9 to 2.1 mg-N/L. Prior to this experiment, absolutely no nitrite was observed at the study site, confirming that this limited range is a definite change. It is clear the layers corresponding to ports ML7-3, ML7-4, and ML7-7 feature very high hydraulic conductivity estimates. Although there is proof of some limited in situ bioremediation, it appears the rapid groundwater flow through these units prevented the establishment of anaerobic conditions due to the constant influx of dissolved oxygen and brief acetate residence times. For the in situ treatment system to be effective,

these fast flowing units, which transport the majority of the nitrate mass, must be more aggressively stimulated. This issue is further addressed in Section 4.5.

The results collected at ports ML7-2, ML7-5, and ML7-6 are more positive in terms of nitrate reduction. The NO_3^- concentrations at these ports over the 25-hour sampling period ranged from 2.9 to 9.4 mg-N/L and featured an average value of 7.0 mg-N/L. This average concentration is 46 percent lower than the mean background concentration of 13.0 mg-N/L, indicating denitrification was successfully stimulated at these depths. Despite this achievement, however, a great deal of nitrite was generated, suggesting denitrification did not proceed to completion. The nitrite values generated at these three ports ranged from 1.1 to 5.6 mg-N/L and produced an average value of 3.3 mg-N/L. It is important to stress that all nitrite samples collected at ML7-2, ML7-5, and ML7-6 during the 25-hour sampling effort featured concentrations above the MAC for nitrite of 1.0 mg-N/L. Fortunately, due to the relatively small 5-m wide target zone, these concentrations will not affect the nitrite mass produced by the supply wells of the Thornton Well Field. However, if this project proceeds to the next phase, a full-scale system capable of treating the 54-m wide window of interest, nitrite concentrations of this magnitude could potentially impact drinking water quality at the production wells, posing risk to the community. Further discussion of this issue is presented in Section 4.5.

The results collected at the final port, ML7-1, provide encouragement for future efforts. All ML7-1 samples collected over the 25-hour sampling period feature nitrate concentrations below the detection limit of 0.5 mg-N/L, suggesting a 100 percent reduction. In addition, very little nitrite was produced, with concentrations ranging from 0.5 to 1.5 mg-N/L and averaging 0.9 mg-N/L. It is clear that, despite transporting the lowest acetate concentrations, port ML7-1 produced the most positive results. The relatively low hydraulic conductivity of this layer appears to have prevented fresh oxygen from overwhelming the system, leading to its denitrification success.

The information presented here is summarized further in Figure 4.31, which displays four cross-sectional contour plots representing concentrations of nitrate and nitrite at experiment times of approximately 0.5 and 7.5 hours. Note that these cross-sections illustrate horizontal layers and, therefore, do not support the theory of dipping hydrostratigraphic aquifer layers presented in Section 4.4.2.2. Consistent with the breakthrough curves presented in Figure 4.30, the plots indicate the presence of multiple units. A second observation is the correlation between nitrite and nitrate distribution. Wherever nitrate concentrations are at their maximum (13 to 14 mg-N/L) or minimum (0 mg-N/L), nitrite concentrations are low. Alternatively, wherever mid-range nitrate concentrations exist, elevated nitrite concentrations also appear, which is consistent with the observed partial denitrification at ports ML7-2, ML7-5, and ML7-6. This phenomenon is also illustrated in Figure 4.32, which displays plots of nitrate concentration versus nitrite concentration at experiment times of approximately 0.5 and 7.5 hours. Figure 4.32, which includes data from multi-level bundles ML5, ML6, ML7, and ML8, clearly demonstrates that maximum nitrite concentrations are associated with mid-range nitrate values.

To supplement the visual representations, two nitrate mass flux calculations were carried out for the 5-m wide treatment area (Table 4.13). The first calculation represents the subsurface conditions prior to the addition of any acetate, while the second calculation is based on nitrate concentrations measured at the ports of ML7 during and directly following injection 13. The calculations combine nitrate concentrations with the flow properties of the hydrogeologic conceptual model to produce estimates of the total nitrate mass flux between injection-extraction wells WO78 and WO79. Prior to the acetate injections, the total mass flux across all six layers summed to 0.35 metric tons of nitrate (as nitrogen) per year. Directly following injection 13, however, this value fell to 0.31 metric tons of nitrate (as nitrogen) per year, yielding a percent difference of 11.4 percent. Note that this percent difference is based on the mean background nitrate concentration of 13.0 mg-N/L. The calculation was also performed using background concentrations of 10.4 and 15.6 mg-N/L, representing one standard deviation from the mean value (calculations not shown). These

concentrations generated minimum and maximum percent differences of 7.1 and 11.9 percent, respectively. For the in situ bioremediation effort to be deemed a viable treatment option for the Thornton Well Field, it is clear that higher removal percentages will have to be achieved. Nevertheless, the presence of denitrifying bacteria in this aquifer has been demonstrated, and what remains is overcoming the hydrogeological problem of acetate delivery.

In summary, varying degrees of denitrification were observed at the ports of ML7. These results clearly demonstrate the impact of the K-profile on stimulating in situ bioremediation. While the high-K layers were able to transport the greatest amount of acetate, little denitrification was observed in these units. Alternatively, the low-K layers, which transported a much smaller quantity of acetate mass, yielded lower nitrate concentrations. The results of this initial testing provide encouragement for future work at the site, while outlining several challenges that must be overcome.

4.4.2.6 Injection 13: Trends in Groundwater Isotope Composition

The NO_3^- - ^{15}N and NO_3^- - ^{18}O isotope data collected from ML5, ML6, and ML7 during Injection Phase 2, in addition to one point representing the average background conditions, are illustrated in Figure 4.33 and listed in Table H.5 (Appendix H). Note that, due to time and cost constraints, no nitrous oxide isotope samples were analyzed. Figure 4.33 (a) clearly displays a relationship between ^{15}N enrichment and decreasing nitrate concentrations, which is indicative of microbial denitrification (Aravena and Robertson, 1998). Comparing the injection phase data presented in Table H.5 with the mean background values of $\delta^{15}\text{N}$ (6.3 ‰) and $\delta^{18}\text{O}$ (1.3 ‰), it appears as though varying degrees of denitrification were stimulated in all aquifer layers. The minimum $\delta^{15}\text{N}$ and $\delta^{18}\text{O}$ values collected during Injection Phase 2, corresponding to a highly permeable zone and an average nitrate concentration of 12.9 mg-N/L, are 9.8 ‰ and 5.7 ‰, respectively. As is consistent with the elevated nitrite concentrations observed at this depth and despite the stable nitrate values, the enriched isotope numbers suggest a small degree of denitrification was stimulated in

this area of the aquifer. Also, the highly enriched isotope numbers pertaining to the lower permeability layers indicate substantial denitrification, supporting the nitrate concentration data.

Using Figure 4.33 (a), the isotopic enrichment factor for denitrification (ϵ) was computed for ^{15}N in nitrate using a simplified Rayleigh equation (Mariotti et al., 1981; Aravena and Robertson, 1998):

$$\delta^{15}\text{N}_r = \delta^{15}\text{N}_o + \epsilon \ln f \quad (4.2)$$

where $\delta^{15}\text{N}_r$ and $\delta^{15}\text{N}_o$ respectively represent the isotopic composition of the residual and initial nitrate, and f is a ratio of the initial nitrate concentration to the final nitrate concentration (Aravena and Robertson, 1998). The resultant enrichment factor was estimated to be -9.77 ‰. This value falls within the range of enrichment factors presented in the literature (Table 4.14). The wide range of enrichment values listed in Table 4.14 can be attributed to the variety of processes and conditions affecting each field site, such as the substrate concentration, temperature, denitrification rate, and type of microorganisms involved (Bottcher et al., 1990; Lund et al., 2000).

The $\delta^{18}\text{O}$ values collected during the second injection phase also confirm the occurrence of denitrification. Figure 4.33 (b) displays a clear linear relationship between $\delta^{18}\text{O}$ values and $\delta^{15}\text{N}$ values, indicative of denitrification. The slope of the line denotes a $^{15}\text{N}:^{18}\text{O}$ fractionation ratio of approximately 2.1:1. This ratio is consistent with those presented in the literature (Bottcher et al., 1990; Aravena and Robertson, 1998).

In summary, the clearly enriched ^{15}N and ^{18}O isotope measurements collected during Injection Phase 2 provide additional evidence confirming the successful stimulation of in situ denitrification in all aquifer layers. The high-K layers demonstrated limited enrichment, while the low-K layers experienced elevated enrichment, suggesting varying degrees of denitrification.

4.4.2.7 Additional Anion Monitoring Throughout Injection Phase 2

Anion samples were collected from multi-level bundle ML-7 on each of the 19 injection days of Injection Phase 2. Only samples collected from ML7-1 and ML7-2 were analyzed for nitrate and nitrite concentrations. Port ML7-1 was selected as it yielded the lowest oxygen concentrations throughout the second injection phase in addition to a 100 percent reduction in nitrate following injection 13. Port ML7-2 was chosen as it also generated results indicative of denitrification. Furthermore, the geochemical changes observed at ML7-2 were very similar to those observed at ML7-5 and ML7-6, suggesting the ML7-2 results could be used to predict behaviour at these depths. Samples collected at ports ML7-3, ML7-4, and ML7-7 were not analyzed due to the seemingly unresponsive nature of these ports throughout Injection Phase 2. All nitrate and nitrite results discussed in this section were generated by a commercial lab (ALS Laboratory Group).

Results of the additional anion monitoring effort are graphically displayed in Figure 4.34 and summarized in Table H.6 (Appendix H). Figure 4.34 indicates nitrate concentrations began to decline in the first injection stage, between September 18 (injection 6) and September 20 (injection 8). This decline is consistent with the oxygen data previously presented in Figure 4.26, although a two-day lag time is observed between minimum oxygen concentrations and minimum nitrate concentrations. This lag time can be attributed to the acclimation of denitrifying microbial populations. Once again, this confirms the hypothesis that several consecutive injections were required to facilitate oxygen consumption and subsequent denitrification.

As is consistent with the nitrate and nitrite data collected during and following injection 13, the depth corresponding to ML7-1 achieved a higher degree of denitrification than the unit represented by ML7-2. Port ML7-1 reached a minimum nitrate concentration of less than the detection limit of 0.5 mg-N/L (September 20), while ML7-2 reached a minimum value of only 4.2 mg-N/L (September 21). The nitrite concentrations are also consistent with the injection 13 results, suggesting a higher level of nitrite production at ML7-2 than ML7-1. For

port ML7-2, the maximum nitrite value of 7.2 mg-N/L corresponds to the minimum nitrate value of 4.2 mg-N/L, suggesting partial denitrification.

Injections 14 to 20, performed at an interval of every other day following daily injections 2 to 13, feature a rebound in nitrate concentrations at both well ports. This rebound is more pronounced in the ML7-2 dataset, which includes elevated nitrate concentrations of 10.8 to 11.5 mg-N/L throughout the final injection stage. Alternatively, the maximum nitrate concentration observed at ML7-1 during this stage was 2.6 mg-N/L, suggesting slower rebound. In addition, nitrite concentrations returned to the background level during this time. This geochemical change is inconsistent with the oxygen data collected during injections 14 to 20, which mimicked the estimates produced between daily injections 2 to 13. Note that the oxygen and nitrate samples were collected at the same time following each injection and, therefore, represent identical conditions. The oxygen dataset provided evidence that an injection interval of every other day is sufficient following the establishment of proper bacterial populations. This hypothesis, however, is challenged by the nitrate and nitrite data, which indicate the extended every other day injection interval cannot sustain denitrification, especially for the mid-range-K layer corresponding to port ML7-2. It appears as though an injection interval of every other day provided enough acetate to support oxygen consumption within the aquifer but not nitrate reduction. Following the final injection, the nitrate concentrations increased at ports ML7-1 and ML-2 towards background levels.

4.5 Site-Specific Challenges

The main challenges relating to this treatment system revolve around the physical and chemical properties of the aquifer system. In particular, the rapid groundwater flow in the high-K aquifer layers generated acetate residence times that were too brief to sustain sufficient oxygen consumption and subsequent denitrification. In addition, the fast flow provided a constant flux of additional dissolved oxygen to the treatment vicinity, further hindering the remediation effort. It is possible, however, that additional denitrification did

occur in these high-K layers further downgradient, beyond the multi-level well network. Dispersion would have laterally spread the injected substrate plumes from the pulsed injections, increasing the residence time of acetate downgradient. The installation of additional multi-level monitoring wells would be required to confirm this conjecture. As demonstrated by the results collected at ML7-1, elevated dissolved oxygen concentrations were not an issue for the layers with low to moderate hydraulic conductivity values. In these layers, residence times were much longer, permitting the necessary oxygen consumption and resulting denitrification.

The rapid groundwater flow and highly aerobic nature of the aquifer have led to two factors that must be overcome to implement the system at full scale: (1) incomplete denitrification in the high-K layers and (2) nitrite generation in nearly all units. As previously mentioned, the high-K layers are able to transport the greatest amount of nitrate mass to the production wells of the Thornton Well Field. Therefore, the ability to successfully stimulate in situ denitrification in these units is of critical importance. Testing various injection concentrations and durations is recommended to determine whether or not this treatment strategy will work in the high-K zones. It is hypothesized that longer, more closely spaced injections may produce sufficient residence times and facilitate adequate oxygen consumption in these layers.

The second principle limitation of this treatment system is nitrite production. Typically, as an increasing number of injections occur, bacterial populations develop and adapt. This natural adaptation may eventually lead to complete denitrification, preventing the production of nitrite. Several denitrification experiments have demonstrated this phenomenon (Hamon and Fustec, 1991; Constantin et al., 1996; Gierczak et al., 2007). As a secondary strategy, increasing the injection concentration may promote complete denitrification by providing additional substrate to denitrifiers.

4.6 Critical Next Steps and an Approach for Up-Scaling Treatment

Additional work is required before stimulated in situ denitrification can be considered an appropriate treatment option for the Thornton Well Field. The planning and execution of a third injection phase is the first recommended step. Ideally, this phase would consist of several consecutive injections, designed specifically to test various pulsing intervals and injection concentrations. It is clear the pulsing interval and acetate concentrations used in Injection Phase 2 were insufficient for the faster flowing layers. Longer, more closely spaced injections with higher acetate concentrations are therefore recommended for this third phase. It is anticipated that once the proper pulsing interval and injection concentration are identified, nitrate and nitrite levels will decline in all layers. If altering these parameters does not produce positive results, testing additional electron donors may prove advantageous. Additionally, it is recommended the third injection phase be longer than the second. This will allow the microbial communities in the high-K units more time to adapt, facilitating oxygen consumption and subsequent denitrification. Further research regarding the use of a packer system is also suggested. It is apparent the low-K zones require less acetate than the high-K zones to successfully stimulate in situ denitrification. Relying on a packer system would permit the use of different pulsing intervals and injection concentrations in these distinct layers.

Once the ideal pulsing interval(s) and injection concentration(s) are identified and the stimulation of uniform in situ denitrification with no nitrite production has been proven, up-scaling the treatment system can follow. Gradual up-scaling with detailed monitoring is recommended to prevent nitrite generation at a scale that may affect the Thornton Well Field. This research has proven that stimulating in situ denitrification at the Woodstock site is primarily dependent on the K-profile, which will vary laterally across the 54-m wide target window. As the system expands into unexamined territory, the risk of nitrite production will increase and the pulsing interval and injection concentration may require refinement. The gradual up-scaling process would involve the installation of several additional injection-extraction wells, oriented in a line perpendicular to ambient groundwater flow, spanning

the 54-m wide window. An injection-extraction well spacing of 10 m was recommended by the three-dimensional groundwater modelling. Additional modelling based on the acetate injection results may be required to confirm this decision. Finally, it is suggested that time and money be invested into an automated injection-extraction system as it would be nearly impossible to properly run the up-scaled treatment system manually.

4.7 Application of the System beyond the Study Site

This research clearly demonstrates that stimulating in situ denitrification in a highly conductive, aerobic aquifer is challenging, but certainly possible. Despite dissolved oxygen concentrations close to saturation, four out of the seven ports of ML7 produced very positive results. Depths corresponding to ML7-2, ML7-5, and ML7-6 demonstrated a 46 percent reduction in nitrate, while results from ML7-1 featured a 100 percent reduction. This provides encouragement to other nitrate-contaminated aquifers with elevated dissolved oxygen concentrations. With proper initial testing to determine ideal injection durations, concentrations, and intervals, this versatile treatment method could be successfully applied at many contaminated agricultural sites. The flexible nature of the system, in terms of well spacing, substrate selection, and injection details, make it highly adaptable. Prior to stimulating denitrification, however, the site of interest must be extremely well characterized. As demonstrated by this research, the subsurface geology is one of the most important factors controlling the success of an in situ denitrification experiment.

4.8 Overall Implications

This research has identified several implications relating to the development of a full-scale in situ treatment system. As an initial point, it is clear the hydraulic conductivity profile dominated the transport of acetate within the aquifer and ultimately controlled the success of the cross-injection scheme. This confirms the need for thorough site characterization prior to stimulating in situ bioremediation. The initial characterization phase is required to

outline the nature of the heterogeneity, allowing the researcher to properly design a remediation strategy.

In addition, the geochemical characterization suggested that thick, unconfined aquifer systems can contain very high amounts of oxygen over the entire profile. This occurs when the flow system permits deep movement of young water. The resulting implication is that aerobic conditions can persist very deep in unconfined aquifer systems. At Woodstock and many other agricultural sites, this is why very little denitrification tends to occur naturally and nitrate persists regionally. As a second implication, the elevated oxygen values throughout the profile significantly challenge the ability to stimulate in situ denitrification, an anaerobic reaction. This must be overcome during the design phase of remediation, prior to up-scaling.

This work also indicated that multiple, consecutive injections are required to adequately stimulate the required microbial populations. Figure 4.26 indicates that four to six injections were required to stimulate sufficient microbial oxygen consumption within the aquifer, reducing concentrations to an acceptable range. In addition, Figure 4.34 suggests that six to eight injections were needed to initiate nitrate reduction. It is clear that a specific conditioning period is required and a single injection cannot be expected to establish the proper conditions, as was demonstrated in Injection Phase 1. It is thought that this conditioning period is site specific, depending on several subsurface properties such as the rate of groundwater flow and the amount of oxygen present in the system. Also regarding the injection process, field experiments demonstrated that different aquifer units may require various injection durations, rates, and concentrations, specifically tailored to the properties of the flow system. This implies that, in a naturally heterogeneous system, the development of the most effective system may require very sophisticated design consideration.

The experiment results demonstrated that nitrite can be easily generated by the cross-injection system. Nitrite concentrations as high as 5.6 mg-N/L were observed during this initial testing. Considering the low MAC for nitrite in drinking water (1.0 mg-N/L) and the close proximity of this research to the Thornton Well Field, this is a potential problem that requires significant attention. Prior to up-scaling, this issue must be completely resolved. As previously mentioned, natural bacterial adaptation may eventually lead to complete denitrification, preventing the production of nitrite. Also, increasing the injection concentration may promote complete denitrification by providing additional substrate to denitrifiers.

Although only an eleven percent reduction in nitrate mass crossing the 5-m wide treatment wall was observed, it is believed that this approach has incredible potential at the study site. With additional work, it is thought that the challenges outlined here and in Section 4.5 can be overcome, eventually resulting in a system capable of reducing the nitrate concentrations at the Thornton Well Field. This belief is based on several observations. As an initial observation, the second phase injections indicated that varying degrees of denitrification were stimulated at all aquifer depths, even in the highest-K layers. This indicates the presence of denitrifying bacteria in all units and provides encouragement for future work at the site. In addition, the 100 percent reduction in nitrate in the low-K unit indicates that the elevated oxygen at the site can be overcome with the proper injection interval and concentration. It appears as though the everyday injection interval and acetate injection concentrations of 125 to 152 mg/L used in Injection Phase 2 were ideal for the lower-K units. Additional work will reveal the ideal injection scenario for the higher-K units. The optimism regarding the cross-injection scheme also stems from the great number of scientific avenues that have yet to be pursued. This research only examined a single electron donor (acetate), one injection duration (6 hours), two injection intervals (everyday and every other day), and a handful of injection concentrations (103 to 152 mg/L). Endless combinations of additional electron donors, injection durations, intervals, and concentrations remain to be explored. It seems certain that one of these combinations will

provide the ideal injection scenario for the higher-K units, leading to the desired outcome of complete denitrification in all aquifer units with no nitrite production. The work that remains, therefore, is identifying the proper combination of injection details.

The overall hypothesis of this research was: large-scale in situ denitrification can be initiated in a heterogeneous, aerobic aquifer through the introduction of a carbon source and electron donor using a controlled injection system. This hypothesis has been proven by the results of Injection Phase 2, which indicated varying degrees of denitrification at all aquifer depths. This achievement can be considered a unique contribution to science. All previous research regarding in situ remediation strategies have focused on sites with much slower groundwater flow and lower dissolved oxygen concentrations. This work also provides an initial foundation for examining the integrated approach, which has not been previously examined in the literature. Once the ideal injection scenario for the higher-K layers has been identified and a full-scale cross-injection scheme is established at the site, it is thought that the stimulation of in situ denitrification will accelerate nitrate remediation at the Thornton Well Field, bridging the gap between BMP implementation and the resulting decline in aquifer nitrate concentrations.

Table 4.1: Hydraulic conductivity results from conventional slug tests.

Test ID	Hydraulic Conductivity (m/s)				
	WO74-S	WO74-M	WO74-D	WO75-S	WO75-D
Falling Head 1	5.9E-04	7.0E-04	5.0E-04	-	3.7E-04
Rising Head 1	1.7E-03	1.1E-03	1.3E-03	8.5E-04	8.1E-04
Falling Head 2	5.9E-04	9.0E-04	7.3E-04	6.0E-04	3.6E-04
Rising Head 2	9.2E-04	1.8E-03	1.3E-03	9.0E-04	1.0E-03
Falling Head 3	5.9E-04	8.2E-04	4.9E-04	8.2E-04	4.6E-04
Rising Head 3	9.1E-04	2.0E-03	1.4E-03	7.6E-04	6.2E-04
Falling Head 4	5.5E-04	8.0E-04	5.4E-04	8.4E-04	4.3E-04
Rising Head 4	1.2E-03	1.0E-03	1.4E-03	9.4E-04	6.5E-04
Falling Head 5	5.3E-04	-	4.8E-04	-	4.0E-04
Rising Head 5	1.1E-03	-	1.5E-03	-	7.3E-04
Falling Head 6	-	-	-	-	4.5E-04
Rising Head 6	-	-	-	-	6.1E-04
Minimum	5.3E-04	7.0E-04	4.8E-04	6.0E-04	3.6E-04
Maximum	1.7E-03	2.0E-03	1.5E-03	9.4E-04	1.0E-03
Arithmetic Mean	8.7E-04	1.1E-03	9.6E-04	8.2E-04	5.7E-04
Standard Deviation	3.5E-04	4.5E-04	4.3E-04	1.0E-04	1.9E-04

Table 4.2: Hydraulic conductivity results from multi-level slug testing.

Depth (masl)	Average Hydraulic Conductivity (m/s)
294.0	3.0E-04
293.0	2.3E-04
292.0	2.6E-04
291.0	2.7E-04
290.0	2.9E-04
289.0	3.0E-04
288.0	3.1E-04
287.0	3.1E-04
286.0	2.9E-04
285.3	3.2E-04
Minimum	2.3E-04
Maximum	3.2E-04
Arithmetic Mean	2.9E-04
Standard Deviation	2.6E-05

Table 4.3: 2008 monthly gradients across the study site.

Month	Gradient
January	3.0E-03
February	3.0E-03
April	3.7E-03
May	3.4E-03
June	3.0E-03
July	3.0E-03
August	2.9E-03
September	4.3E-03
October	2.4E-03
December	3.9E-03
Minimum	2.4E-03
Maximum	4.3E-03
Arithmetic Mean	3.3E-03
Standard Deviation	5.4E-04

Table 4.4: Summary of CLOUDPE and PULSEPE tracer test results.

Test ID	Well ID	Depth (masl)	Dispersivity (m)	Velocity (m/s)	Hydraulic Conductivity ^a (m/s)
Forced Gradient Tracer Test 1	ML12-2	293.08	0.23	1.78E-04	-
	ML12-3	291.38	0.38	1.81E-04	-
	ML12-4	289.68	0.87	3.36E-04	-
Forced Gradient Tracer Test 2	ML5-2	295.54	0.40	6.82E-06	6.82E-04
	ML5-3	293.84	0.36	2.13E-05	2.13E-03
	ML5-4	292.14	0.34	2.88E-05	2.88E-03
	ML5-5	290.44	0.65	3.86E-05	3.86E-03
	ML5-6	288.74	1.78	7.29E-06	7.29E-04
	ML5-7	287.04	0.88	9.45E-06	9.45E-04
	ML6-2	293.45	0.76	1.69E-05	1.69E-03
	ML6-3	291.75	0.73	2.52E-05	2.52E-03
	ML6-4	290.05	1.34	4.59E-05	4.59E-03
	ML6-6	286.65	0.42	1.73E-05	1.73E-03
	ML6-7	284.95	0.42	2.96E-05	2.96E-03
	ML7-2	293.47	0.60	1.15E-05	1.15E-03
	ML7-3	291.77	1.42	3.73E-05	3.73E-03
	ML7-4	290.07	23.15	5.05E-04	5.05E-02
	ML7-5	288.37	1.25	2.20E-05	2.20E-03
ML8-3	291.14	0.90	2.47E-05	2.47E-03	
Natural Gradient Tracer Test	ML10-3	291.19	1.03	2.58E-04	2.6E-02
	ML10-4	289.49	0.34	5.05E-04	5.1E-02
	ML10-7	284.39	0.67	2.38E-04	2.4E-02

^a Hydraulic conductivity calculated with average gradient of 3.3×10^{-3} and average porosity of 0.33.

Table 4.5: Hydrogeologic parameters for the three-layer model (Gale, 2009).

	Depth range (masl)	Conductivity (cm/s)	Longitudinal dispersivity (m)
Upper unit	>294.5	3.3E-02	0.5
Middle unit	289.5 – 294.5	1.0E-01	0.5
Lower unit	<289.5	1.8E-02	0.5

Table 4.6: Hydrogeologic parameters for the initial five-layer model (Gale, 2009).

Zone	Depth range (masl)	Conductivity (cm/s)	Longitudinal dispersivity (m)
1	>294.5	3.3E-02	0.50
2	292 – 294.5	1.6E-01	0.25
3	290 - 292	4.5E-02	0.37
4	289.5 – 290	3.2E-01	0.80
5	<289.5	1.8E-02	0.50

Table 4.7: Layer-specific parameters for the calibrated five-layer model (Gale, 2009).

Layer	Depth range (masl)	Conductivity (cm/s)	Longitudinal dispersivity (m)	Vertical Conductivity (cm/s)
1	>294.6	8.0E-03	0.5	8.0E-03
2	292.2 – 294.6	1.5E-01	0.2	1.5E-01
3	290 – 292.2	1.2E-01	0.3	3.0E-02
4	289.6 – 290	3.5E-01	0.7	1.0E-01
5	<289.6	8.0E-03	0.5	8.0E-03

Table 4.8: Universal parameters for the calibrated five-layer model (Gale, 2009).

Property	Value	Units
Transverse vertical dispersivity	0.005* α_L	m
Transverse horizontal dispersivity	0.025* α_L	m
Effective porosity	0.33	-

Table 4.9: Summary of normalized sensitivity coefficients; the grey cells represent NSC values greater than 0.1 and less than -0.1, indicating significant sensitivity (modified from Gale, 2009).

Model Parameter	Normalized sensitivity coefficients					
	Peak Concentration			Peak Arrival Time		
	Port 2	Port 3	Port 4	Port 2	Port 3	Port 4
$K_1 = K_5 = 1.2E-02$ cm/s	0.031	-0.013	-0.032	0.027	0	-0.105
$K_2 = 1.3E-01$ cm/s (isotropic)	0.391	-0.19	-0.041	-0.507	0.38	0.091
$K_{x3} = 1.5E-01$ cm/s	-0.625	0.051	-0.238	0.703	-0.152	0.145
$K_4 = 2.5E-01$ cm/s	-0.146	-0.111	0.265	0.047	0.151	-0.071
$K_{z1} = K_{z5} = 2.0E-03$ cm/s (anisotropic)	0.125	0.135	0.05	-0.173	-0.084	0.011
$K_{z3} = 1.2E-01$ (isotropic)	0.007	-0.011	-0.011	0	0.004	0.003
$\alpha_{L4} = 0.9$ m	0.055	0	-0.284	0.095	0	0
$\alpha_{L3} = 0.4$ m	0.016	-0.323	0	0	-0.076	0
$\alpha_{L2} = 0.35$ m	-0.188	0	0	-0.072	0	0
$\alpha_{L1} = \alpha_{L5} = 0.2$ m	0	0	0	0	0	0
$\alpha_{TH} = 0.05\alpha_L$	0.005	-0.019	-0.016	0.019	0.005	0
$\alpha_{TV} = 0.01\alpha_L$	0.026	0.006	-0.054	0.041	-0.013	0
Pumping rate = 4.17 L/s (250 L/min)	0.434	0.552	0.171	-0.375	-0.462	0
$n_e = 0.28$	-0.55	-0.585	-0.178	0.446	0.418	0.213

Table 4.10: Summary of hydraulic conductivity estimates generated by various methods.

Parameter	Location	Average K (m/s)	Standard Deviation
K grain size	Core 1	1.3E-03	1.9E-03
K grain size	Core 2	1.5E-03	1.9E-03
K grain size	Core 3	2.5E-04	2.6E-04
K grain size	Core 4	1.3E-03	2.7E-03
K flowmeter	WO77	1.2E-03	1.5E-03
K flowmeter	WO78	1.7E-03	2.1E-03
K flowmeter	WO79	1.2E-03	2.1E-03
K flowmeter	WO80	1.9E-03	2.1E-03
K slug test	WO74-S	8.7E-04	3.5E-04
K slug test	WO74-M	1.1E-03	4.5E-04
K slug test	WO74-D	9.6E-04	4.3E-04
K slug test	WO75-S	8.2E-04	1.0E-04
K slug test	WO75-D	5.7E-04	1.9E-04
K tracer test	ML5	1.9E-03	1.3E-03
K tracer test	ML6	2.4E-03	1.2E-03
K tracer test	ML7	1.4E-02	2.4E-02
K tracer test	ML10	3.3E-02	1.5E-02
K calibrated model	-	1.3E-03	1.4E-03

Table 4.11: Nitrate mass flux calculations for municipal supply wells 01, 03, 05, 08, and 11.

Well Name	2008 Average Pumping Rate (m ³ /min)	1999-2006 Average Aqueous Nitrate (mg/L NO ₃ -N)	1999-2006 Average Aqueous Nitrate (mg/m ³ NO ₃ -N)	Nitrate Mass Flux (mg NO ₃ -N per min)	Nitrate Mass Flux (t*-N per year)
Well01	0.78	9.34	9.3E+03	7.2E+03	3.8
Well03	0.16	9.18	9.2E+03	1.4E+03	0.8
Well05	0.09	9.49	9.5E+03	8.7E+02	0.5
Well08	1.48	6.86	6.9E+03	1.0E+04	5.3
Well11	2.07	5.38	5.4E+03	1.1E+04	5.9
Total					16.2

*metric ton

Table 4.13: Calculations comparing the nitrate mass flux prior to the addition of acetate and following the 13th injection.

Ave. Annual Gradient		3.3E-03	-								
Ave. Porosity		0.33	-								
Ave. Water Table Elevation (Y ₂)		297.6	masl								
Ave. Top of Aquitard Elev. (Y ₁)		283	masl								
Total Y ₂ - Y ₁		14.6	m								
<div style="border: 1px solid black; padding: 5px; width: fit-content; margin: 0 auto;"> $Nitrate\ Mass\ Flux = Velocity \times Nitrate\ Concentration \times Area \times Porosity$ </div>											
Parameters											
Layer ID	K (m/s)	V (m/s)	ΔY (m)	ΔX (m)	Area (m ²)	Before Acetate Injections		After Injection 13 (ML7 NO ₃ conc.)			
						Nitrate Conc. (mg-N/m ³)	Nitrate Mass Flux (mg-N/s)	Nitrate Mass Flux (t*-N per year)	Nitrate Conc. (mg-N/m ³)	Nitrate Mass Flux (mg-N/s)	Nitrate Mass Flux (t*-N per year)
1	4.77E-04	4.70E-06	3.1	5	15.5	1.3E+04	3.1E-01	0.01	0.0E+00	0.0E+00	0.00
2	1.64E-03	1.61E-05	2	5	10.0	1.3E+04	6.9E-01	0.02	7.0E+03	3.7E-01	0.01
3	5.87E-03	5.79E-05	2	5	10.0	1.3E+04	2.5E+00	0.08	1.3E+04	2.5E+00	0.08
4	1.91E-02	1.88E-04	1.1	5	5.5	1.3E+04	4.4E+00	0.14	1.3E+04	4.4E+00	0.14
5	1.22E-03	1.20E-05	4.4	5	22.0	1.3E+04	1.1E+00	0.04	7.0E+03	6.1E-01	0.02
6	4.87E-03	4.81E-05	2.0	5	10.0	1.3E+04	2.1E+00	0.07	1.3E+04	2.1E+00	0.07
TOTAL						TOTAL		0.35	TOTAL		
								0.31			
								PERCENT DIFFERENCE (%)		11.4	

*metric ton

Table 4.14: Estimates of nitrogen isotope enrichment factors for denitrification.

Citation	Type of Study	Enrichment Factor (‰)
Mariotti et al. (1988)	Groundwater	-4.7 to -5.0
Spalding and Parrot (1994)	Groundwater	-9.6
Aravena and Robertson (1998)	Groundwater	-22.9
Bottcher et al. (1990)	Groundwater	-15.9
Fukada et al. (2003)	Groundwater	-13.6
Mengis et al. (1999)	Groundwater	-27.6

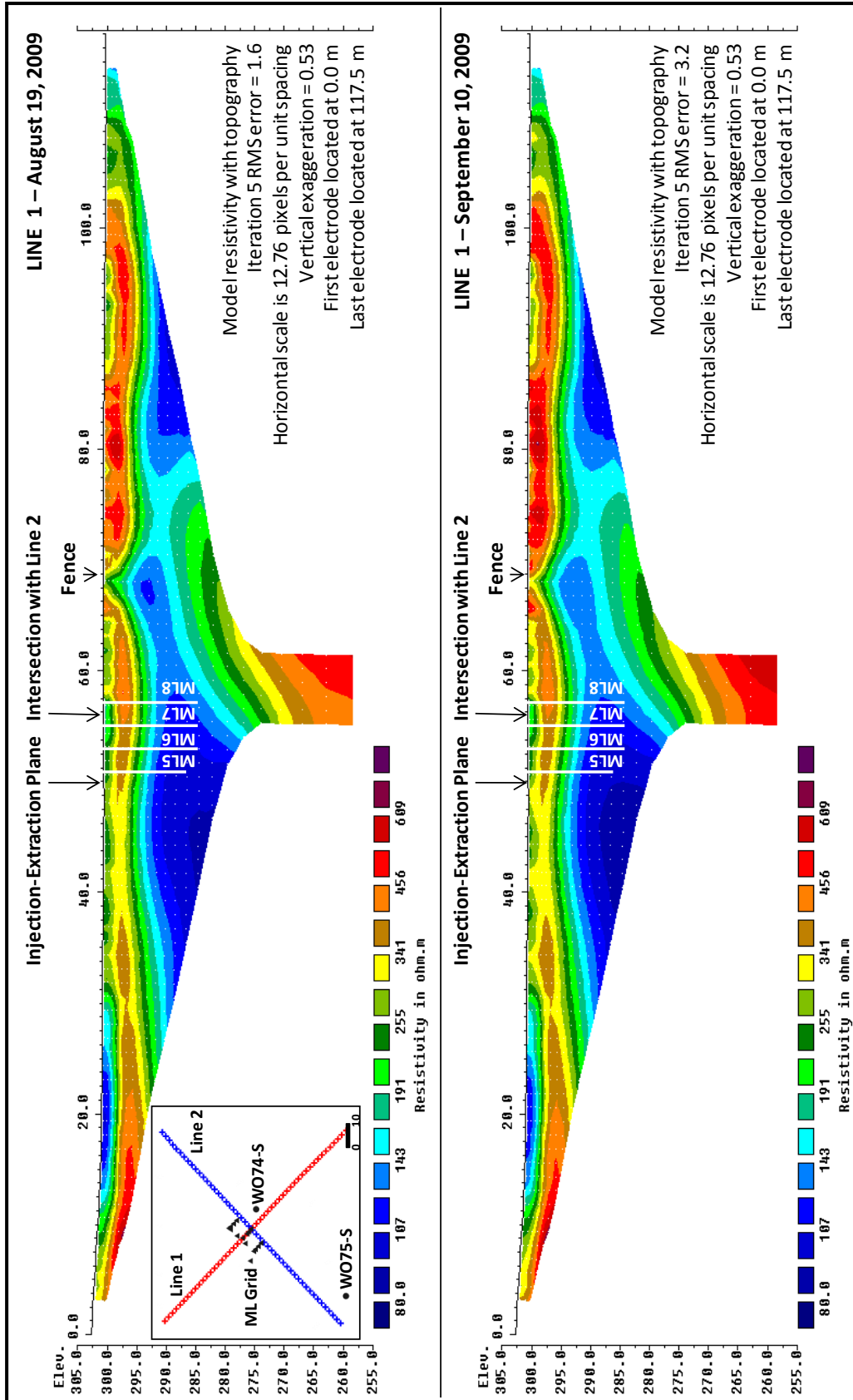


Figure 4.1: The August 19, 2009 and September 10, 2009 resistivity results for Line 1.

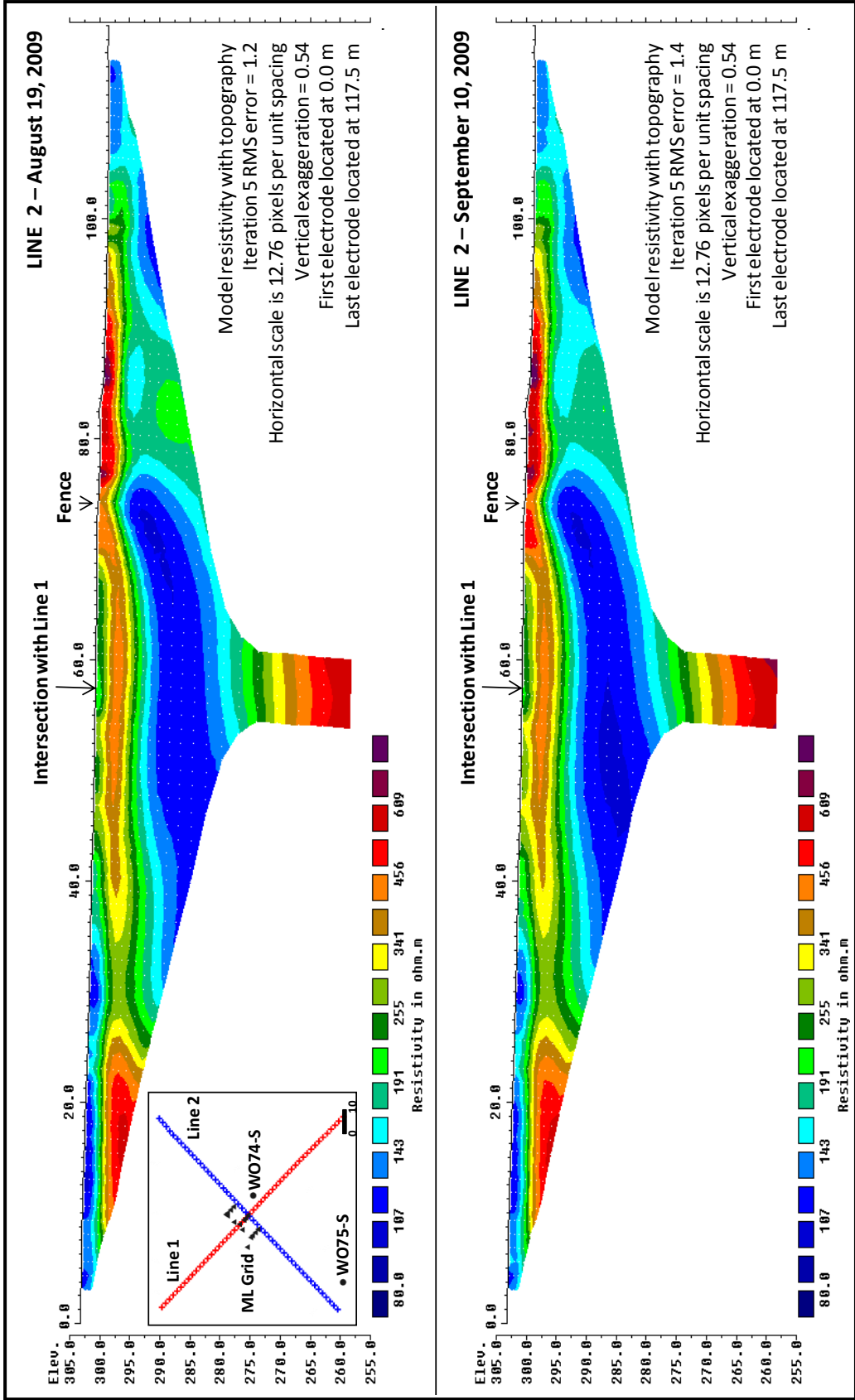


Figure 4.2: The August 19, 2009 and September 10, 2009 resistivity results for Line 2.

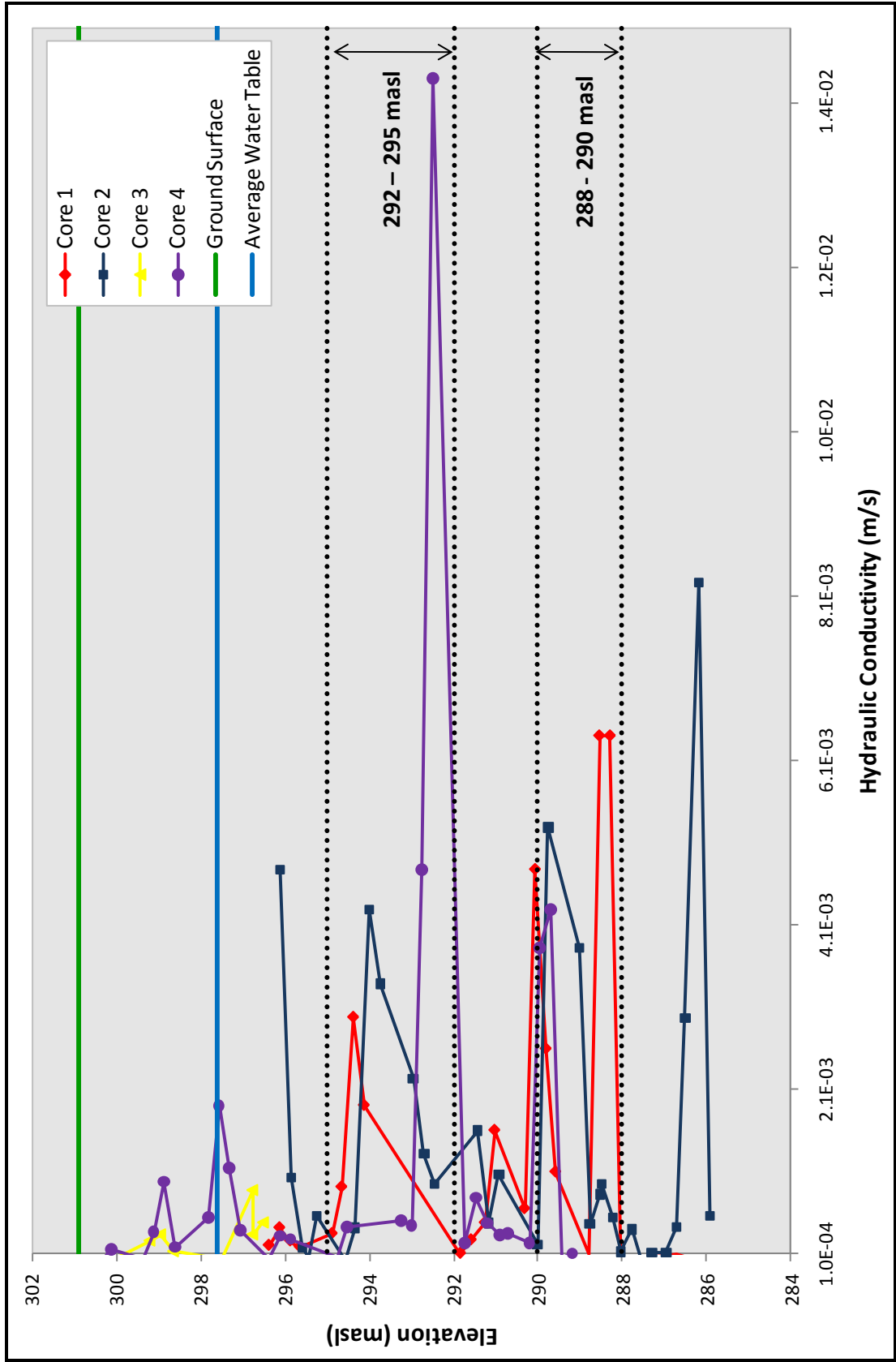


Figure 4.3: Grain size analysis results plotted as hydraulic conductivity with depth.

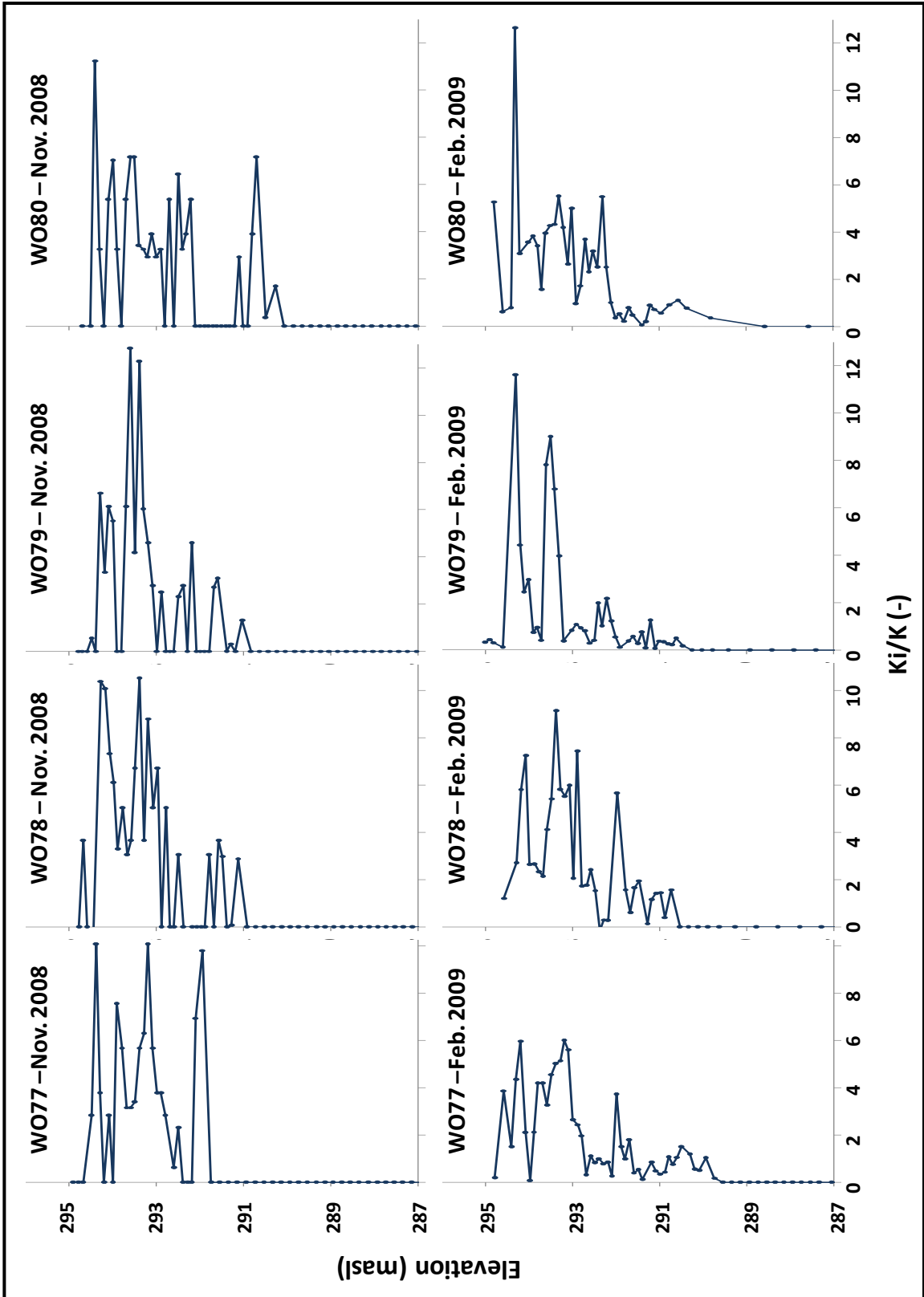


Figure 4.4: Borehole flowmeter test results for wells WO77, WO78, WO79, and WO80.

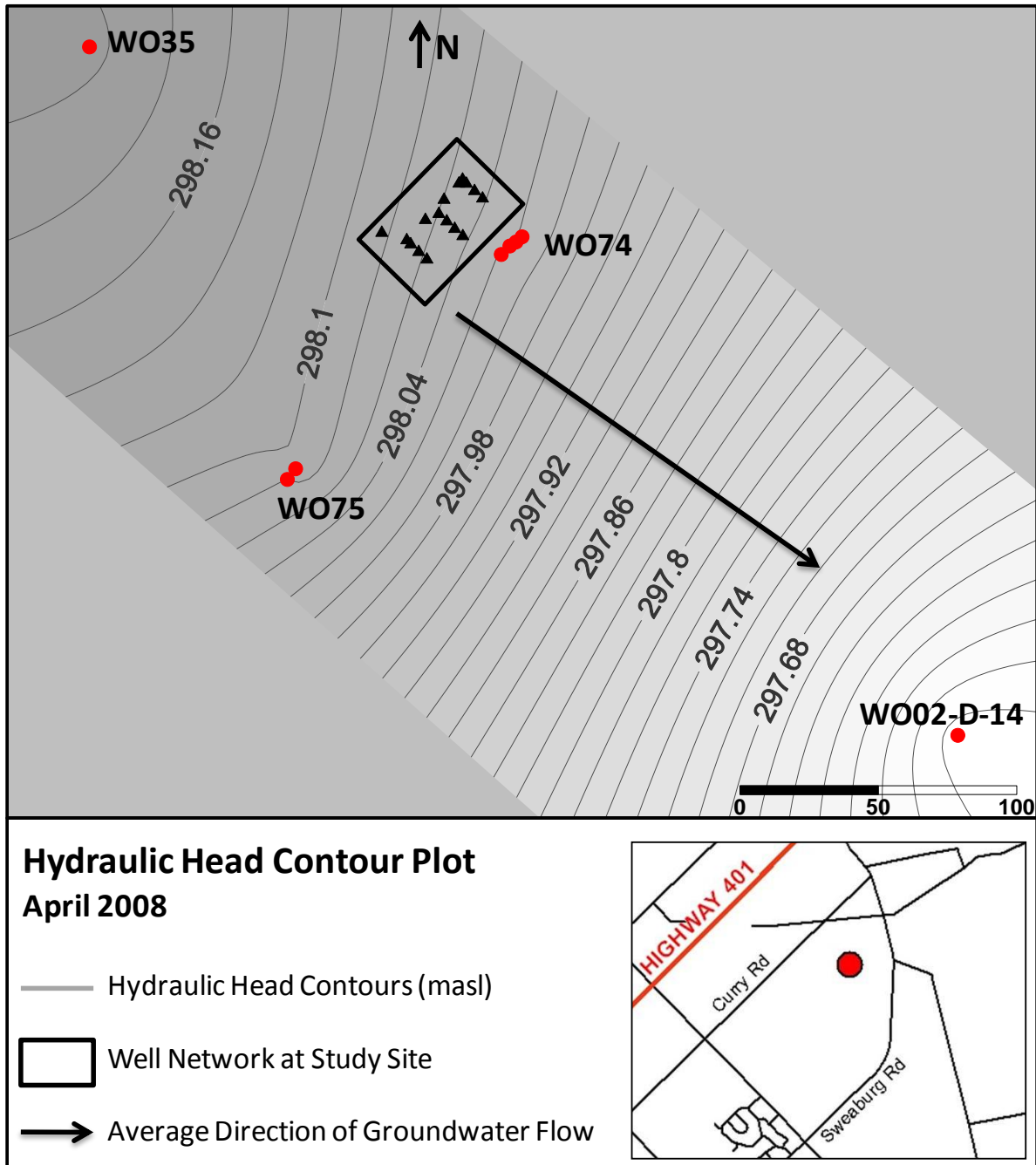


Figure 4.5: Hydraulic head contour plot displaying direction of ambient groundwater flow.

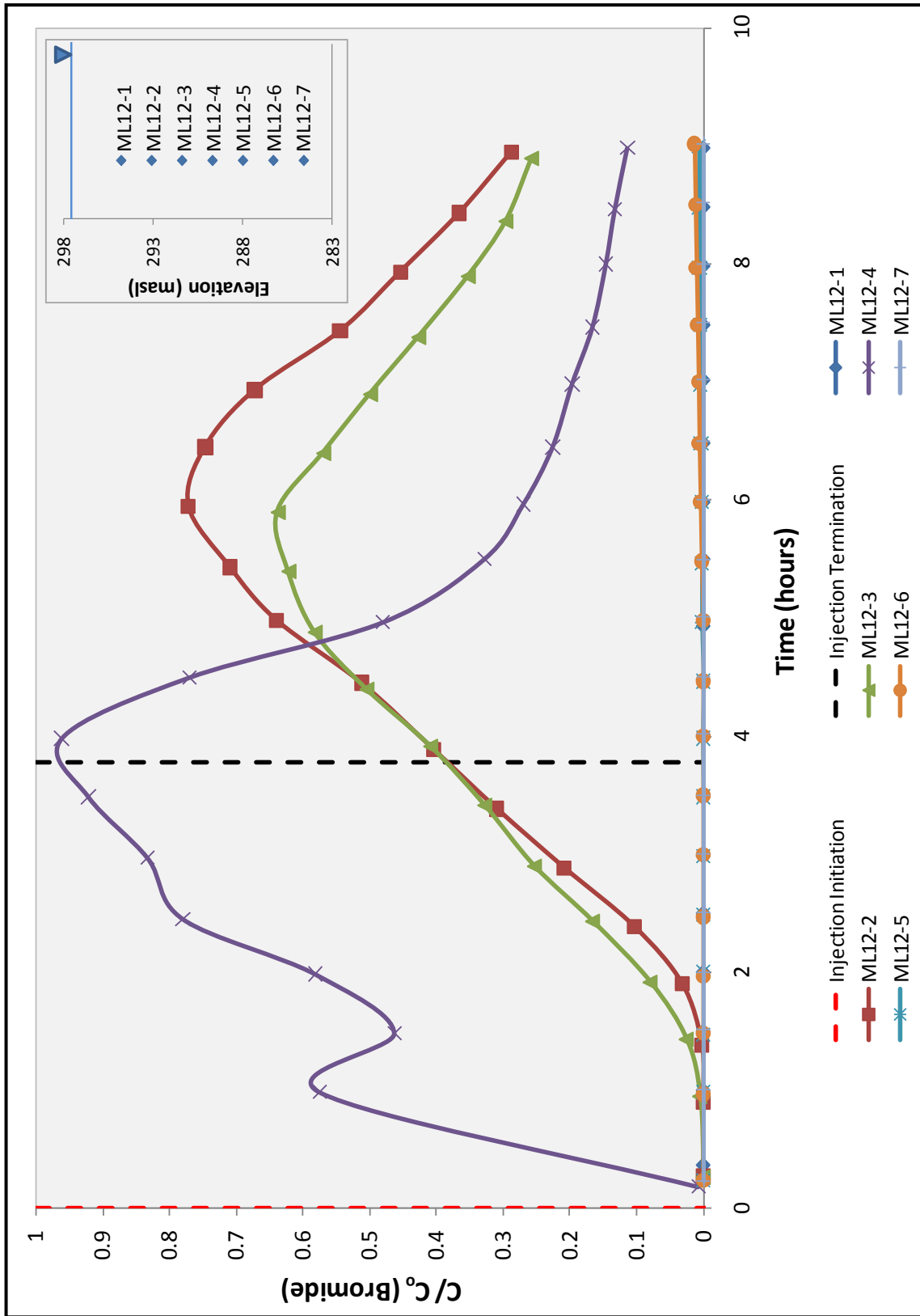


Figure 4.6: Bromide breakthrough curves from the first forced gradient tracer test.

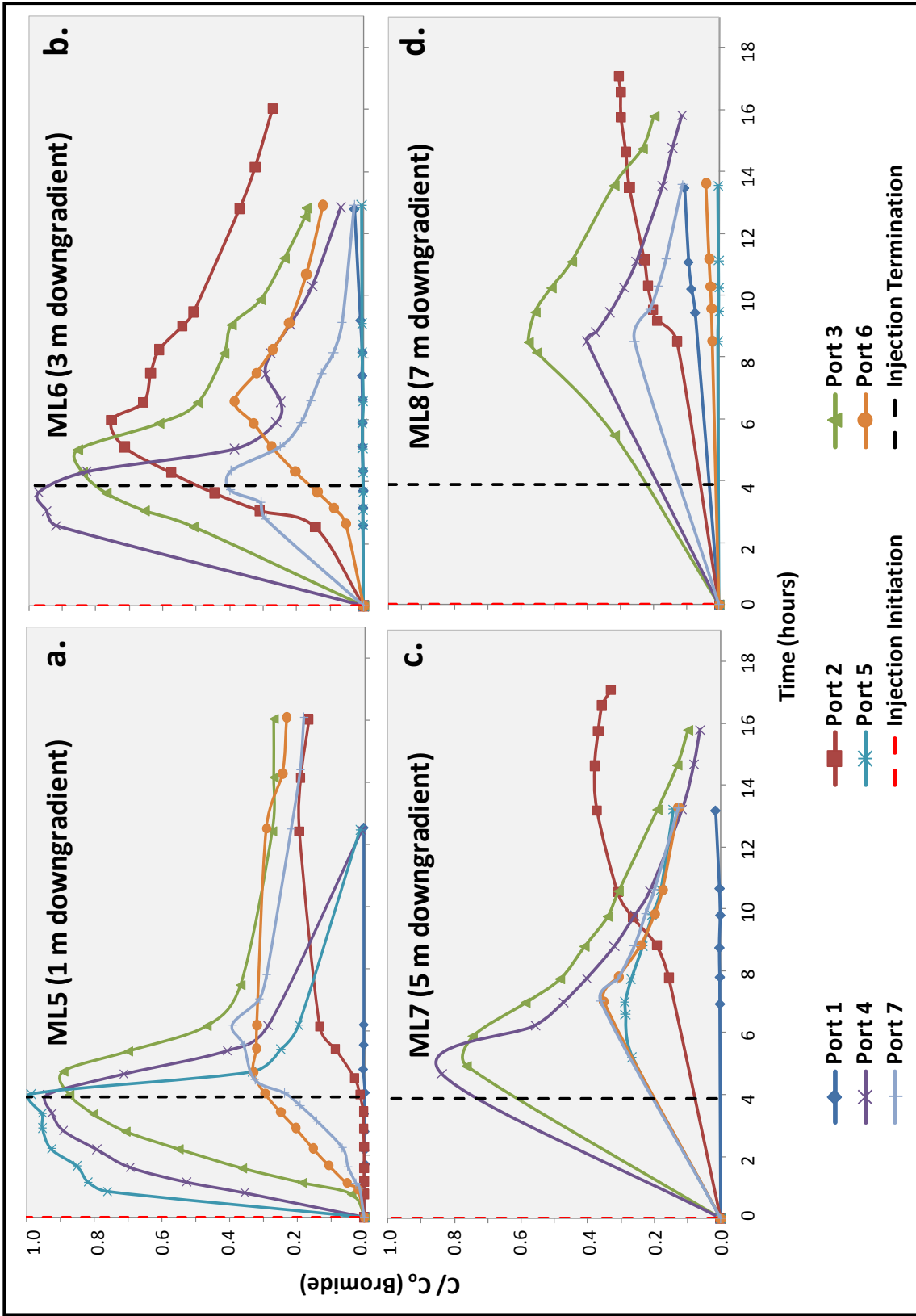


Figure 4.7: Breakthrough curves from the second forced gradient tracer test for (a) ML5, (b) ML6, (c) ML7, and (d) ML8.

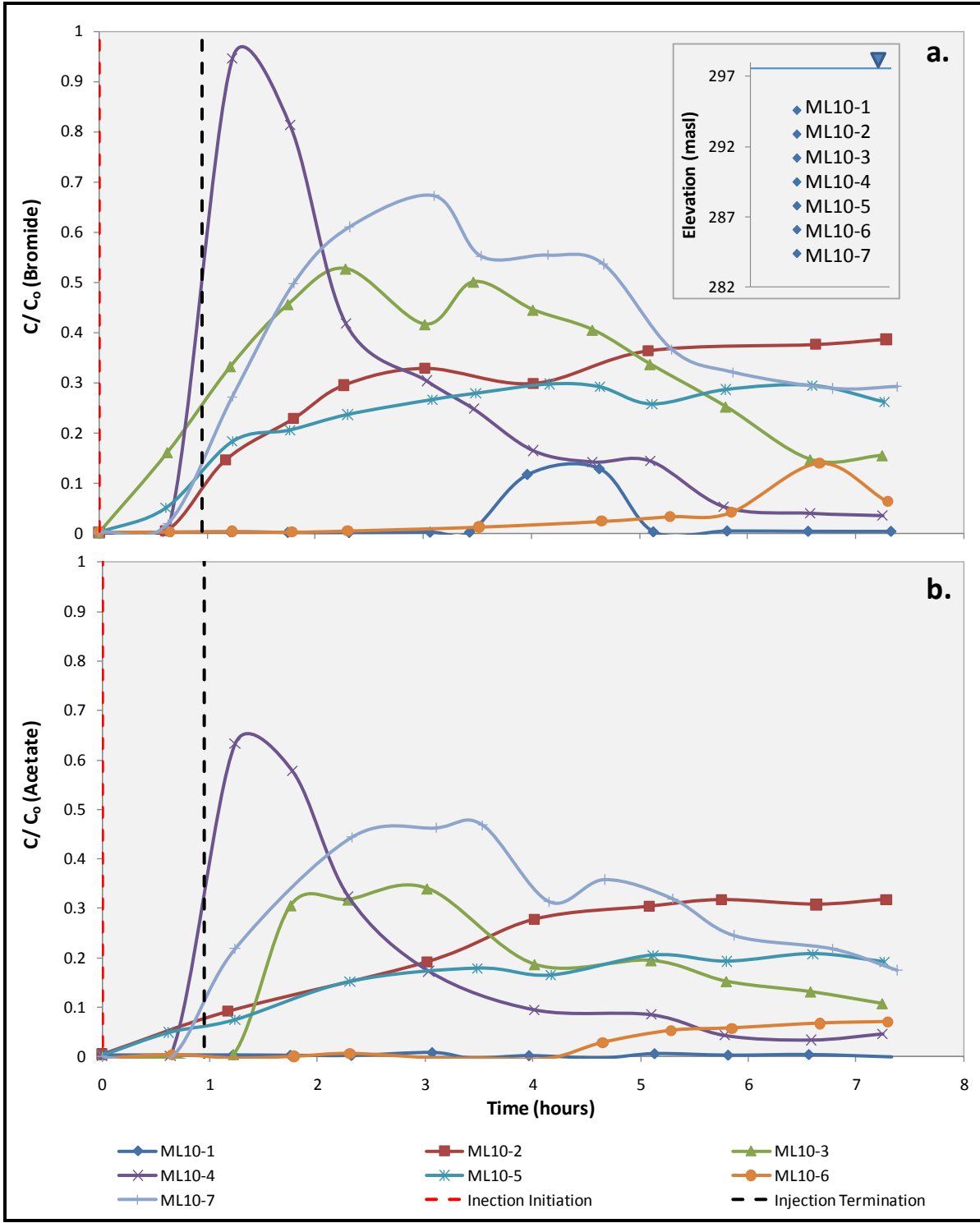


Figure 4.8: Natural gradient tracer test breakthrough curves for (a) bromide and (b) acetate.

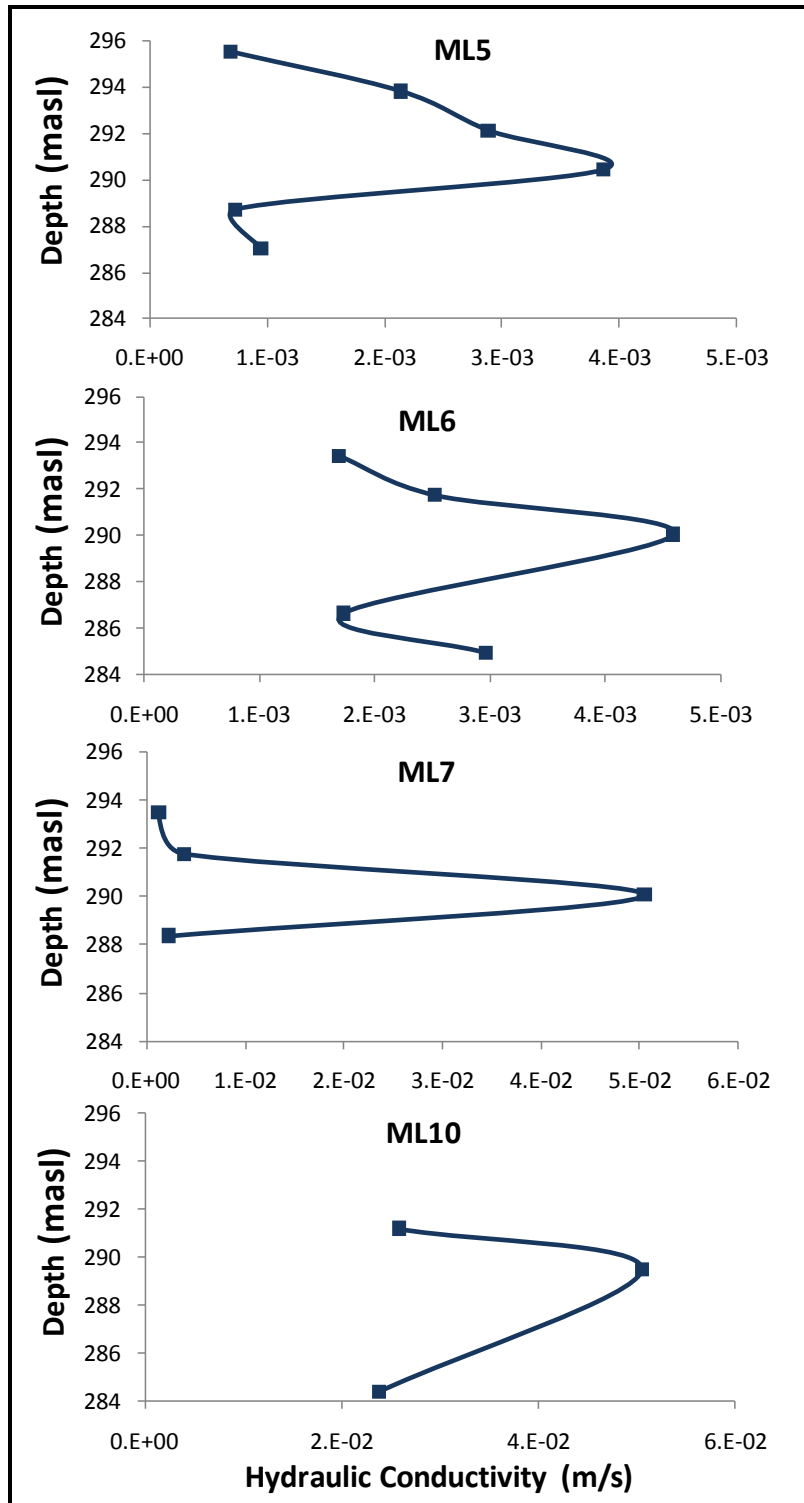


Figure 4.9: Comparison of hydraulic conductivity values determined from tracer testing; note the different horizontal scales.

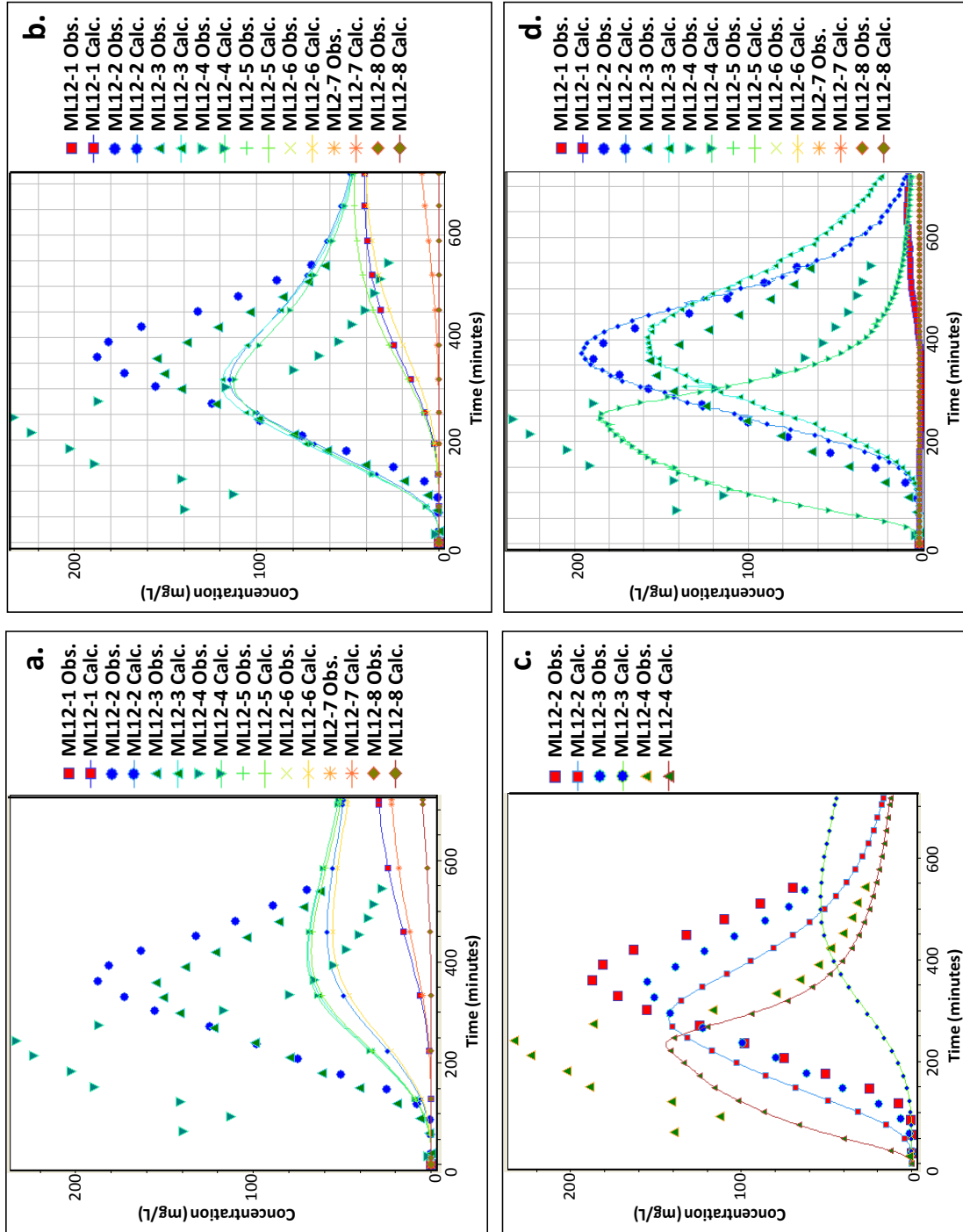


Figure 4.10: Observed and simulated breakthrough curves for (a) the homogeneous case, (b) the three-layer case, (c) the initial five-layer case, and (d) the calibrated five-layer case (Gale, 2009).

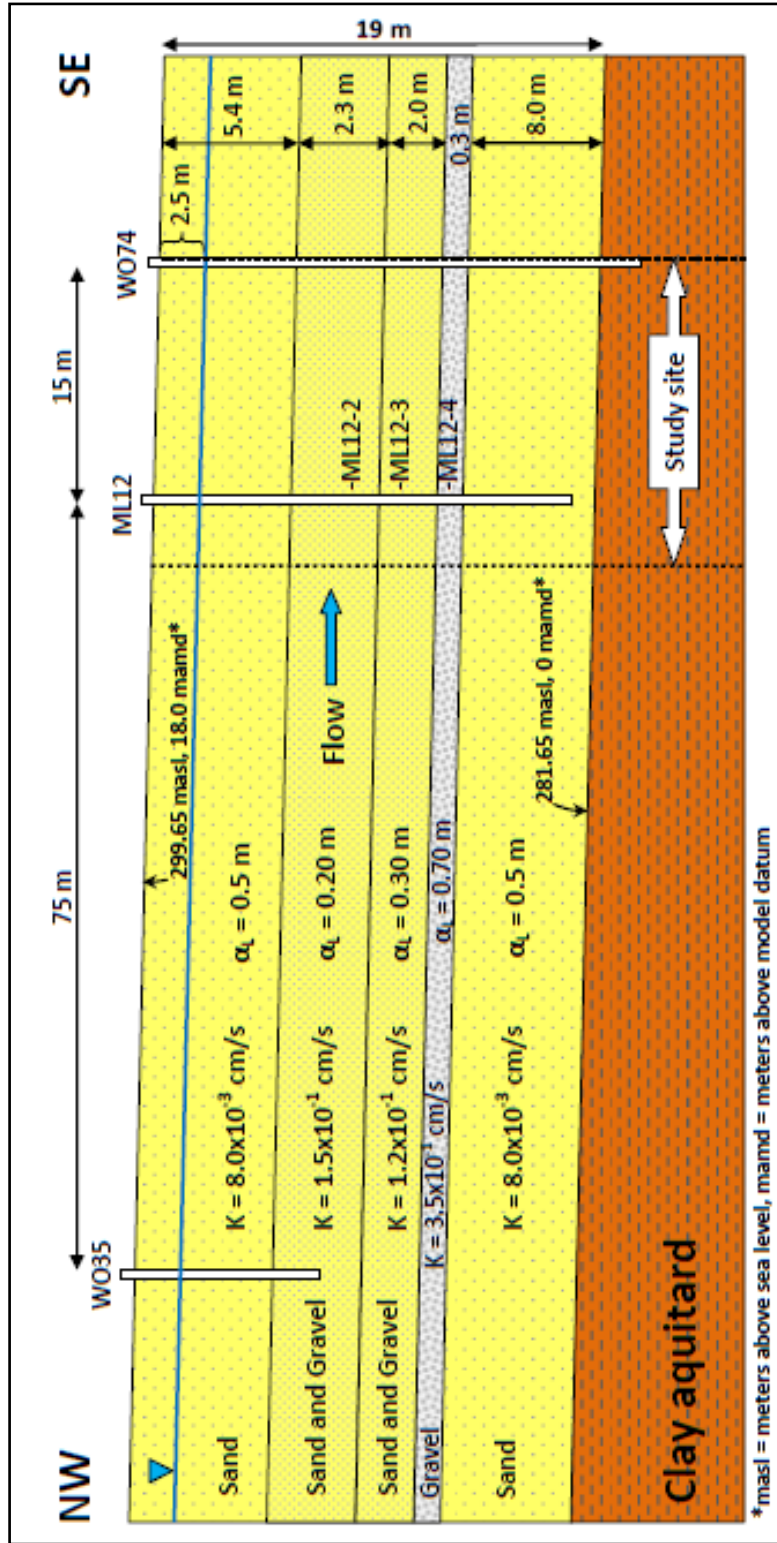


Figure 4.11: Five-layer conceptual model (not to scale) (Gale, 2009).

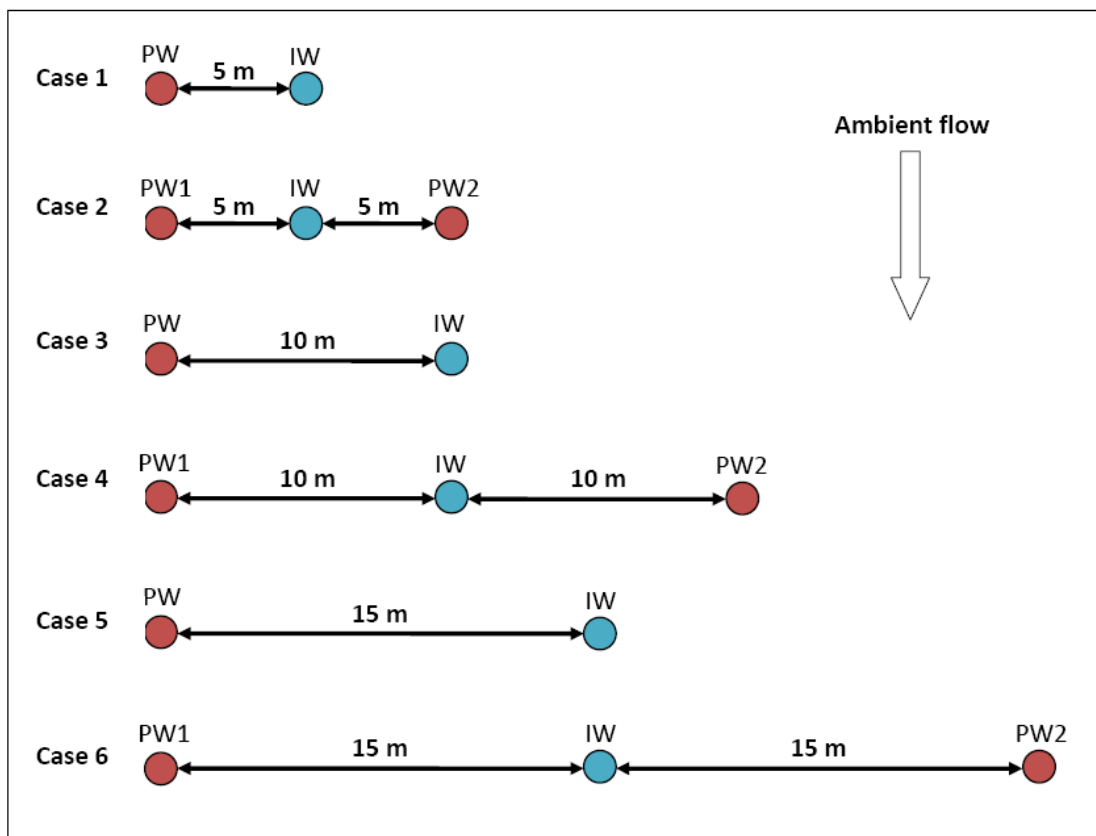


Figure 4.12: Prospective pumping and injection well (PW, IW) arrangements (Gale, 2009).

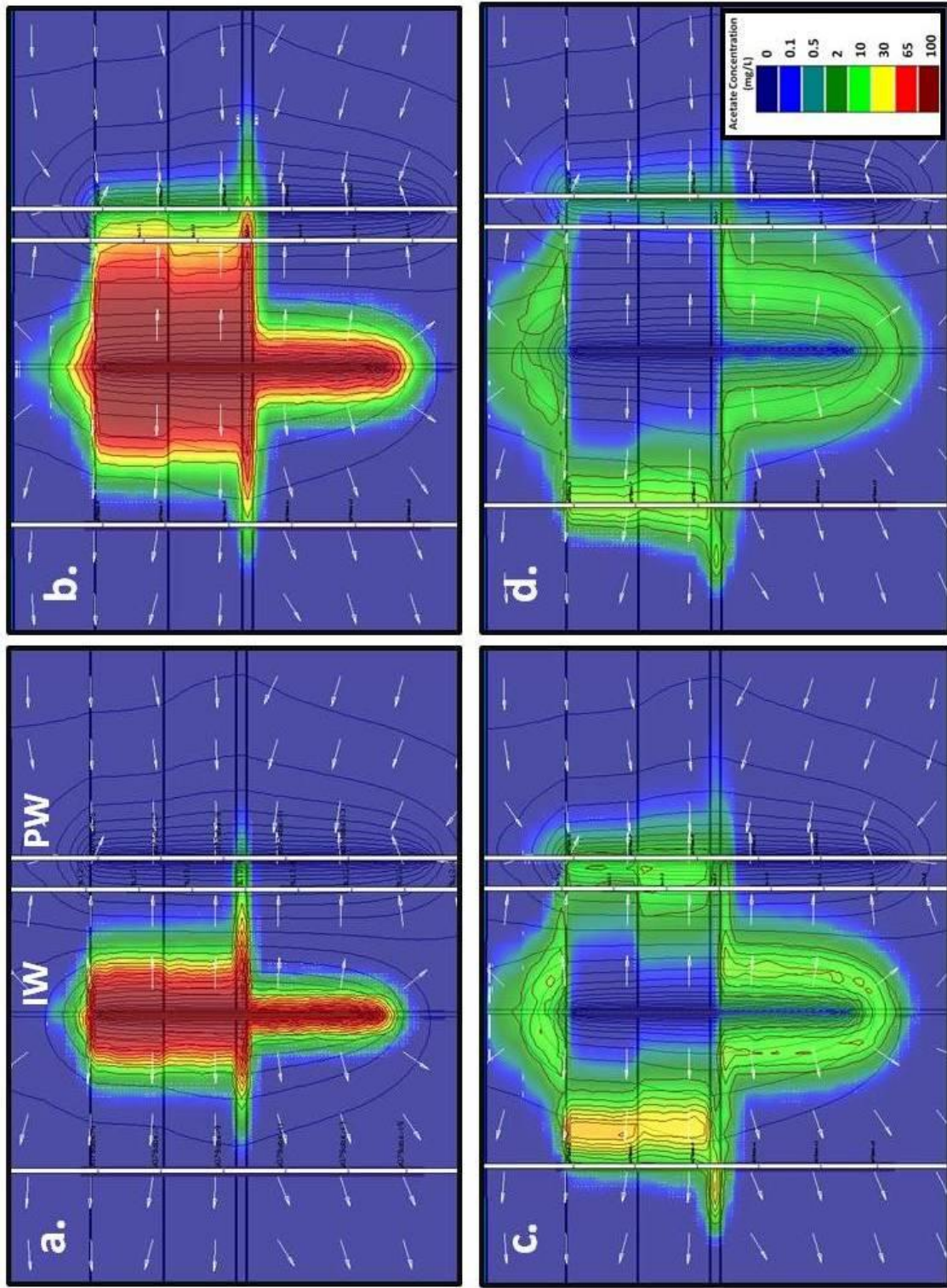


Figure 4.13: Case 1 (5 m separation distance, single extraction well) model-generated acetate plume along the injection-extraction well plane at (a) $t = 50$ minutes, (b) $t = 240$ minutes, (c) $t = 720$ minutes, and (d) $t = 1440$ minutes (Gale, 2009).

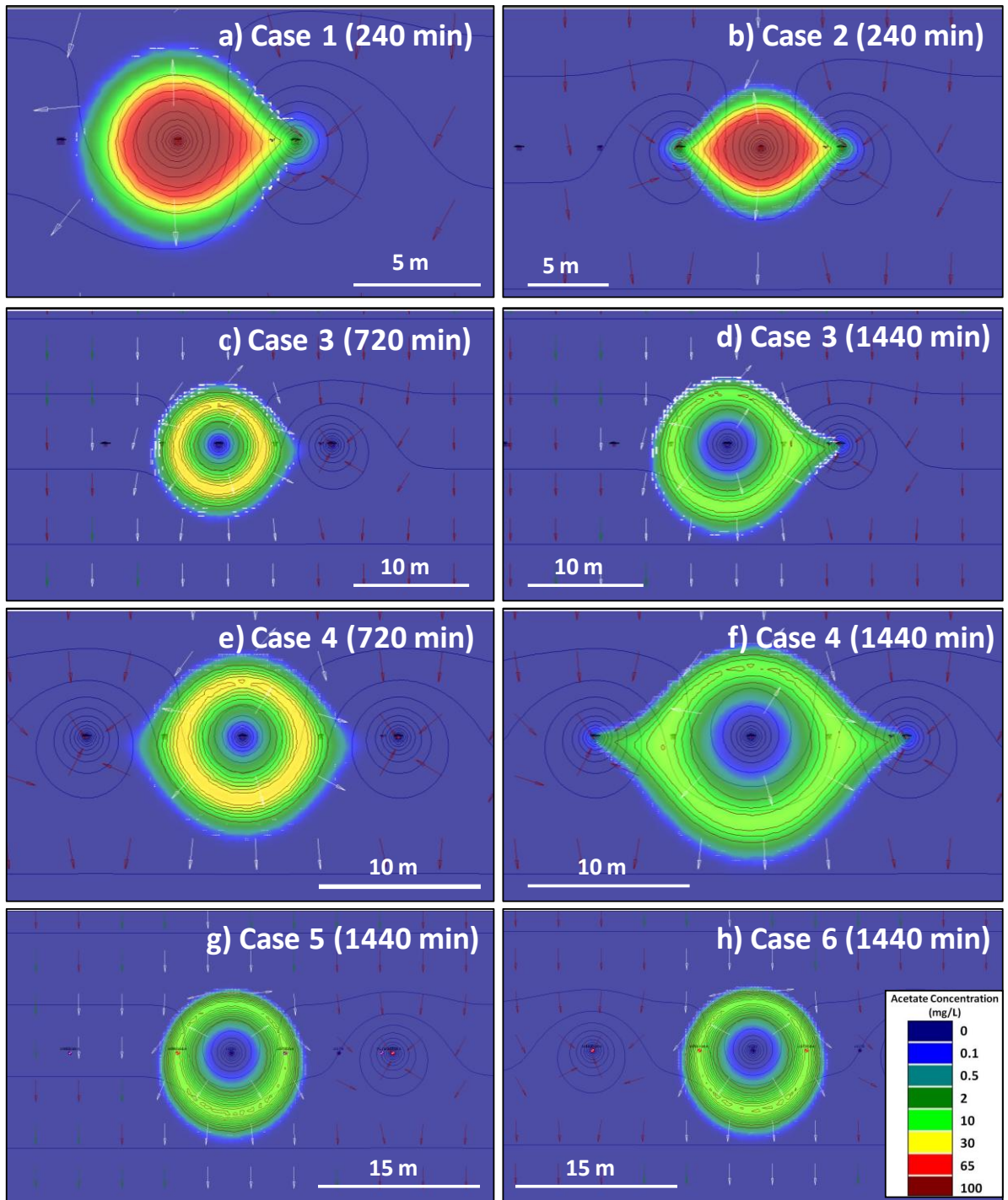


Figure 4.14: Plan view diagrams illustrating the injectate plume in the third layer ($K = 1.2 \times 10^{-1} \text{ cm/s}$) for (a) Case 1 at 240 minutes, (b) Case 2 at 240 minutes, (c) Case 3 at 720 minutes, (d) Case 3 at 1440 minutes, (e) Case 4 at 720 minutes, (f) Case 4 at 1440 minutes, (g) Case 5 at 1440 minutes, and (h) Case 6 at 1440 minutes (modified from Gale, 2009).

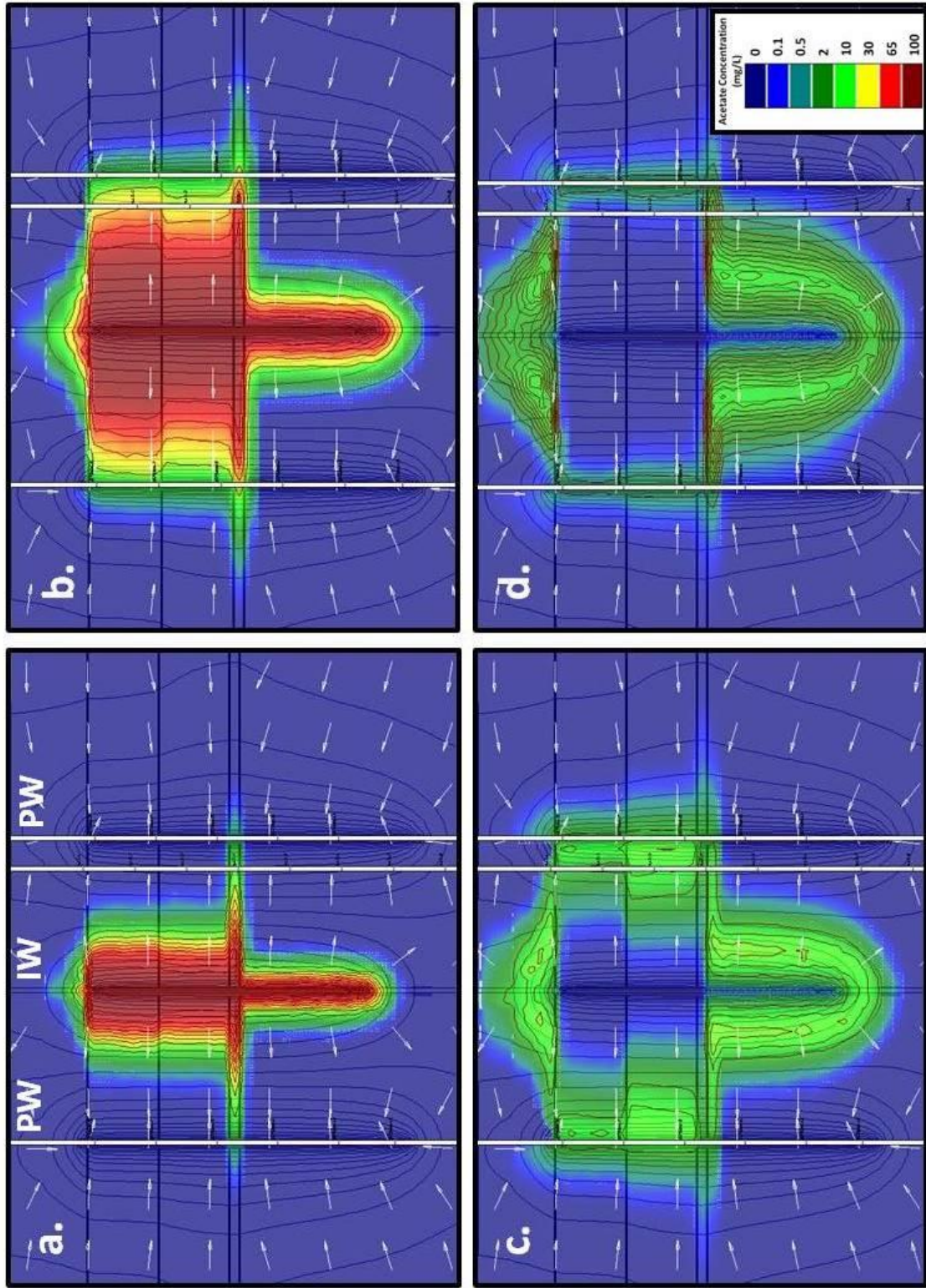


Figure 4.15: Case 2 (5 m separation distance, two extraction wells) model-generated acetate plume along the injection-extraction well plane at (a) $t = 50$ minutes, (b) $t = 240$ minutes, (c) $t = 720$ minutes, and (d) $t = 1440$ minutes (Gale, 2009).

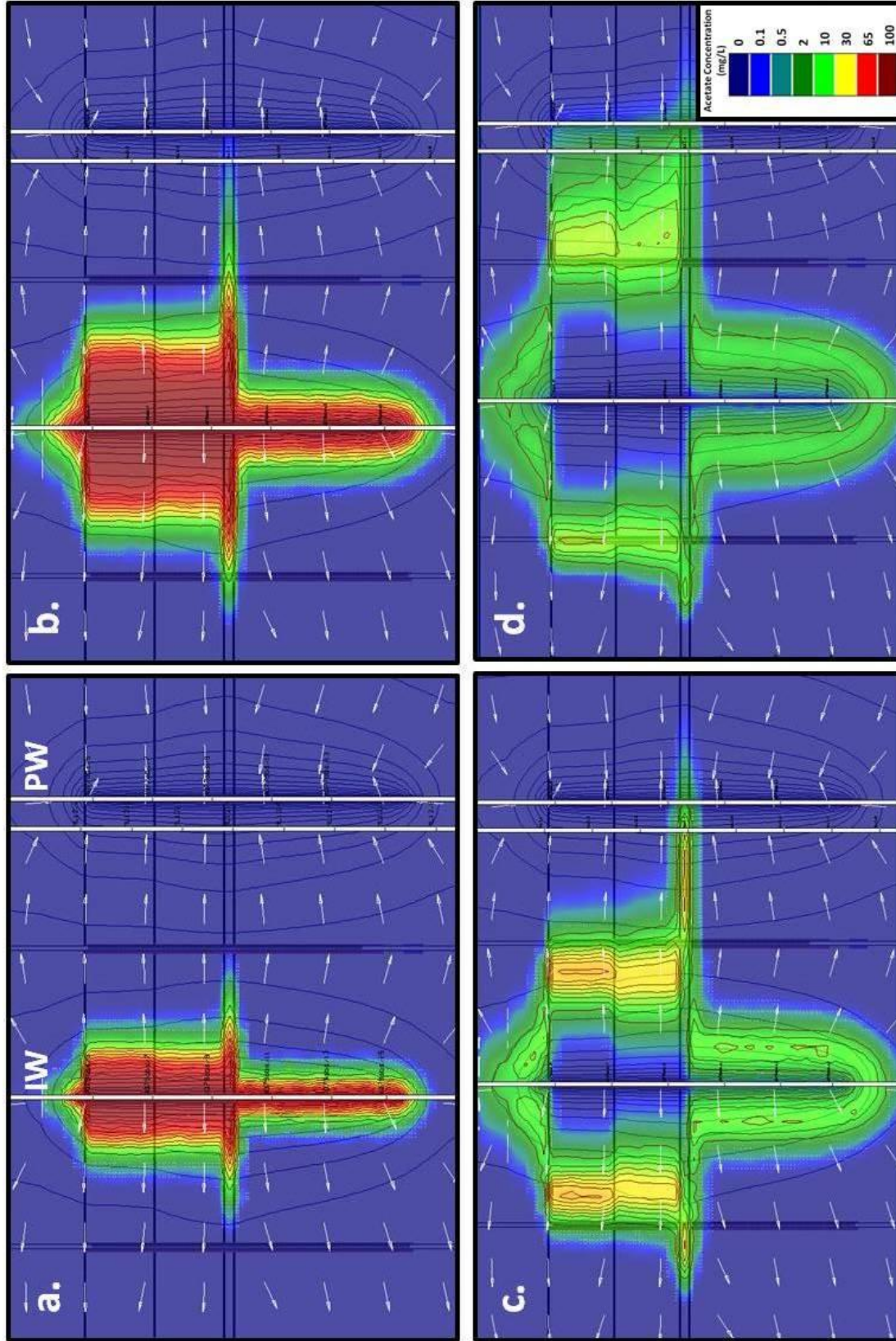


Figure 4.16: Case 3 (10 m separation distance, single extraction well) model-generated acetate plume along the injection-extraction well plane at (a) $t = 50$ minutes, (b) $t = 240$ minutes, (c) $t = 720$ minutes, and (d) $t = 1440$ minutes (Gale, 2009).

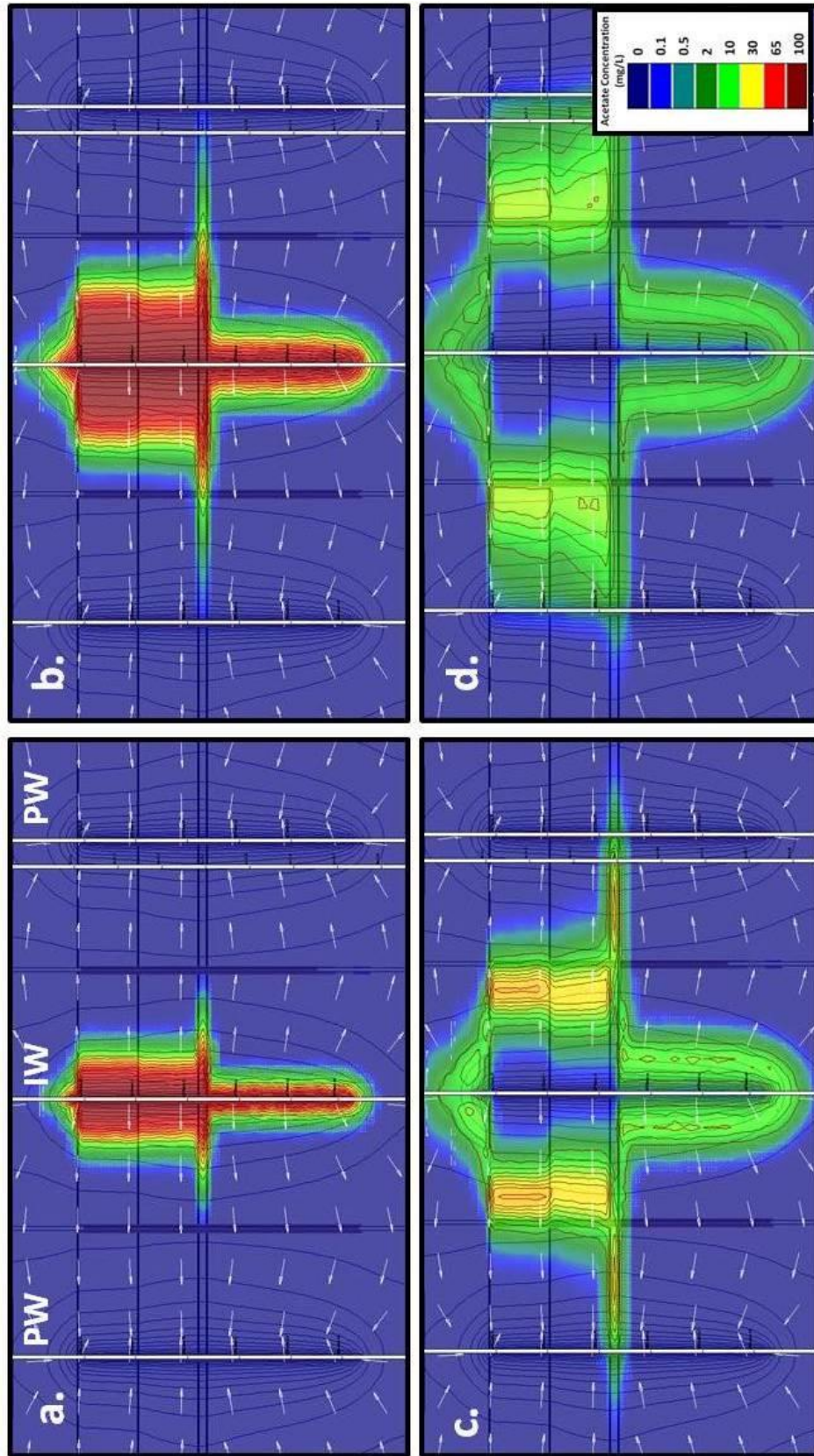


Figure 4.17: Case 4 (10 m separation distance, two extraction wells) model-generated acetate plume along the injection-extraction well plane at (a) $t = 50$ minutes, (b) $t = 240$ minutes, (c) $t = 720$ minutes, and (d) $t = 1440$ minutes (Gale, 2009).

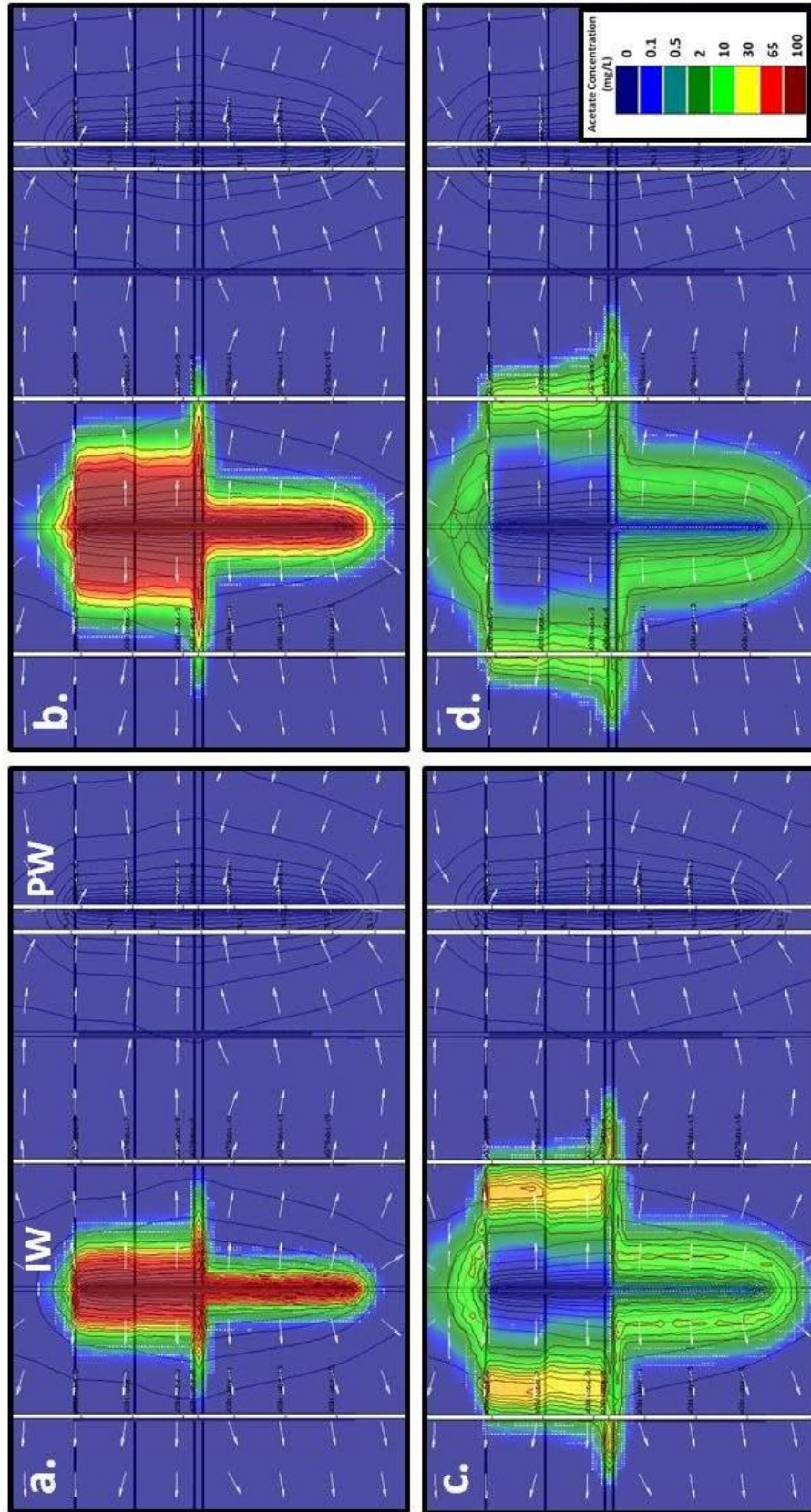


Figure 4.18: Case 5 (15 m separation distance, single extraction well) model-generated acetate plume along the injection-extraction well plane at (a) $t = 50$ minutes, (b) $t = 240$ minutes, (c) $t = 720$ minutes, and (d) $t = 1440$ minutes (Gale, 2009).

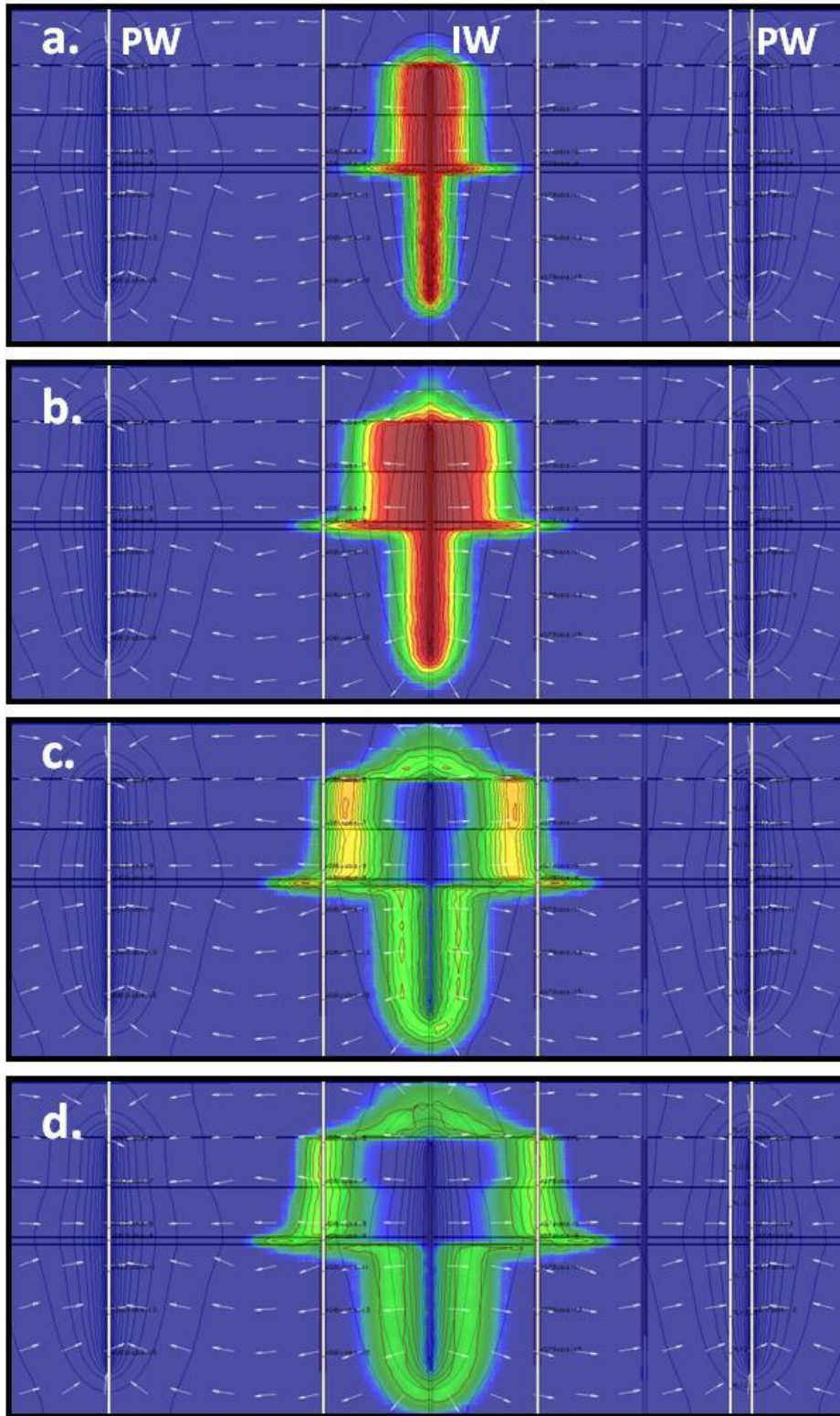


Figure 4.19: Case 6 (15 m separation distance, two extraction wells) model-generated acetate plume along the injection-extraction well plane at (a) $t = 50$ minutes, (b) $t = 240$ minutes, (c) $t = 720$ minutes, and (d) $t = 1440$ minutes (Gale, 2009).

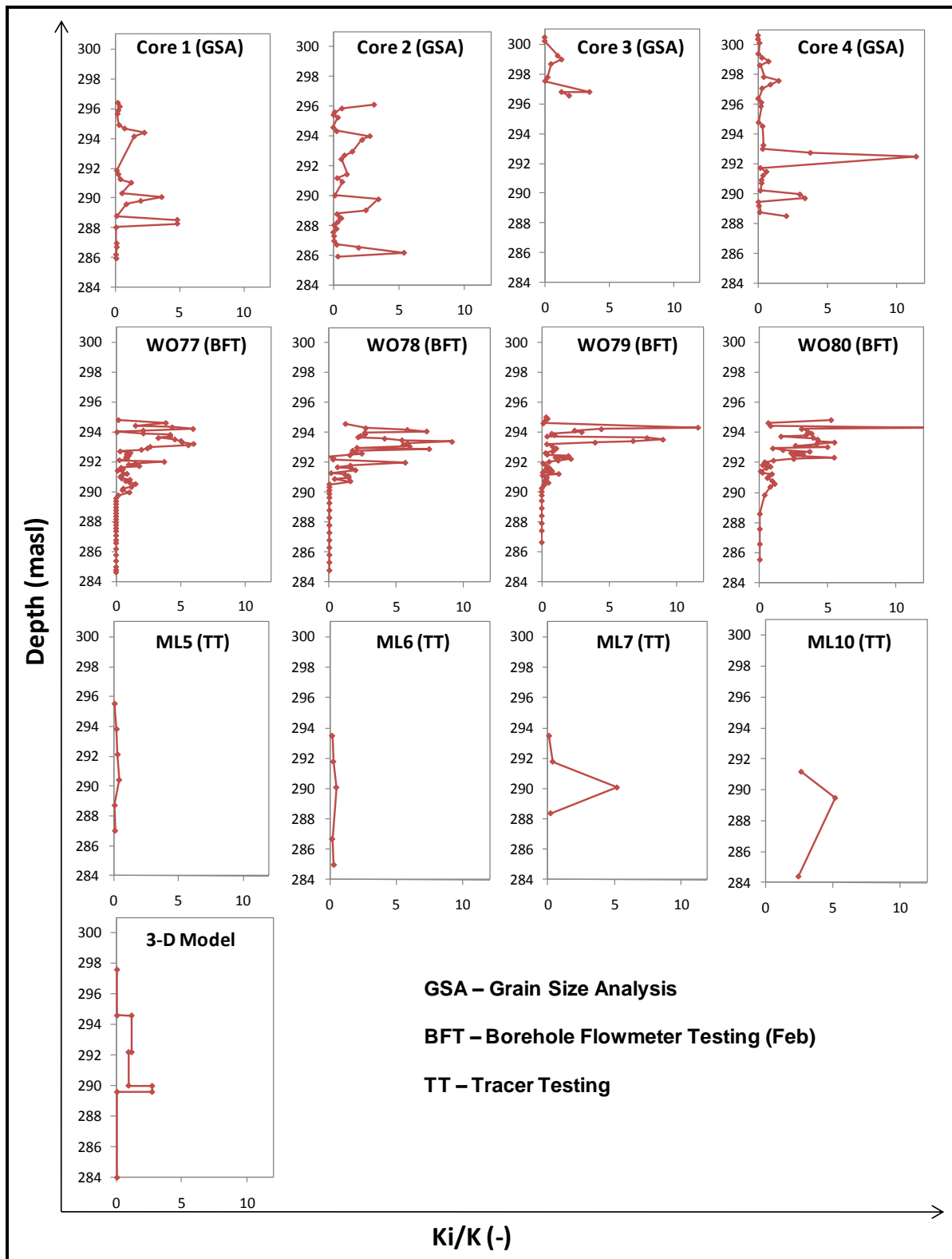


Figure 4.20: Graphical summary of all hydraulic conductivity profile estimates.

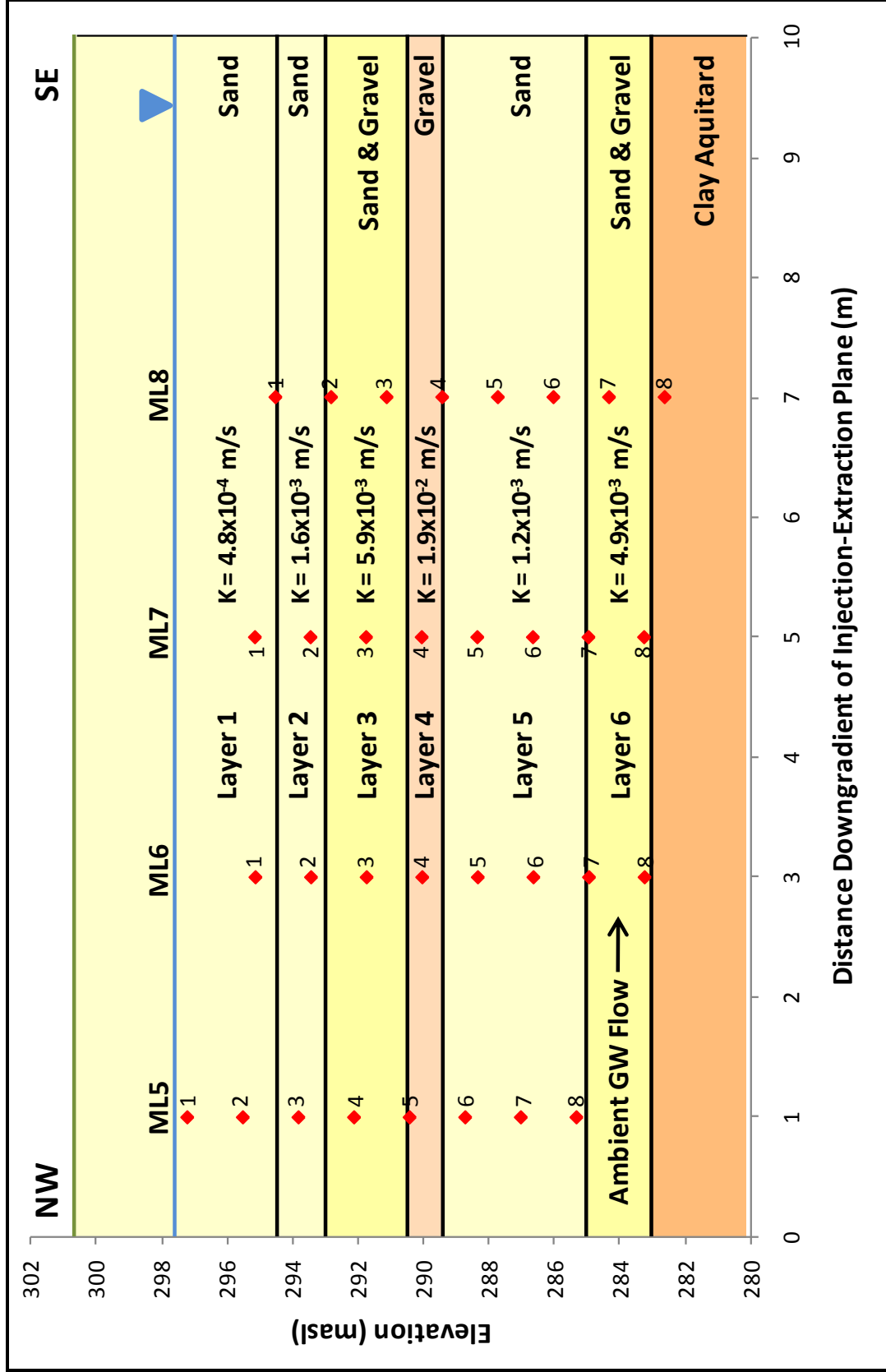


Figure 4.21: The hydrogeologic conceptual model for the study site.

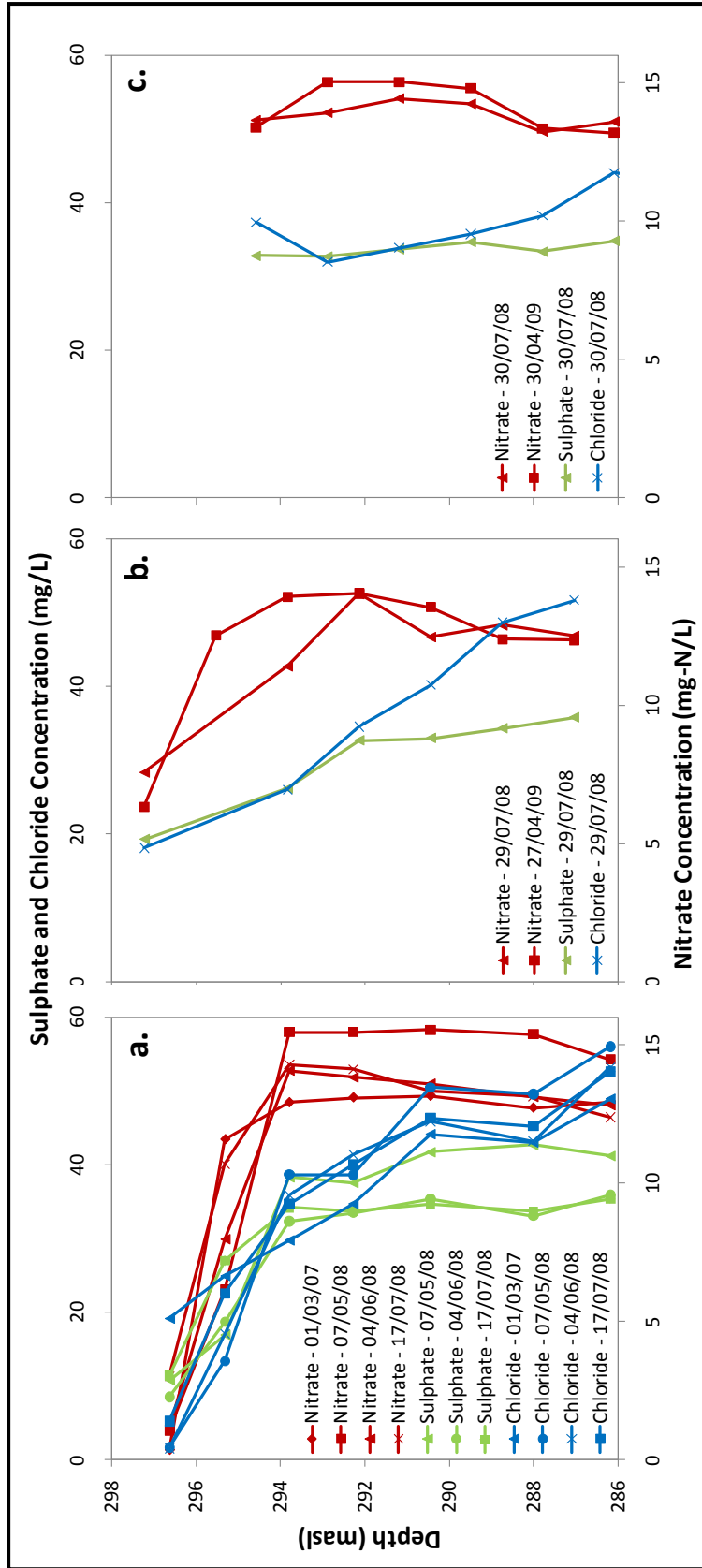


Figure 4.22: Background nitrate, sulphate, and chloride concentration profiles for (a) WO74-ML, (b) ML5, and (c) ML10.

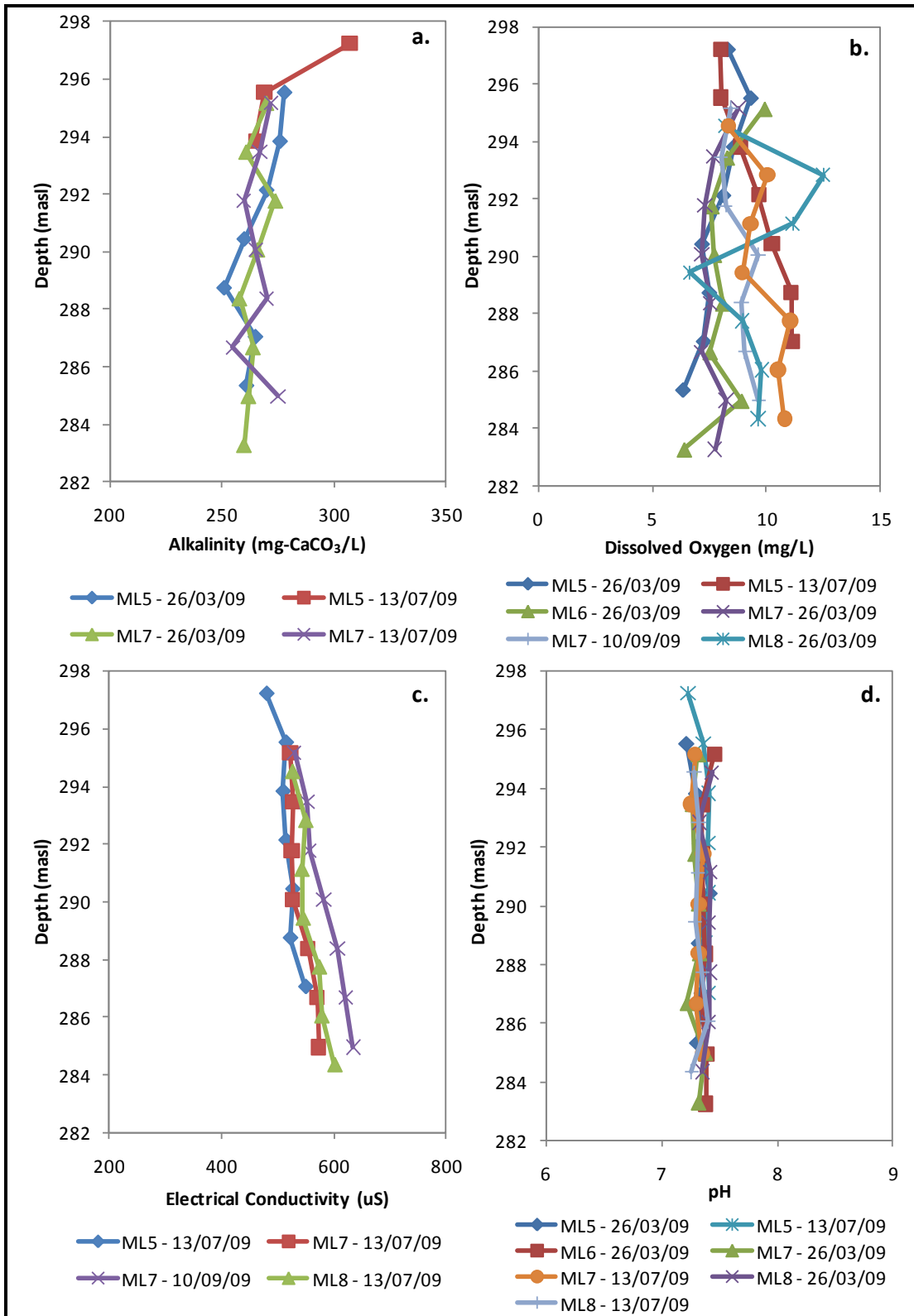


Figure 4.23: Vertical profiles of (a) alkalinity, (b) dissolved oxygen, (c) electrical conductivity, and (d) pH.

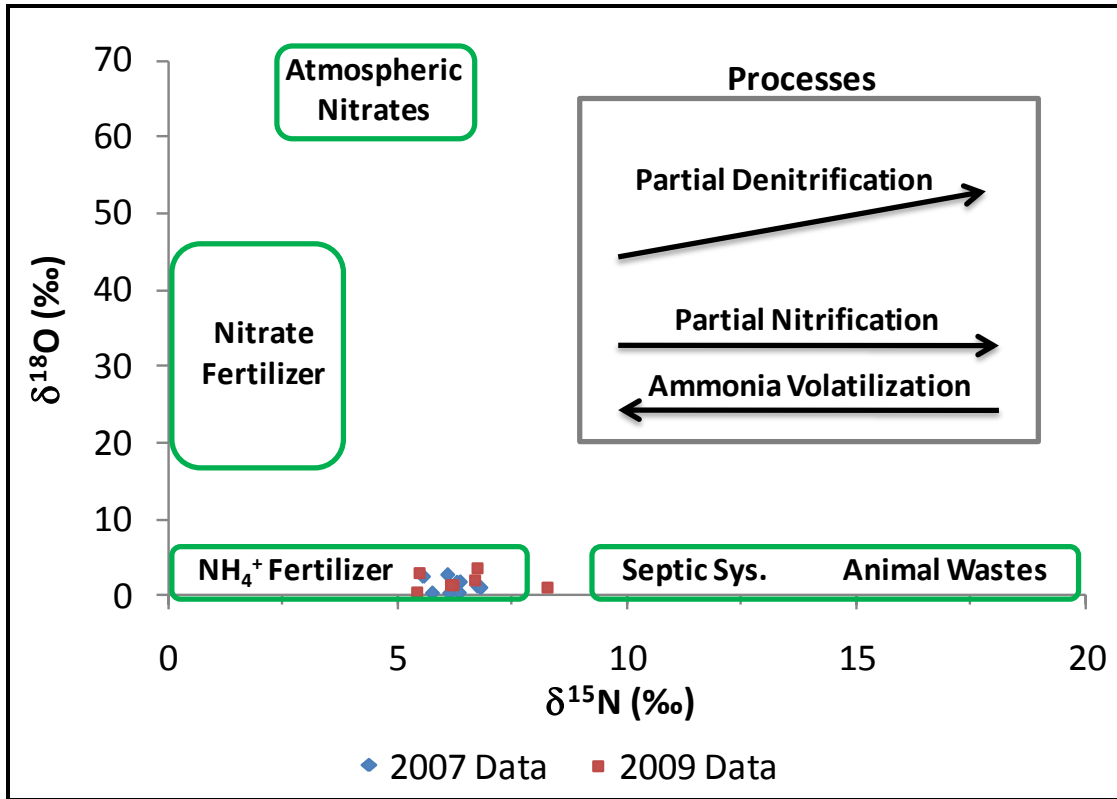


Figure 4.24: 2007 and 2009 nitrate isotope data plotted amongst various categories of nitrate sources (modified from Bleifuss et al., 2001).

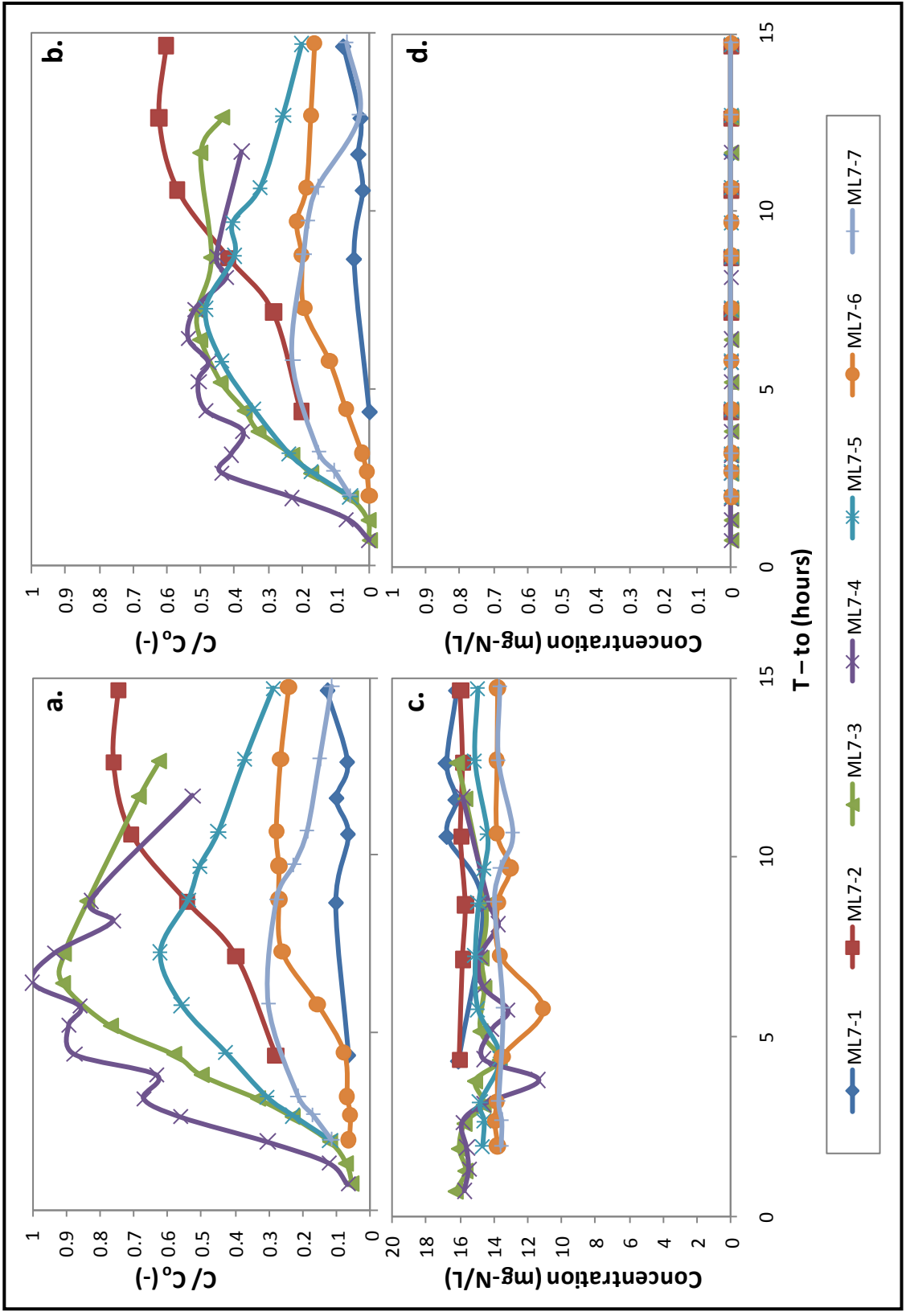


Figure 4.25: ML7 (a) Bromide, (b) acetate, (c) nitrate, and (d) nitrite results from the first injection phase.

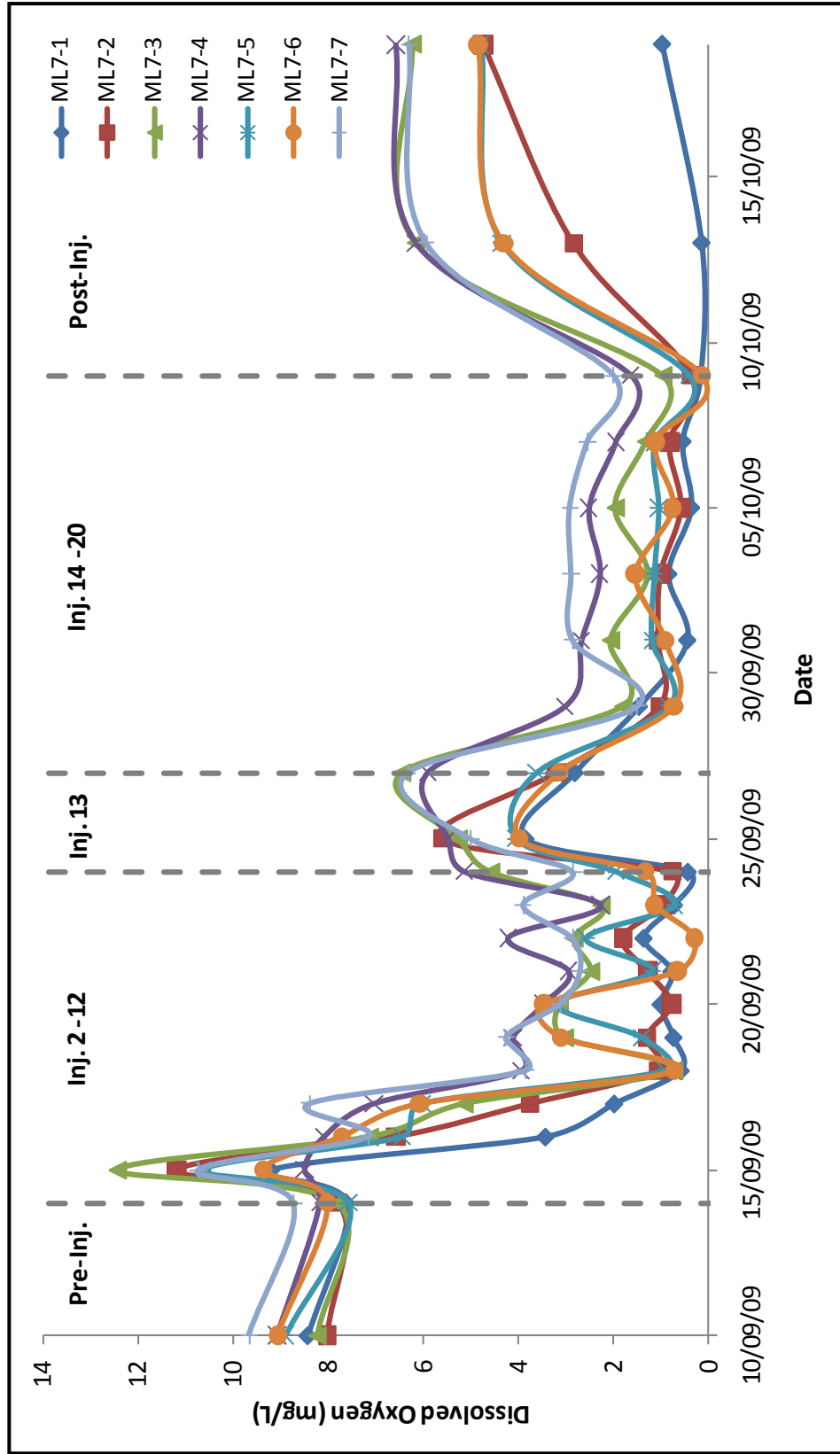


Figure 4.26: Dissolved oxygen results from the second injection phase.

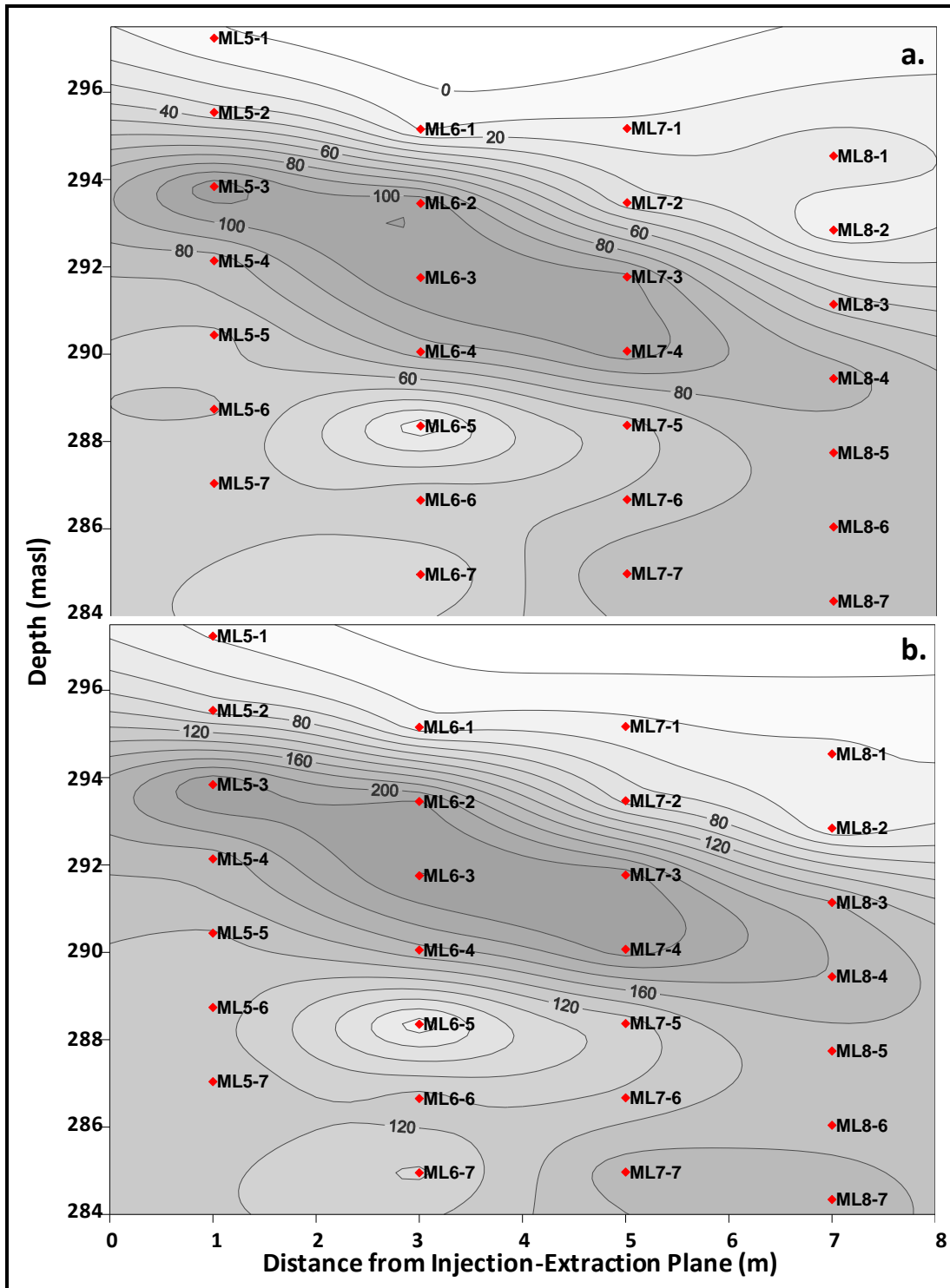


Figure 4.27: Cross-sectional contour plots along the line of multi-level wells representing concentrations of (a) acetate at $T_{to} = 7.5$ hours and (b) bromide at $T_{to} = 7.5$ hours.

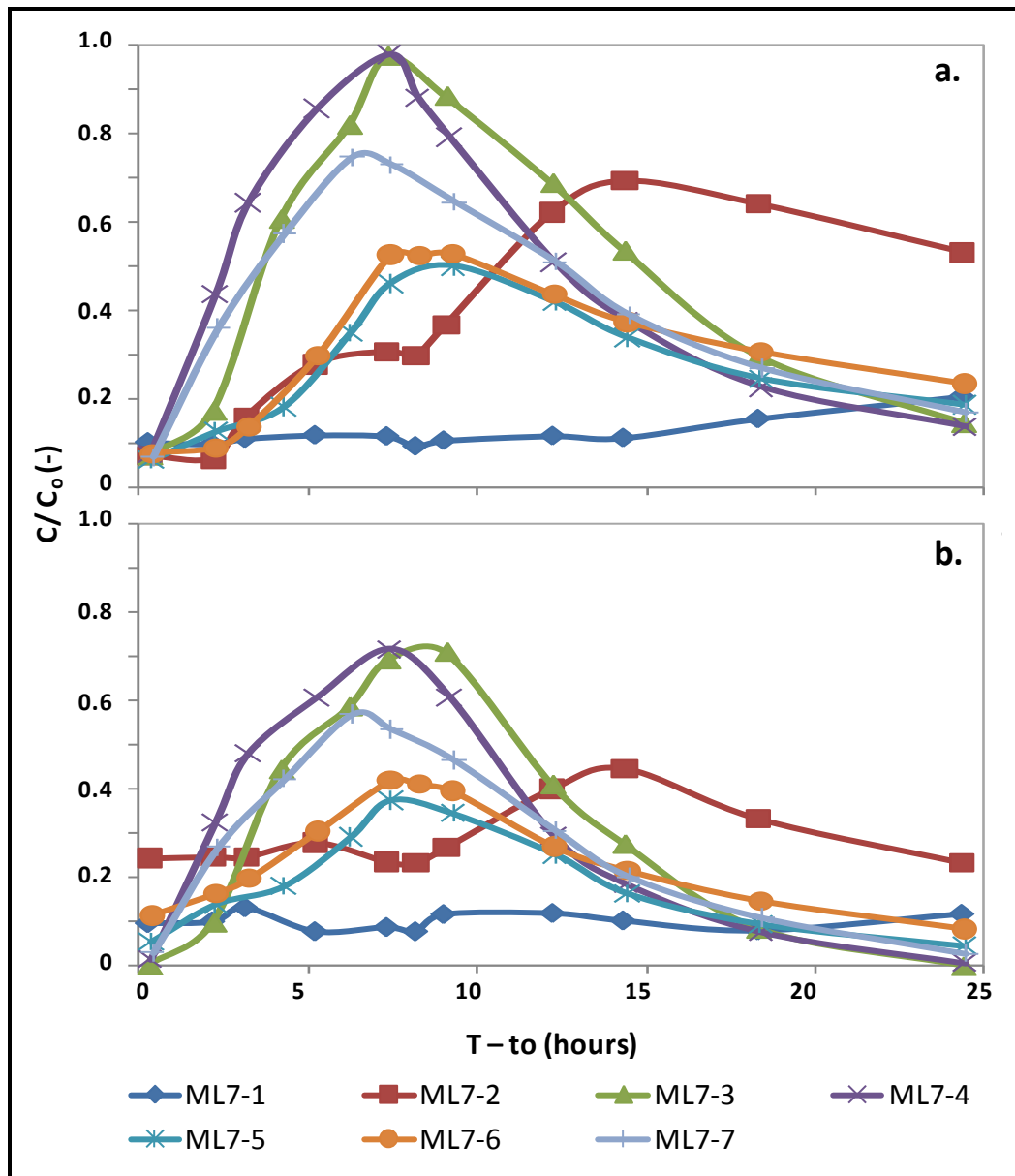


Figure 4.28: ML7 (a) bromide and (b) acetate breakthrough curves from the 25-hour sampling effort that took place during and following injection 13.

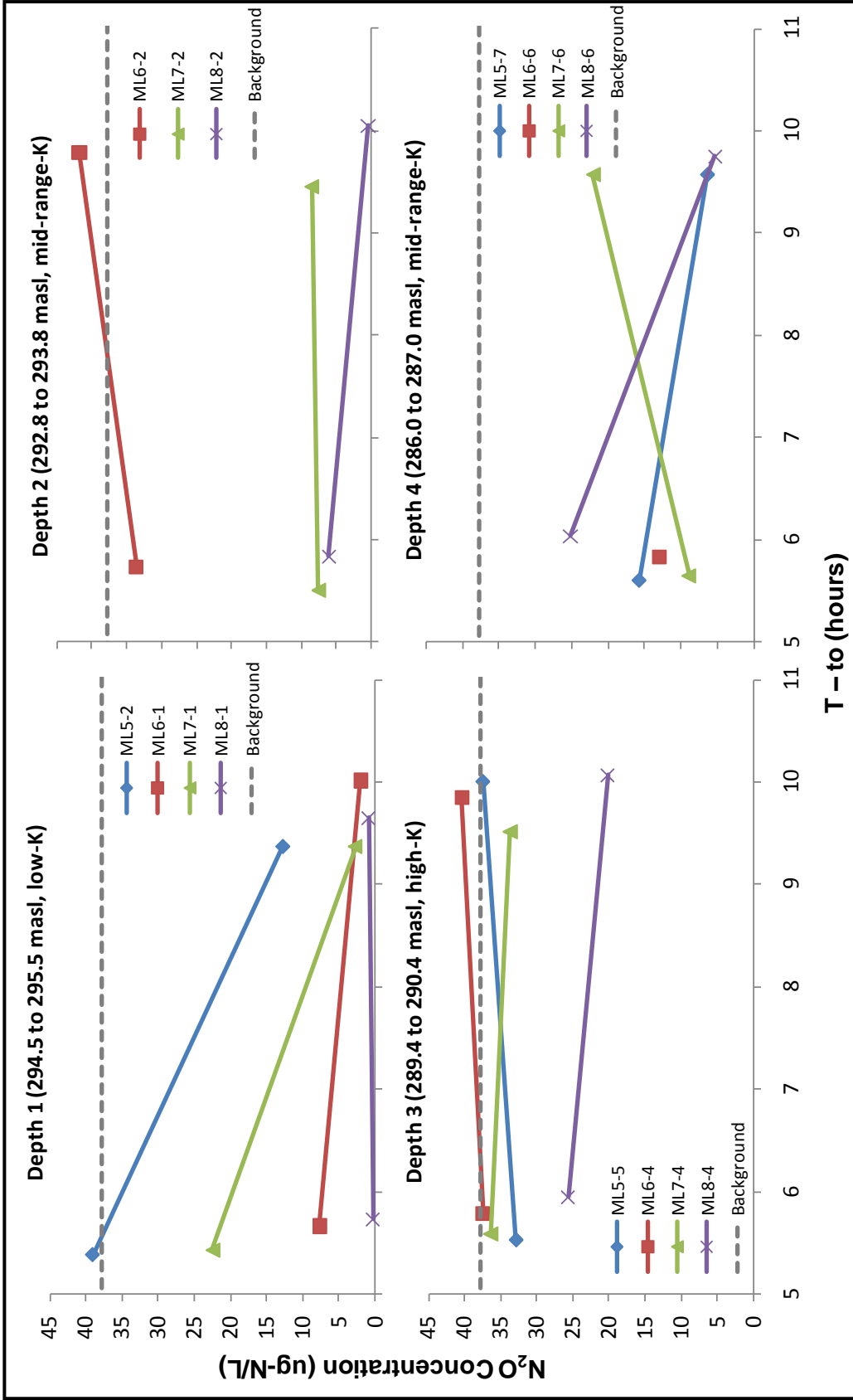


Figure 4.29: Nitrous oxide concentrations determined from samples collected during injection 13.

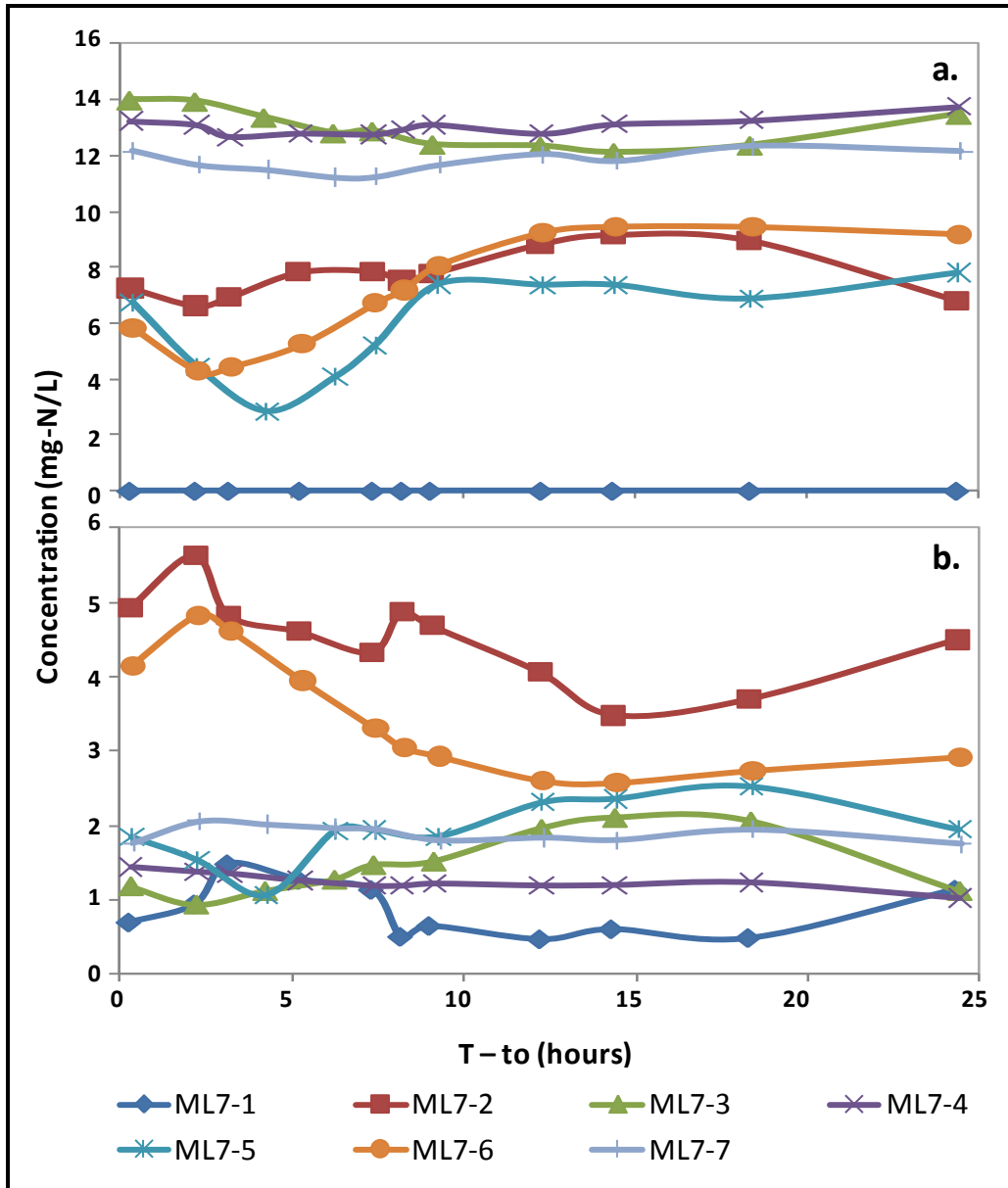


Figure 4.30: ML7 (a) nitrate and (b) nitrite results from the 25-hour sampling effort.

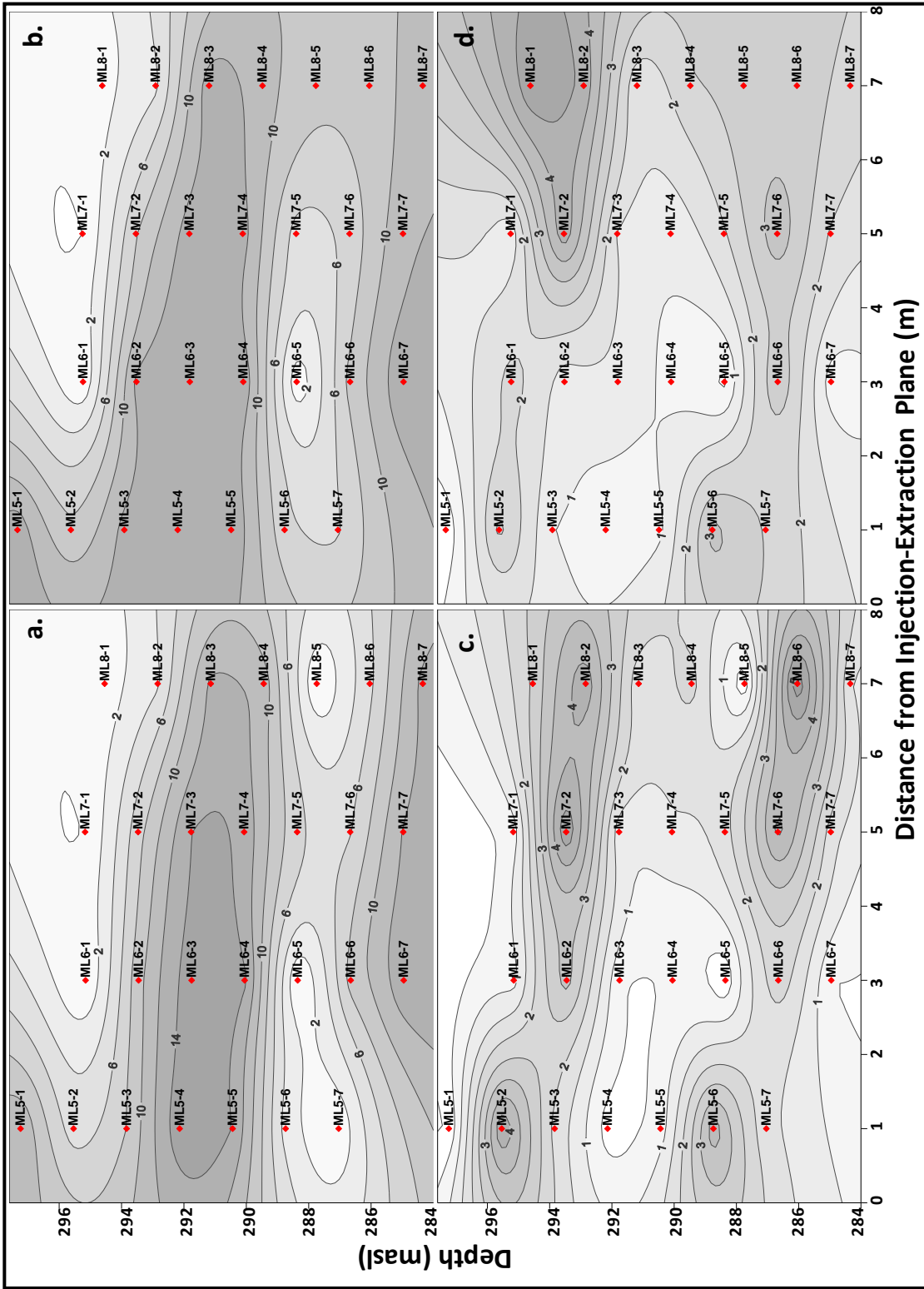


Figure 4.31: Cross-sectional contour plots along the line of multi-level wells representing concentrations of (a) nitrate at T-to = 0.5 hours, (b) nitrate at T-to = 7.5 hours, (c) nitrite at T-to = 0.5 hours, and (d) nitrite at T-to = 7.5 hours.

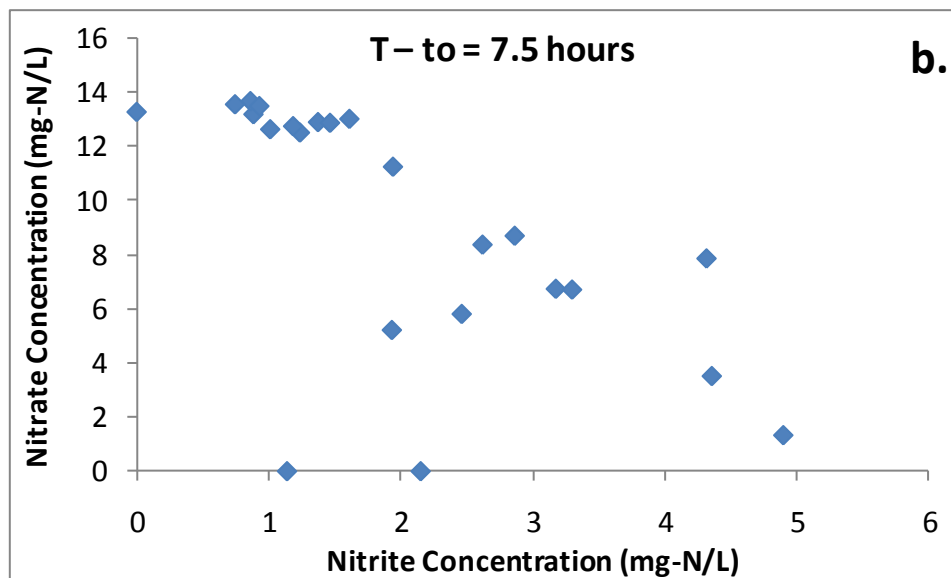
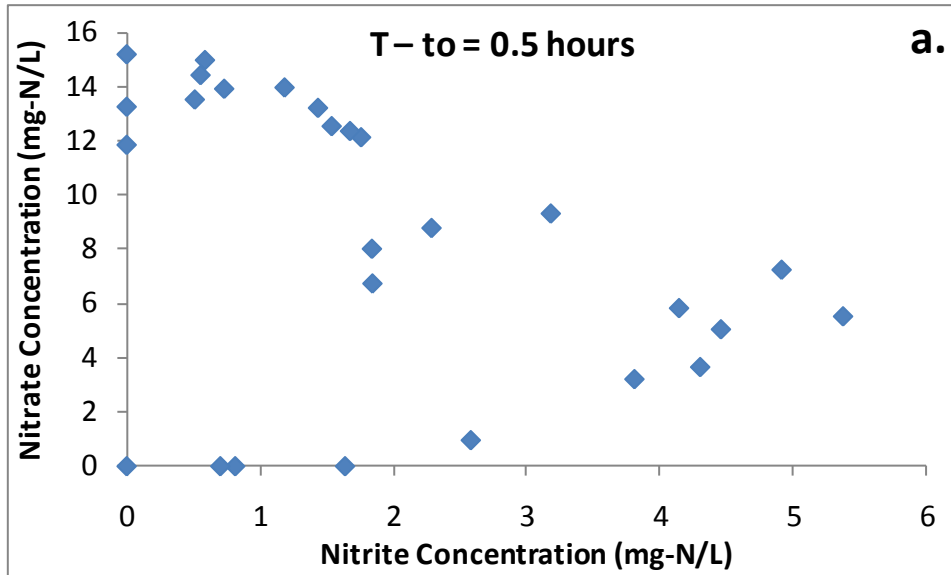


Figure 4.32: Nitrate concentration plotted against nitrite concentration for experiment times of (a) T – to = 0.5 hours and (b) T – to = 7.5 hours.

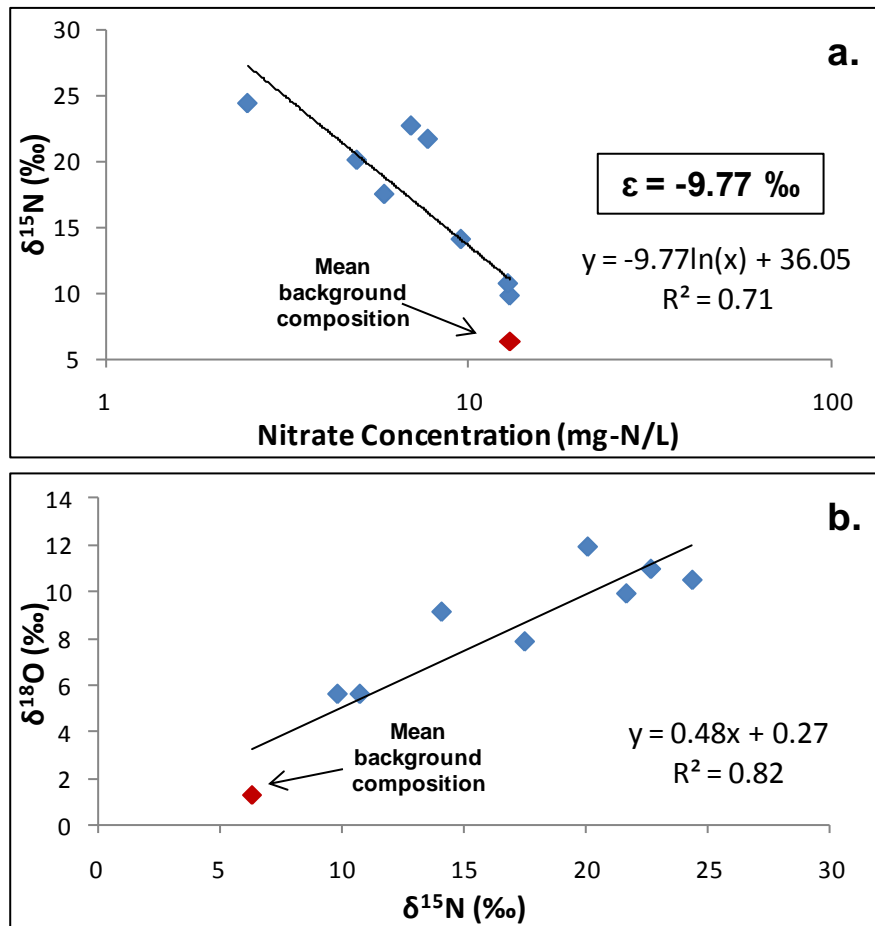


Figure 4.33: ML5, ML6, and ML7 nitrate isotope results from the second injection phase.

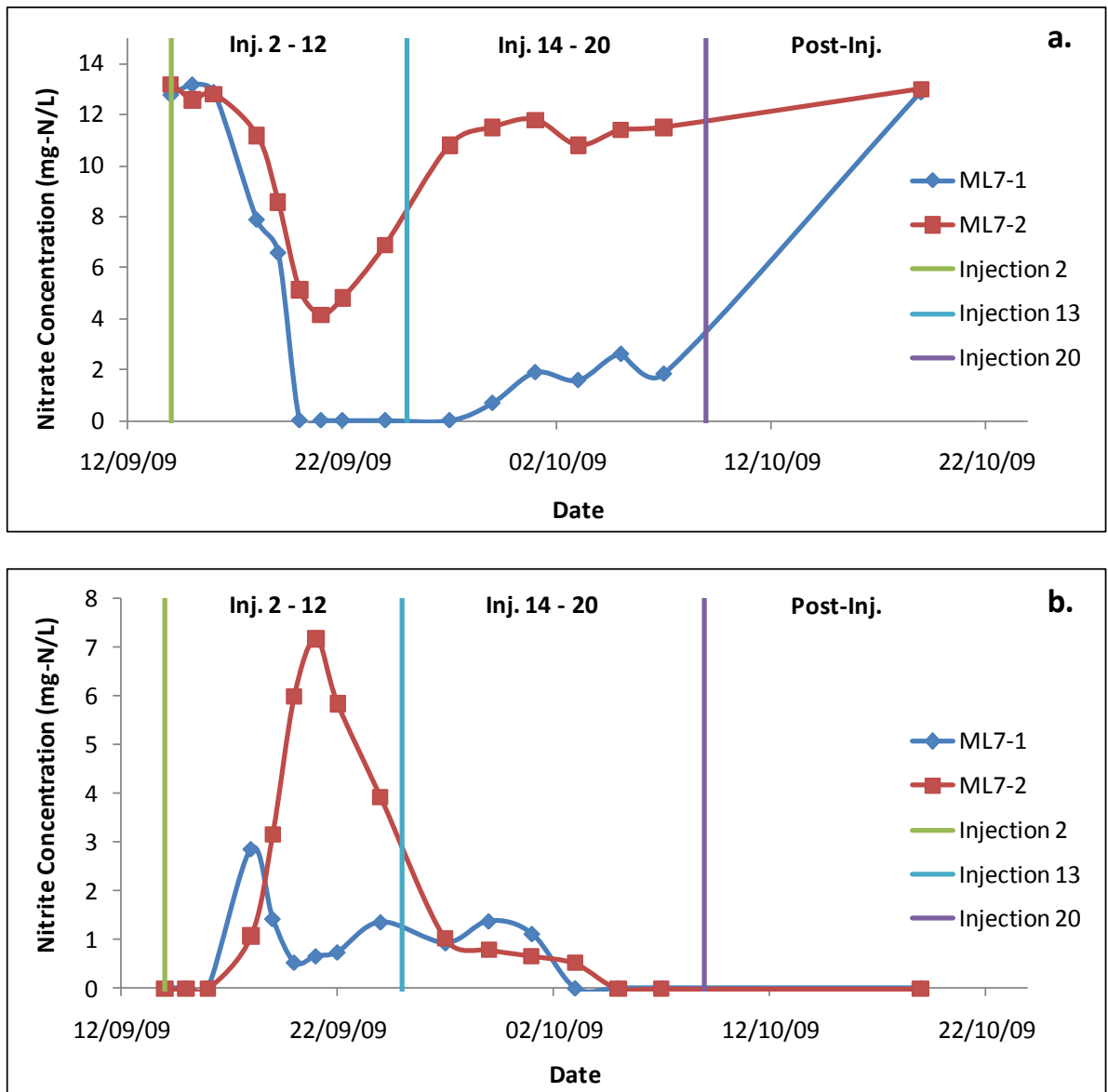


Figure 4.34: Additional (a) nitrate and (b) nitrite monitoring throughout Injection Phase 2.

5. Conclusions and Recommendations

5.1 Conclusions

This research revolved around the development of a cross-injection scheme for stimulating in situ denitrification in an aerobic, highly permeable aquifer. Several methods of physical characterization revealed the complexity of the target aquifer. This unconfined aquifer was found to consist of six main hydrostratigraphic layers with varying hydraulic conductivity values. While the aquifer featured great hydrogeologic complexity, its geochemistry was fairly uniform with depth. This uniformity was observed in the anion, cation, alkalinity, pH, dissolved oxygen, and nitrous oxide data.

Following an unsuccessful initial acetate injection phase, it was determined that multiple, repetitive acetate injections would be required to tackle the aerobic nature of the aquifer and support the growth and reproduction of denitrifying populations. The 19 individual injection experiments of the second acetate injection phase successfully lowered the dissolved oxygen concentrations within the target aquifer to an average range of 0 to 4 mg/L. The least conductive layers featured the lowest oxygen concentrations, while the high-K layers maintained elevated oxygen concentrations throughout the second injection phase. This is despite the uneven distribution of injected acetate, which displayed maximum concentrations in the fast flowing units. The nitrite, nitrate and NO_3^- - ^{15}N and NO_3^- - ^{18}O isotope data were consistent with the oxygen results, suggesting a high degree of stimulated denitrification in the least conductive layers and a limited degree in the high-K layers. These results confirmed the presence of denitrifying bacteria at all aquifer depths. The units corresponding to multi-level well ports ML7-2, ML7-5, and ML7-6 achieved a 46 percent reduction in nitrate, while the layer represented by ML7-1 attained a 100 percent reduction in nitrate. In contrast, very little denitrification was observed in the fast flowing layers corresponding to ports ML7-3, ML7-4, and ML7-7. A total percent reduction, in terms of nitrate mass crossing the treatment lens, of only eleven percent was calculated. Based on these results, it was concluded that the K-profile had an incredible impact on the ability to successfully stimulate in situ denitrification in the target aquifer.

While the treatment system generated harmful nitrite at all aquifer depths and was unable to stimulate denitrification within the highly permeable layers, it is still thought to have great potential at the study site. Additional experimentation is clearly required, however, prior to up-scaling. Once the ideal pulsing interval, injection duration, and injection concentration are determined for the high-K layers, it is believed that this system will have the ability to reduce the nitrate concentrations at the Thornton Well Field. The full-scale system will accelerate nitrate attenuation at the site, eliminating the extensive time lag associated with the BMPs.

5.2 Recommendations

The results of this research have led to the development of several recommendations for future work at the study site.

- 1) The installation of additional downgradient multi-level monitoring bundles: these wells will provide further information regarding the fate of the injected substrate, nitrate, and nitrite during future testing.
- 2) The development and implementation of Injection Phase 3: this phase should feature multiple, consecutive substrate injections designed to systematically test various pulsing intervals, injection concentrations, and electron donors. The data collected will reveal whether or not stimulated in situ denitrification is a viable treatment option for the Thornton Well Field.
- 3) Packer system research: this research should examine the advantages and disadvantages of relying on a packer system to facilitate uniform substrate distribution and denitrification stimulation with depth.

- 4) Additional groundwater modelling: both chemical and physical groundwater modelling should be used to make predictions regarding the third injection phase and to determine the effects of up-scaling treatment.

- 5) Continued site monitoring: groundwater samples should be continuously collected to detect any changes in geochemistry with depth, whether natural or relating to BMPs.

- 6) Refinement of the up-scaling procedure: based on information gathered during the third injection phase, the method for up-scaling treatment should be improved.

Bibliography

- Addiscott, T. M. and N. Benjamin. 2004. Nitrate and Human Health. *Soil Use and Management* 20: 98-104.
- Addy, K. L., A. J. Gold, P. M. Groffman, and P. A. Jacinthe. 1999. Ground Water Nitrate Removal in Subsoil of Forested and Mowed Riparian Buffer Zones. *Journal of Environmental Quality* 28: 962–970.
- Aeschbach-Hertig, W., P. Schlosser, M. Stute, H. J. Simpson, A. Ludin, and J. F. Clark. 1998. A $^3\text{H}/^3\text{He}$ Study of Ground Water Flow in a Fractured Bedrock Aquifer. *Ground Water* 36(4): 661-670.
- Albus, W.L. and R. E. Knighton. 1998. Water Quality in a Sand Plain after Conversion from Dryland to Irrigation: Tillage and Cropping Systems Compared. *Soil and Tillage Research* 48: 195-206.
- American Society for Testing Materials. 2006. *D2487-06, Standard Practice for Classification of Soils for Engineering Purposes (Unified Soil Classification System)*.
- American Society for Testing Materials. 2007. *D422-63, Standard Test Method for Particle-Size Analysis of Soils*.
- Anderson, I. C. and J. S. Levine. 1986. Relative Rates of Nitric Oxide and Nitrous Oxide Production by Nitrifiers, Denitrifiers, and Nitrate Respirers. *Applied and Environmental Microbiology* 51(5): 938-945.
- Appelo, C. A. J., and D. Postma. 2005. *Geochemistry, Groundwater and Pollution, Second Edition*. Amsterdam, Netherlands: A.A. Balkema Publishers.
- Aravena, R., and W. D. Robertson. 1998. Use of Multiple Isotope Tracers to Evaluate Denitrification in Groundwater: Case Study of Nitrate from a Large-Flux Septic System Plume. *Ground Water* 36: 975- 982.
- Barford, C. C., J. P. Montoya, M. A. Altabet, and R. Mitchell. 1999. Steady-State Nitrogen Isotope Effects of N_2 and N_2O Production in *Paracoccus denitrificans*. *Applied and Environmental Microbiology* 65(3): 989-994.
- Bekeris, L. 2007. *Field-Scale Evaluation of Enhanced Agricultural Management Practices Using a Novel Unsaturated Zone Nitrate Mass Load Approach*. Master's thesis, University of Waterloo.

Bleifuss, P. S., G. N. Hanson, and M. A. A Schoonen. 2001. Tracing Sources of Nitrate in the Long Island Aquifer System. Long Island Geology Research Papers. The State University of New York. <http://pbisotopes.ess.sunysb.edu/reports/bleifuss/>.

Blowes, D. W., C. J. Ptacek, S. G. Benner, C. W. T. McRae, T. A. Bennett, and R. W. Puls. 2000. Treatment of Inorganic Contaminants Using Permeable Reactive Barriers. *Journal of Contaminant Hydrology* 45: 123-137.

Bottcher, J., O. Strelbel, S. Voerkelius, and H. L. Schmidt. 1990. Using Isotope Fractionation of Nitrate-Nitrogen and Nitrate-Oxygen for Evaluation of Microbial Denitrification in a Sandy Aquifer. *Journal of Hydrology* 114: 413-424.

Bradbury, K. R. and M. A. Muldoon. 1990. Hydraulic Conductivity Determinations in Unlithified Glacial and Fluvial Sediments. In *Groundwater and Vadose Zone Monitoring, ASTM Special Technical Publication 1053*. American Society for Testing Materials, Philadelphia, 138-151.

Bunn, M. 2010. Information regarding the Interpretation of Resistivity Surveys. Personal Communication.

Butler, J. J. Jr., C. D. McElwee, and W. Z. Liu. 1996. Improving the Reliability of Parameter Estimates Obtained from Slug Tests. *Ground Water* 34(3): 480-490.

Cambardella, C. A., T. B. Moorman, D. B. Jaynes, J. L. Hatfield, T. B. Parkin, W. W. Simpkins, and D. L. Karlen. 1999. Water Quality in Walnut Creek Watershed: Nitrate-Nitrogen in Soils, Subsurface Drainage Water and Shallow Groundwater. *Journal of Environmental Quality* 28: 25-34.

Canter, L.W. 1997. *Nitrates in Groundwater*. Boca Raton, Florida: CRC Press.

Cey, E. E., D. L. Rudolph, R. Aravena, and G. Parkin. 1999. Role of the Riparian Zone in Controlling the Distribution and Fate of Agricultural Nitrogen near a Small Stream in Southern Ontario. *Journal of Contaminant Hydrology* 37: 45-67.

Cole, J. 2008. *Quantification of the Long-Term Effects from Nutrient Reductions on Groundwater Nitrate Concentrations in an Agricultural Setting*. Master's thesis, University of Waterloo.

Constantin, H. and M. Fick. 1997. Influence of C-sources on the Denitrification Rate of a High-Nitrate Concentrated Industrial Wastewater. *Water Research* 31(3): 583-589.

Constantin, H., S. Raoult, W. Montigny, and M. Fick. 1996. Denitrification of Concentrated Industrial Wastewater: Microorganism Selection and Kinetic Studies. *Environmental Technology* 17: 831-840.

Corporation of the County of Oxford. 2001. Quaternary Geology: The Corporation of the County of Oxford, Woodstock, Ontario, Canada.

Corporation of the County of Oxford. 2003b. Municipal Water Wells: The Corporation of the County of Oxford, Woodstock, Ontario, Canada.

Corporation of the County of Oxford. 2003c. Roads: The Corporation of the County of Oxford, Woodstock, Ontario, Canada.

Cowan, W. R. 1975. *Quaternary geology of the Woodstock Area, Southern Ontario*. Geological Report 119, Ontario Division of Mines, Ministry of Natural Resources.

Crop Nutrients Council. 2009. Beneficial Management Practices. Agriculture and Agri-Food Canada. http://www.cropnutrients.ca/Beneficial_Management_Practices/.

Devlin, J. F. and J. F. Barker. 1994. A Semipassive Nutrient Injection Scheme for Enhanced In Situ Denitrification. *Groundwater* 32(3): 374-380.

Devlin, J. F., and J. F. Barker. 1996. Field Investigation of Nutrient Pulse Mixing in an In Situ Biostimulation Experiment. *Water Resources Research* 32(9): 2869-2877.

Devlin, J. F., R. Eedy, and B. J. Butler. 2000. The Effects of Electron Donor and Granular Iron on Nitrate Transformation Rates in Sediments from a Municipal Water Supply Aquifer. *Journal of Contaminant Hydrology* 46: 81-97.

Di, H. J., and K. C. Cameron. 2002. Nitrate Leaching in Temperate Agroecosystems: Sources, Factors, and Mitigating Strategies. *Nutrient Cycling in Agroecosystems* 46: 237-256.

Dinnes, D. L., D. L. Karlen, D. B. Jaynes, T. C. Kaspar, J. L. Hatfield, T. S. Colvin, and C. A. Cambadella. 2002. Nitrogen Management Strategies to Reduce Nitrate Leaching in Tile-Drained Midwestern Soils. *Agronomy Journal* 94: 153-171.

DMTI CanMap Streetfiles [computer file]. 2005. Markham, Ontario: DMTI Spatial Incorporated.

DMTI Census Geography [computer file]. 2003. Markham, Ontario: DMTI Spatial Incorporated.

- Drury, C. F., C. S. Tan, J. D. Gaynor, T. O. Oloya, and T. W. Welacky. 1996. Influence of Controlled Drainage-Subirrigation on Surface and Tile Drainage Nitrate Loss. *Journal of Environmental Quality* 25: 317-324.
- Dybas, M.J., D. W. Hyndman, R. Heine, J. Tiedje, K. Linning, D. Wiggert, T. Voice, X. Zhao, L. Dybas, and C. S. Criddle. 2002. Development, Operation and Long-Term Performance of a Full-Scale Biocurtain Utilizing Bioaugmentation. *Environmental Science and Technology* 36(16): 3635–3644.
- Endres, T. 2010. Electrical Method: Rock and Soil Properties. In Earth 461/668: Advanced Applied Geophysics Class Notes (Set 1). University of Waterloo.
- Englert, A., S. S. Hubbard, K. H. Williams, L. Li, and C. I. Steefel. 2009. Feedbacks Between Hydrogeological Heterogeneity and Bioremediation Induced Biogeochemical Transformations. *Environmental Science and Technology* 43(14): 5197-5204.
- Fan, A. M. and V. E. Steinberg. 1996. Health Implications of Nitrate and Nitrite in Drinking Water: An Update on Methemoglobinemia Occurrence and Reproductive and Developmental Toxicity. *Regulatory Toxicology and Pharmacology* 23: 35–43.
- Foth, H. D. 1984. *Fundamentals of Soil Science*. New York: John Wiley & Sons.
- Freeze, R. A. and J. A. Cherry. 1979. *Groundwater*. Englewood Cliffs, New Jersey: Prentice Hall.
- Fukada, T., K. M. Hiscock, P. F. Dennis, T. Grishek. 2003. A Dual Isotope Approach to Identify Denitrification in Groundwater at a River-Bank Infiltration Site. *Water Research* 37: 3070-3078.
- Gale, T. 2009. *Optimizing Solute Delivery Parameters for the Cross-Injection Scheme Groundwater Nitrate Remediation Technique using Numerical Modelling, Phase II Report*. Bachelor's thesis, University of Waterloo.
- Gelberg, K.H., L. Church, G. Casey, M. London, D. S. Roerig, J. Boyd, and M. Hill. 1999. Nitrate Levels in Drinking Water in Rural New York State. *Environmental Research* 80(1): 34-40.
- Gierczak, R., J. F. Devlin, and D. L. Rudolph. 2006. Combined Use of Field and Laboratory Testing to Predict Preferred Flow Paths in an Heterogeneous Aquifer. *Journal of Contaminant Hydrology* 82: 75-98.

Gierczak, R., J. F. Devlin, and D. L. Rudolph. 2007. Field Test of a Cross-Injection Scheme for Stimulating In Situ Denitrification near a Municipal Water Supply Well. *Journal of Contaminant Hydrology* 89: 48-70.

Gilbert, T. W., T. D. Behymer, and H. B. Castaneda. 1982. Determination of Dissolved Oxygen in Natural and Wastewaters. ASTM D 888-87. *American Laboratory* 14(3): 119-134.

Hamon, M. and E. Fustec. 1991. Laboratory and Field Study of an In Situ Groundwater Denitrification Reactor. *Research Journal of the Water Pollution Control Federation* 63(7): 942-949.

Haslauer, C. P. 2005. *Hydrogeologic Analysis of a Complex Aquifer System and Impacts of Changes in Agricultural Practices on Nitrate Concentrations in a Municipal Well Field: Woodstock, Ontario*. Master's thesis, University of Waterloo.

Heagle, D. J. 2000. *Nitrate Geochemistry of a Regional Aquifer in an Agricultural Landscape, Woodstock, Ontario*. Master's thesis, University of Waterloo.

Health Canada. 2008. Guidelines for Canadian Drinking Water Quality: Summary Table. Prepared by the Federal-Provincial-Territorial Committee on Drinking Water. http://www.hc-sc.gc.ca/ewh-semt/pubs/water-eau/sum_guide-res_recom/index-eng.php.

Hendry, M. J., T. G. Kotzer, and D. K. Solomon. 2005. Sources of Radiogenic Helium in a Clay Aquitard and its Use to Evaluate the Timing of Geologic Events. *Geochimica et Cosmochimica Acta* 69(2): 475-483.

Herman, R. 2001. An Introduction to Electrical Resistivity in Geophysics. *American Journal of Physics* 69(9): 943-952.

Honisch, M., C. Hellmeier, and K. Weiss. 2002. Response of Surface and Subsurface Water Quality to Land Use Changes. *Geoderma* 105: 277-298.

Javandel, I. and P. A. Witherspoon. 1969. A Method of Analyzing Transient Fluid Flow in Multilayered Aquifers. *Water Resources Research* 5: 856-869.

Johnson, C. J., P. A. Bonrod, T. I. Dosch, A. W. Kilness, K. A. Senger, D. C. Busch, and M. R. Meyer. 1987. Fatal Outcome of Methemoglobinemia in an Infant. *Journal of the American Medical Association* 257: 2796-2797.

Khan, I. A. and R. F. Spalding. 2003. Development of a Procedure for Sustainable In Situ Aquifer Denitrification. *Remediation* 13(2): 53-69.

- Khan, I. A. and R. F. Spalding. 2004. Enhanced In Situ Denitrification for a Municipal Well. *Water Research* 38: 3382–3388.
- Knobeloch, L., B. Salna, A. Hogan, J. Postle, and H. Anderson. 2000. Blue Babies and Nitrate-Contaminated Well Water. *Environmental Health Perspectives* 108(7): 675-678.
- Koch, J. 2009. *Evaluating Regional Aquifer Vulnerability and BMP Performance in an Agricultural Environment Using A Multi-Scale Data Integration Approach*. Master's thesis, University of Waterloo.
- Lee, M., J. A. Saunders, and L. W. Wolf. 2000. Effects of Geologic Heterogeneities on Pump-and-Treat and In Situ Bioremediation: A Stochastic Analysis. *Environmental Engineering Science* 17(3): 183-189.
- Logan, J. D. 2001. *Transport Modeling in Hydrogeochemical Systems*. New York: Springer-Verlag.
- Loke, M. H. 1999. *Electrical Imaging Surveys for Environmental and Engineering Studies: A Practical Guide to 2-D and 3-D Surveys*. Heritage Geophysics Incorporated.
- Lund, L. J., A. J. Horne, and A. E. Williams. 2000. Estimating Denitrification in a Large Constructed Wetland using Stable Nitrogen Isotope Ratios. *Ecological Engineering* 14: 67-76.
- Mackay, D. M. 1990. Characterization of the Distribution and Behavior of Contaminants in the Subsurface. pages 70-90. In: *Ground Water and Soil Contamination Remediation: Toward Compatible Science, Policy and Public Perception*. Report on a Colloquium Sponsored by the Water Science and Technology Board. Washington, District of Columbia: National Academy Press.
- Mackay, D. M. and J. A. Cherry. 1989. Remediation of Subsurface Contamination: Limitations of Pump and Treat Programs. *Environmental Science and Technology* 23(6): 630-636.
- Mackay, D. M., P. V. Roberts, and J. A. Cherry. 1985. Transport of Organic Contaminants in Groundwater. *Environmental Science and Technology* 19(5): 384-392.
- Manassaram, D. M., L. C. Backer, and D. M. Moll. 2006. A Review of Nitrate in Drinking Water: Maternal Exposure and Adverse Reproductive and Developmental Outcomes. *Environmental Health Perspectives* 114(3): 320-327.

- Mariotti, A., J. C. Germon, P. Hubert, P. Kaiser, R. Letolle, A. Tardieux, and P. Tardieux. 1981. Experimental Determination of Nitrogen Kinetic Isotope Fractionation: Some Principles; Illustration for the Denitrification and Nitrification Processes. *Plant Soil* 62: 413-430.
- Mariotti, A., A Landreau, and B. Simon. 1988. ¹⁵N Isotope Biogeochemistry and Natural Denitrification Process in Groundwater: Application to the Chalk Aquifer in Northern France. *Geochimica Cosmochimica Acta* 52(7): 1869-1878.
- Martinez, J. and G. Guiraud. 1990. A Lysimeter Study of the Effects of a Rye Grass Catch Crop during Wheat/Maize Rotation on Leaching and on the Following Crop. *Journal of Soil Science* 41(1): 5-16.
- Mateju, V., S. Cizinsica, J. Krejci, and T. Janoch. 1992. Biological Water Denitrification. *Enzyme and Microbiological Technology* 14: 170-183.
- McKague, K., K. Reid, and H. Simpson. 2005. Environmental Impacts of Nitrogen Use in Agriculture. Ontario Ministry of Agriculture, Food, and Rural Affairs. <http://www.omafra.gov.on.ca/english/engineer/facts/05-073.htm>.
- Meisinger, J. J. and J. A. Delgado. 2002. Principles for Managing Nitrogen Leaching. *Journal of Soil and Water Conservation* 57: 485-498.
- Meisinger, J. J., W. L. Hargrove, R. B. Mikkelsen, J. R. Williams, and V. W. Benson. 1991. Effect of Cover Crops on Groundwater Quality. pages 57-68. In: *Cover Crops for Clean Water*. Proceedings of International Conference on Cover Crops for Clean Water. Soil and Water Conservation Society of America. Ankeny, New York.
- Meissner, R., J. Seeger, and H. Rupp. 2002. Effects of Agricultural Land Use Changes on Diffuse Pollution of Water Resources. *Irrigation and Drainage* 51:119-127.
- Mengis M., S. L. Schiff, M. Harris, M. C. English, R. Aravena, R. J. Elgood, and A. MacLean. 1999. Multiple Geochemical and Isotopic Approaches for Assessing Ground Water NO₃⁻ Elimination in a Riparian Zone. *Ground Water* 37(3): 448-457.
- Moltz, F. J., R. H. Morin, A. E. Hess, J. G. Melville, and O. Güven. 1989. The Impeller Meter for Measuring Aquifer Permeability Variations: Evaluation and Comparison with other Tests. *Water Resources Research* 25(7): 1677-1683.
- Natural Resources and Values Information System [computer file]. 2008. Toronto, Ontario: The Ontario Ministry of Natural Resources.
- Neville, C. J. 2001. *ONED_1 Analytical Solution: User's Guide*.

Ontario Ministry of Agriculture, Food, and Rural Affairs, 2009. Nutrient Management – Legislation, Regulations, and Protocols. <http://www.omafra.gov.on.ca/english/environment/laws.htm>.

Ontario Ministry of the Environment, 2008. Nutrient Management – Regulation and Protocols. http://www.ene.gov.on.ca/envision/land/nutrient_management.htm.

Padusenko, G. 2001. Regional Hydrogeologic Evaluation of a Complex Glacial Aquifer System in an Agricultural Landscape: Implications for Nitrate Distribution. Master's thesis, University of Waterloo.

Peyton, B. 1996. Improved Biomass Distribution using Pulsed Injections of Electron Donor and Acceptor. *Water Research* 30(3): 756–758.

Price, R. M., Z. Top, J. D. Happell, and P. K. Swart. 2003. Use of Tritium and Helium to Define Groundwater Flow Conditions in Everglades National Park. *Water Resources Research* 39(9): 1267-1279.

Randall, G. W., D. R. Huggins, M. P. Russelle, D. J. Fuchs, W. W. Nelson, and J. L. Anderson. 1997. Nitrate Losses through Subsurface Tile Drainage in CRP, Alfalfa, and Row Crop Systems. *Journal of Environmental Quality* 26: 1240–1247.

Randall, G. W. and D. J. Mulla. 2001. Nitrate Nitrogen in Surface Waters as Influenced by Climatic Conditions and Agricultural Practices. *Journal of Environmental Quality* 30: 337-344.

Rausch, R., W. Schafer, R. Therrien, and C. Wagner. 2005. *Solute Transport Modelling: An Introduction to Models and Solution Strategies*. Stuttgart, Germany: Gebr. Borntraeger Verlagsbuchhandlung Science Publishers.

Riding, R. E. and S. M. Awramik (eds). 2000. *Microbial Sediments*. Heidelberg, Germany: Springer-Verlag.

Robertson, W. D., D. W. Blowes, C. J. Ptacek, and J. A. Cherry. 2000. Long-Term Performance of In Situ Reactive Barriers for Nitrate Remediation. *Ground Water* 38(5): 689-695.

Robertson, W. D. and J. A. Cherry. 1995. In Situ Denitrification of Septic-System Nitrate Using Reactive Porous Media Barriers: Field Trials. *Ground Water* 33(1): 99-111.

Ross, H. C. and C. D. McElwee. 2007. Multi-Level Slug Tests to Measure 3-D Hydraulic Conductivity Distributions. *Natural Resources Research* 16(1): 67-79.

Sanchez, C. A. and A. M. Blackmer. 1988. Recovery of Anhydrous Ammonia-Derived Nitrogen-15 during Three Years of Corn Production in Iowa. *Agronomy Journal* 80: 102-108.

- Scherer, M. M., S. Richter, R. L. Valentine, and P. J. J. Alvarez. 2000. Chemistry and Microbiology of Permeable Reactive Barriers for In Situ Groundwater Clean up. *Critical Reviews in Microbiology* 26(4): 221-264.
- Schulze-Makuch, D., D. A. Carlson, D. S. Cherkauer, and P. Malik. 1999. Scale Dependency of Hydraulic Conductivity in Heterogeneous Media. *Ground Water* 37(6): 904-919.
- Sebol, L. A. 2004. Evaluating Shallow Groundwater Age Tracers: Br⁻, CFCs, ³H/³He, SF₆, and HCFCs/HFCs. PhD thesis, University of Waterloo.
- Silliman, S. E. and G. Mantz. 2000. The Effect of Measurement Error on Estimating the Hydraulic Gradient in Three Dimensions. *Ground Water* 38 (1): 114-120.
- Soares, M. I. M. 2000. Biological Denitrification of Groundwater. *Water, Air, and Soil Pollution* 123: 183-193.
- Sobieszuk, P. and K. W. Szewczyk. 2006. Estimation of (C/N) Ratio for Microbial Denitrification. *Environmental Technology* 27: 103-108.
- Solomon, D. K., R. J. Poreda, P. G. Cook, and A. Hunt. 1995. Site Characterization Using ³H/³He Ground-Water Ages, Cape Cod, Massachusetts. *Ground Water* 33(6): 988-996.
- Solomon, D. K., R. J. Poreda, S. L. Schiff, and J. A. Cherry. 1992. Tritium and Helium 3 as Groundwater Age Tracers in the Borden Aquifer. *Water Resources Research* 28(3): 741-755.
- Solomon, D. K., S. L. Schiff, R. J. Poreda, and W. B. Clarke. 1993. A Validation of the ³H/³He-Method for Determining Groundwater Recharge. *Water Resources Research* 29(2): 2951-2962.
- Solomon, D. K. and E. A. Sudicky. 1991. Tritium and Helium 3 Isotope Ratios for Direct Estimation of Spatial Variations in Groundwater Recharge. *Water Resources Research* 27(9): 2309-2319.
- Southwestern Ontario Orthoimagery Project [computer file]. 2006. First Base Solutions.
- Spalding, R. F. and M. E. Exner. 1993. Occurrence of Nitrate in Groundwater: A Review. *Journal of Environmental Quality* 22: 392-402.
- Spalding, R. F. and J. D. Parrott. 1994. Shallow Groundwater Denitrification. *The Science of the Total Environment* 141: 17-25.

- Springer, R. K. and L. W. Gelhar. 1991. Characterization of Large-Scale Aquifer Heterogeneity in Glacial Outwash by Analysis of Slug Tests with Oscillatory Response, Cape Cod, Massachusetts. U.S. Geological Survey Water Resources Investigation Report 91-4034: 36-40.
- Spruill, T.B. 2000. Statistical Evaluation of Effects of Riparian Buffers on Nitrate and Ground Water Quality. *Journal of Environmental Quality* 29: 1523–1538.
- Svenson, E., T. Schweisinger, and L. C. Murdoch. 2005. Air-Slug Low-Pressure Straddle-Packer System to Facilitate Characterization of Fractured Bedrock. Proceedings of the 2005 Georgia Water Resources Conference, April 25-27, 2005, University of Georgia.
- Szabo, Z., D. E. Rice, L. N. Plummer, E. Busenberg, S. Drenkard, and P. Schlosser. 1996. Age Dating of Shallow Groundwater with Chlorofluorocarbons, Tritium/Helium 3, and Flow Path Analysis, Southern New Jersey Coastal Plain. *Water Resources Research* 32(4): 1023-1038.
- Terzaghi, K. 1925. *Erdbaumechanik auf Bodenphysikalischer Grundlage*. Franz Deuticke, Leipzig.
- Tomer, M. D. and M. R. Burkart. 2003. Long-Term Effects of Nitrogen Fertilizer Use on Groundwater Nitrate in Two Small Watersheds. *Journal of Environmental Quality* 32: 2158-2171.
- Ward, M. H., S. D. Mark, K. P. Cantor, D. D. Weisenburger, A. Correa-Villasenor, and S. H. Zahm. 1996. Drinking Water Nitrate and the Risk of Non-Hodgkin's Lymphoma. *Epidemiology* 7(5): 465–471.
- Wassenaar, L. I., M. J. Hendry, and N. Harrington. 2006. Decadal Geochemical and Isotopic Trends for Nitrate in a Transboundary Aquifer and Implications for Agricultural Beneficial Management Practices. *Environmental Science and Technology* 40: 4626-4632.
- Weed, D. A. J. and R. S. Kanwar. 1996. Nitrate and Water Present in and Flowing from Root-Zone Soil. *Journal of Environmental Quality* 25: 709–719.
- Yang, C. Y., M. F. Cheng, S. S. Tsai, and Y. L. Hsieh. 1998. Calcium, Magnesium, and Nitrate in Drinking Water and Gastric Cancer Mortality. *Japanese Journal of Cancer Research* 89: 124-130.
- Yang, Y. S., K. L. McGeough, R. M. Kalin, and K. W. Dickson. 2003. Numerical Modeling for Remediation of Contaminated Land and Groundwater. *Bulletin of Environmental Contamination Toxicology* 71: 729-736.

Young, E. O. and R. D. Briggs. 2005. Shallow Ground Water Nitrate-N and Ammonium-N in cropland and Riparian Buffers. *Agriculture, Ecosystems and Environment* 109(3-4): 297-309.

Zemansky, G. M. and C. D. McElwee. 2005. High-Resolution Slug Testing. *Ground Water* 43(2): 222-230.

Zheng, C. and P. P. Wang. 1999. *MT3DMS: A Modular Three-Dimensional Multispecies Transport Model*. Contract Report for the U.S. Army Corps of Engineers Strategic Environmental Research and Development Program (SERDP).

Zlotnik, V. A. and V. L. McGuire. 1998. Multi-Level Slug Tests in Highly Permeable Formations: 2. Hydraulic Conductivity Identification, Method Verification, and Field Applications. *Journal of Hydrology* 204: 283-296.

Appendices

Appendix A: Well Location and Construction Information

Table A.1: Construction and location information for the injection-extraction wells.

Well ID	[UTM NAD 83 17 N]		Ground Surface Elevation (masl)	Top of Casing Elevation (masl)	Total Depth (masl)	Top of Screen Depth (masl)	Length of Screen (m)
	Easting (m)	Northing (m)					
WO77	520045.40	4770166.24	300.47	300.69	283.90	294.56	10.67
WO78	520041.97	4770162.58	300.52	301.15	283.70	294.37	10.67
WO79	520038.57	4770158.89	300.67	301.31	285.32	294.47	9.14
WO80	520035.13	4770155.04	300.85	301.21	284.00	294.66	10.67

Table A.2: Construction and location information for the multi-level monitoring wells installed in 2008.

Well ID	[UTM NAD 83 17 N]		Ground Surface Elevation (masl)	Top of Casing Elevation (masl)	Port ID	Depth to Centre of Screen (mbgs)	Depth to Centre of Screen (masl)
	Easting (m)	Northing (m)					
ML1	520030.78	4770156.59	301.01	301.70	1	3.88	297.13
					2	5.38	295.63
					3	6.88	294.13
					4	8.38	292.63
					5	9.88	291.13
					6	11.38	289.63
					7	12.88	288.13
ML2	520046.05	4770165.48	300.52	301.02	1	5.89	294.62
					2	7.59	292.92
					3	9.29	291.22
					4	10.99	289.52
					5	12.69	287.82
					6	14.39	286.12
					7	16.09	284.42
					8	17.79	282.72
ML3	520047.44	4770164.16	300.53	301.12	1	5.93	294.59
					2	7.63	292.89
					3	9.33	291.19
					4	11.03	289.49
					5	12.73	287.79
					6	14.43	286.09
					7	16.13	284.39
					8	17.83	282.69
ML4	520048.89	4770162.76	300.54	301.12	1	6.07	294.47
					2	7.77	292.77
					3	9.47	291.07
					4	11.17	289.37
					5	12.87	287.67
					6	14.57	285.97
					7	16.27	284.27
					8	17.97	282.57

Table A.2: (continued)

Well ID	[UTM NAD 83 17 N]		Ground Surface Elevation (masl)	Top of Casing Elevation (masl)	Port ID	Depth to Centre of Screen (mbgs)	Depth to Centre of Screen (masl)
	Easting (m)	Northing (m)					
ML5	520041.03	4770160.03	300.64	301.19	1	3.40	297.24
					2	5.10	295.54
					3	6.80	293.84
					4	8.50	292.14
					5	10.20	290.44
					6	11.90	288.74
					7	13.60	287.04
					8	15.30	285.34
ML6	520042.42	4770158.54	300.67	301.29	1	5.51	295.15
					2	7.21	293.45
					3	8.91	291.75
					4	10.61	290.05
					5	12.31	288.35
					6	14.01	286.65
					7	15.71	284.95
					8	17.41	283.25
ML7	520043.83	4770157.27	300.69	301.28	1	5.52	295.17
					2	7.22	293.47
					3	8.92	291.77
					4	10.62	290.07
					5	12.32	288.37
					6	14.02	286.67
					7	15.72	284.97
					8	17.42	283.27
ML8	520045.07	4770156.28	300.73	301.35	1	6.19	294.54
					2	7.89	292.84
					3	9.59	291.14
					4	11.29	289.44
					5	12.99	287.74
					6	14.69	286.04
					7	16.39	284.34
					8	18.09	282.64

Table A.2: (continued)

Well ID	[UTM NAD 83 17 N]		Ground Surface Elevation (masl)	Top of Casing Elevation (masl)	Port ID	Depth to Centre of Screen (mbgs)	Depth to Centre of Screen (masl)
	Easting (m)	Northing (m)					
ML9	520036.00	4770154.31	300.85	301.70	1	5.07	295.78
					2	6.77	294.08
					3	8.47	292.38
					4	10.17	290.68
					5	11.87	288.98
					6	13.57	287.28
					7	15.27	285.58
					8	17.02	283.83
ML10	520037.37	4770153.01	300.92	301.45	1	6.33	294.59
					2	8.03	292.89
					3	9.73	291.19
					4	11.43	289.49
					5	13.13	287.79
					6	14.83	286.09
					7	16.53	284.39
					8	18.23	282.69
ML11	520038.80	4770151.82	300.91	301.35	1	6.38	294.53
					2	8.08	292.83
					3	9.78	291.13
					4	11.48	289.43
					5	13.18	287.73
					6	14.88	286.03
					7	16.58	284.33
					8	18.28	282.63
ML12	520044.84	4770165.49	300.49	301.20	1	5.71	294.78
					2	7.41	293.08
					3	9.11	291.38
					4	10.81	289.68
					5	12.51	287.98
					6	14.21	286.28
					7	15.91	284.58
					8	17.61	282.88

Table A.3: Construction and location information for the Solinst® CMT Multi-level Systems.

Well ID	[UTM NAD 83 17 N]		Ground Surface Elevation (masl)	Top of Casing Elevation (masl)	Port ID	Depth to Centre of Screen (mbgs)	Depth to Centre of Screen (masl)
	Easting (m)	Northing (m)					
WO74-ML	520051.31	4770151.86	300.81	301.28	1	4.17	296.64
					2	5.49	295.32
					3	7.01	293.80
					4	8.53	292.28
					5	10.36	290.45
					6	12.80	288.01
					7	14.63	286.18
WO75-ML	520014.39	4770113.06	302.82	303.22	1	3.81	299.01
					2	5.03	297.79
					3	7.47	295.35
					4	9.30	293.52
					5	11.13	291.69
					6	12.95	289.87
					7	14.78	288.04

Table A.4: Construction and location information for larger diameter, single-screen, existing monitoring wells.

Well ID	[UTM NAD 83 17 N]		Ground Surface Elevation	Top of Casing Elevation (masl)	Total Depth (masl)	Top of Screen Depth (masl)	Length of Screen (m)
	Easting (m)	Northing (m)					
WO74-S	520053.90	4770154.28	300.75	301.64	290.39	291.61	1.22
WO74-WT	520052.33	4770152.75	300.75	301.64	294.81	297.70	2.89
WO74-M	520055.03	4770154.97	300.74	301.63	287.02	288.24	1.22
WO74-D	520056.14	4770155.97	300.75	301.62	282.77	285.81	3.04
WO75-S	520015.09	4770112.00	302.68	303.58	292.32	293.84	1.52
WO75-D	520013.59	4770112.04	302.80	303.62	281.46	284.51	3.05
WO35	519977.82	4770190.29	302.57	303.00	295.87	297.39	1.52
WO02-D-14	520134.99	4770065.73	300.89	301.08	286.74	289.24	2.50

Appendix B: Geologic Core Logs

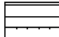




WO74-D (Monitoring Well)



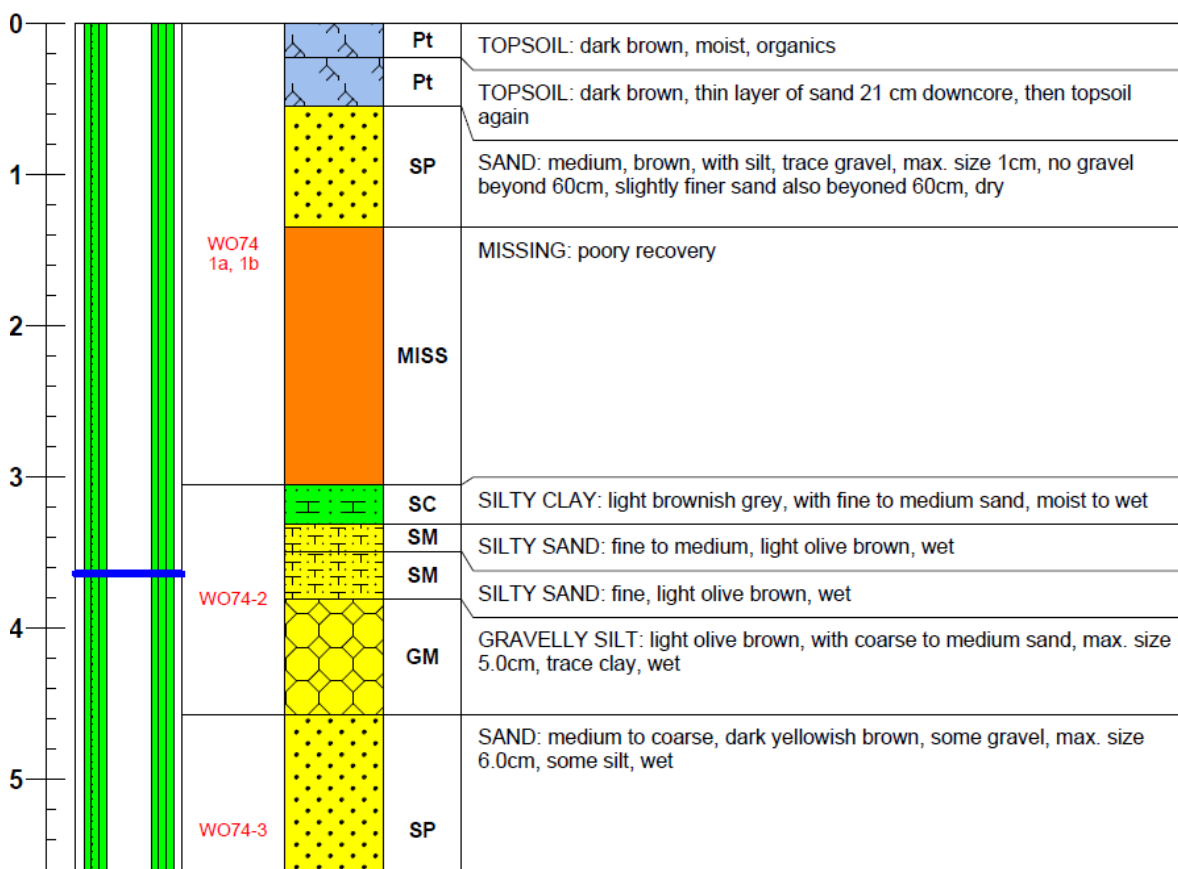
Date Drilled: December 20, 2006
 Drilling Inspector: Joanna Passmore
 Drillers: Boart Longyear - SDS Drilling
 Method: Rotosonic Mini Sonic Drill Rig 4x6" system
 Total Depth of Boring: 21.34m
 Depth to water: 3.64mbgs (NAD83) (Measured January 10, 2007)
 Ground Elevation: 300.75masl (NAD83)
 Top of PVC riser elevation: 301.62m (NAD83)
 Location: UTM17 North 4770155.97m, East 520056.14m
 Originally Surveyed: March 28, 2007
 Elevations Re-Surveyed: July 20, 2007
 Survey Corrected: July 25, 2007
 Installation: - 2.00" Schedule 40 PVC riser and screen
 - holeplug from 13.56mbgs to 16.61mbgs
 - screen from 14.94mbgs to 17.98mbgs
 - sand pack from 16.61mbgs to 20.42mbgs
 - grout from 0mbgs to 13.56mbgs
 Logged By: Geoff Moroz, Jaqueline Kreller
 Last Updated: July 25, 2007

USCS = Unified Soil Classification System
 mbgs = Metres Below Ground Surface
 masl = Metres Above Sea Level

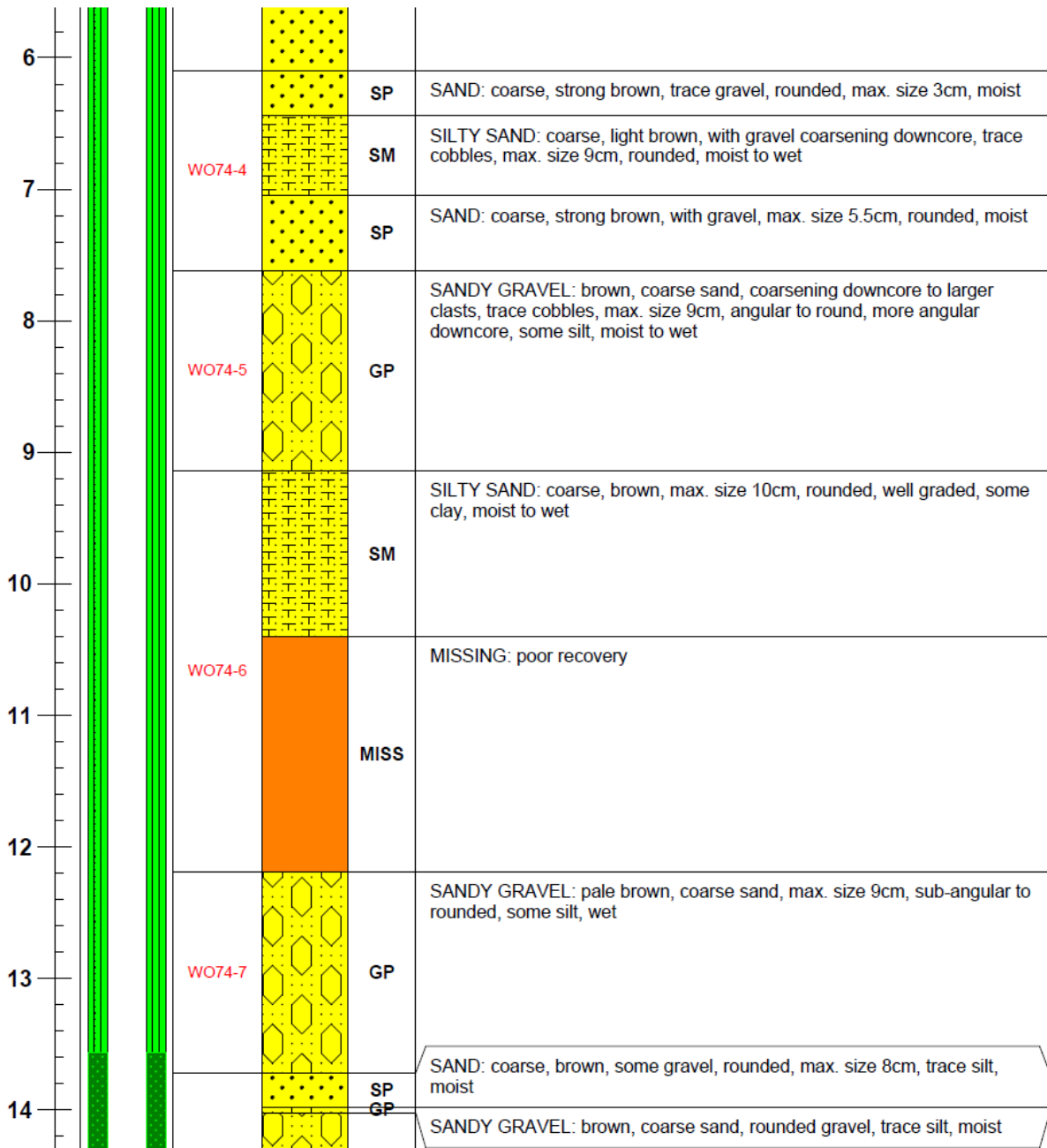
Well Construction Legend:

	Well Screen		Water Level
	Hole Plug		
	Bentonite Grout		
	Sand pack		

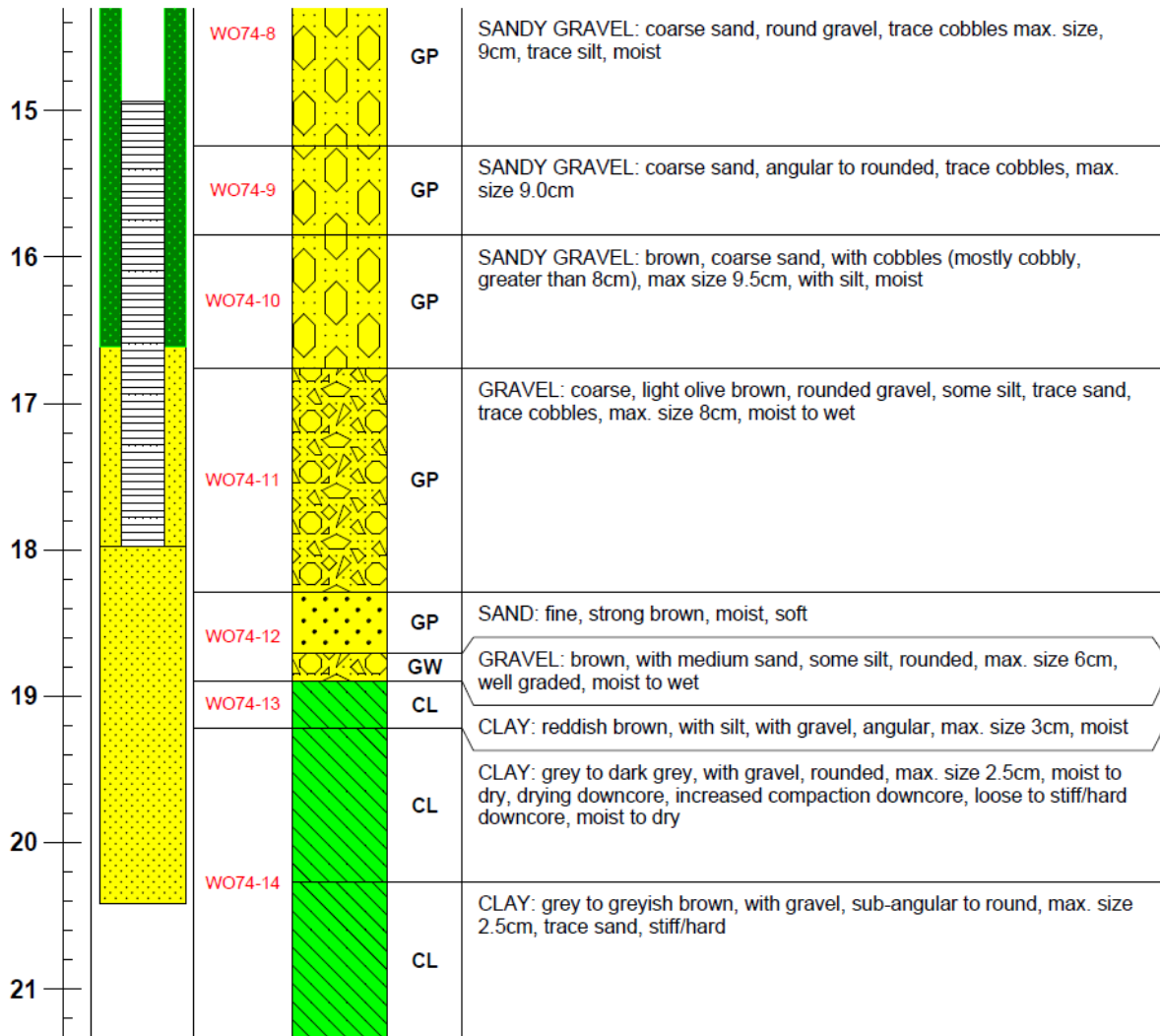
Depth (m)	Well Construction	Core No. and % Recovery	Lithology	USCS	Lithological Description
-----------	-------------------	-------------------------	-----------	------	--------------------------



WO74-D (Monitoring Well)					
Depth (m)	Well Construction	Core No. and % Recovery	Lithology	USCS	Lithological Description



WO74-D (Monitoring Well)					
Depth (m)	Well Construction	Core No. and % Recovery	Lithology	USCS	Lithological Description



Notes:

- for 5' cores, percent recovery based on a total core length of 1.524m
- developed January 10, 2007 with a Monsoon pump
- pumped water until clear; total water pumped 90L
- well is down and around driveway into the back left corner of farmers field on left of Curry Rd.
- water level measured from top of PVC pipe, stickup: 0.92m

WO74-M (Monitoring Well)



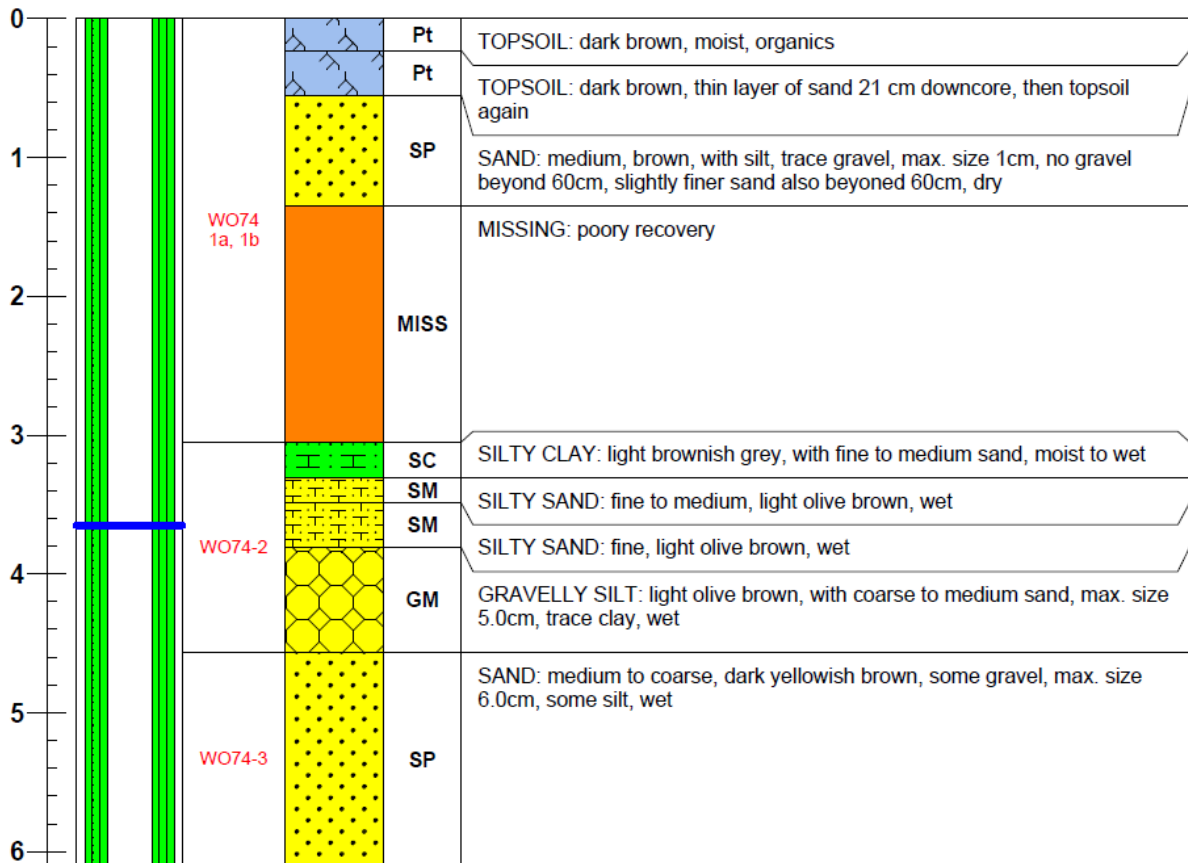
Date Drilled: December 20, 2006
 Drilling Inspector: Joanna Passmore
 Drillers: Boart Longyear - SDS Drilling
 Method: Rotasonic Mini Sonic Drill Rig 4x6" system
 Total Depth of Boring: 14.02m
 Depth to water: 3.65mbgs (NAD83) (Measured March 29, 2007)
 Ground Elevation: 300.74masl (NAD83)
 Top of PVC riser elevation: 301.63m (NAD83)
 Location: UTM17 North 4770154.97m, East 520055.03m
 Originally Surveyed: March 28, 2007
 Elevations Re-Surveyed: July 20, 2007
 Survey Corrected: July 25, 2007
 Installation: - 2.00" Schedule 40 PVC riser and screen
 - holeplug from 9.14mbgs to 11.89mbgs
 - screen from 12.50mbgs to 13.72mbgs
 - sand pack from 11.89mbgs to 14.02mbgs
 - grout from 0mbgs to 9.14mbgs
 Logged By: Geoff Moroz, Jaqueline Kreller
 Last Updated: July 25, 2007

USCS = Unified Soil Classification System
 mbgs = Metres Below Ground Surface
 masl = Metres Above Sea Level

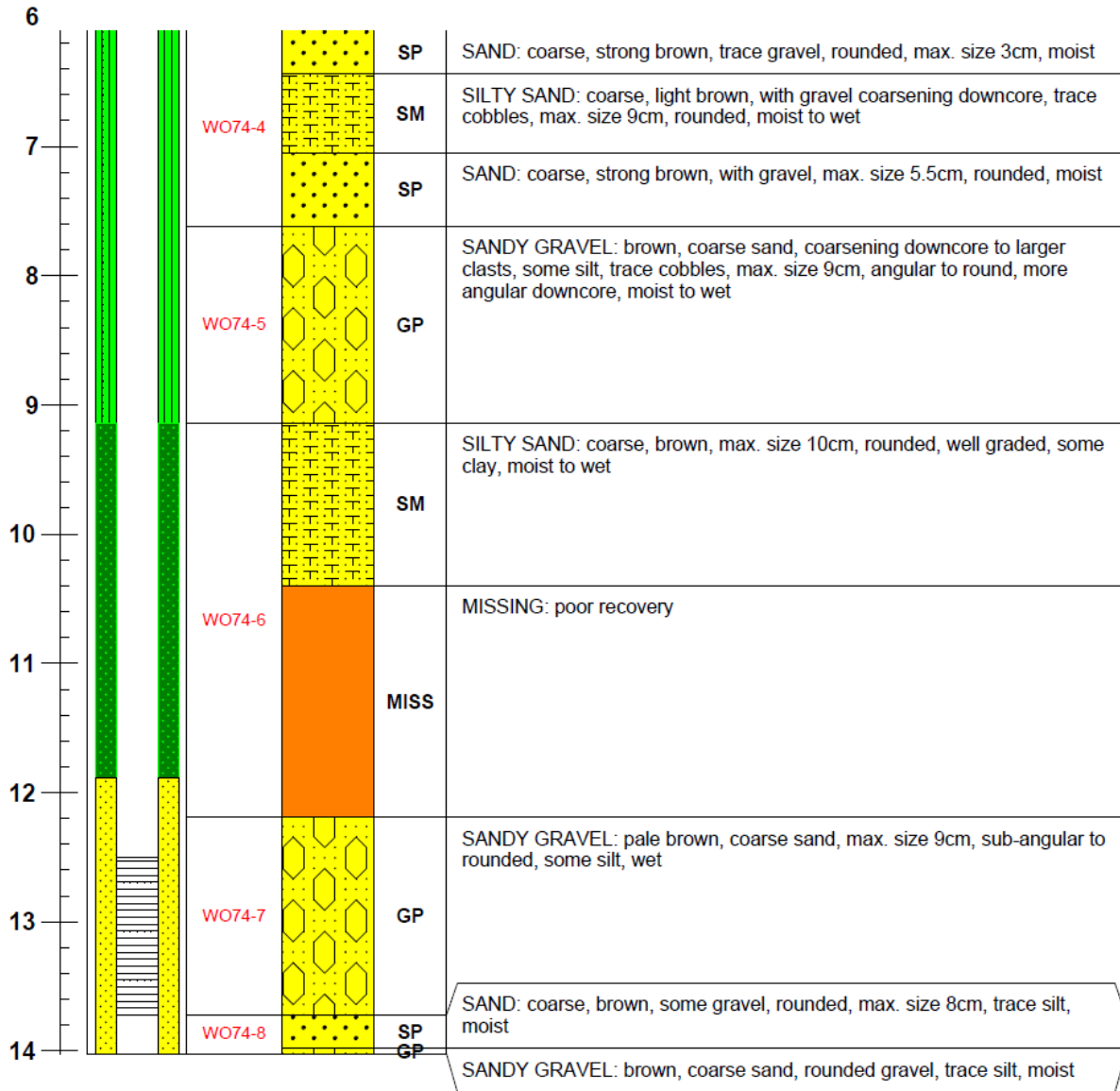
Well Construction Legend:

	Well Screen		Water Level
	Hole Plug		
	Bentonite Grout		
	Sand pack		

Depth (m)	Well Construction	Core No. and % Recovery	Lithology	USCS	Lithological Description
-----------	-------------------	-------------------------	-----------	------	--------------------------



WO74-M (Monitoring Well)					
Depth (m)	Well Construction	Core No. and % Recovery	Lithology	USCS	Lithological Description



Notes:

- for 5' cores, percent recovery based on a total core length of 1.524m
- developed January 10, 2007 with a Monsoon pump
- pumped water until clear; total water pumped 105L
- well is down and around driveway into the back left corner of farmers field on left of Curry Rd.
- water level measured from top of PVC pipe, stickup: 0.89m

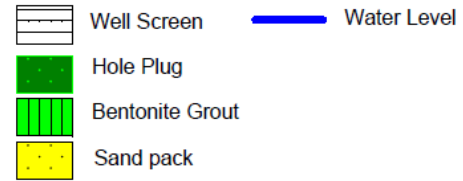
WO74-S (Monitoring Well)



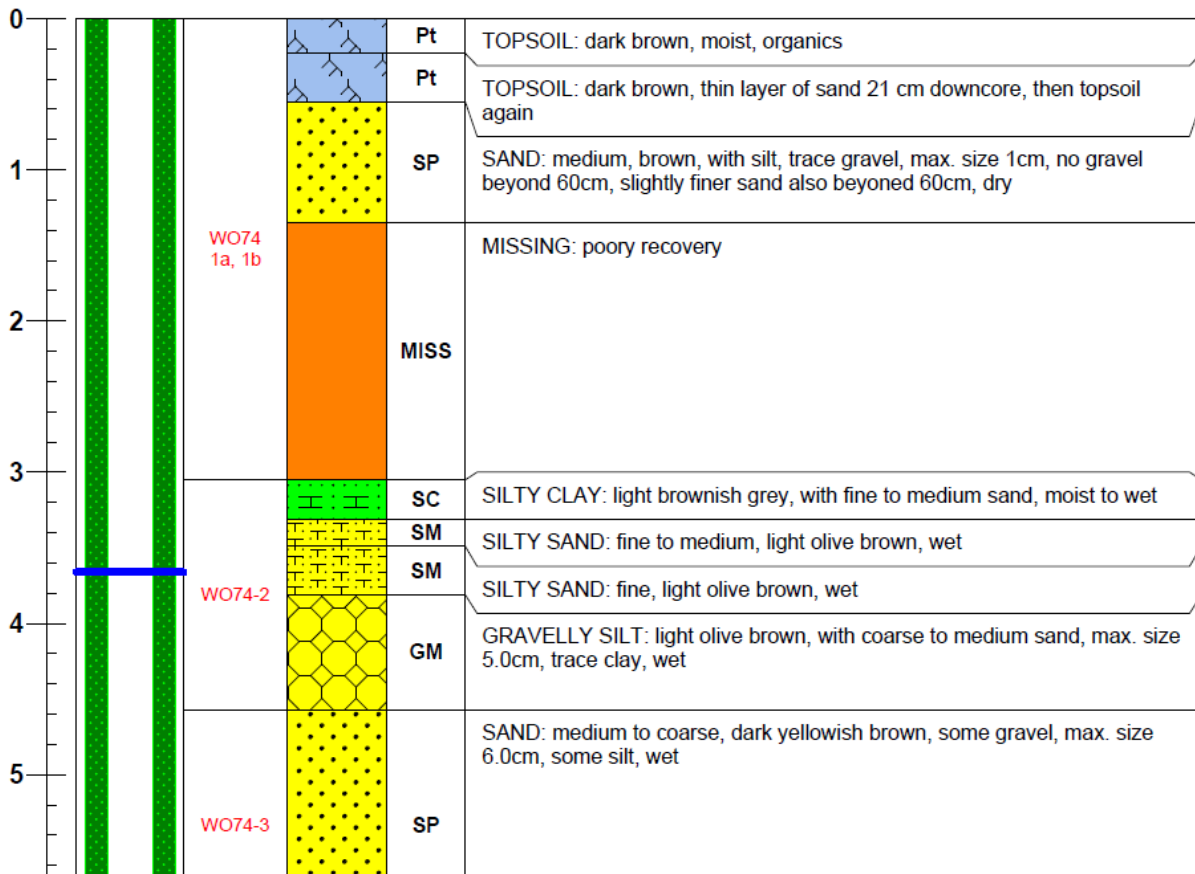
Date Drilled: December 20, 2006
 Drilling Inspector: Joanna Passmore
 Drillers: Boart Longyear - SDS Drilling
 Method: Rotasonic Mini Sonic Drill Rig 4x6" system
 Total Depth of Boring: 10.67m
 Depth to water: 3.66mbgs (NAD83) (Measured March 29, 2007)
 Ground Elevation: 300.75masl (NAD83)
 Top of PVC riser elevation: 301.64m (NAD83)
 Location: UTM17 North 4770154.28m, East 520053.90m
 Originally Surveyed: March 28, 2007
 Elevations Re-Surveyed: July 20, 2007
 Survey Corrected: July 25, 2007
 Installation: - 2.00" Schedule 40 PVC riser and screen
 - holeplug from 0mbgs to 7.92mbgs
 - screen from 9.14mbgs to 10.36mbgs
 - sand pack from 7.92mbgs to 10.67mbgs
 Logged By: Geoff Moroz, Jaqueline Kreller
 Last Updated: July 25, 2007

USCS = Unified Soil Classification System
 mbgs = Metres Below Ground Surface
 masl = Metres Above Sea Level

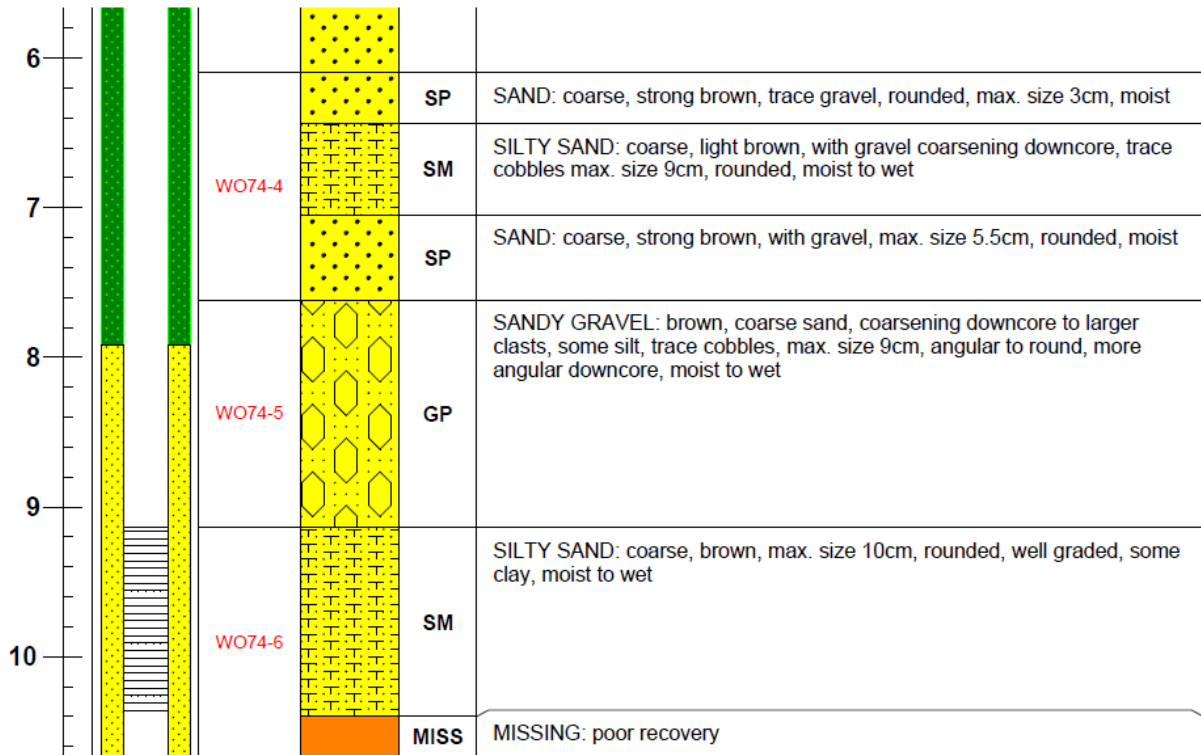
Well Construction Legend:



Depth (m)	Well Construction	Core No. and % Recovery	Lithology	USCS	Lithological Description
-----------	-------------------	-------------------------	-----------	------	--------------------------



WO74-S (Monitoring Well)					
Depth (m)	Well Construction	Core No. and % Recovery	Lithology	USCS	Lithological Description



Notes:

- for 5' cores, percent recovery based on a total core length of 1.524m
- developed January 10, 2007 with a Monsoon pump
- pumped water until clear; total water pumped 135L
- well is down and around driveway into the back left corner of farmers field on left of Curry Rd.
- water level measured from top of PVC pipe, stickup: 0.87m

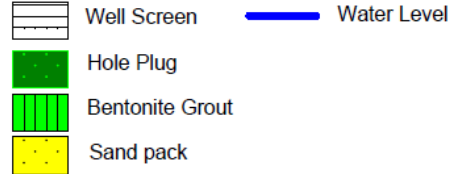
WO74-WT (Monitoring Well)



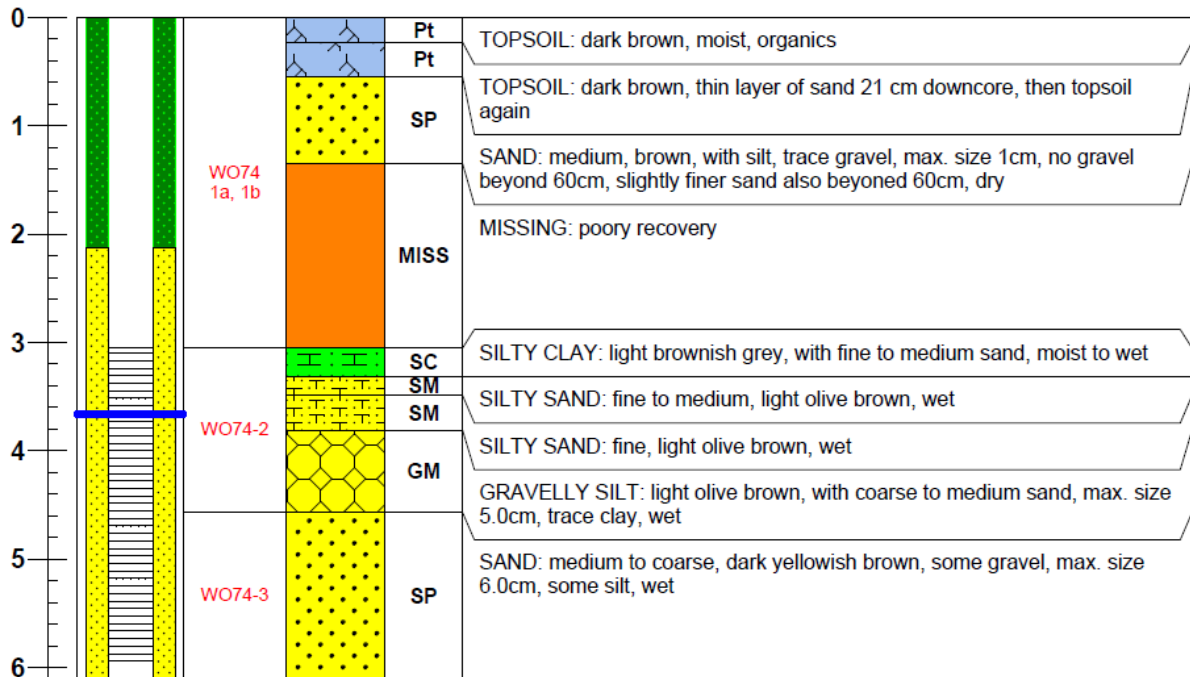
Date Drilled: December 20, 2006
 Drilling Inspector: Joanna Passmore
 Drillers: Boart Longyear - SDS Drilling
 Method: Rotasonic Mini Sonic Drill Rig 4x6" system
 Total Depth of Boring: 6.10m
 Depth to water: 3.66mbgs (NAD83) (Measured March 29, 2007)
 Ground Elevation: 300.75masl (NAD83)
 Top of PVC riser elevation: 301.64m (NAD83)
 Location: UTM17 North 4770152.75m, East 520052.33m
 Originally Surveyed: March 28, 2007
 Elevations Re-Surveyed: July 20, 2007
 Survey Corrected: July 25, 2007
 Installation: - 2.00" Schedule 40 PVC riser and screen
 - holeplug from 0mbgs to 2.13bgs
 - screen from 3.05mbgs to 5.94mbgs
 - sand pack from 2.13mbgs to 6.10mbgs
 Logged By: Geoff Moroz, Jaqueline Kreller
 Last Updated: July 25, 2007

USCS = Unified Soil Classification System
 mbgs = Metres Below Ground Surface
 masl = Metres Above Sea Level

Well Construction Legend:



Depth (m)	Well Construction	Core No. and % Recovery	Lithology	USCS	Lithological Description
-----------	-------------------	-------------------------	-----------	------	--------------------------



Notes:

- for 5' cores, percent recovery based on a total core length of 1.524m
- developed January 10, 2007 with a Monsoon pump
- pumped water until clear; total water pumped 120L
- well is down and around driveway into the back left corner of farmers field on left of Curry Rd.
- water level measured from top of PVC pipe, stickup: 0.80m


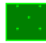



WO75-D (Monitoring Well)



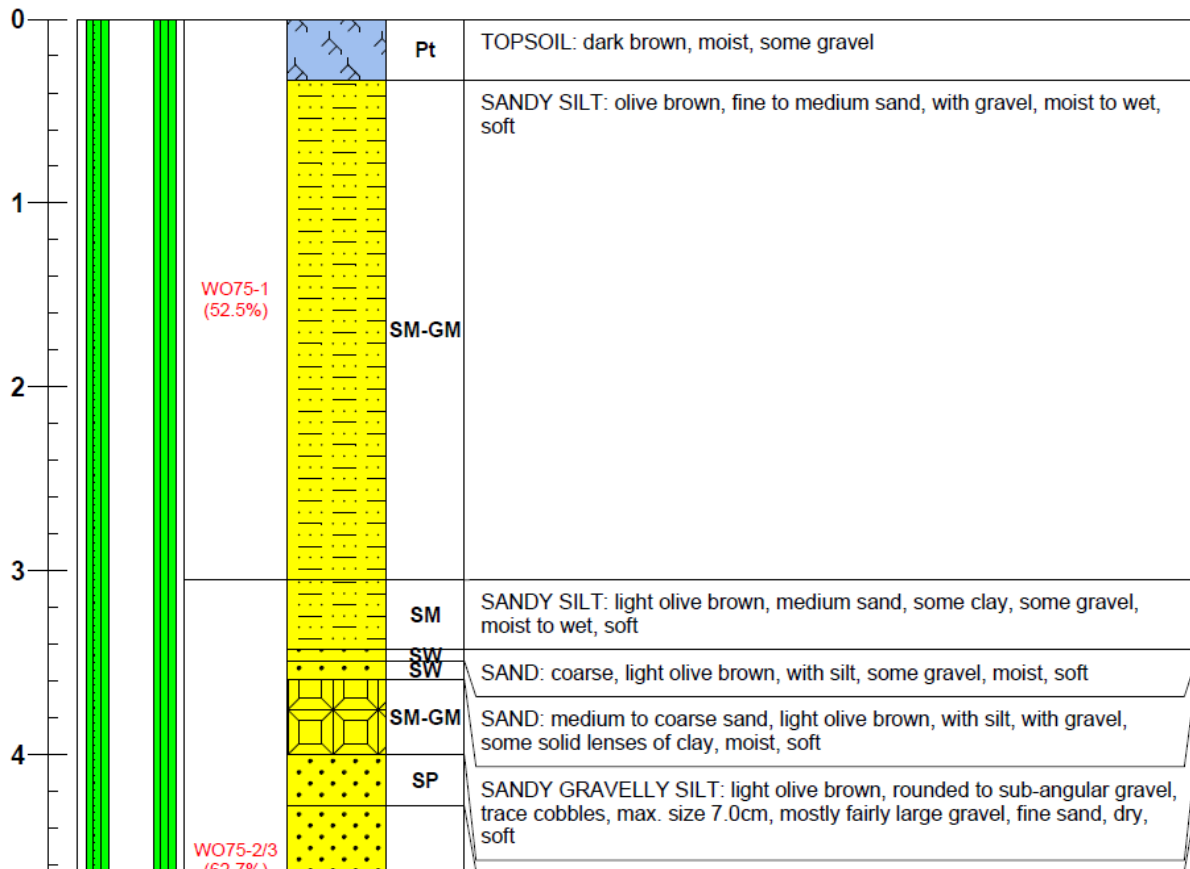
Date Drilled: January 10, 2007
 Drilling Inspector: Joanna Passmore
 Drillers: Boart Longyear - SDS Drilling
 Method: Rotasonic Mini Sonic Drill Rig 4x6" system
 Total Depth of Boring: 24.38m
 Depth to water: 5.57mbgs (NAD83) (Measured March 29, 2007)
 Ground Elevation: 302.80masl (NAD83)
 Top of PVC riser elevation: 303.62m (NAD83)
 Location: UTM17 North 4770112.04m, East 520013.59m
 Originally Surveyed: March 28, 2007
 Elevations Re-Surveyed: July 20, 2007
 Survey Corrected: July 25, 2007
 Installation: - 2.00" Schedule 40 PVC riser and screen
 - holeplug from 15.24mbgs to 16.92mbgs & 22.10mbgs to 22.86mbgs
 - screen from 18.29mbgs to 21.34mbgs
 - sand pack from 16.92mbgs to 22.10mbgs
 - grout from 0mbgs to 12.19mbgs
 Logged By: Geoff Moroz, Jaqueline Kreller
 Last Updated: July 25, 2007

USCS = Unified Soil Classification System
 mbgs = Metres Below Ground Surface
 masl = Metres Above Sea Level

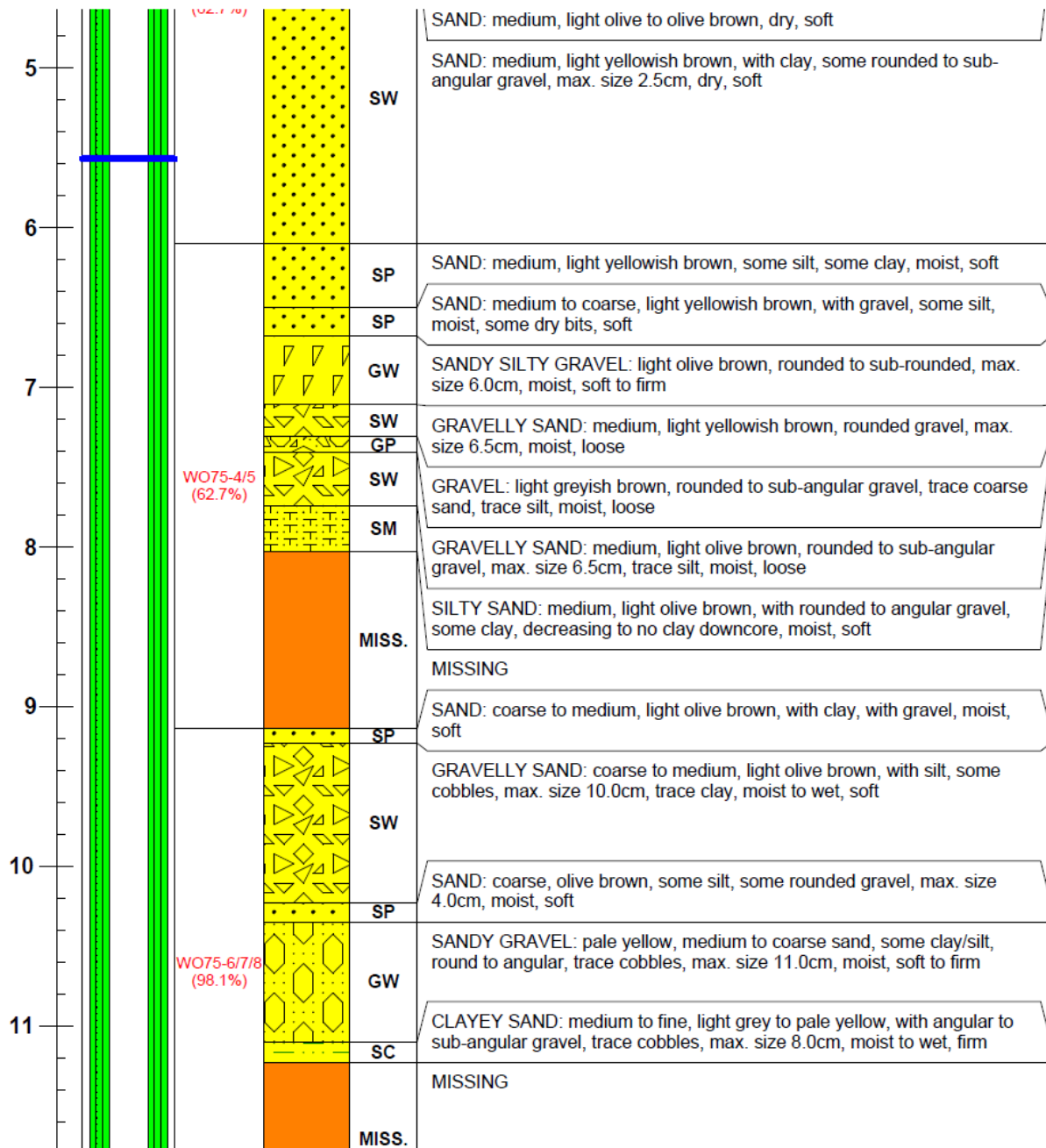
Well Construction Legend:

-  Well Screen
-  Hole Plug
-  Bentonite Grout
-  Sand pack
-  Water Level

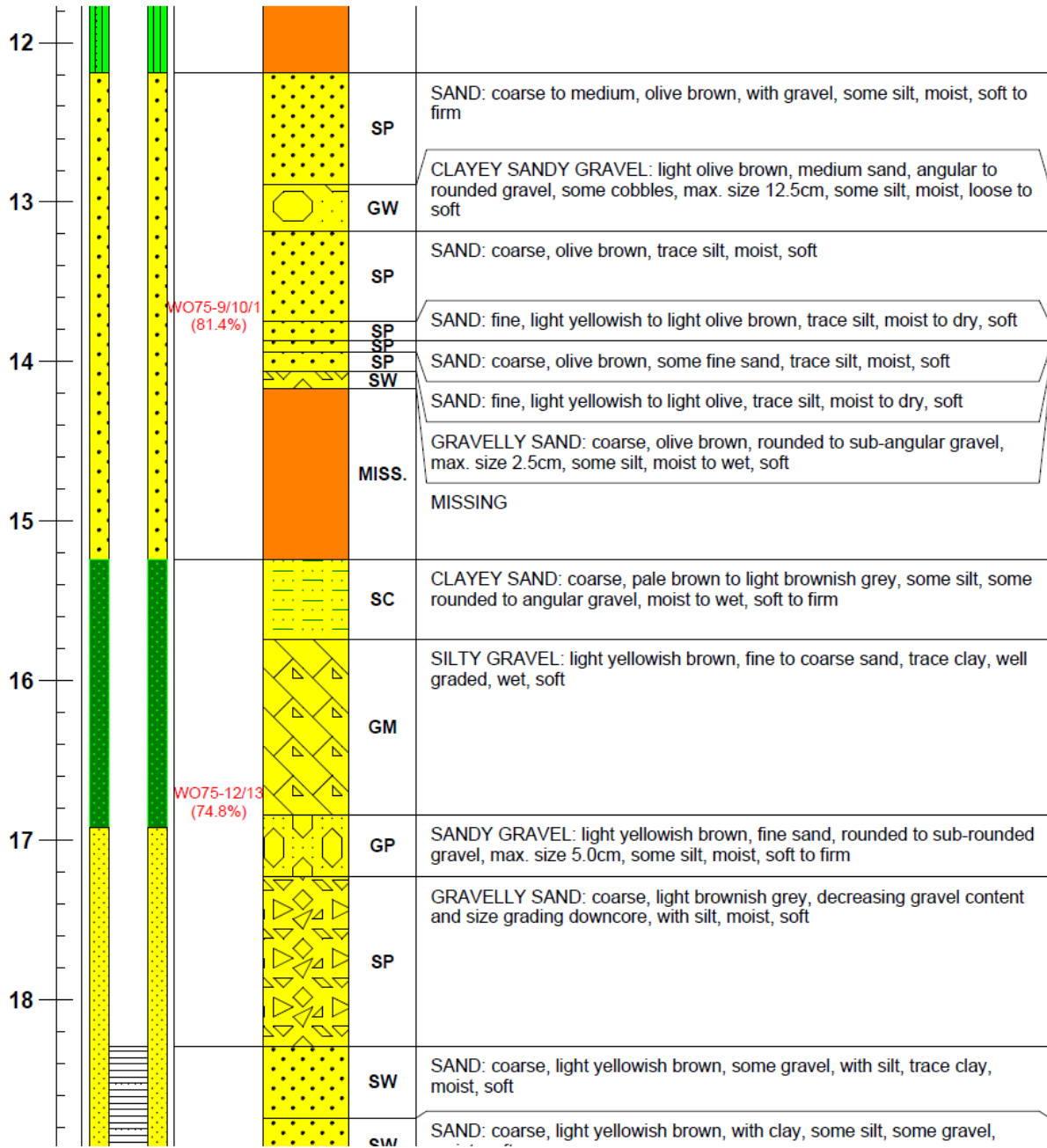
Depth (m)	Well Construction	Core No. and % Recovery	Lithology	USCS	Lithological Description
-----------	-------------------	-------------------------	-----------	------	--------------------------



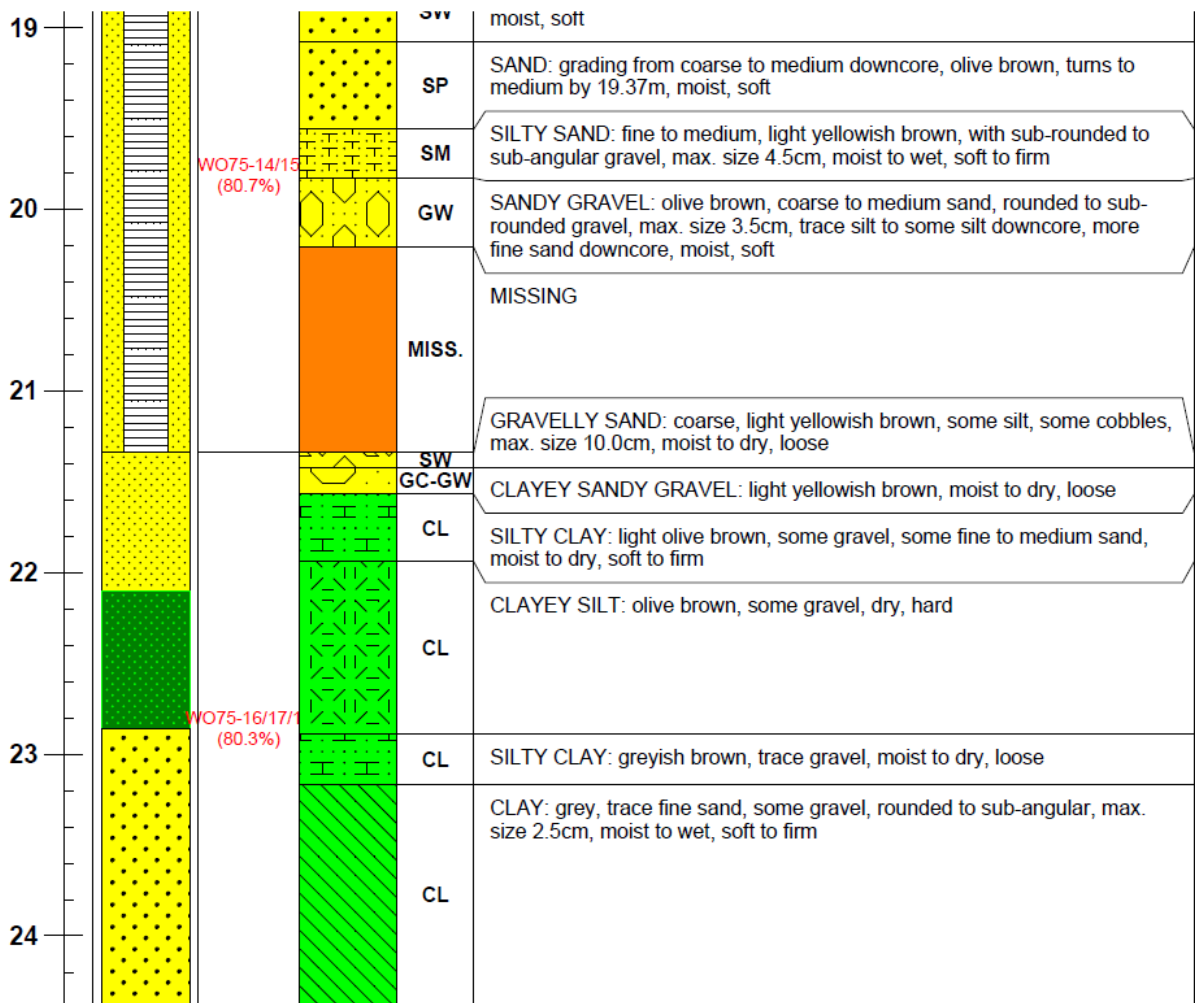
WO75-D (Monitoring Well)					
Depth (m)	Well Construction	Core No. and % Recovery	Lithology	USCS	Lithological Description



WO75-D (Monitoring Well)					
Depth (m)	Well Construction	Core No. and % Recovery	Lithology	USCS	Lithological Description



WO75-D (Monitoring Well)					
Depth (m)	Well Construction	Core No. and % Recovery	Lithology	USCS	Lithological Description



Notes:

- for 5' cores, percent recovery based on a total core length of 1.524m
- developed February 22, 2007 with a Monsoon pump
- pumped water until clear; total water pumped 225L
- well is down and around driveway into the back left corner of farmers field on left of Curry Rd.
- water level measured from top of PVC pipe, stickup: 0.84m
- sand came up into casing to 45' after putting in holeplug
- lots of sand pushing up into casing; high pressure at this location
- had 40' of sand pushed up into casing when drilling

WO75-S (Monitoring Well)



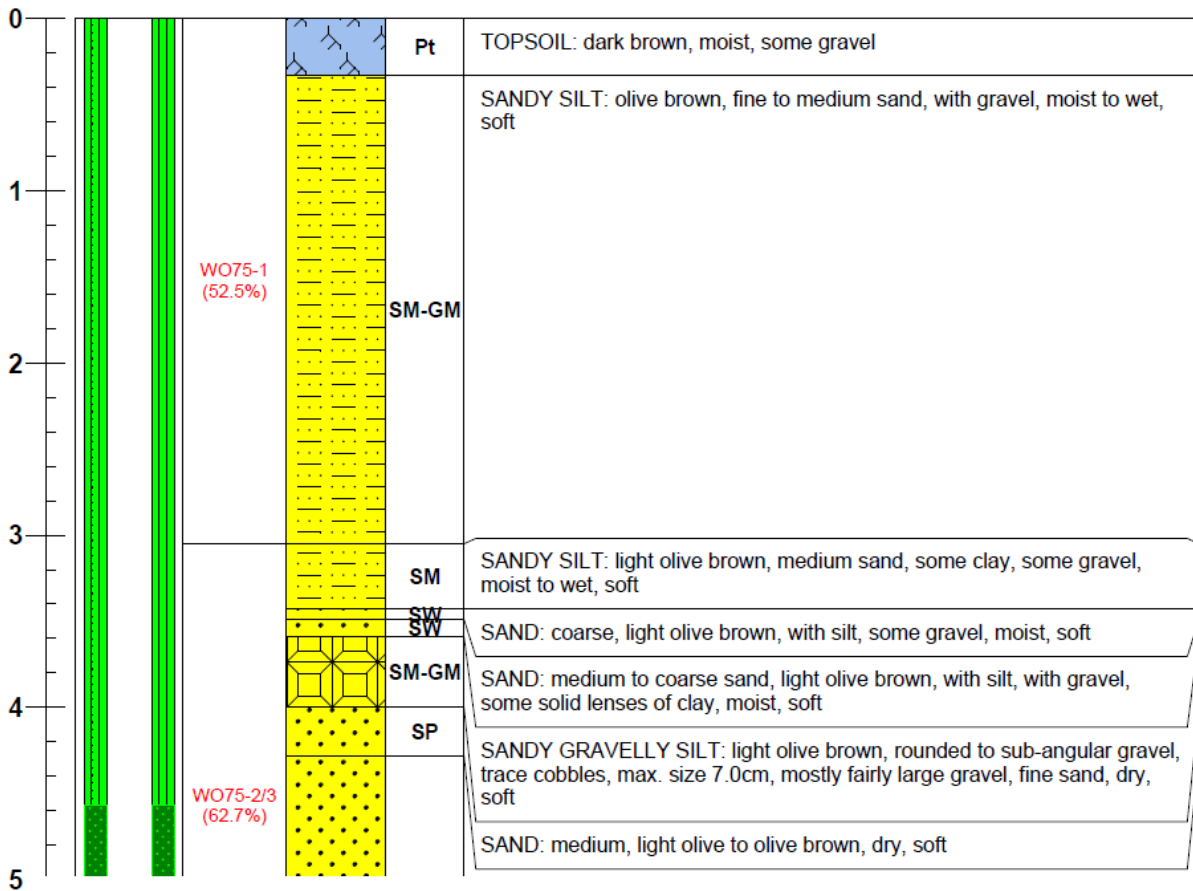
Date Drilled: January 10, 2007
 Drilling Inspector: Joanna Passmore
 Drillers: Boart Longyear - SDS Drilling
 Method: Rotasonic Mini Sonic Drill Rig 4x6" system
 Total Depth of Boring: 10.67m
 Depth to water: 5.57mbgs (NAD83) (Measured March 29, 2007)
 Ground Elevation: 302.68masl (NAD83)
 Top of PVC riser elevation: 303.58m (NAD83)
 Location: UTM17 North 4770112.00m, East 520015.09m
 Originally Surveyed: March 28, 2007
 Elevations Re-Surveyed: July 20, 2007
 Survey Corrected: July 25, 2007
 Installation: - 2.00" Schedule 40 PVC riser and screen
 - holeplug from 4.57mbgs to 7.92mbgs
 - screen from 8.84mbgs to 10.36mbgs
 - sand pack from 7.92mbgs to 10.67mbgs
 - grout from 0mbgs to 4.57mbgs
 Logged By: Geoff Moroz, Jaqueline Kreller
 Last Updated: July 25, 2007

USCS = Unified Soil Classification System
 mbgs = Metres Below Ground Surface
 masl = Metres Above Sea Level

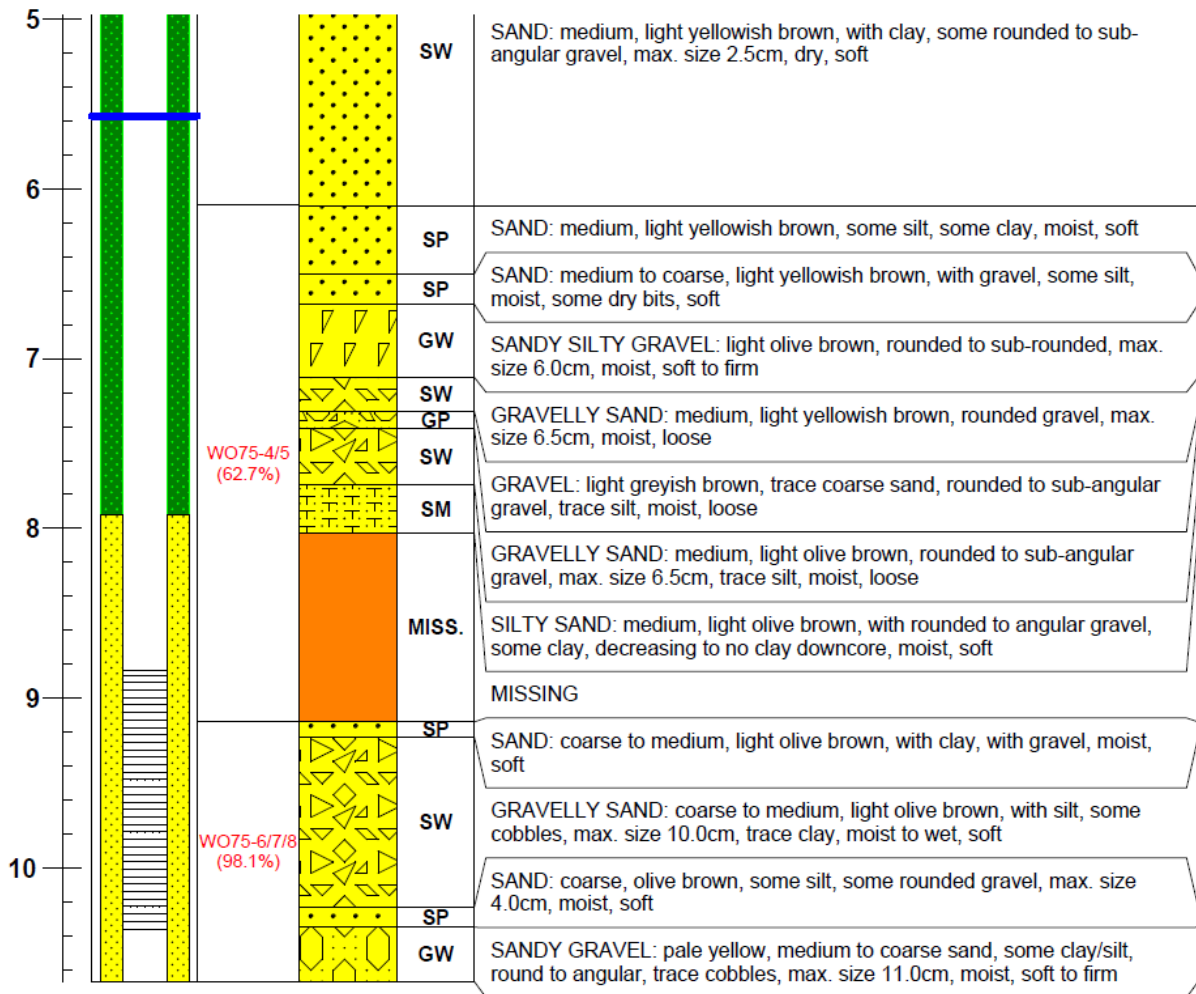
Well Construction Legend:

	Well Screen		Water Level
	Hole Plug		
	Bentonite Grout		
	Sand pack		

Depth (m)	Well Construction	Core No. and % Recovery	Lithology	USCS	Lithological Description
-----------	-------------------	-------------------------	-----------	------	--------------------------



WO75-S (Monitoring Well)					
Depth (m)	Well Construction	Core No. and % Recovery	Lithology	USCS	Lithological Description



Notes:

- for 5' cores, percent recovery based on a total core length of 1.524m
- developed February 22, 2007 with a Monsoon pump
- pumped water until clear; total water pumped 165L
- well is down and around driveway into the back left corner of farmers field on left of Curry Rd.
- water level measured from top of PVC pipe, stickup: 0.93m
- sand came up into casing to 45' after putting in holeplug
- lots of sand pushing up into casing; high pressure at this location
- had 40' of sand pushed up into casing when drilling


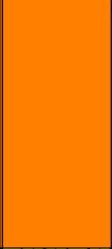

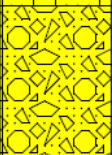
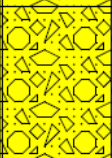
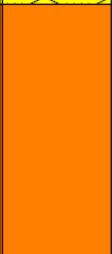

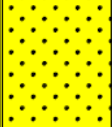



Core 1

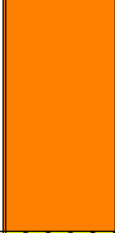
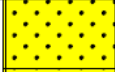
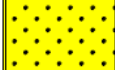














Point velocity probe (PVP) installation
 Date Drilled: October 6, 2008
 Drilling Inspector: Kate Critchley, Peter Schillig
 Drillers: Paul Johnson, Bob Ingleton
 Method: Geoprobe® direct push rig
 Total Depth of Boring: 15.24 mbgs
 Ground Surface Elevation: 301.02 masl (NAD83)
 Location: UTM17 North 4770157.50 m, East 520030.15 m
 Survey Date: September 3, 2009
 Logged By: Kate Critchley
 Last Updated: October 26, 2009

mbgs = Metres Below Ground Surface
 masl = Metres Above Sea Level

Depth (mbgs)	Core Number	% Recovery	Lithology	Lithological Description
5	C 1-1	53.3		GRAVELLY SAND: Gravelly medium to coarse sand, fine to coarse gravel, trace fines, angular to subrounded clasts, maximum diameter = 5.1cm, poorly sorted
				GRAVELLY SAND: Gravelly medium to coarse sand, fine gravel, trace fines, angular to subrounded clasts, maximum diameter = 1.3cm, poorly sorted
				SAND: Medium to coarse sand with fine gravel, trace fines, fining with depth, subangular to subrounded clasts, fairly well sorted
				MISSING: Not Recovered
6	C 1-2	61.7		SAND: Medium to coarse sand with fine gravel, trace fines, coarsening with depth, angular to subrounded clasts, fairly well sorted
				GRAVEL: Fine to medium gravel with medium to coarse sand, trace fines, angular to subrounded clasts, maximum diameter = 1cm, poorly sorted
				GRAVEL: Fine to coarse gravel with coarse sand, trace fines, subangular to rounded clasts, maximum diameter = 5.1cm, poorly sorted
				GRAVEL: Fine to medium gravel with medium to coarse sand, trace fines, angular to subrounded clasts, maximum diameter = 1cm, poorly sorted
				GRAVEL: Medium to coarse gravel, trace coarse sand, fine gravel and fines, subangular to rounded clasts, maximum diameter = 3.8cm, well sorted

Core 1				
Depth (mbgs)	Core Number	% Recovery	Lithology	Lithological Description
7				GRAVEL: Coarse sand and fine gravel, trace fines, subangular to subrounded clasts, maximum diameter =2.5cm, fairly well sorted with exception of one large piece of gravel
				GRAVEL: Coarse gravel with fine gravel and coarse sand, trace fines, coarsening with depth, subangular to subrounded clasts, maximum diameter = 3.8cm, poorly sorted MISSING: Not Recovered
8	C 1-3	46.9		SANDY GRAVEL: Coarse sand to fine gravel, angular to subangular clasts, brown
				GRAVEL: Medium gravel with coarse sand, angular to subangular clasts, brown
				GRAVEL: Coarse gravel with fine to coarse sand, trace silt and clay, angular to subangular clasts, yellow/ brown
				MISSING: Not Recovered
9				SAND: Medium sand with coarse sand, trace fines, subangular clasts, well sorted
				SAND: Coarse sand with medium sand and fine gravel, trace fines, subangular to subrounded clasts, maximum diameter = 1.3cm, poorly sorted
				GRAVEL: Fine to coarse gravel with fine to coarse sand, angular to subangular clasts, yellow/brown
				GRAVEL: Fine to coarse gravel with coarse sand, trace fines, subangular to subrounded clasts, maximum diameter = 3.8cm, poorly sorted
				
10	C 1-4	64.5		

Core 1				
Depth (mbgs)	Core Number	% Recovery	Lithology	Lithological Description
				MISSING: Not Recovered
11	C 1-5	87.0		SAND: Coarse sand with fine gravel, trace silt and clay, angular to subangular clasts, yellow/brown
				SAND: Coarse sand with fine gravel, trace fines, coarsening with depth, subangular to rounded clasts, well sorted
				SANDY GRAVEL: Sandy fine gravel, coarse sand, trace fines, angular to rounded clasts
				GRAVEL: Fine to coarse gravel with medium to coarse sand, trace fines, rounded clasts, maximum diameter = 2.5cm
				SANDY GRAVEL: Sandy fine to coarse gravel, medium to coarse sand, trace fines, maximum diameter = 3.3cm, poorly sorted
				GRAVEL: Coarse gravel with coarse sand and fine gravel, trace fines, subangular clasts, maximum diameter = 5.1cm
12				SANDY GRAVEL: Fine to coarse sand and gravel, trace silt and clay, angular to subangular clasts, poorly sorted
				MISSING: Not Recovered
13	C 1-6	68.0		SAND: Medium to coarse sand with fine gravel, trace fines, mostly subangular clasts, maximum diameter = 1.0cm, well sorted
				GRAVEL: Fine to coarse (mostly fine) gravel with coarse sand, trace fines, angular to subrounded clasts, maximum diameter = 2.5cm
				GRAVEL: Fine to coarse (mostly coarse) gravel with coarse sand, trace fines, subangular to rounded clasts, maximum diameter = 3.8cm
				SANDY GRAVEL: Sandy coarse gravel with fines, fine sand, angular to subrounded clasts, maximum diameter = 5.8cm, poorly sorted
				SAND: Medium to coarse sand with fine sand, trace silt and clay, angular to subangular clasts
				MISSING: Not Recovered

Core 1				
Depth (mbgs)	Core Number	% Recovery	Lithology	Lithological Description
14	C 1-7	88.5		SAND: Medium to coarse sand, subangular clasts, well sorted, grey/brown
				SAND: Fine to coarse sand with fine gravel, trace fines, angular to subrounded clasts, maximum diameter = 1.0cm, poorly sorted
				SANDY GRAVEL: Sandy fine to coarse gravel, fine to coarse sand, trace fines, angular to subrounded clasts, maximum diameter = 3.8cm, poorly sorted
				GRAVEL: Coarse gravel with fine gravel and fine to coarse sand, trace fines, rounded to subangular clasts, maximum diameter = 3.8cm, fairly well sorted
15				SILTY SAND: Silty fine sand, trace clay, well sorted; note that fines may have washed from this unit into upper layers in the core barrel
				SAND: Fine to medium sand, trace coarse sand, fine gravel, and fines, angular to subrounded clasts, maximum diameter = 1.0cm
				SAND: Fine to coarse sand, trace fine gravel and fines, coarsening with depth, angular to subrounded clasts, poorly sorted
				GRAVELLY SAND: Gravelly fine to coarse sand, fine to coarse gravel, trace fines, subangular to rounded clasts, maximum diameter = 2.5cm, poorly sorted
				MISSING: Not Recovered

Notes:

- assumed top of core represented the actual top and all lost material was lost from the bottom
- for 5' cores, percent recovery based on a total core length of 1.52m
- for 3' cores, percent recovery based on a total core length of 0.9144m

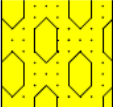
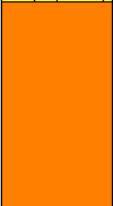
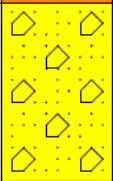

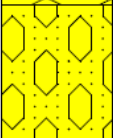
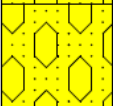
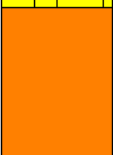
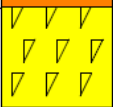

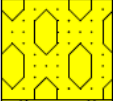
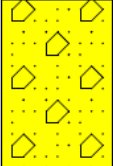
Core 2







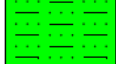
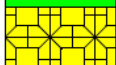


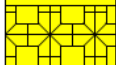







Point velocity probe (PVP) installation
 Date Drilled: October 7, 2008
 Drilling Inspector: Kate Critchley, Peter Schillig
 Drillers: Paul Johnson, Bob Ingleton
 Method: Geoprobe® direct push rig
 Total Depth of Boring: 15.24mbgs
 Ground Surface Elevation: 300.72 masl (NAD83)
 Location: UTM17 North 4770156.45 m, East 520039.34 m
 Survey Date: September 3, 2009
 Logged By: Kate Critchley
 Last Updated: October 26, 2009

mbgs = Metres Below Ground Surface
 masl = Metres Above Sea Level

Depth (mbgs)	Core Number	% Recovery	Lithology	Lithological Description
5	C 2-1	62.1		SANDY GRAVEL: Sandy fine to coarse gravel, medium to coarse sand, trace fines, subangular to subrounded clasts, maximum diameter = 3.8cm, poorly sorted
				GRAVEL: Fine to coarse gravel with fine to coarse sand and fines, subangular to subrounded clasts, maximum diameter = 3.8cm, poorly sorted
				GRAVELLY SAND: Gravelly medium to coarse sand with fines, fine to coarse gravel, angular to subrounded clasts, maximum diameter = 3.8cm, poorly sorted
				MISSING: Not Recovered
6	C 2-2	68.8		SAND: Fine to medium sand with fines, well sorted
				SAND: Medium to coarse sand with fine gravel, trace fines, coarsening with depth, angular to subrounded clasts, maximum diameter = 1.5cm, fairly well sorted
				SANDY GRAVEL: Sandy medium to coarse gravel, fine to coarse sand, trace silt and clay, angular to subangular clasts, yellow/brown
				SANDY GRAVEL: Sandy fine to coarse gravel, fine to coarse sand, trace fines, subangular to subrounded clasts, maximum diameter = 5.1cm, poorly sorted

Core 2				
Depth (mbgs)	Core Number	% Recovery	Lithology	Lithological Description
7				
				MISSING: Not Recovered
8	C 2-3	76.9		SILTY SANDY GRAVEL: Silty, sandy gravel with clay, angular to subangular clasts, grey/brown sand and yellow/brown fines
				GRAVEL: Fine to coarse gravel with fine to coarse sand, trace fines, angular to subrounded clasts, maximum diameter = 3.8cm, poorly sorted
				SANDY GRAVEL: Sandy fine to coarse gravel with fines, fine to coarse sand, subangular to subrounded clasts, maximum diameter = 3.8cm, poorly sorted
				SANDY GRAVEL: Sandy fine to coarse gravel, medium to coarse sand, trace fines, subangular to subrounded clasts, maximum diameter = 3.8cm, poorly sorted
				MISSING: Not Recovered
9				SANDY SILTY GRAVEL: Sandy, silty fine to medium gravel, 30% silt
				SILTY GRAVEL: Silty medium to coarse gravel, 30% silt
				SANDY GRAVEL: Sandy fine to coarse gravel with fines, coarse sand, angular to subrounded clasts, maximum diameter = 3.8cm, poorly sorted
10	C 2-4	74.3		SILTY SANDY GRAVEL: Silty, sandy fine to coarse gravel, fine to coarse sand, angular to subrounded clasts, maximum diameter = 3.8cm, poorly sorted

Core 2				
Depth (mbgs)	Core Number	% Recovery	Lithology	Lithological Description
				
				MISSIN: Not Recovered
11	C 2-5	92.3		SAND: Medium to coarse sand with fines, angular to subrounded clasts, well sorted
				GRAVEL: Fine to coarse gravel with coarse sand and fines, angular to subrounded clasts, maximum diameter = 1.9cm, poorly sorted
				GRAVELLY SAND: Gravelly coarse sand, fine to coarse gravel, trace fines, coarsening with depth, maximum diameter = 3.8cm, poorly sorted
				SANDY GRAVEL: Sandy fine gravel, coarse sand, trace fines, maximum diameter = 1.6cm, poorly sorted
				GRAVELLY CLAY: Gravelly clay, 90% clay, yellow/brown
				SANDY SILTY CLAY: Sandy, silty clay, fine to coarse sand, trace gravel, coarsening with depth, subrounded clasts, maximum diameter = 3.8cm, poorly sorted, aquitard material
12				SANDY SILTY CLAYEY GRAVEL: Sandy, silty, clayey fine to coarse gravel (mostly coarse), fine to coarse sand, angular to subrounded clasts, maximum diameter = 3.8cm, poorly sorted
				SANDY SILTY CLAYEY GRAVEL: Sandy, silty, clayey fine to coarse gravel (mostly fine), fine to coarse sand, angular to subrounded clasts, maximum diameter = 2.5cm, poorly sorted
13	C 2-6	91.2		MISSING: Not Recovered
				SAND: Medium sand with fine to coarse components in smaller percentages, <20% silt, yellow/brown
				SANDY SILTY CLAYEY GRAVEL: Sandy, silty, clayey fine to coarse gravel, fine to coarse sand, subangular to rounded clasts, maximum diameter = 3.3, poorly sorted
				GRAVELLY SAND: Gravelly fine to coarse sand with fines, fine to coarse gravel, subangular clasts, maximum diameter = 3.8cm, poorly sorted
				SANDY GRAVEL: Sandy fine to coarse gravel with fines, fine to coarse sand, subangular to subrounded clasts, maximum diameter = 5.1cm, poorly sorted
				SANDY SILTY CLAYEY GRAVEL: Sandy, silty, clayey, gravel, poorly sorted, poor visibility in core for better description
				SANDY GRAVEL: Sandy fine to coarse gravel with fines, fine to coarse sand, subrounded clasts, maximum diameter = 3.8cm, poorly sorted

Core 2				
Depth (mbgs)	Core Number	% Recovery	Lithology	Lithological Description
14	C 2-7	81.8		SANDY SILTY CLAYEY GRAVEL: Sandy, silty, clayey fine to coarse gravel, fine to coarse sand, subrounded clasts, maximum diameter = 2.5cm, poorly sorted
				SILTY CLAYEY GRAVELLY SAND: Silty, clayey, gravelly fine to coarse sand, fine gravel, subrounded clasts, maximum diameter = 1.5cm, poorly sorted
				MISSING: Not Recovered
				SAND: Medium sand with fines, well sorted
				GRAVELLY SAND: Gravelly medium to coarse sand with fines, fine gravel, subangular to subrounded clasts, maximum diameter = 1.8cm, poorly sorted
				SANDY GRAVEL: Sandy fine to coarse gravel with fines, fine to coarse sand, subrounded clasts, maximum diameter = 5.1cm, poorly sorted
				SILTY CLAYEY SAND: Silty, clayey medium to coarse sand, angular to subangular clasts, yellow/brown
				GRAVEL: Fine to coarse gravel with fine to coarse sand and fines, subangular to subrounded clasts, maximum diameter = 2.5cm, poorly sorted
				GRAVELLY SAND: Gravelly fine to coarse sand with fines, fine to coarse gravel, subangular clasts, maximum diameter = 5.1cm, poorly sorted
			15	

Notes:

- assumed top of core represented the actual top and all lost material was lost from the bottom
- for 5' cores, percent recovery based on a total core length of 1.52m
- for 3' cores, percent recovery based on a total core length of 0.9144m


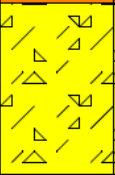
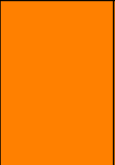



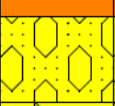
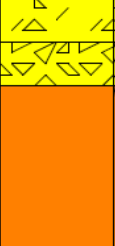
Core 3



Hole used for groundwater profiling
 Date Drilled: May 13, 2008
 Drilling Inspector: Kate Critchley
 Drillers: Paul Johnson, Bob Ingleton
 Method: Vibra-Push® direct push rig equipped with Enviro-Core® sampling system
 Total Depth of Boring: 5.79 mbgs
 Ground Surface Elevation: 300.90 masl (NAD83)
 Location: UTM17 North 4770154.26 m, East 520033.56 m
 Survey Date: September 3, 2009
 Logged By: Kate Critchley
 Last Updated: October 26, 2009

mbgs = Metres Below Ground Surface
 masl = Metres Above Sea Level

Depth (mbgs)	Core Number	% Recovery	Lithology	Lithological Description
0	3-1	100		TOPSOIL: Topsoil, fine sandy silt at top grading to silty fine sand at bottom, well sorted, roots and organic matter present
				SILTY SAND: Silty fine sand, trace fine gravel, subangular to subrounded clasts, maximum diameter = 1cm, well sorted
1	3-2	55.6		SILTY CLAYEY SAND: Silty, clayey fine sand, trace fine to coarse gravel, angular clasts, maximum diameter = 3cm, poorly sorted; note that the gravel pieces appear to be fragments of a single broken cobble
				MISSING: Not Recovered
2	3-3	100		SILTY SAND: Silty fine sand, trace fine to coarse gravel (mostly fine), angular clasts, maximum diameter = 3cm, poorly sorted
				SANDY GRAVEL: Sandy fine to coarse gravel with silt, fine to coarse sand, subrounded clsts, maximum diameter = 3.8cm, poorly sorted
	3-4	23.6		GRAVELLY SAND: Gravelly fine to coarse sand, fine to coarse gravel, trace fines, subangular to subrounded clasts, maximum diameter = 2.5cm, poorly sorted; note that the bottom of the core liner was deformed from pushing gravel
				MISSING: Not Recovered

Core 3				
Depth (mbgs)	Core Number	% Recovery	Lithology	Lithological Description
3	3-5	50.0		
				GRAVELLY SILTY CLAYEY SAND: Gravelly, silty, clayey fine to coarse sand, fine to coarse gravel, subangular clasts, maximum diameter = 2.5cm, poorly sorted
4	3-6	34.2		MISSING: Not Recovered
				GRAVELLY SAND: Gravelly medium to coarse sand with fines, fine to coarse gravel, subrounded to subangular clasts, maximum diameter = 5.1cm, poorly sorted
5	3-7	51.4		SANDY GRAVEL: Sandy fine to coarse gravel with fines, fine to coarse sand, angular clasts, maximum diameter = 3.8cm, poorly sorted; note that gravel pieces are made up of rock fragments shattered by drilling
				GRAVELLY SILTY CLAYEY SAND: Gravelly, silty, clayey fine to coarse sand, fine to coarse gravel, angular clasts, maximum diameter = 3.8cm, poorly sorted
				GRAVELLY SAND: Gravelly fine to coarse sand, fine to coarse gravel, trace fines, subrounded to rounded clasts, maximum diameter = 5.1cm, poorly sorted
				MISSING: Not Recovered

Notes:

- assumed top of core represented the actual top and all lost material was lost from the bottom
- for 5' cores, percent recovery based on a total core length of 1.52m
- for 3' cores, percent recovery based on a total core length of 0.9144m

Core 4



Multi-level monitoring well
 Date Drilled: June 24-25, 2008
 Drilling Inspector: Kate Critchley
 Drillers: Paul Johnson, Bob Ingleton
 Method: Geoprobe® direct push rig
 Total Depth of Boring: 13.72 m
 Ground Elevation: 301.01 masl (NAD83)
 Top of PVC centre stock elevation: 301.70 masl (NAD83)
 Location: UTM17 North 4770156.59 m, East 520030.78 m
 Surveyed: September 3, 2009
 Installation: - 7 1/4" polyethylene tubes secured to a 1/2" PVC centre stock
 - natural collapse from 4.15mbgs to 13.72mbgs
 - sand from 3.50mbgs to 4.15mbgs
 - bentonite chips from ground surface to 3.50mbgs
 Logged By: Kate Critchley
 Last Updated: October 26, 2009

mbgs = Metres Below Ground Surface
 masl = Metres Above Sea Level

Well Construction Legend

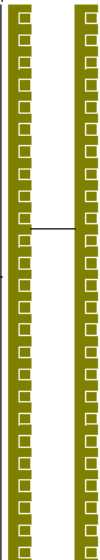
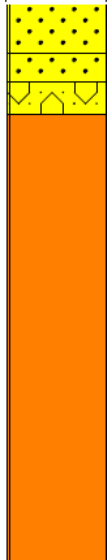
- Screen Port
- Sand Pack
- Bentonite Chips
- Natural Collapse

Depth (m)	Well Construction	Core Number	% Recovery	Lithology	Lithological Description
0		ML1-1	75		TOPSOIL: Topsoil, silty fine sand, trace fine to coarse gravel from 8" - 12" bgs, angular clasts, maximum diameter = 4.6cm, well sorted, roots and organic matter present
				SILTY SAND: Silty fine sand, trace coarse gravel, one angular clast, maximum diameter = 3.3cm, well sorted except for one large piece of gravel	
				SILTY CLAYEY GRAVELLY SAND: Silty, clayey, gravelly fine to medium sand, fine to coarse gravel, subrounded to angular clasts, maximum diameter = 3.8cm, poorly sorted	
				SILT: Silt, trace fine to coarse gravel, angular to subrounded clsts, maximum diameter = 2.5cm, poorly sorted	
				SAND: Fine to coarse sand with fine to coarse gravel, trace fines, subangular to subrounded clasts, maximum diameter = 2.4cm, sand is well sorted	
				MISSING: Not Recovered	
				SAND: Fine sand, trace fines and medium to coarse sand, well sorted	
1					GRAVELLY SAND: Gravelly fine to coarse sand, fine to coarse gravel, trace fines, angular to subrounded clasts, maximum diameter = 5.1cm, poorly sorted
2					

Core 4					
Depth (m)	Well Construction	Core Number	% Recovery	Lithology	Lithological Description
3		ML1-2	72.5		
					MISSING: Not Recovered
4		ML1-3	60.8		GRAVELLY CLAYEY SAND: Gravelly, clayey fine to coarse sand, fine to coarse gravel (mostly coarse), subangular to angular clasts, maximum diameter = 3.8cm, poorly sorted
					GRAVELLY SAND: Gravelly fine to coarse sand with fines, fine to coarse gravel, subangular to subrounded clasts, maximum diameter = 2.5cm, poorly sorted
5		ML1-4	40		CLAYEY SILTY SANDY GRAVEL: Clayey, silty, sandy fine to coarse gravel, fine to coarse sand, angular to subangular clasts, maximum diameter = 5.1cm, poorly sorted
					SANDY SILTY CLAYEY GRAVEL: Sandy, silty, clayey fine to coarse gravel, fine to coarse sand, subangular to subrounded clasts, maximum diameter = 3.8cm, poorly sorted
5		ML1-4	40		GRAVELLY SAND: Gravelly fine to coarse sand with fines, fine to coarse gravel, subangular to subrounded clsts, maximum diameter = 3.8cm, poorly sorted
					MISSING: Not Recovered
5		ML1-4	40		SILTY CLAYEY SAND: Silty, clayey fine to coarse sand, trace fine gravel, angular to subrounded clasts, poorly sorted
					SAND: Fine to coarse sand with fine to coarse gravel, trace fines, angular to subrounded clasts, maximum diameter = 2cm, poorly sorted
5		ML1-4	40		GRAVELLY SILTY CLAYEY SAND: Gravelly, silty, clayey fine to coarse sand, fine to coarse gravel, angular to subrounded clasts, maximum diameter = 5.1cm, poorly sorted
					SAND: Fine to coarse sand with fine to coarse gravel, trace fines, angular to subrounded clasts, maximum diameter = 3.3cm, poorly sorted
		ML1-4	40		MISSING: Not Recovered

Core 4					
Depth (m)	Well Construction	Core Number	% Recovery	Lithology	Lithological Description
6					
		ML1-5	40.8		SANDY CLAYEY SILT: Sandy fines (silt, clay), fine sand, well sorted, aquitard material
					SILTY CLAYEY SAND: Silty, clayey medium sand, well sorted
					SAND: Sand with fines, medium sand grading to medium to coarse sand
					SAND: Medium to coarse sand with fine to coarse gravel, trace fines, angular to subrounded clasts, maximum diameter = 3.8cm, fairly well sorted
7					MISSING: Not Recovered
8		ML1-6	72.5		SAND: Medium to coarse sand with fine to coarse gravel, trace fines, angular to subrounded clasts, maximum diameter = 3.8cm, fairly well sorted
					SANDY GRAVEL: Sandy fine to coarse gravel, medium to coarse sand, trace fines, angular to rounded clasts
					MISSING: Not Recovered

Core 4					
Depth (m)	Well Construction	Core Number	% Recovery	Lithology	Lithological Description
9		ML1-7	82.5		
					SAND: Coarse sand, trace fines, angular to subrounded grains, well sorted GRAVELLY SAND: Gravelly fine to coarse sand, fine to coarse gravel, grading from trace fines near top to silty and clayey near bottom, angular to rounded clasts, maximum diameter = 3.8cm, poorly sorted
10					MISSING: Not Recovered
11		ML1-8	81.7		SAND: Medium to coarse sand, trace fines, angular to subangular grains, well sorted
					SAND: Medium to coarse sand with fine gravel, trace fines, subangular to subrounded clasts, maximum diameter = 1cm, fairly well sorted
					SANDY GRAVEL: Sandy fine to coarse gravel with fines, fine to coarse sand, angular to rounded clasts, maximum diameter = 5.1cm, poorly sorted
					SAND: Medium to coarse sand, trace fine gravel and fines, subangular to rounded clasts, maximum diameter = 1.8cm, fairly well sorted
12					GRAVEL: Fine to coarse gravel with fine to coarse sand and fines, angular to subrounded clasts, maximum diameter = 3.8cm, poorly sorted
					MISSING: Not Recovered
					SAND: Fine sand at top of section grading to coarse sand at bottom of section, trace fines, angular to rounded grains, well sorted

Core 4					
Depth (m)	Well Construction	Core Number	% Recovery	Lithology	Lithological Description
13		ML1-9	26.7		<p>SAND: Coarse sand with fine gravel, trace fines, angular to rounded clasts, maximum diameter = 1.5cm, well sorted</p> <p>SANDY GRAVEL: Sandy fine to coarse gravel, coarse sand, trace fines, rounded to subrounded clasts, maximum diameter = 2cm; note that the entire section graded evenly from fine sand at the top to fine to coarse gravel at the bottom</p> <p>MISSING: Not Recovered</p>

Notes:

- assumed top of core represented the actual top and all lost material was lost from the bottom
- for 5' cores, percent recovery based on a total core length of 1.52m
- for 3' cores, percent recovery based on a total core length of 0.9144m

Appendix C: Grain Size Analysis Data

Table C.1: Grain size analysis results for Core 1.

Core ID	Depth of Sample Centre (masl)	Terzaghi Method K (angular) (m/s)	Terzaghi Method K (rounded) (m/s)	Terzaghi Mean (m/s)
Core 1	296.39	1.5E-04	2.6E-04	2.0E-04
	296.14	3.0E-04	5.3E-04	4.1E-04
	295.88	1.9E-04	3.3E-04	2.6E-04
	295.65	1.3E-04	2.3E-04	1.8E-04
	294.89	2.5E-04	4.4E-04	3.4E-04
	294.66	6.6E-04	1.2E-03	9.1E-04
	294.38	2.2E-03	3.8E-03	3.0E-03
	294.13	1.4E-03	2.4E-03	1.9E-03
	291.84	7.6E-05	1.3E-04	1.0E-04
	291.59	2.0E-04	3.4E-04	2.7E-04
	291.26	3.5E-04	6.0E-04	4.8E-04
	291.03	1.2E-03	2.0E-03	1.6E-03
	290.32	4.7E-04	8.2E-04	6.5E-04
	290.06	3.5E-03	6.1E-03	4.8E-03
	289.81	1.9E-03	3.3E-03	2.6E-03
	289.58	8.0E-04	1.4E-03	1.1E-03
	288.79	7.0E-05	1.2E-04	9.6E-05
	288.54	4.7E-03	8.1E-03	6.4E-03
	288.29	4.7E-03	8.1E-03	6.4E-03
	288.03	3.1E-05	5.4E-05	4.3E-05
	286.97	6.0E-05	1.0E-04	8.3E-05
	286.71	7.0E-05	1.2E-04	9.6E-05
	286.20	1.4E-05	2.4E-05	1.9E-05
285.95	3.9E-05	6.7E-05	5.3E-05	
Minimum				1.9E-05
Maximum				6.4E-03
Arithmetic Mean				1.3E-03
Standard Deviation				1.9E-03

Table C.2: Grain size analysis results for Core 2.

Core ID	Depth of Sample Centre (masl)	Terzaghi Method K (angular) (m/s)	Terzaghi Method K (rounded) (m/s)	Terzaghi Mean (m/s)
Core 2	296.11	3.5E-03	6.1E-03	4.8E-03
	295.85	7.5E-04	1.3E-03	1.0E-03
	295.60	1.2E-04	2.2E-04	1.7E-04
	295.42	3.9E-05	6.7E-05	5.3E-05
	295.25	4.1E-04	7.1E-04	5.6E-04
	294.58	9.3E-06	1.6E-05	1.3E-05
	294.33	3.0E-04	5.3E-04	4.1E-04
	294.00	3.1E-03	5.4E-03	4.3E-03
	293.75	2.5E-03	4.3E-03	3.4E-03
	292.96	1.6E-03	2.8E-03	2.2E-03
	292.71	9.6E-04	1.7E-03	1.3E-03
	292.45	7.0E-04	1.2E-03	9.5E-04
	291.44	1.2E-03	2.0E-03	1.6E-03
	291.18	3.5E-04	6.0E-04	4.8E-04
	290.93	7.8E-04	1.4E-03	1.1E-03
	290.01	1.5E-04	2.7E-04	2.1E-04
	289.76	3.9E-03	6.7E-03	5.3E-03
	289.02	2.8E-03	4.9E-03	3.8E-03
	288.77	3.4E-04	5.8E-04	4.6E-04
	288.51	6.0E-04	1.0E-03	8.2E-04
	288.49	7.0E-04	1.2E-03	9.5E-04
	288.23	4.0E-04	6.9E-04	5.4E-04
	288.03	9.3E-05	1.6E-04	1.3E-04
	287.78	2.9E-04	5.1E-04	4.0E-04
	287.55	1.4E-05	2.4E-05	1.9E-05
	287.30	8.5E-05	1.5E-04	1.2E-04
	286.96	8.7E-05	1.5E-04	1.2E-04
	286.71	3.1E-04	5.5E-04	4.3E-04
	286.51	2.2E-03	3.8E-03	3.0E-03
	286.18	6.0E-03	1.0E-02	8.3E-03
285.92	4.1E-04	7.1E-04	5.6E-04	
Minimum				1.3E-05
Maximum				8.3E-03
Arithmetic Mean				1.5E-03
Standard Deviation				1.9E-03

Table C.3: Grain size analysis results for Core 3.

Core ID	Depth of Sample Centre (masl)	Terzaghi Method K (angular) (m/s)	Terzaghi Method K (rounded) (m/s)	Terzaghi Mean (m/s)
Core 3	300.46	4.7E-06	8.2E-06	6.5E-06
	300.20	5.6E-06	9.7E-06	7.6E-06
	299.21	1.9E-04	3.3E-04	2.6E-04
	298.96	2.4E-04	4.2E-04	3.3E-04
	298.65	9.3E-05	1.6E-04	1.3E-04
	297.77	4.7E-05	8.1E-05	6.4E-05
	297.51	1.2E-05	2.0E-05	1.6E-05
	296.77	6.3E-04	1.1E-03	8.7E-04
	296.77	2.4E-04	4.2E-04	3.3E-04
	296.52	3.5E-04	6.0E-04	4.8E-04
Minimum				6.5E-06
Maximum				8.7E-04
Arithmetic Mean				2.5E-04
Standard Deviation				2.6E-04

Table C.4: Grain size analysis results for Core 4.

Core ID	Depth of Sample Centre (masl)	Terzaghi Method K (angular) (m/s)	Terzaghi Method K (rounded) (m/s)	Terzaghi Mean (m/s)
Core 4	300.62	8.7E-06	1.5E-05	1.2E-05
	300.36	9.1E-06	1.6E-05	1.2E-05
	300.11	1.1E-04	1.9E-04	1.5E-04
	299.37	2.8E-05	4.9E-05	3.8E-05
	299.12	2.7E-04	4.7E-04	3.7E-04
	298.87	7.1E-04	1.2E-03	9.8E-04
	298.61	1.3E-04	2.3E-04	1.8E-04
	297.82	4.0E-04	6.9E-04	5.4E-04
	297.57	1.4E-03	2.4E-03	1.9E-03
	297.32	8.3E-04	1.5E-03	1.1E-03
	297.06	2.8E-04	4.9E-04	3.9E-04
	296.38	2.2E-05	3.8E-05	3.0E-05
	296.12	2.3E-04	4.0E-04	3.2E-04
	295.87	2.0E-04	3.6E-04	2.8E-04
	294.78	4.7E-05	8.1E-05	6.4E-05
	294.52	3.1E-04	5.5E-04	4.3E-04
	293.25	3.7E-04	6.5E-04	5.1E-04
	293.00	3.2E-04	5.6E-04	4.4E-04
	292.74	3.5E-03	6.1E-03	4.8E-03
	292.49	1.1E-02	1.8E-02	1.4E-02
	291.73	1.7E-04	3.0E-04	2.3E-04
	291.47	5.7E-04	1.0E-03	7.8E-04
	291.22	3.5E-04	6.0E-04	4.8E-04
	290.92	2.4E-04	4.2E-04	3.3E-04
	290.71	2.5E-04	4.4E-04	3.4E-04
	290.20	1.7E-04	3.0E-04	2.3E-04
	289.95	2.8E-03	4.9E-03	3.8E-03
	289.70	3.1E-03	5.4E-03	4.3E-03
	289.44	4.3E-05	7.4E-05	5.8E-05
	289.19	7.6E-05	1.3E-04	1.0E-04
288.76	1.3E-04	2.3E-04	1.8E-04	
288.50	1.9E-03	3.3E-03	2.6E-03	
Minimum				1.2E-05
Maximum				1.4E-02
Arithmetic Mean				1.3E-03
Standard Deviation				2.7E-03

Appendix D: Manual Water Level Measurements

Table D.1: Manual water level measurements used to compute the regional hydraulic gradient estimates.

Date	Manual Water Level (masl)							
	WO2D-14	WO35	WO74-S	WO74-M	WO74-D	WO74-WT	WO75-S	WO75-D
Jan	297.03	297.57	297.42	297.42	297.43	297.42	297.50	297.47
Feb	297.17	297.74	297.56	297.56	297.55	297.55	297.64	297.61
April	297.53	298.21	298.02	298.02	298.02	298.02	298.10	298.08
May	297.26	297.89	297.74	297.74	297.75	297.75	297.81	-
June	297.22	297.79	297.64	297.63	297.64	297.64	297.73	297.70
July	297.05	297.62	297.44	297.44	297.45	297.44	297.52	297.50
Aug	296.96	297.51	297.35	297.34	297.36	297.35	297.43	297.41
Sept	296.80	297.58	297.44	297.43	297.44	297.43	297.51	297.48
Oct	297.08	-	297.45	297.45	297.46	297.45	297.54	297.50
Dec	296.99	-	297.63	297.63	297.63	297.65	297.71	297.68

Appendix E: Complete CLOUDPE and PULSEPE Tracer Test Results

Table E.1: CLOUDPE and PULSEPE results from the first forced gradient tracer test.

Well ID	ML12-2	ML12-3	ML12-4	Arithmetic Mean	
Depth (masl)	293.08	291.38	289.68	-	
Best Fit Parameter Estimates	PULSEPE Velocity (m/s)	1.78E-04	1.81E-04	3.36E-04	2.31E-04
	CLOUDPE Velocity (m/s)	1.81E-04	1.90E-04	3.34E-04	2.35E-04
	PULSEPE Dispersivity (m)	0.23	0.38	0.87	0.50
	CLOUDPE Dispersivity (m)	0.27	0.35	0.72	0.45
	PULSEPE Source Width (m)	2.46	2.33	5.00	3.26
	CLOUDPE Mass (ug)	2.09E+05	1.96E+05	4.02E+05	2.69E+05
Approximate 95% Confidence Intervals^a	PULSEPE Velocity (m/s)	3.60E-06	3.70E-06	3.69E-05	1.47E-05
	CLOUDPE Velocity (m/s)	1.50E-05	1.50E-05	1.07E-04	4.57E-05
	PULSEPE Dispersivity (m)	0.05	0.07	0.88	0.33
	CLOUDPE Dispersivity (m)	0.01	0.03	0.13	0.06
	PULSEPE Source Width (m)	0.15	0.14	0.75	0.35
	CLOUDPE Mass (ug)	2.90E+04	2.70E+04	1.25E+05	6.03E+04
Solution with Better Fit	PULSEPE	PULSEPE	PULSEPE	-	
Disp. Based on Better Fit	0.23	0.38	0.87	0.50	
Velocity Based on Better Fit (m/s)	1.78E-04	1.81E-04	3.36E-04	2.31E-04	
Velocity Based on Better Fit (m/day)	15.4	15.6	29.0	20.0	

^a Actual confidence intervals are not symmetrical around the best fit parameters in all cases.

Table E.2: CLOUDPE and PULSEPE results from the second forced gradient tracer test.

WellID	ML5-2	ML5-3	ML5-4	ML5-5	ML5-6	ML5-7	ML6-2	ML6-3	ML6-4	ML6-6	ML6-7	ML7-2	ML7-3	ML7-4	ML7-5	ML8-3	Arithmetic Mean
Depth (masl)	295.54	293.84	292.14	290.44	288.74	287.04	293.45	291.75	290.05	286.65	284.95	293.47	291.77	290.07	288.37	291.14	-
PULSEPE Velocity (m/s)	5.29E-05	1.79E-04	2.42E-04	3.24E-04	4.78E-05	7.14E-05	1.40E-04	2.26E-04	4.30E-04	1.38E-04	2.37E-04	9.15E-05	2.62E-04	3.07E-04	1.60E-04	2.07E-04	1.95E-04
CLOUDPE Velocity (m/s)	6.16E-05	1.44E-04	2.34E-04	2.98E-04	6.12E-05	8.72E-05	1.42E-04	2.12E-04	3.41E-04	1.52E-04	2.60E-04	1.02E-04	3.13E-04	4.24E-03	2.09E-04	3.07E-05	4.30E-04
PULSEPE Dispersivity (m)	0.45	0.36	0.34	0.65	2.97	1.10	0.92	1.10	1.90	0.47	0.46	0.69	1.59	1.56	1.47	0.90	1.06
CLOUDPE Dispersivity (m)	0.35	0.90	0.75	0.91	1.78	0.65	0.76	0.73	0.78	0.38	0.38	0.51	1.42	23.15	1.04	1.13	2.23
PULSEPE Source Width (m)	0.70	2.89	3.61	5.38	1.67	1.27	3.58	4.40	7.81	1.39	1.49	2.23	5.75	5.96	2.04	4.39	3.41
CLOUDPE Mass (ug)	6.62E+04	3.56E+05	3.94E+05	4.80E+05	1.96E+05	1.38E+05	3.64E+05	4.05E+05	5.19E+05	1.29E+05	1.40E+05	2.01E+05	7.08E+05	2.11E+07	2.10E+05	9.95E+06	2.21E+06
PULSEPE Velocity (m/s)	4.76E-06	6.45E-05	1.69E-05	3.57E-05	6.21E-06	1.71E-05	5.17E-05	9.25E-05	6.87E-05	1.38E-05	4.03E-05	3.66E-06	5.24E-05	6.45E-05	1.12E-05	8.30E-06	3.45E-05
CLOUDPE Velocity (m/s)	6.20E-06	5.70E-05	9.30E-05	1.78E-04	1.04E-05	1.92E-05	1.90E-05	3.60E-05	1.12E-04	1.90E-05	4.60E-05	6.20E-06	2.50E-05	8.00E-05	2.50E-05	4.11E-05	4.83E-05
PULSEPE Dispersivity (m)	0.10	1.24	0.31	0.75	1.19	0.77	1.63	2.58	6.38	0.18	0.38	0.11	1.97	2.31	0.28	0.17	1.27
CLOUDPE Dispersivity (m)	0.00	0.01	0.02	0.11	0.00	0.01	0.02	0.03	0.07	0.01	0.07	0.00	0.07	3.00	0.00	1.13	0.28
PULSEPE Source Width (m)	0.11	1.33	0.36	0.70	0.25	0.32	1.33	2.64	1.41	0.22	0.37	0.13	1.50	1.73	0.12	0.18	0.79
CLOUDPE Mass (ug)	8.60E+03	4.30E+04	6.60E+04	1.44E+05	2.00E+04	1.40E+04	4.40E+04	6.50E+04	2.44E+05	1.50E+04	3.60E+04	2.00E+04	1.49E+05	2.10E+06	3.60E+04	1.00E+06	2.50E+05
Solution with Better Fit	na	PULSEPE	PULSEPE	PULSEPE	CLOUDPE	CLOUDPE	CLOUDPE	CLOUDPE	na	na	na	na	CLOUDPE	CLOUDPE	na	PULSEPE	-
Disp. Based on Better Fit	0.40	0.36	0.34	0.65	1.78	0.88	0.76	0.73	1.34	0.42	0.42	0.60	1.42	23.15	1.25	0.90	0.82 ^c
Velocity Based on Better Fit (m/s)	5.73E-05	1.79E-04	2.42E-04	3.24E-04	6.12E-05	7.93E-05	1.42E-04	2.12E-04	3.85E-04	1.45E-04	2.49E-04	9.67E-05	3.13E-04	4.24E-03	1.84E-04	2.07E-04	4.45E-04
Relative Velocity	1.35E-02	4.23E-02	5.71E-02	7.65E-02	1.44E-02	1.87E-02	3.35E-02	5.00E-02	9.09E-02	3.42E-02	5.86E-02	2.28E-02	7.39E-02	1.00E+00	4.35E-02	4.89E-02	1.05E-01
V Calibrated to Natural Gradient TT (m/s)	6.82E-06	2.13E-05	2.88E-05	3.86E-05	7.29E-06	9.45E-06	1.69E-05	2.52E-05	4.59E-05	1.73E-05	2.96E-05	1.15E-05	3.73E-05	5.05E-04	2.20E-05	2.47E-05	5.30E-05
V Calibrated to Natural Gradient TT (m/day)	0.59	1.84	2.49	3.34	0.63	0.82	1.46	2.18	3.96	1.49	2.56	1.00	3.22	43.63	1.90	2.13	4.58
Hydraulic Conductivity ^b (m/s)	6.8E-04	2.1E-03	2.9E-03	3.9E-03	7.3E-04	9.5E-04	1.7E-03	2.5E-03	4.6E-03	1.7E-03	3.0E-03	1.2E-03	3.7E-03	5.1E-02	2.2E-03	2.5E-03	5.9E-03

^a Actual confidence intervals are not symmetrical around the best fit parameters in all cases.

^b Hydraulic conductivity calculated with average gradient of 3.3x10⁻³ and average porosity of 0.33.

^c Value calculated without the ML7-4 dispersivity estimate of 23.15 metres.

Table E.3: CLOUDPE and PULSEPE results from the natural gradient tracer test.

Well ID	ML10-3	ML10-4	ML10-7	Arithmetic Mean	
Depth (masl)	291.19	289.49	284.39	-	
Best Fit Parameter Estimates	PULSEPE Velocity (m/s)	1.78E-04	4.82E-04	2.11E-04	2.90E-04
	CLOUDPE Velocity (m/s)	2.58E-04	5.05E-04	2.38E-04	3.34E-04
	PULSEPE Dispersivity (m)	2.85	0.36	0.91	1.38
	CLOUDPE Dispersivity (m)	1.03	0.34	0.67	0.68
	PULSEPE Source Width (m)	2.35	2.56	2.64	2.51
	CLOUDPE Mass (ug)	1.08E+05	1.15E+05	1.13E+05	1.12E+05
Approximate 95% Confidence Intervals^a	PULSEPE Velocity (m/s)	5.34E-05	3.04E-04	6.33E-05	1.40E-04
	CLOUDPE Velocity (m/s)	8.50E-05	1.82E-04	3.30E-05	1.00E-04
	PULSEPE Dispersivity (m)	4.02	2.43	1.23	2.56
	CLOUDPE Dispersivity (m)	0.01	0.00	0.02	0.01
	PULSEPE Source Width (m)	0.71	2.22	0.84	1.26
	CLOUDPE Mass (ug)	2.18E+04	2.80E+04	1.80E+04	2.26E+04
Solution with Better Fit	CLOUDPE	CLOUDPE	CLOUDPE	-	
Disp. Based on Better Fit	1.03	0.34	0.67	0.68	
Velocity Based on Better Fit (m/s)	2.58E-04	5.05E-04	2.38E-04	3.34E-04	
Velocity Based on Better Fit (m/day)	22.3	43.7	20.5	28.8	
Hydraulic Conductivity^b (m/s)	2.6E-02	5.1E-02	2.4E-02	3.3E-02	

^a Actual confidence intervals are not symmetrical around the best fit parameters in all cases.

^b Hydraulic conductivity calculated with average gradient of 3.3×10^{-3} and average porosity of 0.33.

Appendix F: Background Geochemical Data

Table F.1: Anion data collected at the study site, listed in chronological order.

Date	Well ID	Depth	Nitrate (mg-N/L)	Nitrite (mg-N/L)	Sulphate (mg-SO ₄ /L)	Chloride (mg-Cl/L)	Bromide (mg-Br/L)	Acetate (mg-CH ₃ COO/L)
28/02/2007	WO75-ML-1	299.01	-	-	-	-	-	-
	WO75-ML-2	297.79	-	-	-	-	-	-
	WO75-ML-3	295.35	14.1	0.0	-	26.9	-	-
	WO75-ML-4	293.52	14.6	0.0	-	28.9	-	-
	WO75-ML-5	291.69	15.0	0.0	-	29.2	-	-
	WO75-ML-6	289.87	13.3	0.0	-	29.3	-	-
	WO75-ML-7	288.04	14.0	0.0	-	31.8	-	-
01/03/2007	WO74-ML-1	296.64	0.3	0.0	-	19.1	-	-
	WO74-ML-2	295.32	11.6	0.0	-	24.9	-	-
	WO74-ML-3	293.80	12.9	0.0	-	29.7	-	-
	WO74-ML-4	292.28	13.1	0.0	-	34.6	-	-
	WO74-ML-5	290.45	13.1	0.0	-	44.1	-	-
	WO74-ML-6	288.01	12.7	0.0	-	43.0	-	-
	WO74-ML-7	286.18	12.9	0.0	-	48.9	-	-
07/05/2008	WO74-ML-1	296.64	1.1	0.0	10.7	1.6	-	-
	WO74-ML-2	295.32	6.1	0.0	16.9	13.4	-	-
	WO74-ML-3	293.80	15.4	0.0	38.3	38.6	-	-
	WO74-ML-4	292.28	15.5	0.0	37.5	38.6	-	-
	WO74-ML-5	290.45	15.5	0.0	41.7	50.4	-	-
	WO74-ML-6	288.01	15.4	0.0	42.7	49.5	-	-
	WO74-ML-7	286.18	14.5	0.0	41.2	56.0	-	-
07/05/2008	WO75-ML-1	299.01	-	-	-	-	-	-
	WO75-ML-2	297.79	-	-	-	-	-	-
	WO75-ML-3	295.35	16.5	0.0	40.5	33.3	-	-
	WO75-ML-4	293.52	16.5	0.0	41.8	34.3	-	-
	WO75-ML-5	291.69	16.0	0.0	41.8	34.6	-	-
	WO75-ML-6	289.87	15.3	0.0	39.0	35.5	-	-
	WO75-ML-7	288.04	16.1	0.0	40.5	37.3	-	-

Table F.1: (continued)

Date	Well ID	Depth	Nitrate (mg-N/L)	Nitrite (mg-N/L)	Sulphate (mg-SO ₄ /L)	Chloride (mg-Cl/L)	Bromide (mg-Br/L)	Acetate (mg-CH ₃ COO/L)
04/06/2008	WO74-ML-1	296.64	1.1	0.0	8.5	1.5	-	-
	WO74-ML-2	295.32	8.0	0.0	18.6	17.0	-	-
	WO74-ML-3	293.80	14.1	0.0	32.3	35.9	-	-
	WO74-ML-4	292.28	13.8	0.0	33.4	41.3	-	-
	WO74-ML-5	290.45	13.6	0.0	35.3	45.9	-	-
	WO74-ML-6	288.01	13.1	0.0	33.0	43.2	-	-
	WO74-ML-7	286.18	12.8	0.0	35.9	53.2	-	-
	WO75-ML-1	299.01	-	-	-	-	-	-
	WO75-ML-2	297.79	-	-	-	-	-	-
	WO75-ML-3	295.35	14.5	0.0	34.6	29.7	-	-
	WO75-ML-4	293.52	14.6	0.0	34.1	30.0	-	-
	WO75-ML-5	291.69	14.6	0.0	34.2	30.8	-	-
	WO75-ML-6	289.87	14.1	0.0	34.2	33.1	-	-
	WO75-ML-7	288.04	14.2	0.0	34.8	33.9	-	-
17/07/2008	WO74-ML-1	296.64	3.0	0.0	11.4	5.2	-	-
	WO74-ML-2	295.32	10.7	0.0	27.0	22.5	-	-
	WO74-ML-3	293.80	14.3	0.0	34.1	34.7	-	-
	WO74-ML-4	292.28	14.1	0.0	33.7	39.9	-	-
	WO74-ML-5	290.45	13.3	0.0	34.6	46.3	-	-
	WO74-ML-6	288.01	13.1	0.0	33.6	45.2	-	-
	WO74-ML-7	286.18	12.4	0.0	35.3	52.5	-	-
	WO75-ML-1	299.01	-	-	-	-	-	-
	WO75-ML-2	297.79	-	-	-	-	-	-
	WO75-ML-3	295.35	14.1	0.0	35.1	29.3	-	-
	WO75-ML-4	293.52	14.3	0.0	34.2	29.1	-	-
	WO75-ML-5	291.69	14.3	0.0	35.0	29.4	-	-
	WO75-ML-6	289.87	14.0	0.0	35.4	32.0	-	-
	WO75-ML-7	288.04	14.0	0.0	35.4	32.1	-	-

Table F.1: (continued)

Date	Well ID	Depth	Nitrate (mg-N/L)	Nitrite (mg-N/L)	Sulphate (mg-SO ₄ /L)	Chloride (mg-Cl/L)	Bromide (mg-Br/L)	Acetate (mg-CH ₃ COO/L)
17/07/2008	ML1-1	297.13	13.3	0.0	32.6	31.5	-	-
	ML1-2	295.63	14.2	0.0	30.2	31.0	-	-
	ML1-3	294.13	14.2	0.0	32.5	36.7	-	-
	ML1-4	292.63	13.9	0.0	33.4	36.1	-	-
	ML1-5	291.13	14.2	0.0	33.7	36.0	-	-
	ML1-6	289.63	13.5	0.0	32.6	40.3	-	-
	ML1-7	288.13	13.1	0.0	33.3	43.0	-	-
24/07/2008	ML2-1	294.62	13.7	0.0	30.6	31.4	-	-
	ML2-2	292.92	14.5	0.0	33.5	37.0	-	-
	ML2-3	291.22	14.0	0.0	32.5	38.4	-	-
	ML2-4	289.52	13.6	0.0	33.2	40.9	-	-
	ML2-5	287.82	13.1	0.0	32.6	41.5	-	-
	ML2-6	286.12	-	-	-	-	-	-
	ML2-7	284.42	11.9	0.0	33.0	56.5	-	-
	ML2-8	282.72	12.0	0.0	34.1	55.0	-	-
24/07/2008	ML3-1	294.59	13.7	0.0	29.9	32.2	-	-
	ML3-2	292.89	14.3	0.0	32.4	37.2	-	-
	ML3-3	291.19	13.7	0.0	33.9	39.6	-	-
	ML3-4	289.49	13.6	0.0	32.2	38.6	-	-
	ML3-5	287.79	13.1	0.0	34.0	47.2	-	-
	ML3-6	286.09	10.7	0.0	30.1	48.8	-	-
	ML3-7	284.39	12.5	0.0	32.4	49.4	-	-
	ML3-8	282.69	12.1	0.0	34.6	56.6	-	-

Table F.1: (continued)

Date	Well ID	Depth	Nitrate (mg-N/L)	Nitrite (mg-N/L)	Sulphate (mg-SO ₄ /L)	Chloride (mg-Cl/L)	Bromide (mg-Br/L)	Acetate (mg-CH ₃ COO/L)
25/07/2008	ML4-1	294.47	13.9	0.0	30.6	33.5	-	-
	ML4-2	292.77	14.4	0.0	31.9	37.9	-	-
	ML4-3	291.07	13.6	0.0	34.5	40.4	-	-
	ML4-4	289.37	13.7	0.0	32.8	39.9	-	-
	ML4-5	287.67	12.7	0.0	33.2	46.3	-	-
	ML4-6	285.97	11.9	0.0	34.6	53.4	-	-
	ML4-7	284.27	12.0	0.0	33.3	54.7	-	-
	ML4-8	282.57	11.9	0.0	33.6	55.6	-	-
25/07/2008	ML7-1	295.17	14.0	0.0	30.7	31.3	-	-
	ML7-2	293.47	14.3	0.0	32.2	34.9	-	-
	ML7-3	291.77	14.0	0.0	34.1	39.8	-	-
	ML7-4	290.07	13.5	0.0	32.7	43.1	-	-
	ML7-5	288.37	12.6	0.0	33.8	46.7	-	-
	ML7-6	286.67	12.3	0.0	33.0	54.4	-	-
	ML7-7	284.97	-	-	-	-	-	-
	ML7-8	283.27	-	-	-	-	-	-
25/07/2008	ML8-1	294.54	14.3	0.0	31.3	33.4	-	-
	ML8-2	292.84	13.9	0.0	32.4	38.2	-	-
	ML8-3	291.14	13.7	0.0	34.9	41.6	-	-
	ML8-4	289.44	13.3	0.0	33.1	44.1	-	-
	ML8-5	287.74	12.8	0.0	35.1	52.4	-	-
	ML8-6	286.04	12.4	0.0	34.6	53.9	-	-
	ML8-7	284.34	12.5	0.0	34.2	49.6	-	-
	ML8-8	282.64	-	-	-	-	-	-

Table F.1: (continued)

Date	Well ID	Depth	Nitrate (mg-N/L)	Nitrite (mg-N/L)	Sulphate (mg-SO ₄ /L)	Chloride (mg-Cl/L)	Bromide (mg-Br/L)	Acetate (mg-CH ₃ COO/L)
29/07/2008	ML5-1	297.24	7.6	0.0	19.3	18.2	-	-
	ML5-2	295.54	-	-	-	-	-	-
	ML5-3	293.84	11.4	0.0	26.2	26.0	-	-
	ML5-4	292.14	14.0	0.0	32.7	34.6	-	-
	ML5-5	290.44	12.5	0.0	33.0	40.2	-	-
	ML5-6	288.74	12.9	0.0	34.3	48.7	-	-
	ML5-7	287.04	12.5	0.0	35.8	51.7	-	-
	ML5-8	285.34	-	0.0	-	-	-	-
29/07/2008	ML6-1	295.15	13.5	0.0	29.7	29.3	-	-
	ML6-2	293.45	-	-	-	-	-	-
	ML6-3	291.75	13.5	0.0	32.8	35.4	-	-
	ML6-4	290.05	-	-	-	-	-	-
	ML6-5	288.35	12.9	0.0	35.1	49.7	-	-
	ML6-6	286.65	12.2	0.0	35.0	53.1	-	-
	ML6-7	284.95	12.0	0.0	34.2	50.1	-	-
	ML6-8	283.25	-	-	-	-	-	-
30/07/2008	ML10-1	294.59	13.6	0.0	32.8	37.4	-	-
	ML10-2	292.89	13.9	0.0	32.7	32.0	-	-
	ML10-3	291.19	14.4	0.0	33.7	33.9	-	-
	ML10-4	289.49	14.2	0.0	34.7	35.7	-	-
	ML10-5	287.79	13.2	0.0	33.4	38.3	-	-
	ML10-6	286.09	13.6	0.0	34.9	44.1	-	-
	ML10-7	284.39	12.9	0.0	33.5	42.6	-	-
	ML10-8	282.69	-	-	-	-	-	-

Table F.1: (continued)

Date	Well ID	Depth	Nitrate (mg-N/L)	Nitrite (mg-N/L)	Sulphate (mg-SO ₄ /L)	Chloride (mg-Cl/L)	Bromide (mg-Br/L)	Acetate (mg-CH ₃ COO/L)
30/07/2008	ML11-1	294.53	14.0	0.0	32.2	35.4	-	-
	ML11-2	292.83	14.4	0.0	33.6	33.5	-	-
	ML11-3	291.13	14.0	0.0	34.2	32.7	-	-
	ML11-4	289.43	13.0	0.0	32.4	33.4	-	-
	ML11-5	287.73	13.3	0.0	34.0	40.3	-	-
	ML11-6	286.03	12.1	0.0	33.2	40.8	-	-
	ML11-7	284.33	12.5	0.0	34.2	42.7	-	-
	ML11-8	282.63	-	-	-	-	-	-
08/08/2008	ML9-1	295.78	13.8	0.0	32.2	31.8	-	-
	ML9-2	294.08	14.2	0.0	34.5	33.8	-	-
	ML9-3	292.38	14.1	0.0	33.4	31.7	-	-
	ML9-4	290.68	14.2	0.0	34.0	32.3	-	-
	ML9-5	288.98	13.6	0.0	33.3	38.0	-	-
	ML9-6	287.28	13.2	0.0	34.8	42.2	-	-
	ML9-7	285.58	13.5	0.0	34.6	42.3	-	-
	ML9-8	283.83	-	-	-	-	-	-
08/08/2008	WO77	-	13.9	0.0	33.6	39.7	-	-
	WO80	-	14.2	0.0	34.1	34.7	-	-

Table F.1: (continued)

Date	Well ID	Depth	Nitrate (mg-N/L)	Nitrite (mg-N/L)	Sulphate (mg-SO ₄ /L)	Chloride (mg-Cl/L)	Bromide (mg-Br/L)	Acetate (mg-CH ₃ COO/L)
27/04/2009	ML5-1	297.24	6.33	-	-	-	0.0	-
	ML5-2	295.54	12.52	-	-	-	0.0	-
	ML5-3	293.84	13.92	-	-	-	0.0	-
	ML5-4	292.14	14.04	-	-	-	0.0	-
	ML5-5	290.44	13.53	-	-	-	0.0	-
	ML5-6	288.74	12.38	-	-	-	0.0	-
	ML5-7	287.04	12.36	-	-	-	0.0	-
	ML5-8	285.34	-	-	-	-	-	-
30/04/2009	ML10-1	294.59	13.4	0.0	-	-	0.0	0.0
	ML10-2	292.89	15.0	0.0	-	-	0.0	0.0
	ML10-3	291.19	15.0	0.0	-	-	0.0	0.0
	ML10-4	289.49	14.8	0.0	-	-	0.0	0.0
	ML10-5	287.79	13.4	0.0	-	-	0.0	0.0
	ML10-6	286.09	13.2	0.0	-	-	0.0	0.0
	ML10-7	284.39	12.9	0.0	-	-	0.0	0.0
	ML10-8	282.69	-	-	-	-	-	-
Arithmetic Mean			13.0	0.0	32.9	38.1	0.0	0.0
Standard Deviation			2.6	0.0	5.2	10.5	0.0	0.0

Table F.2: Cation data collected at the study site.

Date	Well ID	Depth	Calcium (mg/L)	Aluminum (mg/L)	Silicon (mg/L)	Manganese (mg/L)	Iron (mg/L)
26/03/2009	ML5-1	297.24	112.0	0.0	5.0	0.0	0.0
	ML5-2	295.54	96.3	0.0	5.4	0.0	0.0
	ML5-3	293.84	102.0	0.0	6.0	0.0	0.0
	ML5-4	292.14	104.0	0.0	6.2	0.0	0.0
	ML5-5	290.44	108.0	0.0	6.2	0.0	0.0
	ML5-6	288.74	103.0	0.0	6.0	0.0	0.0
	ML5-7	287.04	103.0	0.0	6.0	0.0	0.0
	ML5-8	285.34	103.0	0.0	5.8	0.1	0.0
26/03/2009	ML7-1	295.17	99.3	0.0	5.7	0.0	0.0
	ML7-2	293.47	104.0	0.0	6.1	0.0	0.0
	ML7-3	291.77	104.0	0.0	6.2	0.0	0.0
	ML7-4	290.07	105.0	0.0	6.2	0.0	0.0
	ML7-5	288.37	106.0	0.0	6.2	0.0	0.0
	ML7-6	286.67	106.0	0.0	6.1	0.0	0.0
	ML7-7	284.97	102.0	0.0	6.0	0.0	0.0
	ML7-8	283.27	106.0	0.0	6.1	0.0	0.0
Arithmetic Mean			104.0	0.0	5.9	0.0	0.0
Standard Deviation			3.5	0.0	0.3	0.0	0.0

Table F.3: Alkalinity, dissolved oxygen, electrical conductivity, temperature, and pH data collected at the study site.

Date	Well ID	Depth	pH	Temperature (degrees C)	Electrical Conductivity Corrected for T (uS)	Dissolved Oxygen (mg/L)	Alkalinity (mg-CaCO ₃ /L)
26/03/2009	ML5-1	297.24	-	5.4	-	8.3	-
	ML5-2	295.54	7.2	6.4	-	9.3	278.0
	ML5-3	293.84	7.3	7.5	-	8.6	276.0
	ML5-4	292.14	7.3	7.9	-	8.1	270.0
	ML5-5	290.44	7.4	8.2	-	7.2	260.0
	ML5-6	288.74	7.3	8.3	-	7.5	251.0
	ML5-7	287.04	7.3	8.3	-	7.3	265.0
	ML5-8	285.34	7.3	8.4	-	6.4	261.0
26/03/2009	ML6-1	295.15	7.5	7.9	-	9.9	-
	ML6-2	293.45	7.4	8.9	-	8.3	-
	ML6-3	291.75	7.3	9.3	-	7.6	-
	ML6-4	290.05	7.4	9.7	-	7.7	-
	ML6-5	288.35	7.4	9.9	-	8.1	-
	ML6-6	286.65	7.3	9.4	-	7.5	-
	ML6-7	284.95	7.4	9.4	-	8.9	-
	ML6-8	283.25	7.4	10.0	-	6.4	-
26/03/2009	ML7-1	295.17	7.3	6.7	-	8.8	270.0
	ML7-2	293.47	7.3	7.9	-	7.7	261.0
	ML7-3	291.77	7.3	8.0	-	7.3	274.0
	ML7-4	290.07	7.3	7.9	-	7.2	266.0
	ML7-5	288.37	7.3	8.2	-	7.6	258.0
	ML7-6	286.67	7.2	8.3	-	7.1	264.0
	ML7-7	284.97	7.4	8.1	-	8.2	262.0
	ML7-8	283.27	7.3	8.3	-	7.7	260.0

Table F.3: (continued)

Date	Well ID	Depth	pH	Temperature (degrees C)	Electrical Conductivity Corrected for T (uS)	Dissolved Oxygen (mg/L)	Alkalinity (mg-CaCO ₃ /L)
26/03/2009	ML8-1	294.54	7.4	8.9	-	8.2	-
	ML8-2	292.84	7.3	9.5	-	12.5	-
	ML8-3	291.14	7.4	9.8	-	11.2	-
	ML8-4	289.44	7.4	10.0	-	6.7	-
	ML8-5	287.74	7.4	9.8	-	9.0	-
	ML8-6	286.04	7.4	9.8	-	9.8	-
	ML8-7	284.34	7.4	9.6	-	9.7	-
	ML8-8	282.64	-	-	-	-	-
13/07/2009	ML5-1	297.24	7.2	13.2	479.9	8.0	307.0
	ML5-2	295.54	7.4	12.3	514.8	8.0	269.0
	ML5-3	293.84	7.4	11.5	509.4	8.9	265.0
	ML5-4	292.14	7.4	11.6	514.5	9.7	-
	ML5-5	290.44	7.4	11.6	526.7	10.3	-
	ML5-6	288.74	7.4	11.5	522.3	11.1	-
	ML5-7	287.04	7.4	12.2	549.9	11.1	-
	ML5-8	285.34	-	-	-	-	-
13/07/2009	ML7-1	295.17	7.3	13.1	522.1	-	272.0
	ML7-2	293.47	7.3	11.6	528.2	-	267.0
	ML7-3	291.77	7.4	12.2	525.0	-	260.0
	ML7-4	290.07	7.3	12.5	526.6	-	265.0
	ML7-5	288.37	7.3	12.4	553.8	-	270.0
	ML7-6	286.67	7.3	13.4	570.3	-	255.0
	ML7-7	284.97	7.4	13.9	572.9	-	275.0
	ML7-8	283.27	-	-	-	-	-

Table F.3: (continued)

Date	Well ID	Depth	pH	Temperature (degrees C)	Electrical Conductivity Corrected for T (uS)	Dissolved Oxygen (mg/L)	Alkalinity (mg-CaCO ₃ /L)
13/07/2009	ML8-1	294.54	7.3	11.6	526.0	8.3	-
	ML8-2	292.84	7.3	12.2	549.9	10.0	-
	ML8-3	291.14	7.3	12.5	542.8	9.3	-
	ML8-4	289.44	7.3	12.8	545.2	9.0	-
	ML8-5	287.74	7.4	14.1	574.5	11.0	-
	ML8-6	286.04	7.4	13.6	578.8	10.5	-
	ML8-7	284.34	7.3	16.2	602.4	10.8	-
	ML8-8	282.64	-	-	-	-	-
10/09/2009	ML7-1	295.17	-	15.1	529.9	8.4	-
	ML7-2	293.47	-	13.3	552.1	8.0	-
	ML7-3	291.77	-	13.7	556.8	8.2	-
	ML7-4	290.07	-	13.6	582.6	9.6	-
	ML7-5	288.37	-	14.3	607.1	8.9	-
	ML7-6	286.67	-	14.8	620.8	9.1	-
	ML7-7	284.97	-	14.8	634.9	9.7	-
	ML7-8	283.27	-	-	-	-	-
Arithmetic Mean			7.3	10.8	550.7	8.7	267.2
Standard Deviation			0.1	2.5	36.3	1.4	10.6

Table F.4: Background nitrous oxide concentration data collected at the site.

Date	Well ID	Depth	N ₂ O Concentration (ug-N/L)
13/07/2009	ML8-1	294.54	40.1
	ML8-2	292.84	36.4
	ML8-3	291.14	41.0
	ML8-4	289.44	38.3
	ML8-5	287.74	36.4
	ML8-6	286.04	35.5
	ML8-7	284.34	36.7
Arithmetic Mean			37.8
Standard Deviation			2.1

Table F.5: Background nitrate isotope data collected at the site.

Date	Well ID	Depth	$\delta^{15}\text{N-NO}_3$ (‰)	$\delta^{18}\text{O-NO}_3$ (‰)
08/2007 to 09/2007 ¹	WO72-S	294.19	5.6	2.4
	WO62	292.16	5.8	0.3
	WO11-6	296.78	5.2	-0.3
	WO11-8	294.63	6.1	0.2
	WO11-13	290.64	6.8	1.1
	Supply Well 1	267.00	6.1	2.7
	Supply Well 5	269.40	6.4	1.7
	WO63	288.56	6.8	1.0
	WO74-S	291.00	6.4	0.3
WO74-D	284.29	6.3	1.7	
26/03/2009	ML5-1	297.24	8.3	1.0
	ML5-2	295.54	5.5	0.6
	ML5-3	293.84	6.3	1.4
	ML5-4	292.14	7.3	-0.2
	ML5-5	290.44	5.5	3.0
	ML5-6	288.74	6.7	2.1
	ML5-7	287.04	6.7	3.6
	ML5-8	285.34	6.2	1.4
Arithmetic Mean			6.3	1.3
Standard Deviation			0.7	1.1

Data from Koch, 2009

Appendix G: Geochemical Results from Acetate Injection Phase 1

Table G.1: Anion data collected at ML7 during the first acetate injection phase.

Port ID	T - to (hours)	Nitrite (mg-N/L)	Nitrate (mg-N/L)	Acetate (mg/L)	Bromide (mg/L)
ML7-1	4.3	0.0	16.1	0.0	18.8
	8.6	0.0	14.6	4.8	29.8
	10.6	0.0	16.8	2.1	19.1
	11.6	0.0	16.2	3.5	29.3
	12.6	0.0	16.8	2.8	19.8
	14.6	0.0	16.2	8.0	37.3
ML7-2	4.4	0.0	16.0	20.8	81.8
	7.2	0.0	15.8	29.3	116.3
	8.7	0.0	15.7	43.0	158.3
	10.6	0.0	15.9	58.6	206.3
	12.6	0.0	15.8	64.3	221.7
	14.7	0.0	16.0	62.2	217.7
ML7-3	0.7	0.0	16.2	0.0	16.3
	1.3	0.0	15.7	0.0	21.1
	1.9	0.0	16.0	5.7	34.8
	2.6	0.0	15.7	17.8	67.2
	3.1	0.0	14.6	23.6	97.1
	3.8	0.0	15.1	33.8	145.8
	4.4	0.0	13.7	38.0	169.6
	5.2	0.0	14.8	45.3	224.2
	6.4	0.0	14.6	51.5	265.7
	7.2	0.0	14.7	52.5	265.0
	8.7	0.0	14.5	48.2	244.9
	11.6	0.0	15.7	51.5	200.2
12.6	0.0	16.2	44.9	182.8	
ML7-4	0.7	0.0	15.7	0.0	19.2
	1.3	0.0	15.5	7.0	35.4
	1.9	0.0	15.6	23.6	88.7
	2.6	0.0	15.9	45.1	163.6
	3.1	0.0	14.6	42.2	195.5
	3.8	0.0	11.4	38.6	184.5

Table G.1: (continued)

Port ID	T - to (hours)	Nitrite (mg-N/L)	Nitrate (mg-N/L)	Acetate (mg/L)	Bromide (mg/L)
ML7-4	4.4	0.0	14.6	50.1	255.5
	5.2	0.0	14.1	52.2	260.3
	5.7	0.0	13.2	49.1	250.7
	6.4	0.0	14.6	55.2	291.6
	7.2	0.0	14.8	53.1	272.3
	8.1	0.0	13.7	43.5	222.1
	8.7	0.0	14.3	46.6	241.5
	11.7	0.0	15.8	39.0	153.4
ML7-5	2.0	0.0	14.7	5.9	35.0
	2.7	0.0	14.6	17.7	67.6
	3.2	0.0	14.8	24.6	89.7
	4.4	0.0	13.7	35.4	125.0
	5.8	0.0	15.0	45.1	163.3
	7.3	0.0	15.1	50.0	181.6
	8.7	0.0	14.9	41.2	157.4
	9.7	0.0	14.6	41.7	147.8
	10.7	0.0	14.4	33.4	131.4
	12.7	0.0	15.1	26.4	108.7
	14.7	0.0	15.0	20.6	84.1
ML7-6	2.0	0.0	13.8	0.0	18.8
	2.7	0.0	14.0	0.9	18.0
	3.2	0.0	13.8	2.3	20.6
	4.4	0.0	13.5	7.2	23.3
	5.8	0.0	11.1	12.2	45.9
	7.3	0.0	13.7	20.0	76.3
	8.8	0.0	13.8	20.7	79.2
	9.7	0.0	13.1	22.3	79.2
	10.7	0.0	13.8	19.3	81.4
	12.7	0.0	13.8	17.9	77.6
	14.7	0.0	13.8	16.8	70.8
ML7-7	2.0	0.0	13.6	6.1	33.7
	2.7	0.0	13.6	10.9	49.8
	3.2	0.0	13.7	15.5	62.5
	5.8	0.0	13.5	23.4	88.6
	8.8	0.0	14.0	19.9	81.3
	9.7	0.0	13.6	18.7	66.4
	10.7	0.0	12.9	15.8	54.7
	12.7	0.0	13.7	3.1	43.9
	14.8	0.0	13.7	7.0	33.5
Arithmetic Mean		0.0	14.7	26.6	116.0
Standard Deviation		0.0	1.1	19.1	83.0

Table G.2: Cation results from the first acetate injection phase.

Well ID	T - to (hours)	Depth (masl)	Calcium (mg/L)	Aluminum (mg/L)	Silicon (mg/L)	Manganese (mg/L)	Iron (mg/L)
ML5-1	1.0	297.24	113.4	0.0	5.0	0.0	0.0
ML5-2	1.0	295.54	107.1	0.0	5.4	0.0	0.0
ML5-3	1.1	293.84	113.8	0.0	5.9	0.0	0.0
ML5-4	1.1	292.14	125.0	0.0	5.8	0.0	0.0
ML5-5	1.2	290.44	112.2	0.0	5.8	0.0	0.0
ML5-6	1.2	288.74	101.8	0.0	5.7	0.0	0.0
ML5-7	1.2	287.04	101.9	0.0	5.8	0.0	0.0
ML5-1	5.4	297.24	114.0	0.0	5.0	0.0	0.0
ML5-2	5.5	295.54	140.3	0.1	5.8	0.0	0.1
ML5-3	5.5	293.84	146.9	0.1	5.9	0.0	0.1
ML5-4	5.6	292.14	125.9	0.0	5.8	0.0	0.0
ML5-5	5.6	290.44	105.9	0.0	5.8	0.0	0.0
ML5-6	5.5	288.74	103.7	0.0	5.8	0.0	0.0
ML5-7	5.5	287.04	106.2	0.0	5.9	0.0	0.0
ML8-1	17.6	294.54	125.0	0.0	5.8	0.0	0.0
ML8-2	17.7	292.84	132.5	0.0	6.0	0.0	0.0
ML8-3	17.5	291.14	122.3	0.0	5.8	0.0	0.0
ML8-4	17.6	289.44	111.2	0.0	5.9	0.0	0.0
ML8-5	17.5	287.74	103.7	0.0	5.9	0.0	0.0
ML8-6	17.7	286.04	108.3	0.0	5.8	0.0	0.0
ML8-7	17.6	284.34	103.1	0.0	5.8	0.0	0.0
Arithmetic Mean			115.4	0.0	5.7	0.0	0.0
Standard Deviation			13.0	0.0	0.3	0.0	0.0

Table G.3: Nitrous oxide concentrations data collected during the pilot acetate injection.

Well ID	T - to (hours)	N ₂ O Concentration (ug-N/L)
ML5-2	4.3	35.8
ML5-2	8.4	40.1
ML5-2	15.2	33.7
ML5-3	4.3	32.0
ML5-3	8.4	33.1
ML5-3	15.3	33.1
ML5-4	4.3	33.5
ML5-4	8.5	35.4
ML5-4	15.4	37.3
ML5-5	4.3	35.7
ML5-5	8.5	35.4
ML5-5	15.4	36.4
ML6-2	4.0	35.3
ML6-3	4.0	33.6
ML6-3	8.1	34.3
ML6-3	15.5	41.5
ML6-4	4.0	34.4
ML6-4	8.1	33.6
ML6-4	15.5	35.4
ML6-5	4.0	33.1
ML6-5	8.1	31.1
ML6-5	15.6	34.4
ML6-6	4.1	31.5
ML6-6	8.2	32.5
ML6-6	15.7	34.6
ML7-3	4.0	38.8
ML7-3	8.3	34.3
ML7-3	15.2	37.9
ML7-4	4.0	33.4
ML7-4	8.4	36.6

Table G.3: (continued)

Well ID	T - to (hours)	N ₂ O Concentration (ug-N/L)
ML7-4	15.3	36.5
ML7-5	4.0	38.7
ML7-5	8.5	33.9
ML7-5	15.3	42.4
ML7-6	4.1	33.5
ML7-6	8.5	33.8
ML7-6	15.4	38.6
ML8-3	4.3	37.4
ML8-3	8.0	36.7
ML8-3	15.5	37.8
ML8-4	4.3	40.8
ML8-4	8.1	39.5
ML8-4	15.5	35.0
ML8-5	4.4	35.5
ML8-5	8.1	34.1
ML8-5	15.6	36.7
ML8-6	4.4	32.8
ML8-6	8.2	25.9
ML8-6	15.7	37.5
Arithmetic Mean		35.4
Standard Deviation		2.9

Table G.4: Nitrous oxide isotope data collected prior to and during Injection Phase 1.

Well ID	T - to (hours)	Depth	$\delta^{15}\text{N-N}_2\text{O}$ (‰)	$\delta^{18}\text{O-N}_2\text{O}$ (‰)
ML5-4-1	4.3	292.14	-15.2	33.4
ML5-4-2	8.5	292.14	-14.9	33.8
ML5-4-3	15.4	292.14	-14.6	33.7
ML8-3-0	0.0	291.14	-14.9	34.0
Arithmetic Mean			-14.9	33.7
Standard Deviation			0.2	0.2

Appendix H: Geochemical Results from Acetate Injection Phase 2

Table H.1: Dissolved oxygen data collected before, during, and following Injection Phase 2.

Injection ID	Date	Dissolved Oxygen Concentration (mg/L)						
		ML7-1	ML7-2	ML7-3	ML7-4	ML7-5	ML7-6	ML7-7
0	10/09/09	8.4	8.0	8.2	9.1	8.9	9.1	9.7
2	14/09/09	7.6	7.8	7.8	8.2	7.6	8.0	8.7
3	15/09/09	9.2	11.2	12.4	8.5	10.6	9.4	10.7
4	16/09/09	3.4	6.6	7.1	8.1	6.5	7.7	7.2
5	17/09/09	2.0	3.7	5.1	7.0	6.0	6.1	8.4
6	18/09/09	0.6	1.0	0.7	3.9	0.9	0.7	3.8
7	19/09/09	0.7	1.3	3.0	4.1	1.4	3.1	4.3
8	20/09/09	1.0	0.8	3.1	3.5	3.2	3.5	3.1
9	21/09/09	0.8	1.3	2.5	2.9	1.2	0.7	2.7
10	22/09/09	1.4	1.8	2.8	4.2	2.6	0.3	2.9
11	23/09/09	0.7	0.9	2.3	2.3	0.7	1.1	3.9
12	24/09/09	0.4	0.7	4.6	5.1	1.9	1.3	2.9
13	25/09/09	3.8	5.6	5.3	5.5	4.0	4.0	5.0
14	27/09/09	2.8	3.2	6.4	5.9	3.6	3.1	6.3
15	29/09/09	1.5	1.0	1.8	3.0	0.8	0.7	1.5
16	01/10/09	0.4	1.0	2.1	2.7	1.2	0.9	2.9
17	03/10/09	0.8	1.0	1.3	2.3	1.1	1.5	2.9
18	05/10/09	0.4	0.6	2.0	2.5	1.0	0.8	2.9
19	07/10/09	0.5	0.8	1.3	2.0	1.1	1.1	2.5
20	09/10/09	0.2	0.3	1.0	1.6	0.4	0.1	2.0
-	13/10/09	0.1	2.8	6.2	6.2	4.3	4.3	5.9
-	19/10/09	1.0	4.7	6.2	6.6	4.8	4.8	6.3
Minimum		0.1	0.3	0.7	1.6	0.4	0.1	1.5
Maximum		9.2	11.2	12.4	9.1	10.6	9.4	10.7
Arithmetic Mean		2.2	3.0	4.2	4.8	3.4	3.3	4.8
Standard Deviation		2.7	3.0	3.0	2.4	2.9	3.0	2.7

Table H.2: Anion data collected during and directly following injection 13.

Well ID	T - to (hours)	Acetate (mg/L)	Nitrite (mg-N/L)	Nitrate (mg-N/L)	Bromide (mg/L)	Chloride (mg/L)	Sulphate (mg/L)
ML5-1	0.5	0.0	0.0	11.9	16.8	24.6	23.1
	7.1	2.2	0.0	13.3	18.3	26.4	26.8
ML5-2	0.5	20.9	4.5	5.1	23.4	33.1	34.1
	3.1	12.7	3.4	7.7	25.7	33.3	35.2
	7.2	34.0	2.6	8.4	72.6	32.9	35.3
	8.2	37.1	2.5	8.7	81.9	33.3	34.0
ML5-3	0.5	37.9	1.8	8.0	17.7	34.6	34.7
	3.2	-	1.2	12.2	204.4	35.5	35.5
	7.2	117.2	1.0	12.6	240.8	35.7	34.4
	8.2	-	1.0	12.8	229.3	35.6	35.2
ML5-4	0.5	22.5	0.0	15.2	56.0	35.1	35.5
	7.2	74.3	0.9	13.2	168.2	36.2	35.5
ML5-5	0.6	82.8	0.7	13.9	163.0	36.5	35.1
	3.2	-	0.9	13.4	257.7	36.0	35.8
	7.2	57.5	0.9	13.7	137.9	37.2	36.6
	8.2	45.9	0.7	13.6	116.2	37.7	35.5
ML5-6	0.6	5.7	3.8	3.2	19.8	42.6	35.2
	7.3	61.3	3.2	6.7	129.6	39.0	36.0
ML5-7	0.6	24.3	1.6	0.0	23.0	39.3	35.5
	3.3	37.8	2.2	2.5	56.1	37.9	34.6
	7.3	56.0	2.5	5.8	139.0	36.2	33.8
	8.3	58.0	2.6	4.9	124.5	37.7	34.8
ML6-1	0.3	0.7	0.8	0.0	26.9	34.9	35.4
	3.4	15.6	1.8	0.0	31.8	34.4	34.8
	7.4	8.8	2.2	0.0	29.1	34.2	33.8
	8.4	-	1.4	0.0	24.1	34.4	35.0
ML6-2	0.3	28.3	3.2	9.3	22.7	36.3	36.2
	3.4	40.6	1.7	11.3	103.1	36.9	34.5
	7.5	108.6	1.2	12.5	223.4	36.2	33.7
	8.5	0.0	1.3	12.2	226.6	34.5	32.3
ML6-3	0.3	0.0	0.6	15.0	18.4	36.4	36.3
	7.5	109.3	1.4	12.9	240.5	36.4	34.5
ML6-4	0.3	3.8	0.6	14.4	26.9	41.0	36.9
	3.5	-	0.9	12.9	234.1	36.2	35.6
	7.5	84.9	0.9	13.5	174.1	37.3	36.1

Table H.2: (continued)

Well ID	T - to (hours)	Acetate (mg/L)	Nitrite (mg-N/L)	Nitrate (mg-N/L)	Bromide (mg/L)	Chloride (mg/L)	Sulphate (mg/L)
ML6-5	0.3	1.6	0.0	0.0	16.8	40.8	37.2
	7.6	13.4	0.0	0.7	27.4	39.1	34.9
ML6-6	0.4	5.7	2.3	8.8	17.5	46.6	36.1
	3.5	29.1	3.3	5.8	51.4	42.0	35.8
	7.6	59.7	2.9	8.7	129.1	41.1	35.9
ML6-7	0.4	0.6	0.5	13.5	16.1	47.3	34.9
	7.6	39.7	0.7	13.6	95.9	43.1	35.6
ML7-1	0.3	14.3	0.7	0.0	24.2	35.1	34.9
	2.2	14.9	0.9	0.0	23.3	34.7	34.7
	3.1	19.5	1.5	0.0	26.1	35.3	34.7
	5.2	11.6	1.3	0.0	28.0	36.7	36.8
	7.3	13.0	1.1	0.0	27.4	36.4	36.1
	8.2	11.6	0.5	0.0	22.1	32.1	31.9
	9.0	17.3	0.7	0.0	25.1	35.8	35.9
	12.2	17.6	0.5	0.0	27.6	35.9	37.2
	14.3	15.2	0.6	0.0	26.5	35.7	35.5
	18.3	11.9	0.5	0.0	36.8	35.5	35.7
24.3	17.4	1.1	0.0	48.7	35.3	34.8	
ML7-2	0.3	36.1	4.9	7.3	16.9	37.3	34.8
	2.2	36.6	5.6	6.6	15.6	37.2	35.4
	3.2	36.6	4.8	6.9	37.9	36.8	34.7
	5.2	41.4	4.6	7.8	66.3	36.6	34.4
	7.3	34.9	4.3	7.9	72.8	35.2	34.8
	8.2	34.4	4.9	7.5	70.7	35.9	34.8
	9.1	39.7	4.7	7.8	87.4	35.8	34.3
	12.2	59.4	4.1	8.8	147.8	36.3	36.0
	14.4	66.0	3.5	9.2	164.3	35.2	35.0
	18.3	49.3	3.7	9.0	152.0	37.1	36.4
24.3	34.6	4.5	6.8	126.1	35.6	34.4	
ML7-3	0.3	0.2	1.2	14.0	17.7	36.5	36.5
	2.2	14.5	0.9	13.9	41.5	36.3	35.6
	4.2	65.8	1.1	13.4	144.0	36.3	35.0
	6.2	86.8	1.3	12.8	194.2	35.8	34.3
	7.4	102.5	1.5	12.9	231.0	35.6	34.5
	9.1	105.0	1.5	12.4	209.6	35.6	33.8
	12.2	60.7	2.0	12.3	163.2	37.0	36.6
	14.4	40.8	2.1	12.1	127.0	36.5	36.0
	18.3	12.5	2.0	12.4	70.7	36.2	36.0
	24.4	0.0	1.1	13.5	34.9	34.7	35.7

Table H.2: (continued)

Well ID	T - to (hours)	Acetate (mg/L)	Nitrite (mg-N/L)	Nitrate (mg-N/L)	Bromide (mg/L)	Chloride (mg/L)	Sulphate (mg/L)
ML7-4	0.3	2.2	1.4	13.2	18.5	39.4	36.6
	2.2	48.2	1.4	13.1	103.7	38.0	36.5
	3.2	71.2	1.3	12.7	152.8	36.6	34.0
	5.3	90.1	1.3	12.8	203.4	36.3	34.8
	7.4	106.2	1.2	12.7	232.1	35.7	33.6
	8.2	-	1.2	12.9	209.0	36.1	35.1
	9.2	90.1	1.2	13.1	187.9	36.6	34.7
	12.3	43.4	1.2	12.8	120.8	36.1	34.7
	14.4	27.5	1.2	13.1	89.6	37.2	35.3
	18.4	11.4	1.2	13.3	54.0	38.0	35.6
	24.4	1.0	1.0	13.8	32.7	38.7	35.9
ML7-5	0.4	8.1	1.8	6.7	15.1	40.1	35.9
	2.3	20.6	1.5	4.4	30.3	38.5	35.6
	4.3	26.7	1.1	2.8	43.5	24.9	-
	6.3	43.2	1.9	4.1	83.2	36.6	34.4
	7.4	55.5	1.9	5.2	109.4	36.8	34.0
	9.3	51.1	1.9	7.4	118.8	37.3	35.2
	12.3	37.5	2.3	7.4	99.4	38.3	36.4
	14.4	24.4	2.4	7.4	80.6	39.4	37.2
	18.4	14.0	2.5	6.9	58.7	38.9	35.1
	24.4	6.7	1.9	7.8	44.7	39.1	35.3
ML7-6	0.4	16.9	4.1	5.8	18.6	41.1	34.9
	2.3	24.4	4.8	4.3	21.4	42.2	36.3
	3.3	29.2	4.6	4.4	32.6	40.6	34.7
	5.3	45.3	3.9	5.2	71.1	39.0	33.5
	7.4	62.2	3.3	6.7	124.9	37.8	33.6
	8.3	60.9	3.0	7.2	124.7	38.0	34.4
	9.3	58.7	2.9	8.1	125.5	39.6	34.5
	12.3	40.0	2.6	9.2	103.5	40.4	35.9
	14.4	32.0	2.6	9.4	89.0	41.0	35.3
	18.4	21.8	2.7	9.4	72.9	42.5	35.7
	24.4	12.4	2.9	9.2	55.8	43.3	34.9

Table H.2: (continued)

Well ID	T - to (hours)	Acetate (mg/L)	Nitrite (mg-N/L)	Nitrate (mg-N/L)	Bromide (mg/L)	Chloride (mg/L)	Sulphate (mg/L)
ML7-7	0.4	4.4	1.8	12.1	16.5	45.9	36.2
	2.3	39.9	2.1	11.7	85.8	42.3	35.3
	4.3	62.7	2.0	11.5	136.3	39.6	35.3
	6.3	84.4	2.0	11.2	177.2	37.6	33.8
	7.5	79.2	1.9	11.2	173.0	37.7	33.9
	9.3	68.9	1.8	11.7	153.3	37.3	34.5
	12.3	45.4	1.8	12.0	121.0	40.5	36.0
	14.5	29.9	1.8	11.8	92.7	41.2	35.3
	18.4	16.1	1.9	12.3	64.0	44.7	36.6
	24.4	4.1	1.7	12.1	40.3	44.6	35.4
ML8-1	0.6	24.1	2.6	1.0	25.6	37.6	37.5
	3.5	31.1	5.2	0.8	21.7	34.0	32.8
	7.6	27.7	4.9	1.3	25.8	37.2	36.4
	8.5	28.5	3.8	1.3	29.8	35.8	34.9
ML8-2	0.6	16.2	4.3	3.7	21.1	36.7	36.6
	3.5	12.7	4.5	4.2	18.0	35.0	34.4
	7.6	11.6	4.4	3.5	25.6	36.0	36.3
	8.6	9.9	4.1	3.6	31.1	35.2	35.5
ML8-3	0.6	0.6	1.7	12.4	16.1	36.0	34.2
	7.7	55.2	1.6	13.0	161.8	37.3	35.0
ML8-4	6.2	1.2	2.2	11.1	14.9	38.4	33.2
	3.5	24.3	2.3	11.1	54.9	38.7	34.8
	8.6	85.3	2.4	10.9	178.7	37.6	36.0
ML8-5	0.6	2.0	0.0	0.0	28.3	39.1	35.8
ML8-6	0.7	1.3	5.4	5.5	16.0	43.9	35.8
	3.6	2.0	5.0	5.6	15.8	42.5	33.9
	8.7	9.2	4.9	5.2	28.0	42.1	34.4
ML8-7	0.7	2.2	1.5	12.6	17.4	47.1	36.0

Table H.3: Nitrous oxide data collected during Injection Phase 2.

Well ID	T - to (hours)	N ₂ O Concentration (ug-N /L)
ML5-2	5.4	39.0
ML5-2	9.4	12.8
ML5-3	5.5	Sample Compromised
ML5-3	9.4	Sample Compromised
ML5-5	5.5	32.8
ML5-5	10.0	37.5
ML5-7	5.6	15.7
ML5-7	9.6	6.4
ML6-1	5.7	7.6
ML6-1	10.0	2.0
ML6-2	5.7	33.6
ML6-2	9.8	41.7
ML6-4	5.8	37.5
ML6-4	9.9	40.4
ML6-6	5.8	13.0
ML6-6	9.7	Sample Compromised
ML7-1	5.4	22.5
ML7-1	9.4	2.7
ML7-2	5.5	7.5
ML7-2	9.5	8.5
ML7-4	5.6	36.3
ML7-4	9.5	33.7
ML7-6	5.7	8.9
ML7-6	9.6	22.1
ML8-1	5.7	0.2
ML8-1	9.7	0.8
ML8-2	5.8	6.1
ML8-2	10.1	0.5
ML8-4	6.0	25.6
ML8-4	10.1	20.1
ML8-6	6.0	25.1
ML8-6	9.8	5.3
Arithmetic Mean		18.8
Standard Deviation		14.3

Table H.4: Cation data collected during Injection Phase 2.

Date	Well ID	T - to (hours)	Depth	Calcium (mg/L)	Aluminum (mg/L)	Silicon (mg/L)	Manganese (mg/L)	Iron (mg/L)
25/09/2009	ML5-2-1	7.0	295.54	104	0.00	5.74	0.02	0.00
	ML5-2-2	14.5	295.54	111	0.00	5.73	0.01	0.00
	ML5-5-1	7.0	290.44	108	0.00	5.71	0.00	0.00
	ML5-5-2	14.5	290.44	102	0.00	5.80	0.00	0.00
	ML7-2-1	7.0	293.47	108	0.00	5.88	0.00	0.01
	ML7-2-2	14.5	293.47	127	0.00	5.90	0.00	0.00
	ML7-4-1	7.0	290.07	124	0.00	5.73	0.00	0.00
	ML7-4-2	14.5	290.07	101	0.00	5.75	0.00	0.01
Arithmetic Mean				110.6	0.0	5.8	0.0	0.0
Standard Deviation				9.7	0.0	0.1	0.0	0.0

Table H.5: Nitrate isotope data collected during Injection Phase 2.

Sample ID	Date Collected	T - to (hours)	$\delta^{15}\text{N}$	$\delta^{18}\text{O}$	Nitrate Concentration
			‰ AIR	‰ VSMOW	mg-N/L
ML5-2-1	25-Sep-09	3.65	21.7	9.9	7.7
ML5-7-1	25-Sep-09	3.73	24.4	10.5	2.5
ML6-4-1	25-Sep-09	3.92	9.8	5.7	12.9
ML6-6-1	25-Sep-09	3.92	17.5	7.9	5.8
ML7-2-1	25-Sep-09	3.65	22.7	11.0	6.9
ML5-3-2	25-Sep-09	8.52	10.7	5.7	12.8
ML5-7-2	25-Sep-09	8.62	20.1	11.9	4.9
ML6-6-2	25-Sep-09	8.75	14.1	9.2	9.5
Minimum	-	-	9.8	5.7	2.5
Maximum	-	-	24.4	11.9	12.9
Mean Values	-	-	17.6	9.0	7.9
Mean Background Values	-	-	6.3	1.3	13.0

Table H.6: Additional nitrate and nitrite results collected during Injection Phase 2.

Port ID	Date Collected	Nitrate (mg-N/L)	Nitrite (mg-N/L)
ML7-1	14/09/2009	12.80	0.00
ML7-1	15/09/2009	13.20	0.00
ML7-1	16/09/2009	12.90	0.00
ML7-1	18/09/2009	7.89	2.87
ML7-1	19/09/2009	6.59	1.43
ML7-1	20/09/2009	0.00	0.53
ML7-1	21/09/2009	0.00	0.66
ML7-1	22/09/2009	0.00	0.74
ML7-1	24/09/2009	0.00	1.36
ML7-1	27/09/2009	0.00	0.93
ML7-1	29/09/2009	0.68	1.38
ML7-1	01/10/2009	1.89	1.12
ML7-1	03/10/2009	1.58	0.00
ML7-1	05/10/2009	2.61	0.00
ML7-1	07/10/2009	1.83	0.00
ML7-1	19/10/2009	12.90	0.00
ML7-2	14/09/2009	13.20	0.00
ML7-2	15/09/2009	12.60	0.00
ML7-2	16/09/2009	12.80	0.00
ML7-2	18/09/2009	11.20	1.08
ML7-2	19/09/2009	8.58	3.16
ML7-2	20/09/2009	5.14	5.99
ML7-2	21/09/2009	4.17	7.17
ML7-2	22/09/2009	4.81	5.84
ML7-2	24/09/2009	6.91	3.92
ML7-2	27/09/2009	10.80	1.02
ML7-2	29/09/2009	11.50	0.80
ML7-2	01/10/2009	11.80	0.67
ML7-2	03/10/2009	10.80	0.52
ML7-2	05/10/2009	11.40	0.00
ML7-2	07/10/2009	11.50	0.00
ML7-2	19/10/2009	13.00	0.00